BEHAVIOUR OF COMPOSITE PIPES UNDER MULTI-AXIAL STRESS

This thesis is submitted with the requirements of Newcastle University for the degree of Doctor of Philosophy

By

Mohd Shukry Bin Abdul Majid

Centre for Composite Materials Engineering,
School of Mechanical and Systems Engineering,
Newcastle University,
Newcastle upon Tyne

January 2012

ABSTRACT

This thesis describes an experimental investigation of the behaviour of filament wound glass fibre reinforced epoxy (GRE) composite pipe under hydrostatic and biaxial load conditions at temperatures up to 95°C. The project was intended to lead to improvements in reliability and quality, and ultimately a reduction in the cost of qualifying GRE oil and gas pipelines. The experiments were designed to be compatible with the procedure currently used by Future Pipe Industries (FPI), employing the concept of ultimate elastic wall stress (UEWS) in the qualification and production control of GRE pipe. The UEWS test appears to provide an attractive means of rating GRE pipes, where weepage resulting from the accumulation of matrix cracks is a common failure mechanism.

A novel test rig capable of performing UEWS tests under various loading conditions from hydrostatic to multi-axial loadings was designed and developed. UEWS tests were conducted under six different stress ratios ranging from pure axial to pure hoop loading at room temperature (RT), 65°C and 95°C. The tests involved the application of groups of ten 1-minute hydrostatic pressure cycles at increasing pressure levels. The intention is to identify, by examining the stress-strain response, a stress level below which damage growth is either negligible or at least sufficiently low to prevent long term failure within the design life. In addition, acoustic emission measurements were also conducted to investigate the nature of the damage mechanisms involved as well as its compatibility to the UEWS results.

Three distinct failure modes were observed: tensile axial failure under pure axial loading, weepage under axial dominated loading from 0.5:1 to 2:1 and localized leakage failure under hoop dominated loading of 4:1 and 1:0. Full tensile-tensile UEWS and leakage based failure envelopes were developed at a range of temperatures from 20°C (RT) to 95°C. Both envelopes showed a strong dependence on stress ratio and test temperature. It was also shown that the UEWS based failure envelope at elevated

temperatures generally degraded, except for the 2:1 loading where UEWS strength increased.

The Miner's law model developed, gives a good account of the effects of cyclic and static loading in UEWS tests. Using a crack growth model similar to Paris Law, damage development can be directly linked to the progressive nucleation of matrix micro cracks. It is also shown that cyclic rather than static loading dominates the UEWS test response. The general lifetime damage model developed in the study shows good agreement with the experimental data from the multiaxial UEWS tests. This approach may therefore be an appropriate procedure for describing the long term performance of GRE pipes under any required combination of static, cyclic fatigue, hydrostatic and non-hydrostatic loading.

ACKNOWLEDGEMENTS

Praise to Allah, the Most Gracious and Most Merciful, for giving me the strength and guidance to finish this thesis.

The research work which led to this thesis was conducted during the period from 22nd September 2008 until 16th September 2011 at Centre of Composite Materials, Newcastle University, UK. Research was funded by Future Pipe Industries (FPI) who also took the role as a joint research partner. I also wish to acknowledge my sponsors, Ministry of Higher Education Malaysia (MOHE) and Universiti Malaysia Perlis (UniMAP) for providing the financial support in their overseas postgraduate programme.

My special thanks go to Professor A.G. Gibson for his guidance and continual support throughout the course of this work. I equally appreciated his wisdom, tolerance, patience and challenging criticism. I would also like to thank Dr. Jack Hale and Dr. George Kotsikos for their expert views, advice and fruitful discussions throughout this project.

I am very grateful to all staff at School of Mechanical and Systems Engineering, especially Ken Madden and his team of skilful technicians, who help with fabrication work, development of the test rig, and for dealing with all of my last minute requests with great humour and professionalism. Many thanks also extended to James Humphrey, Johannes Linden, Tarak Assaleh, Pietro Di Modica and Gordana Vasic for their companionship, helpful insights and friendly working environment.

And most importantly, the unconditional love, support and care from my family, my parents and my beloved wife and kids have been unsurpassed at all times, and for this, I am eternally indebted.

LIST OF PUBLICATIONS

1. **M.S. Abdul Majid**, T.A. Assaleh, A.G. Gibson, J.M., Hale, A. Fahrer, C. A. P. Rookus and M. Hekman, *Ultimate elastic wall stress (UEWS) test of glass fibre reinforced epoxy (GRE) pipe*, Composites Part A: Applied Science and Manufacturing, Volume 42, Issue 10, October 2011, pp. 1500-1508.

2. A.G. Gibson, **M.S. Abdul Majid,** T.A. Assaleh, J.M., Hale, A. Fahrer, C. A. P. Rookus and M. Hekman, *Qualification and lifetime modeling of fibreglass pipe*, Plastics, Rubber and Composites: Macromolecular Engineering (PRC2838), Volume 40, Number 2, March 2011 , pp. 80-85(6)

3. A.G. Gibson, **M.S. Abdul Majid,** T.A. Assaleh, A. Fahrer, C.A.P. Rookus, M. Hekman *Qualification And Test Procedures For GRE Fibreglass Pipe*, DURACOSYS – 2010, 9th International Conference on Durability of Composite Systems 12 – 15 September 2010, Patras – Greece

4. A.G. Gibson, **M.S. Abdul Majid** and T.A. Assaleh, J.M., Hale, *Qualification and Test Procedures for Fiberglass Pipe for Oil and Gas Applications*, 13th Middle East Corrosion Conference, MECC 2010 paper no:10127

TABLE OF CONTENTS

SYMBOLS AND ABBREVIATIONS

Symbols

a	Crack length
A	Proportionality constant
E	Elastic modulus
d	Diameter
E_A	Axial Young's Modulus
E_H	Hoop Young's Modulus
E_f, E_m	Fibre and matrix Youngs' Modulus
$E_{1,}$ E_2	Ply stiffness in the fibre and transverse fibre direction
G	Shear Modulus
G_f, G_m	Fibre and matrix shear modulus
I	Moment of inertia
k_1, k_2	Interaction constants
N_i	Number of cycles applied at stress level σ_i
N_{if}	Number of cycles to failure at stress level σ_i
P	Pressure
R	Radius
t_i	Time applied at stress level σ_i
t_{cf}	Creep failure at stress level σ_i
W	Load
ID_{sg}	Inner diameter at the location of strain gauge
TE_{sg}	Reinforced wall at the location of strain gauge
$[Q]$ $[\overline{Q}]$	Stiffness and transformed stiffness matrix
$[\overline{S}]$	Transformed compliance matrix
$[T]$	Transformation matrix
V_f, V_m	Fibre and matrix volume fraction
σ, ε	Stress and strain
$\sigma_{A,}$ σ_H	Average pipe stress in the axial and hoop direction

$\sigma_{1,}\sigma_2$	Ply stresses in 1-2 direction
$\varepsilon_{A,}\varepsilon_H$	Average pipe strain in the axial and hoop direction
τ, γ	Shear stress and shear strain
$\tau_{12,}\tau_{AH}$	Ply shear stress in the 1-2 and *A-H* plane
$\gamma_{12,}\gamma_{AH}$	Ply shear strain in the 1-2 and *A-H* plane
σ_1^* σ_2^*	Longitudinal and transverse failure stress of a unidirectional ply
τ_{12}^*	Shear failure stress of a unidirectional ply
$\varepsilon_{1,}\varepsilon_{10}$	Strain at the first and the tenth cycle during UEWS test
ε_p	Predicted strain during UEWS test
α	Thermal expansion coefficient
υ_f, υ_m	Fibre and matrix Poisson's ratio
υ_{12}, υ_{12}	Ply Poisson's ratio in the 1-2 and 2-1 plane
δ	Deflection
ρ	Crack density

Abbreviations

AE	Acoustic emission
CTP	Cyclic test pressure
DGEBA	Diglycidyl ether of bisphenol A
FPI	Future pipes industries
FRP	Fibre-reinforced plastics
GRE	Glass fibre-reinforced epoxy
GRP	Glass fibre-reinforced plastics
HDB	Hydrostatic design basis
LCL	Lower confidence limit
MDA	4,4'-methylene-dianiline
PVC	Polyvinyl chloride
RT	Room temperature
UEWS	Ultimate elastic wall stress
WWFE	World wide failure exercise

LIST OF FIGURES

LIST OF TABLES

CHAPTER 1: INTRODUCTION

1.1. Glass fibre reinforced epoxy (GRE) pipes

Glass fibre-reinforced plastics (GRPs) have been successfully employed in many engineering applications, notably in the aerospace, marine, automotive parts, oil and gas industries and consumer goods. This is due to their attractive physical and mechanical properties, particularly their strength to weight ratio and resistance to fatigue and corrosion [1-4]. Other features such as ease of installation, high durability and low maintenance and life cycle costs make them more desirable than conventional materials such as steel. In addition, due to their anisotropic nature, GRPs can be tailored to specific applications to achieve the highest levels of performance required. This allows engineers to design composite structures to match loading systems and gives the ability to fabricate shapes which are difficult to form using conventional materials.

Glass fibre-reinforced epoxy (GRE) composite is one of the most widely used types of GRP. It is used extensively in the marine, building and automotive industries. The present work concerns applications in the offshore oil and gas industry, particularly in composite pipelines for aqueous liquids. GRE pipes are usually designed to withstand high pressure. Their lightweight, relatively thin-walled structure provides ease of handling and transportation [2, 5], which results in reduced installation costs. Their corrosion resistance properties have led to extensive use in the offshore industry to transport highly corrosive fluids (including seawater, aerated water and hydrocarbons) [2]. Almost all the pipes in these applications are produced by a filament winding process, and they are usually subjected to a combination of internal pressure and axial loading.

One of the reasons GRE pipes have proliferated recently in the oil and gas industry and for the transportation of corrosive fluids is their excellent mechanical properties. These are highly dependent on the types of resin used, orientation and placement, and also the

volume fraction of the glass fibre reinforcement. Unlike metals, which are homogenous and isotropic materials, the GRE pipe is considered to be orthotropic in nature. The mechanical properties of GRE pipes are distinct in three mutually perpendicular planes, where the intersection of these planes is known as the principal material axes [6]. This special property permits engineers to design pipes so that they will have greater strength and stiffness in the anticipated load direction. In cases of GRE pipes for transporting fluids, the 'ideal' winding angle of ±55° is always preferred since here the maximum stress is aligned to the direction of the fibres.

However, GRE pipes have low modulus of elasticity in the hoop direction and particularly in the axial direction. Nevertheless, they show promises in their high strength to weight ratio and stiffness, in addition to other excellent properties such as abrasion, corrosion and chemical resistance. As with stiffness and strength, the thermal behaviour of GRE pipes is also dependent on the characteristics and arrangement of their constituents.

As the use of GRE pipe increases, so does the need to define reliable design limit in terms of performance. This will provide engineers with basic guidelines to enable GRE systems to be designed with confidence to a common standard. One of the major challenges concerning the use of filament wound GRE pipe is to predict the onset of first ply damage under combinations of internal pressure and axial loading. As has been thoroughly investigated and documented, the principal failure of GRE pipe is due to weepage, which is a slow leakage of fluid through the pipe wall. This type of failure normally occurs at much lower stress levels than that leading to bursting.

Filament-wound GRE pipe is essentially a layered of unidirectional plies angled sequentially at ±θ°, to the axial direction. In this investigation, the pipes were produced at the ±55° angle, which is considered to be the optimum angle for GRE pipes when subjected to internal pressure alone. However, in practice, pipework is also subject to axial tensile or compressive and bending loads. This implies that the hoop to axial stress ratio could vary significantly from the 2:1 ratio, i.e. internal pressure loading only. The inherently anisotropic mechanical properties of each ply induce complicated stress

states within the laminate when subjected to multiaxial loads such as combined internal pressure and axial loading. This leads to a rather intricate process of crack initiation within the laminates, with cracks running through the resin phase parallel to the fibre direction. However, this may not result in weepage failure since the cracks are restrained by the neighbouring ply at a different orientation, which may still remain intact. This suggests that weepage could have precipitated from combinations of matrix cracks with other forms of damage, for example interlaminar cracks or even delamination between plies.

The stress-strain behaviour of GRE pipe is initially linear elastic, and followed by non-linearity at later stages close to failure, first by weepage and then ultimately bursting. In earlier investigations, many have explained this non-linear response as a consequence of matrix cracking within plies. As the crack density increases with increasing load, the non-linearity becomes more pronounced at higher loads and is found to correspond to degradation in the mechanical properties of the pipe. A comprehensive review of the behaviour of GRE pipes, particularly under multiaxial and fatigue loading, is given in Chapter 2.

Figure 1.1: Glass fibre reinforced epoxy (GRE) pipes for cooling water – courtesy of Future Pipe Industries (FPI).

1.2. Manufacture of GRE pipes

As mentioned above, almost all GRE pipes used for offshore applications are produced by the filament winding process. This process emerged in the 1950s and has evolved since then to become an efficient technique for the mass production of GRE pipes and many other high quality composite components such as vessels, shafts, ducts and most tube-shaped structures [7]. One reason for its ubiquity is that the process can provide high fibre content and hence produces pipes with excellent mechanical properties. A broad range of fibre and matrix systems can be used in this process, depending on the cost and performance levels required. There are a variety of types of winding machine available, such as those using helical, polar, continuous and filament placement [1, 8]. However, the current study only concerns helical winding because this is the most common winding method used to produce GRE pipes.

The winding process for producing GRE pipe is relatively simple. Bundles of continuous fibre strands are either impregnated or wetted by passing them through a resin bath, wound onto a rotating mandrel at the desired angle. The carriage unit responsible for feeding the fibres onto the mandrel travels back and forth along the length of the mandrel while it rotates at a specified speed [6, 9, 10]. The arrangement of the fibres and the winding angle can be easily controlled for specific designs by coordinating mandrel rotation and carriage speed in order to obtain the required axial and hoop properties. Careful monitoring is required to ensure that the mandrel is fully covered by the resin wetted fibre bundles and to produce a product with consistent wall thickness. Usually, numbers of fibre tow are used together to produce bigger bandwidth and reduce winding time. A diagram of the filament winding process for producing GRE parts is shown in Figure 1.2.

Once the mandrel is completely covered to the desired thickness, it is removed from the winder and placed in the oven for curing. The mandrel is then rotated during the curing processes to maintain uniformity in resin content around the circumference of the pipe. Finally, the cured GRE pipe is stripped from the mandrel which has usually been coated with a release agent prior to the winding process for easy removal of the wound

structure. However for some products, such as pressure vessels, the mandrel is not removed and becomes an integral part of the structure.

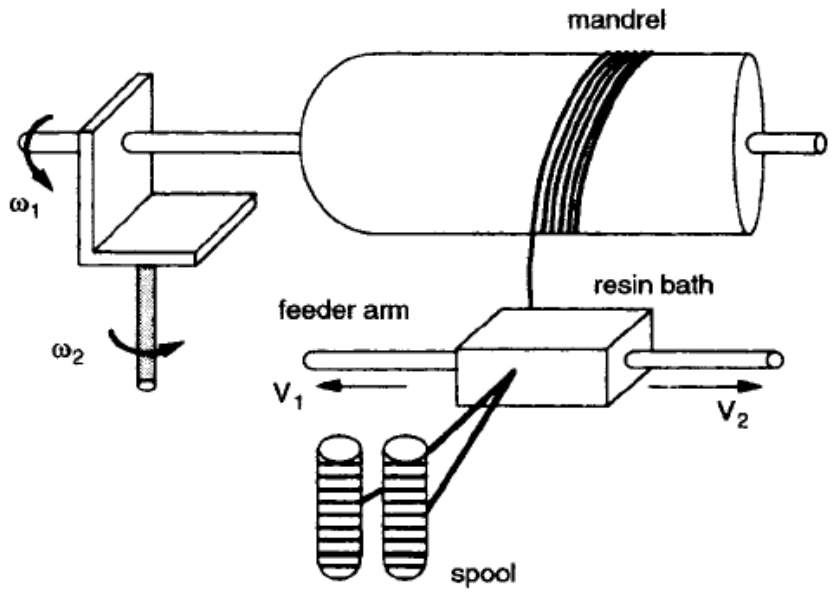

Figure 1.2: Schematic diagrams of the filament winding concept for producing angle ply GRE pipes. The winding angle is controlled by coordination of feeder movement and the rotation of the mandrel [11].

Contemporary filament winding processes offer high precision, very good repeatability and relatively inexpensive compared with other automated methods of manufacturing composite parts. The low cost is perhaps due to their evolved automated system, which allow for high production rates. This subsequently reduces fabrication costs by 50-80% as compared to a manual hand-layup process which relies extensively on human labour [12]. All shapes of GRE pipes can be manufactured using the filament wound process except for those with difficult surface curvatures. Some of the parts, such as the pipe tee, may not appear to be woundable directly, but a combination of two or three plain GRE pipes would often be used to produce such complex parts.

Modern winding machines are numerically controlled with a high degree of precision for laying the exact number of layers of reinforcement in order to ensure that the GRE pipe produced has good mechanical strength in the circumferential and longitudinal directions. However, the mechanical strength of the filament wound parts does not

simply depend on the composition of constituent materials but also on process parameters like winding angle, fibre tension, resin chemistry and curing cycle [7]. Great emphasis has focused on the development of computer operated and user friendly filament winding machine control to improve the quality of GRE products, especially in the mass production of GRE pipes. The development of lower cost filament winding machines encompassing control systems and the software used to produce cylindrical GRE components is now being pursued [9, 13].

1.3. Constituent materials in GRE pipes

The main constituents of GRE components are epoxy resin, aromatic amines as hardener and glass fibre reinforcement. The primary function of the glass fibres in GRE pipes is to increase the mechanical properties of the matrix system and hence provide greater stiffness, strength and thermal ability [14]. They are made from an extrusion of a molten mixture of quarry products (sand, limestone and boric acid) through micro fine bushings before rapid cooling to below the glass transition temperature [15]. Usually, the glass fibre reinforcement used in composite engineering would have a diameter in the range of 10-20μm [6, 10]. Finally, a surface coating, also known as sizing, is applied to the fibres to promote easy fibre wetting and processing, hence creating strong bonding between the resin and fibres. The most commonly used glass reinforcement in GRE products is E-glass, due to its high strength to weight ratio and good corrosion resistance properties.

The epoxy matrix system, on the other hand, serves to transfer and distribute applied loads to the fibre reinforcement and maintain the reinforcement position and orientation. Epoxy matrix also protects the fibres from mechanical damage due to handling and aggressive environments [6, 16]. The most prevalently used epoxy resin in the manufacture of GRE pipes is known as diglycidyl ether of bisphenol A (DGEBA). It is created by the reaction of epichlorohydrin with bisphenol A in the presence of sodium hydroxide. The chemical structure of DGEBA is shown in Figure 1.3(a) [17];

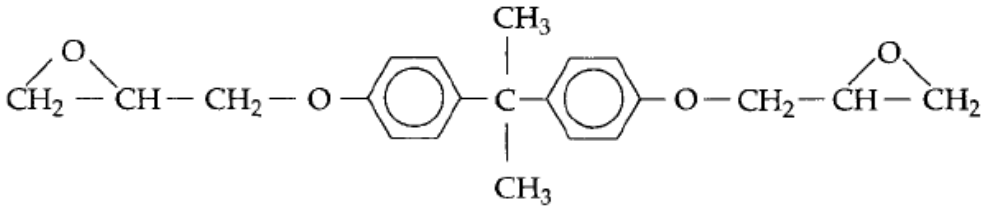

(a)

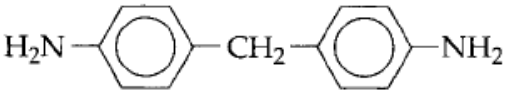

(b)

Figure 1.3: (a) Chemical structure of common epoxy resin (DGEBA) and (b) curing agent, 4,4′-methylene-dianiline (MDA).

DGEBA resin is a difunctional molecule with two terminal epoxide groups instead of the ester groups in polyester resin. The absence of ester groups in epoxy resin imply that it will have better water resistance property and hence, be less susceptible to water attack. The epoxy chain molecule also consists of two ring groups at its centre, which provide superior responses to both mechanical and thermal stresses than linear groups. As a result this gives epoxy resin very good stiffness, toughness and heat resistance properties [15].

Epoxies differ from other resins in that they are cured by a 'hardener' rather than a catalyst. The hardener is normally an amine (cycloaliphatic, IPD or aromatic, MDA) used as the curing agent and is determined by the number of N-H bonds in a molecule. An aromatic amine like 4,4′-methylene-dianiline (MDA) is usually preferred in preparing epoxy resin due to its good chemical and thermal resistance. The chemistry of this 'addition reaction' causes cross-linking, where two epoxy sites react on each amine site producing a C-N bond as shown in Figure 1.4 [18]. This creates a complex three-dimensional molecular structure. While some epoxies are formulated to crosslink at room temperature, many necessitate subsequent post-curing to complete the cross linking to achieve optimum properties.

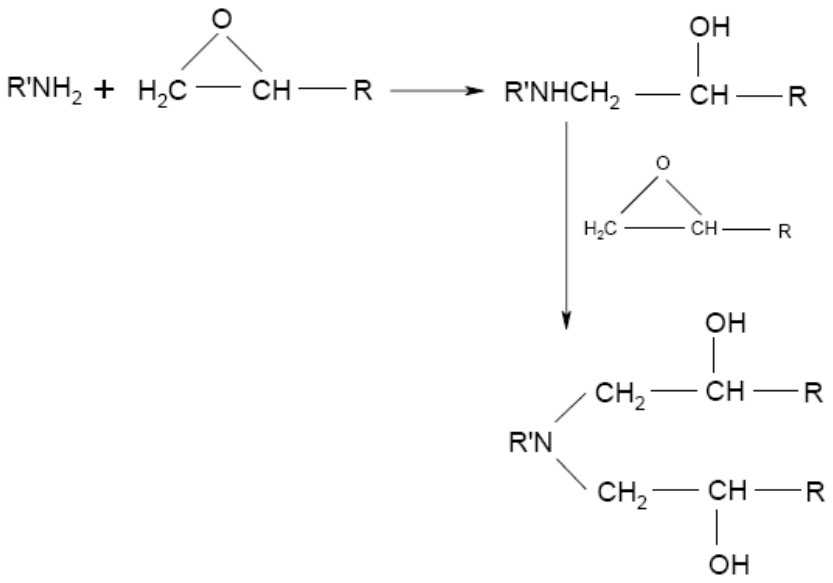

Figure 1.4: The curing reaction scheme between epoxy resin and amine [18].

1.4. Objectives of the project and outline of the thesis

From an industrial point of view, ISO 14692 is the principal standard currently used to predict the maximum service pressure for GRE pipes where a regression curve is determined. Weepage failure is common in this procedure, where slow leakage from the wall of the tube is observed due to the presence of a network of matrix cracks which form over time [19-21]. Although the ISO procedure provides an acceptable and reliable method of predicting behaviour under pure internal pressure, GRE piping is usually subject to complex loading involving combinations of axial load and internal pressure. At present, the understanding of pipe behaviour, particularly under combinations of axial tension and internal pressure, is limited by a lack of experimental data and understanding of the failure mechanisms involved. ISO 14692 provides an approximate method allowing for axial load effects, but may not reflect the true nature of the interaction between internal pressure and axial stress. Furthermore, the ISO 14962 test to predict lifetime based on a regression curve can be very expensive and time consuming. Considering all the limitations of the existing test procedure, there is a need to develop an improved and more rapid method for realistic conditions, supported by experimental data and accurately reflecting the failure mechanisms that may occur.

The aim of this PhD research on lifetime behaviour is that it will lead to improved reliability, quality and cost reduction for qualifying epoxy oil and gas pipelines. This is a partnership project between the Composite Centre of Newcastle University and its industry counterpart, Future Pipe Industries (FPI), to investigate the failure envelope characteristics of GRE pipes under biaxial loading based on a short term test. This research is experimentally based and involves an investigation of the failure envelopes of GRE pipe of realistic diameter over a variety of axial load and internal pressure combinations. It also involves an experimental investigation of the behaviour of GRE under hydrostatic and biaxial load conditions at temperatures up to 95°C.

The format of the experiments has been singled out to be compatible with the FPI procedure which uses the ultimate elastic wall stress (UEWS) concept in the qualification and production control of GRE pipes. The experimental side of the research involves the design of 200mm diameter test spools with an internal pressure ram capable of modifying loading conditions from hydrostatic to multi-axial loading. The design enables an additional pressure chamber to be contained within the envelope of a normal GRE test-spool, without the need for any form of exterior loading frame.

The interpretation and modelling of the results are of equal importance to the experimental work carried out. The key difficulty is in correlating the results of UEWS tests with long term failure data. A model based on Miner's cumulative law is used to illustrate the damage accumulation caused by fatigue cyclic and static loading in UEWS tests. This model then takes into account the fundamental failure mechanism in GRE, namely the propagation of cracks within the resin phase. It is intended that the model be used as a framework within which the results of the experimental study can be interpreted. The prediction of failure envelopes from the UEWS method currently employed by Future Pipe Industries (FPI) is critically investigated and assessed from accurate measurements of stress and strain as well as acoustic emissions during testing. A general lifetime damage model for GRE pipe similar to the Tsai-Hill interactive failure criterion is also employed for this particular purpose.

In this thesis, the relevant literature and background are reviewed in Chapter 2. The review covers on the failure modes and analysis, fatigue behaviour and factors that affect the behaviour of GRE pipes as well as the current qualification process for GRE pipe. Chapter 3 describes the experimental procedures involved in the project, which include the main UEWS test at various loading ratios, the determination of the degradation in properties, the acoustic emission and microscopic analysis procedures. Chapter 4 describes all the modelling work carried out in the project. Chapter 5 presents the results from the UEWS test for all test conditions and the calculations involved in interpreting the data. Results of the acoustic emissions measurement, determination of stiffness property and microscopic analysis are also presented in this chapter. This includes comprehensive discussions of the results obtained. Finally, conclusions from the study and suggestions for future research are drawn in Chapter 6.

CHAPTER 2: LITERATURE REVIEW

2.1. Biaxial loading of filament wound GRE pipes

Multiaxial stress and strain states can occur in a system due to (a) applied multiaxial loadings, for example in pipes, shafts, pressure vessels; (b) geometric discontinuities in notches, reinforcing plates; (c) material discontinuities in bonded structures; and (d) material anisotropy in fibre reinforced composites [22]. Due to the orthotropic nature and tubular shape of GRE pipe, the biaxial stress-strain states encountered is an extremely complex problem. GRE pipe work, which is the subject of the investigation here, is not only subjected to internal pressure loading but also axial tensile or compressive and bending loads due to various factors such as ground movement, improper installation, temperature fluctuation and many more.

Generally, for a thin-walled filament wound fibreglass pipe, internal pressure alone gives a 2:1 hoop to axial stress ratio, which is the case for the ±55 filament wound GRE pipe used in this work. By applying additional axial loading to the system together with differential internal pressure, various hoop to axial stress states can be obtained. The radial component, on the other hand, is relatively low in magnitude compared to the in-plane components and hence, can be ignored. The stresses in the principal plane can be calculated from the following relationship:

$$\sigma_H = \frac{P\,d}{2t}$$
$$\sigma_A = \frac{P\,d}{4t}$$
$$hence;\ \sigma_A = \frac{\sigma_H}{2} \qquad (2.1)$$

where σ_H, σ_A, and are the hoop and axial stresses respectively and d and t are the diameter and thickness of the pipe respectively.

Figure 2.1 shows the conventional experimental setup for attaining a 2:1 hoop to axial ratio and pure hoop loading for composite tubes [23]. In diagram (a), the end caps are secured and axial and hoop stresses are given by equation (2.1). In diagram (b), the pressure is sealed by the rubber o-rings, where the pipe is free to slide and hence eliminate the axial stress to create pure hoop loading. This type of set up is also convenient for studying the stress state in laminate, with the benefits of avoiding edge-effect problems as well as taking advantage of the ease of introducing multiaxial loading into the specimen [21].

Numerous studies of the biaxial testing of filament wound GRP pipes have been conducted. Hull *et al.* [24], for instance, fabricated filament wound glass polyester pipe and subjected it to biaxial and uniaxial hoop pressures to observe failure modes. Rosenow [25] continued Hull's work by further extending the test to include tensile loading. Sodden *et al.* [26] carried out experimental work on bi-directional, ±55 filament wound GRE pipes under a variety of biaxial stress states by applying combinations of internal pressure and axial tensile and compressive loads. Special attention was paid to the end gripping and pressure sealing problem by adding material reinforcement to the end of the pipe to minimize the stress concentration.

Mistry *et al.* [27] designed a test rig to carry out an experimental study on the buckling failure of filament wound GRE pipes under combined external pressure and axial loading. Ellyin and Wolodko [22] developed a new multiaxial testing machine capable of applying axial load differential pressure and torsional force to the composite tube. Recently, Hale *et al.* [28, 29] designed a biaxial test rig suitable for conducting a test on filament wound composite pipe at elevated temperatures. In this test rig, the pipe was thermally regulated by a cartridge heater installed inside the test spool and loading was achieved by the pressurization of the test medium. In the present work, a similar concept to that of Hale's test rig has been adopted. A ram was installed inside the pipe to create two compartments which could be separately pressurized to produce various hoop to axial stress ratios. Further details of the design and arrangement of the set up and test procedures are given in Chapter 3.

(a)

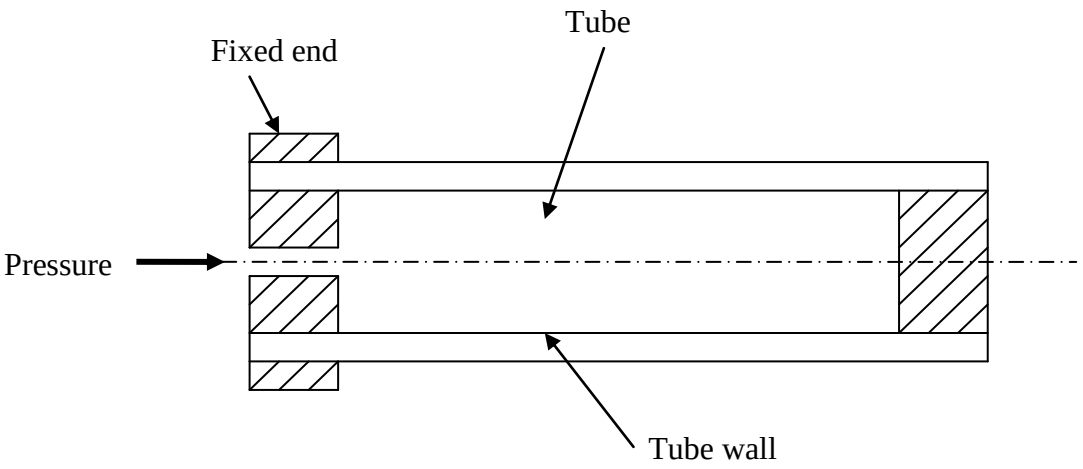

(b)

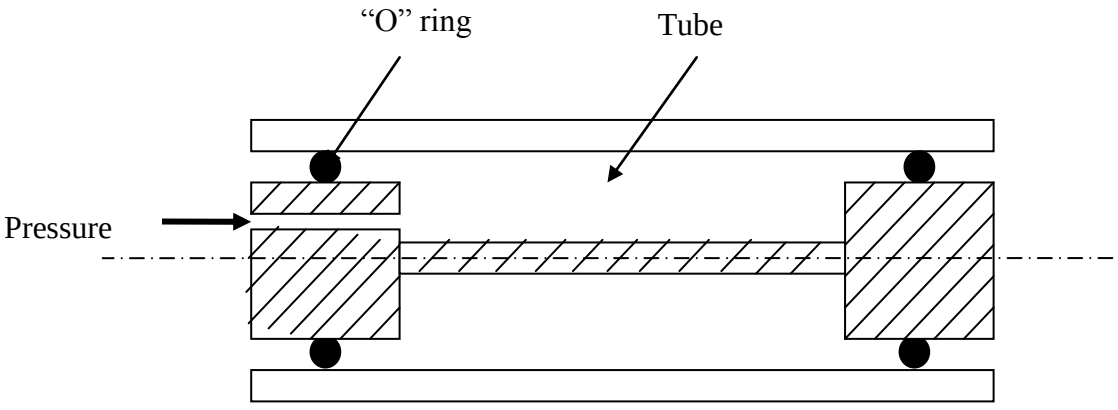

Figure 2.1: Schematic diagram for common biaxial testing rig for composite pipes with: (a) internal pressure loading creating 2:1 hoop to axial stress condition; and (b) pure hoop loading condition [23].

2.2. Failure of filament wound GRE pipes

The failure behaviour of filament wound GRE pipes subjected to biaxial load has been the subject of numerous experimental and modelling investigations spanning decades, as demonstrated in the literature [5, 14, 20, 24, 26, 29-46]. The majority of such investigations have emphasized on the failure envelopes, fatigue strength, leakage and the associated deformation of angle ply laminates similar to those used in GRE pipes. However, whilst most of these studies concentrated on structural failure in composite pipes, the more significant issue of micro structural progressive damage, which leads to the final failure is less clear.

One of the earliest studies of the failure behaviour of fibreglass pipes was conducted by Hull e*t al.* [24] in which pipes were internally pressurized to failure using the closed end and the restricted end as referred to in the previous section (Figure 2.1). Leakage was observed to be the main failure mode for fibreglass reinforced pipes, and leakage modes were distinct for different ratios of axial load to internal pressure. Similar tests were conducted by Soden [26] to investigate leakage and fracture strength in ±55° filament wound GRE pipes. He concluded that fracture strength very much depending on the ratio of hoop to axial stress applied, noting that leakage failure occurred at much lower stresses than that at final failure.

Most of the literature has reported that filament wound composite pipes under fatigue biaxial load failed due to sequences of damage which involve transverse matrix cracking, delamination, weepage and fibre fracture [19]. This is illustrated in Figure 2.2 [47]. Increases in applied load cause the continuous nucleation and accumulation of transverse matrix cracks along the fibre direction. When the matrix crack density reaches saturation, delamination, weepage and fibre fracture may occur hence causing a rapid progression of damage leading to final catastrophic failure.

However, when composite pipes are in use, one must not only consider the final failure of the pipes but also any situations when they lose the practical capability to carry out the requirements of the application. Since weepage and delamination failure occur at much lower pressure than that required to fracture the glass fibres, these types of failure

can be regarded as functional failure rather than the structural failure when total collapse occurs and can no longer bear the load. Hence detecting functional failures in GRE pipes is favoured, since these failures can be regarded as benign failure modes, providing attractive leak-before-break characteristics. Before trying to correlate the damage state, stiffness degradation and fatigue life from the UEWS tests conducted in this investigation, it is imperative to look more closely at these sequences of damage endured by the pipe before functional failure.

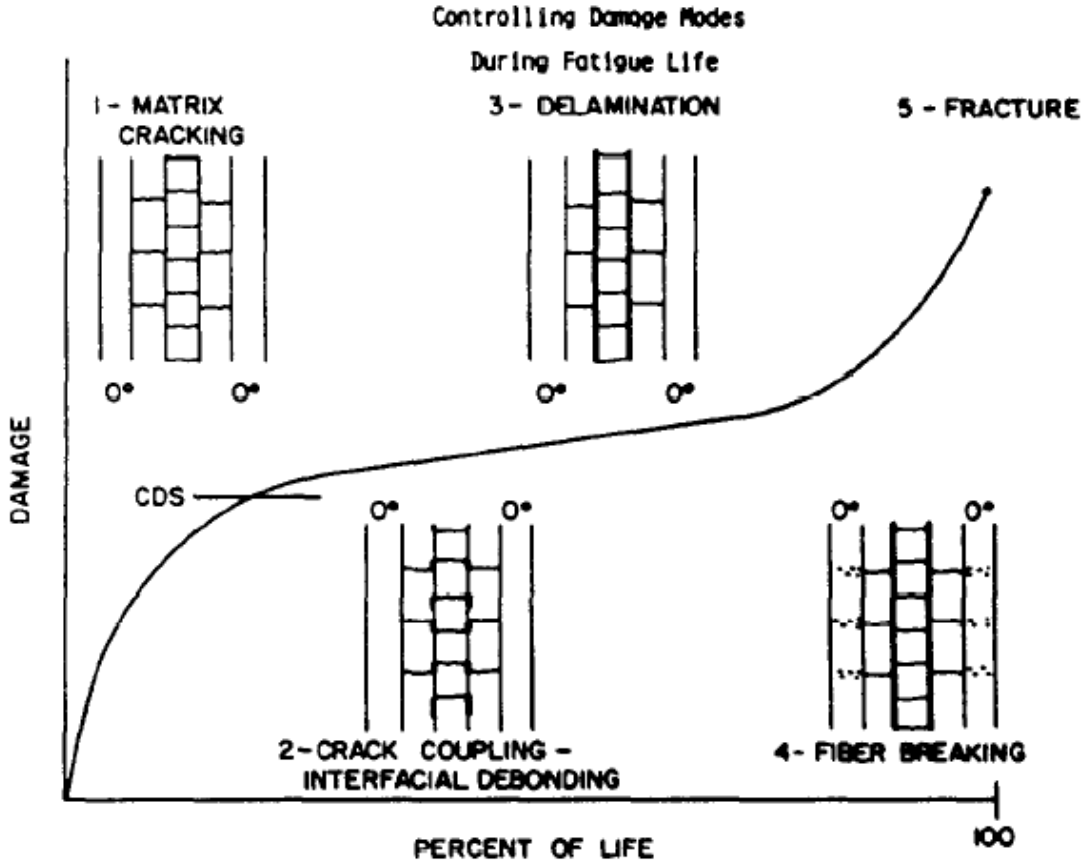

Figure 2.2: Sequence of damage development in composite laminates during fatigue loading [47].

2.2.1 Transverse matrix cracking

The formation and growth of transverse matrix cracking which leads to weepage failure has been a well observed and much studied failure mechanism in filament wound GRE pipes. Increases in the load applied statically or cyclically will cause a progressive nucleation of matrix cracks due to the high stress and strain concentrations in the matrix phase between the tightly packed fibres. Matrix microcracks proceed from the initiation of cracks near regions of high fibre volume fractions or voids, before propagating transversely to the matrix phase around the fibres [19, 48]. However, in some cases, microcracks also observed across the resin rich areas. The numbers of cracks then increase as the load is increased, which results in a significant decline of the effective stiffness and thermal properties of the laminate. This eventually induces stress redistribution in individual plies before considerably affecting the deformation of the pipe and final leakage failure. Throughout the whole failure process, the fibres remain intact [32]. Figure 2.3 shows the transverse matrix cracking commonly observed in angle ply laminate pipes.

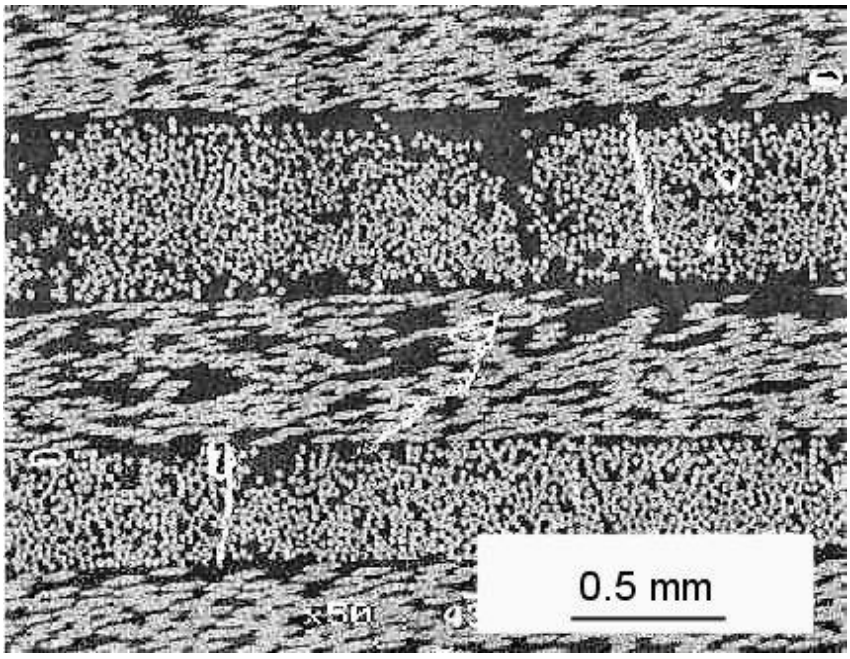

Figure 2.3: Transverse matrix micro-cracks in a filament wound ±55º angle ply glass epoxy tube [49]

Several experimental and modelling studies have been carried out on the initiation and growth of transverse matrix cracks and the influence of various loading combinations, ply fibre orientations and environmental conditions [50-52]. One of the earlier studies, by Broutman and Sahu [53], investigated the initial formation of transverse cracks. Extensive experimental works have also been carried out in [54, 55] to observe matrix cracks. It was found that the cracks formed in the transverse direction of the fibres and crack density increased with increasing applied stress until reaching saturation at which failure occurred. The researcher then went on to revise the multiple fracture theory in studying the effect of ply thickness on predictions of crack spacing in unidirectional composite laminates. It was concluded that the threshold strain for transverse cracking is highly dependent on the thickness of the plies around which cracking occurs. However, Harrison and Barder [56] suggested that, crack density at saturation also depends to the extent on the applied strain levels, rather than just laminate geometry, especially during fatigue loading. Later, Nairn and Hu and Nairn *et al.* [57, 58] successfully conducted a series of experiments on crack density as a function of applied stress. They found that no cracks were observed until the limit stress was reached. However, once initiated, the crack density often increased very rapidly.

Matrix cracking within composite laminates has been recognized as the major factor causing the reduction in stiffness of laminates. Various models have been presented to characterize such degradation in stiffness due to transverse matrix cracking under in-plane uniaxial and multiaxial loading. Among these models are the ply-discount approximation [59], the continuum damage model [48, 60-62], shear lag model [54, 55, 63], self consistent scheme [64], and the variational model proposed by Hashin [65, 66]. Recently, Katerelos *et al.* [67] conducted an analysis of the effect of matrix cracking on the behaviour of angle ply laminates loaded statically using the equivalent constraint model (ECM). The approach showed a good agreement with the experimental results obtained by microscopic strain measurement using the laser Roman spectroscopy technique [68].

A finite element model was proposed by Tao and Sun [69] and Sun and Tao [70], who investigated the effects of matrix cracking on the stiffness degradation of laminates. The

predicted normalized transverse and shear modulus was later plotted against the exponential function of the normalized crack density of a cracked lamina. The following curve fitting expression was then derived from the plot:

$$\frac{E_2}{E_2^{o}} = \exp(-\alpha_E \lambda^*)$$
$$\frac{G_2}{G_2^{o}} = \exp(-\alpha_G \lambda^*) \qquad (2.2)$$

Where;

E_2 and E_2^{o} are effective and initial transverse Young's modulus of ply respectively.

G_2 and G_2^{o} are effective and initial shear modulus of ply respectively.

α_E and α_G are curve fitting constant determined by the finite element analysis.

λ is the normalized crack density function.

The authors concluded that normalized crack density rather than crack density is a more appropriate parameter to be used in predicting cracking damage. It was also inferred that the location of the cracks has very little influence on layer stiffness, but that the constraining layers have a considerable impact on the effective modulus of the cracked layer.

In 1979, Jones and Hull [71] examined the morphology of transverse matrix cracks present in GRE pipe loaded up to final failure, using a standard microscopic technique. According to their observations, white striations parallel to the fibres appeared during pressurization which increased progressively as weepage pressure was approached. The formation of streaks was also accompanied by acoustic emission indicating matrix cracking that took place within the laminates. From micrograph image observations, they found that matrix cracks tended to be initiated at a region with higher fibre content. They subsequently classified these cracks as either transverse, parallel or interlaminar and oblique transverse cracks. Similar observations were made by Bailey and Parvisi [50] in their work on the debonding effects in cross ply laminates of glass fibre composites. They inferred that the whitening effect seen were, in fact, associated with

fibre-matrix debonding. Micrograph images suggested that the transverse cracks then formed as a result of the coalescence and growth of this debonding in the laminates. Recently, Lokman Gemi *et al.* [72] looked at the fatigue behaviour of filament wound GRE pipes under pure internal pressure. Structural observations with a scanning electron microscope (SEM) showed matrix cracking coalescing with voids within the matrix phase, hence precipitating the damage progression process.

Frost *et al.* [42, 73] studied the influence of loading frequency in predicting the long term fatigue behaviour of a GRE pipe. They concluded that the prime failure mechanism observed for short and long term fatigue were leakage as a result of matrix cracking. As mentioned earlier, although transverse matrix cracking may not cause abrupt structural damage in pipeline applications, it is highly detrimental since it leads to weepage failure which, if not treated, can trigger the development of other, more deleterious forms of damage such as fibre breakage or bursting.

2.2.2 Delamination

Another commonly observed failure mode for GRE pipes is delamination, which is also referred to as interlaminar cracks between composite layers. This type of failure is dominated by the properties of the matrix, and given that matrix strength and toughness tend to be relatively low, laminated composites are hence prone to the development of delamination. This type of damage rarely occurs as an independent damage mode, and is usually associated with or triggered by other damage modes such as commonly, transverse matrix cracking.

Delamination damage or interlaminar cracks can be described as the detachment or separation of two adjacent plies. This may result from the interlaminar stresses that develop due to edge effects or large differences in ply stiffness as a consequence of transverse matrix cracks. Delamination damage may also occur due to impact damage and manufacturing inconsistencies such as incomplete curing and poor interplay bonding. Similar to transverse matrix cracking, delamination in GRE pipes significantly reduces the structural integrity of the pipe and may initiate more extreme damage

mechanisms such as weepage or leakage failure and fibre breakage [19, 24, 74]. In many types of composite structure, including GRE pipes, delamination and transverse matrix cracks are the most frequently observed type of damage and combinations of the two constitute the majority of failure mechanisms.

As mentioned in the previous section, transverse matrix cracks tend to occur along the fibre direction within individual layers. As there is relatively little resistance to crack growth in the fibre direction, the cracks, once initiated, grow rapidly in this direction. However, the cracks are restrained by their respective layers due to plies of different orientation lying above and below, which may differ considerably in stiffness properties. As a result, a multiaxial stress state develops at the crack tips and, once the stress level exceeds the resin failure strength, this may be sufficient to initiate interlaminar or delamination failure between the two adjacent layers. Delamination increases the possibility of weepage failure by coalescing with transverse cracks, hence creating multiple pathways for fluid to pass through the pipe wall.

Jones and Hull [19] carried out microscopic observations of the delamination failures of GRE pipes under biaxial loading. They observed that, for pure hoop loading, the pipe buckled and delamination took place on the compressive side of the bent pipes. This was later followed by catastrophic failure involving fibre breakage, which appeared to start in the regions of delamination. Local weepage or small jets of fluid spraying from local sites could be observed if delamination took place along the outermost interlaminar plane, since fluid could escape along the crack length. This was observed by Meijer [35] when GRE pipes were tested at 4:1, 4.5:1 and 5:1 hoop to axial stress states. It was noted that the appearance of the tested pipes changed, becoming opaque over the entire surface due to coarse striations. This characteristic suggested delamination damage. Ellyin and his co-workers [75] studied the behaviour of multidirectional filament wound GRE pipes subjected to biaxial loads of different loading rates. Due to the combinations of fibre winding angles in the plies, matrix micro cracks cause great differences in stiffness in neighbouring layers, creating high interlaminar stress and hence resulting in delamination damage.

A number of studies have been conducted on the delamination damage induced by matrix cracking, most of which has concentrated on the problems of predicting initiation and growth [76-82]. O'Brien [81] was the first to develop an analytical model for predicting matrix crack induced delamination. The model estimates the energy release rate as a function of the modulus of the undamaged laminates and the modulus of the delaminated region. Wang *et al.* [83] carried out a 3D finite element analysis to determine the rate of energy release as delamination grows. Two types of delamination were investigated: one initiating from the intersection of transverse cracks and free edges of the laminates and the other from the intersection of transverse cracks only. Both case studies showed reasonable agreement with the experimental results.

Later, Nairn and Hu [57] and Nagendra *et al.* [84] extended the variational analysis of a transverse matrix cracking proposed by Hashin to model the delamination damage induced at the crack tip. Takeda and Ogihara [80] used a simple one dimensional shear lag analysis to model laminates containing delamination originating from the crack tips and hence predicted the associated decline in modulus properties. However, this study was only concerned with reductions in the axial stiffness, while the effects of delamination on shear modulus and Poisson's ratio remained unexamined. The latter were investigated by Kashtalyan and Soutis [85], whose results revealed that crack induced delamination caused a significant total reduction in shear modulus and Poisson's ratio which in fact, exceeded that caused by transverse cracking. More recently, Noh and Whitcom [86] conducted a very interesting study on the effects of various shapes of cracks induced delamination towards property degradation. It was claimed that the crack opening is closely related to the decline in stiffness of the damaged middle lamina.

2.2.3 Weepage

Weepage is a common type of leakage failure in filament wound GRE pipes as a result of the progressive damage caused by transverse matrix cracking running parallel to the fibre as discussed in previous section. Through-thickness matrix cracks form and propagate due to the integrated effects of transverse tensile and shear stresses. This can

develop either from the effect of long term static pressure (static fatigue), repeated pressure (cyclic fatigue) or a combination of both. This damage mode normally occurs at load levels considerably lower than that of structural bursting or collapse failures.

The cracks start from the debonding process between fibres and the matrix interface. Once debonding takes place, there will be less surface area for stress distribution. This will initiate the development of stress concentrations within the composite system which, in turn, causes further debonding. Ultimately, debonding combined to form a crack parallel to the fibres which then grow in a plane parallel to them. Weepage occurs once the crack concentration increases to a critical level where a fluid path is possible through the pipe wall [24, 36, 74]. Weepage failure is categorized as functional failure due to slow leakage through the pipe wall while it still maintains its structural integrity.

This mechanism can be observed visually from the uniform formation of fluid droplets on the outside surface of the pipe. As loading continues after a significant accumulation, beads of fluid can be seen running down the exterior of the pipe, which eventually progresses into the wetting of the entire surface. Other methods of detecting the onset of weepage include the use of electrical resistance measurement on the pipe surface or by quantifying the changes in the fluid volume within the pipes, which also enables workers to determine the rate at which leakage occurred [75]. Recent work by Mertiny and Gold [87] measured weepage using effective permeability, which is based on the fluid flux through the wall of GRP pipes. They suggested a good correlation between matrix damage and fluid permeation.

Pabiot *et al.* [88] studied the effect of the fibre/matrix interface on the weepage of filament-wound composite pipes. They demonstrated a relationship which shows that weepage failure in GRE pipes subjected to internal pressure loading is very much influenced by the interface in terms of crack initiation and propagation through the wall thickness. Jones and Hull [19] tested ±55° filament wound GRE pipes at 2:1 hoop to axial loading and found them to fail through a weepage mechanism. They went on to suggest that the prevention of weepage failure can be improved by finding a way to inhibit the initiation and propagation of transverse cracks.

Mieras [89] studied the effect of matrix properties on the failure of filament wound GRE pipes. He suggested that weepage failure is very much dependent on the failure strain of the matrix system. Legg and Hull [90] explored the effects of resin flexibility on weepage strength, and found that the weepage strength of ±55° filament wound GRP tested at $\sigma_H=2\sigma_A$ increased with resin flexibility due to changes in failure strains and the initiation and propagation of micro cracks. Later, Tanigushi *et al.* [91] continued these investigations and looked into the influence of the mechanical properties of the matrix system in the GRE pipes with respect to weepage failure. Weepage pressure was observed to be almost proportional to the failure strain of the matrix.

Soden *et al.* [26] conducted an experimental investigation of thin walled GRE tubes subjected to various biaxial stress conditions from combinations of internal pressure and axial loading. They found that the initial failure for all loading conditions was usually leakage at a pressure considerably lower than the final failure pressure. A similar study by Saied [14] also suggested that GRE tubes tend to fail due to a weepage mechanism, which is in agreement with previous findings [19, 24, 26, 34]. A recent study by Meijer and Ellyin [35] investigated first failure modes of GRE pipes subjected to fourteen stress ratios ranging from pure axial loading (0:1 hoop to axial) to pure axial compression (0:-1 hoop to axial). Weepage/leakage was observed for all loading conditions from pure axial to 5:1 hoop to axial loading, except for high hoop dominating loadings and axially compressive loadings where the specimens demonstrated catastrophic failure with sudden bursting.

2.2.4 Fibre breakage

Fibre breakage is the final sequence of the damage mode in GRE pipes. When it occurs the specimen is considered to have lost its structural integrity before progressing quickly to total failure. Combinations of damage modes spread within laminates until either tensile stress in the fibres exceeds the limiting strength of the glass or macro cracks which have nucleated from combinations of interlaminar and intralaminar cracks grow catastrophically. This is often followed by sudden bursting, leaving the fracture

area with very little of the structure of the wound pipe. This type of failure is also sometimes referred to as total structural failure since load can no longer be borne.

An assessment by Orifici *et al.* [92] on the failure of composite laminates implies that failure of fibre in tension is caused by the accumulation of the failures of individual fibre in the plies. This eventually becomes critical when not enough intact fibres remain to bear the load. Failure of fibre in compression loading, on the other hand, was found to occur due to micro buckling.

Spencer and Hull [93] tested GRE pipes to failure under a 2:1 hoop to axial stress ratio at various winding angles. They found no significant fibre rotation prior to weepage failure. However, after weepage was observed, the matrix cracks became very extensive and the pipes developed a large axial elongation and obvious circumferential contractions where the fibres rotated towards an optimum angle of ±55º. Pipes then burst abruptly due to successive and continuous fibre breakage. This can normally be seen from massive macro cracks parallel to the fibre orientation in which the minimum necessary amount of energy has been dissipated for the fibres to pull out and fracture [72]. Similar work was conducted by Soden *et al.* [94] on the study the fracture strength of GRE pipes where weepage failure was suppressed by use of a rubber liner.

Meijer and Ellyin [35] conducted biaxial testing on GRE pipes at high hoop dominating and axial compressive loading. They found that all samples demonstrated catastrophic failure leaving fibres pulled out, which were no longer constrained by the matrix. Similar findings were also observed by Highton *et al.* [95] and Caroll *et al.* [40].

2.3. Stress-strain response for biaxial loading

Many researchers have shown that the behaviour of filament wound GRE pipes is linearly elastic at low strain, followed by non-linearity when approaching failure, first by weepage then ultimately rupture. This behaviour is a consequence of transverse matrix cracking within each ply, which causes a reduction in the stiffness of the pipe. Frost [32, 42] reported that crack density increased with increasing load, which resulted in more pronounced non-linearity in the stress-strain response. He suggested that, as

crack density increased, delamination then took place which allows for ply rotation. This rotation hence caused a more noticeable non linearity response in the axial strain.

Nahas [96] briefly reviewed some of the existing methods for predicting the non-linear response of laminated fibre reinforced composites. He then used the secant modulus and an iteration technique to predict the non-linearity of laminates under load. Sun and Tao [70] later identified this response as primarily resulting from three main sources: material non-linearity, progressive failure in the laminates, and geometric non-linearity. They then modelled stress-strain behaviour using simplified shear-lag and finite element analysis, considering the material's non-linearity and progressive matrix cracking.

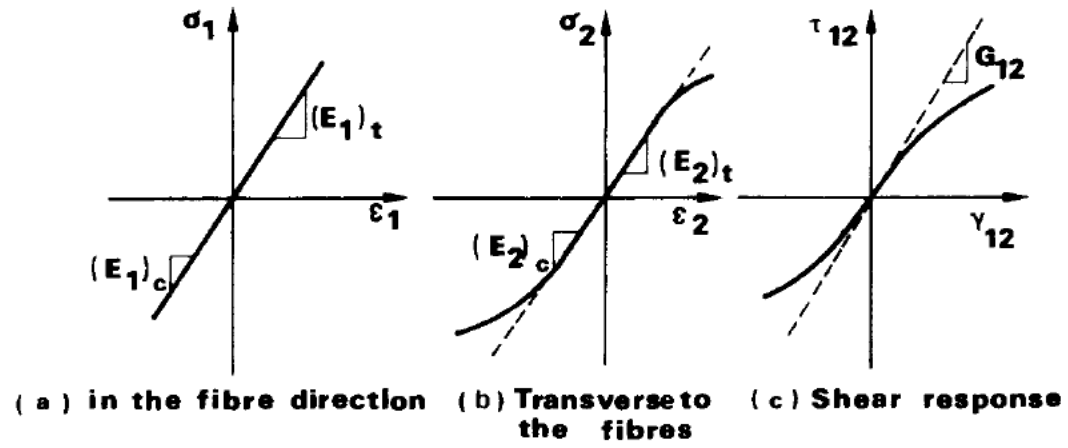

Figure 2.4: Typical stress strain behaviour of fibre reinforced composite materials [96].

Caroll *et al.* [40] experimentally investigated the effects of the rate and stress ratio of biaxial loading on the stress-strain behaviour of GRE pipes. They found that elastic behaviour of the pipe was present at low stress levels. They went on to formulate a relationship between the stress-strain responses to accumulating damage. Later, Ellyin *et al.* [75] analysed the stress-strain response for multidirectional filament wound GRE pipes under biaxial loading. Confirming findings of Caroll, they noted that the elastic behaviour of the tested pipes was not just present at low stress levels but also showed time dependent properties.

Roberts *et al.* [49] examined the effects of micro cracks on the stress-strain relationship in GRE pipes. They developed a crack density model for predicting the stress-strain response in which relationship between crack density and applied stress was established. Good conformity between modelled and experimental results was attained. The non-linearity was also observed to become more pronounced at higher temperatures approaching the resin glass transition temperature, *Tg*. Recently, Meijer and Ellyin [35] conducted a test on ±60° GRE pipes under 14 different stress ratios. They observed that the stress strain response for hoop dominated loading tended to be relatively linear compared to the response in the axial direction which is dominated by the polymer matrix. This again further suggests that the non-linearity of the stress-strain response is a result of changes in transverse stiffness as crack concentration increases leading to weepage failure.

2.4. Micromechanics of GRE pipes

Prior to investigating the failure modes of GRE pipes subjected to a range of multiaxial load ratios, it is important that the micromechanics of GRE pipes is fully understood. Extensive work has been carried out by earlier researchers on the performance behaviour of GRE pipes [23, 24, 26, 35, 36, 38, 42] which is still going on. The primary concerns are the degradation of the mechanical properties of the pipes and their elastic response prior to final failure. The elastic properties of GRE pipe work are often modelled using laminate theory.

2.4.1. Laminate theory

Laminate theory is a powerful mathematical procedure for determining the global elastic response of composite laminates subjected to applied loads or strains. In laminate theory, each ply is assumed to be macroscopically homogeneous and linearly elastic. It may further be assumed that plies also have perfect bonding with the adjacent lamina so that no slippage can occur [23, 74]. Micromechanics theory describes the elastic response of the lamina and the elastic stiffness of its constituents. Laminate theory then allows the stresses induced in each layer to be estimated from the elastic properties of each lamina, which is very significant considering that the failure of GRE

pipes involves progressive fracture such as matrix cracking. The details of the implementation of laminate theory are given in Chapter 4 during the modelling of the elastic properties of the GRE pipe.

2.4.2. Netting analysis

Another quick and simple method of predicting the biaxial strength of filament wound GRE pipe is to employ 'netting analysis'. This was described by Hull [23] and is widely used especially during the early evolution of filament winding techniques. Although the analysis considerably simplifies the nature of the loading taking place, it has been found to provide a fairly good approximation of the rupture strength of composite pipes at 2:1 hoop to axial stress ratios. Perhaps this simplicity and its conservative approach may be the reasons for its continuing use.

Basically, the analysis simply disregards the presence of the matrix and assumes that all the loads applied to the composite system are carried by the reinforcing fibres [16, 23, 26]. This means that the pipe can only support a combination of forces such that the resultant acts in the direction of the fibres, and thus their transverse and shear stress is taken to be zero, that is $\sigma_2=\tau_{12}=0$. Using the inverse of the transformation matrix to relate the stress in pipe's axis and the fibres' principal axis gives:

$$\begin{aligned} \sigma_x &= \sigma_1 \cos^2\theta \\ \sigma_y &= \sigma_1 \sin^2\theta \\ \tau_{xy} &= \sigma_1 \sin\theta\cos\theta \end{aligned} \tag{2.3}$$

By using netting analysis to characterize helically wound GRE pipes under biaxial stress conditions where the in-plane principal stresses are in the ratio of 2:1 hoop to axial stress, it can be derived that:

$$\text{when } \sigma_x = \sigma_A,\ \ \sigma_y = \sigma_H \text{ and } \sigma_H \Big/ \sigma_A = 2$$

$$\frac{\sigma_H}{\sigma_A} = \frac{\sigma_1 \sin^2\theta}{\sigma_1 \cos^2\theta} = \tan^2\theta = 2$$

$$\text{hence,} \quad \theta = \sqrt{2} = 54.7^\circ \tag{2.4}$$

This presumed 'ideal angle' is normally preferred for filament wound fibre-reinforced pipe applications since it gives a good prediction of the load capacity for a 2:1 hoop to axial stress ratio, especially when the stiffness of the matrix is extremely small relative to that of the reinforcing fibres. It is important to note that this 'ideal angle' is only valid for pipes with closed ends, where the application of internal pressure alone will give 2:1 hoop to axial stress ratios. However, for other stress ratios, the predicted strengths become doubtful.

J.T. Evans *et al.* [97] compared the results obtained from netting analysis with the full predictions obtained from laminate theory. The optimum angle predicted by laminate theory was found to deviate from that obtained from netting analysis by a total depending on the matrix to fibre stiffness ratio. According to Soden *et al.* [26, 38], since most of the filament wound pipes for high pressure applications used this 'ideal angle', netting analysis provides a straightforward tool for designing high pressure pipes. In addition, netting analysis can also be used to decide which angle is best suited for particular hoop to axial stress ratios. Most high pressure GRE pipes today which operate at 2:1 hoop to axial stress ratios are reinforced at $\theta = \pm 55°$.

2.5. Failure criteria

Failure criteria for isotropic and homogenous materials like maximum stress, maximum shear and maximum distortional energy theories have been well established [6]. Such theory are then further extended and modified to cater for composite materials by taking into account the anisotropic nature of their strength and stiffness. This development of failure models to characterize the mechanisms that lead to failure has been the matter of

rigorous study for over 30 years by research workers around the world. At present, countless theories available in the literature describe failure in various ways. This includes whether they are founded on strength or fracture mechanic theories, or whether they give general failure predictions or are capable of pin-pointing particular failure modes [92].

Predicting failure in composite materials is complicated due to the multiplicity of failure modes involving either fibres or the matrix or combinations of both [21]. For example, the failure of composite laminates is always preceded by matrix micro cracks within individual plies where the laminate continues to carry the load even though first ply failure has occurred. This is clearly explained in the failure of GRE pipes discussed in previous sections where bursting is often preceded by weepage.

In 1998, initiative was taken by Soden *et al*. to conduct an organized study to test and compare prominent failure theories developed in the past decades [37, 98-100]. Known as the World Wide Failure Exercise (WWFE), the study was conducted by comparing the failure criteria of fibre reinforced plastics (FRP) systems subjected to biaxial stress ratios against a common set of experimental test data, so that consistent comparison could be facilitated. Surprisingly most theories differed significantly from experimental observations even for a simple laminate analysis. It was concluded that, while there are a number of failure criteria available, these were only successful with limited ranges of data. Some failure theories showed a wider range of applications whereas some produced predictions of greater accuracy. However, none were able to accurately predict the weepage failure of FRP systems [100].

Throughout the years, many different categories have been introduced to classify failure criteria. However, failure theories are usually classified as interactive or non-interactive criteria. Non-interactive failure criteria suggest that there is no interaction between stress components and that each failure is unique and independent of others, while in interactive failure criteria, the stress components interact and can be included in a single expression. In the following sections, some widely used failure theories are briefly discussed.

2.5.1 Interactive failure criteria

In these criteria, all stress components interact and contribute simultaneously toward the failure of the composite systems. Tsai-Hill [101] and Tsai-Wu [102] failure criteria are the two most commonly used interactive failure criteria in determining the failure of fibre reinforce polymer structures. The Tsai-Hill criterion allows for interaction between different stress components, whereas the Tsai-Wu criterion provides the capability for interaction between direct and shear stresses and accounts for differences between tensile and compressive strength [103]. These criteria assume linear elastic material properties and expect degradations in stiffness after the first ply failure. However, both criteria state only that the material will fail once the limiting stress is reached and do not explicitly identify failure modes.

Tsai Hill's criterion [101] is based on the Von Mises distortional energy criterion. It was later modified by Hill to cover anisotropic materials before been applied to composite materials by Tsai. For orthotropic materials similar to GRE pipes, the criterion is expressed as:

$$\left(\frac{\sigma_1}{\sigma_1 *}\right)^2 + \left(\frac{\sigma_2}{\sigma_2 *}\right)^2 - \left(\frac{\sigma_1 \sigma_2}{\sigma_1 *}\right)^2 + \left(\frac{\tau_{12}}{\tau_{12} *}\right)^2 = \phi \tag{2.5}$$

where, the subscripts, 1, 2, and 12 indicate, tensile stresses parallel and transverse to the direction of the composite ply and the shear stress respectively. The starred terms refer to stresses at failure for unidirectional lamina. According to this criterion, no failure will occur provided that Φ is less than unity. One disadvantage of the Tsai-Hill criterion is that it does not differentiate between tensile and compressive strength during evaluation.

Another widely used interactive criterion, was first proposed by Tsai-Wu in 1971 [102]. The criterion describes the combined stress failure surface in a quadratic polynomial relation represented by the following expression:

$$F_1\sigma_1 + F_2\sigma_2 + F_{11}\sigma^2{}_1 + F_{22}\sigma^2{}_2 + 2F_{12}\sigma_1\sigma_2 + F_{66}\tau^2{}_6 = 1 \quad (2.6)$$

where F_1, F_2, F_{11}, F_{22} and F_{66} are described in terms of the strengths in the principal directions. F_{12} on the other hand, is experimentally determined by biaxial tensile loading. The Tsai-Wu criterion can be applied to a laminate and used to find the first ply failure. This can be further extended to be related to a progressive damage model to produce a final failure envelope and predicts the stress-strain response of composite laminates. This criterion is widely used in laminate analysis as it is easy to exercise and can be simplified into a single-valued function which enables an extension to cater for cases of three-dimensional failure [98]. The Tsai-Wu criterion was one of only a few that were highly ranked in the WWFE study [100] for predicting the strength of unidirectional laminates under combined loads.

Both the Tsai-Hill and Tsai-Wu failure criteria have been applied extensively in many composite applications. For example, Puck and Schneider [104] modified the Tsai-Hill criterion to construct a micro mechanical failure theory to predict failure strength based on stresses of the fibre, the matrix system and the fibre-matrix interface. Sim and Brogdon [105] formulated probably the first explicit extension of the Tsai Hill static failure criterion to describe the fatigue behaviour of composites under various loading modes. This was achieved by replacing the static strength parameters with a fitting fatigue curve.

Philippidis and Vassilopoulos [106] further extended the Tsai-Wu criterion to cover cyclic loading to predict the fatigue strength of multidirectional laminates, which was tested under multiaxial loading conditions. Hashin [107], on the other hand, modified the Tsai-Wu criterion to establish three dimensional theories for unidirectional fibre composites. He then collaborated with Rotem to develop the Hashin-Rotem failure criterion, which was one of the earliest to concentrate on two separate failure criteria: one for fibres and the other for resin [108]. This criterion also enjoys wide popularity among researchers. However, it appears to be suitable only for defining the onset of

damage and is more sound in the cases of unidirectional and angle ply laminates than for general composite structures.

2.5.2 Non-interactive failure criteria

Non-interactive failure criteria are generally involved in evaluating the failures of the stress components separately rather than those of homogenised material and many are available in the literature. However, the most widely used are the maximum stress and maximum strain criteria and also the more elaborate damage mechanic model. The maximum stress and strain criteria are very similar to the Rankine theory for homogeneous isotropic materials, but have been extended to cater for the orthotropic nature of composite laminates. These theories are based on the assumption that failure will take place when at least one of the stress or strain components along the principal axes exceeds the corresponding strength or ultimate strain critical values. Thus, maximum stress theory is expressed in the following:

$$\frac{\sigma_1}{\sigma_1^{fail}} \geq 1, \quad \frac{\sigma_2}{\sigma_2^{fail}} \geq 1, \quad \frac{\tau_{12}}{\tau_{12}^{fail}} \geq 1 \tag{2.7}$$

where σ_1, σ_2, τ_{12} are longitudinal, transverse and shear stresses respectively in the principal directions and σ_1^{fail}, σ_2^{fail} and τ_{12}^{fail} are the longitudinal, transverse tensile and shear failure strengths of unidirectional lamina. If the normal stresses are compressive, σ_1^{fail} and σ_2^{fail} must be replaced by compressive strength. Similarly, for maximum strain theory:

$$\frac{\varepsilon_1}{\varepsilon_1^{fail}} \geq 1, \quad \frac{\varepsilon_2}{\varepsilon_2^{fail}} \geq 1, \quad \frac{\gamma_{12}}{\gamma_{12}^{fail}} \geq 1 \tag{2.8}$$

where ε_1, ε_2, γ_{12} are longitudinal, transverse and shear strains respectively in the principal directions and ε_1^{fail}, ε_2^{fail} and γ_{12}^{fail} are the corresponding allowable strains.

Although these theories have been extensively investigated in the past, their main drawback is in neglecting the interaction between different stress components, especially in biaxial loading conditions. They generally yield different results and can be less accurate, although they are often used due to their simplicity. However, the Puck theory is a well known non-interactive failure criterion was rated in the WWFE study. Developed by Puck and Schűrmann [109], the theory is based on physical damage and failure mechanisms in the constituents. The theory takes into account the non-linear stress-strain relationship and makes allowances for a continuous and progressive decline in stiffness after the initiation of matrix cracks. This is later used to calculate the elastic constant of the lamina.

2.6. Failure envelope for biaxial loading

The failure strength of composite laminates under biaxial loading can be illustrated in a graphical presentation called the failure envelope. This is generated by conducting a pressure test to failure at various hoop-to-axial loading ratios. For a thin walled pipe, internal pressure alone gives a 2:1 hoop-to-axial stress ratio, and radial stress is minimal and normally neglected. The biaxial failure envelope is then illustrated by plotting the failure points in an axial stress versus hoop stress graph where $\tau_{HA} = 0$. The shape of the failure envelope can vary depending on the loading conditions, mechanical properties of the constituents, and winding angles.

An investigation by Soden *et al.* in 1978 [38, 95] described the failure envelopes for ±45°, ±55° and ±75° wound tubes under a variety of biaxial stresses. It was concluded that the strength of the tubes varied greatly according to the ratio of axial to hoop stresses. It was also noticed that the shape of the failure envelope was highly dependent on the orientation of the fibres. Figure 2.5 illustrates the failure envelopes generated in the study showing the initial and final failure stresses for ±55° filament wound GRE tubes under biaxial loads. Hinton *et al.* [103] then further extended the investigation by comparing those recorded experimental based failure envelopes with five well known failure theories. Carroll *et al.* [40] conducted an experimental investigation into the behaviour of GRE pipes subjected to monotonic biaxial loading of various hoop to axial

stress ratios. A somewhat different failure envelope was constructed with failure stresses in compression loading considerably higher than those seen in Soden's failure envelope.

Sun and Tao [70] constructed failure envelopes for unidirectional composite laminates from linear laminate theory. They used a ply by ply discount method with a parallel spring stiffness model for modelling the envelopes. They then compared their model based failure envelope to the test results used in the WWFE study [110]. Their findings showed a good conformity with the final failure strength where failures were largely dominated by fibre tensile strength. Conversely, the result yielded poor agreement with the experimental failure strains dominated by transverse and shear matrix cracking. An interesting biaxial fatigue failure envelope was constructed by Ellyin and Martens [31] for multidirectional filament-wound GRE pipes. However, the failure envelope presented did not provide a credible insight into the complex behaviour of multidirectional laminate pipe.

Hale *et al.* [28, 29] investigated experimentally the effects of high temperature and wetting conditions on two different matrix based GRE pipes, IPD epoxy and PSX phenolic, under biaxial loading. They noted that the plot for the envelope tends to be skewed towards the origin of the axes as temperature increased. Meijer and Ellyin [35] recently carried out multiaxial stress tests on filament wound GRE pipes under different loading conditions where stress and strain failure envelopes were produced. The maximum strain failure criterion was then fitted to the experimental strain failure envelope. The criterion was found to over-predict strength at stress ratios where failure occurred by local leakage and during axial compressive loading.

Failure envelopes for GRE products are very important, since they provide pipe engineers with the information to take full advantage of the high strength of composite structures whilst maintaining realistic margins of safety against fracture. They can also be used to show potential problems that engineers might face, especially in operating filament wound pipes at high stress levels, so that appropriate preventive measures could be set in place [26].

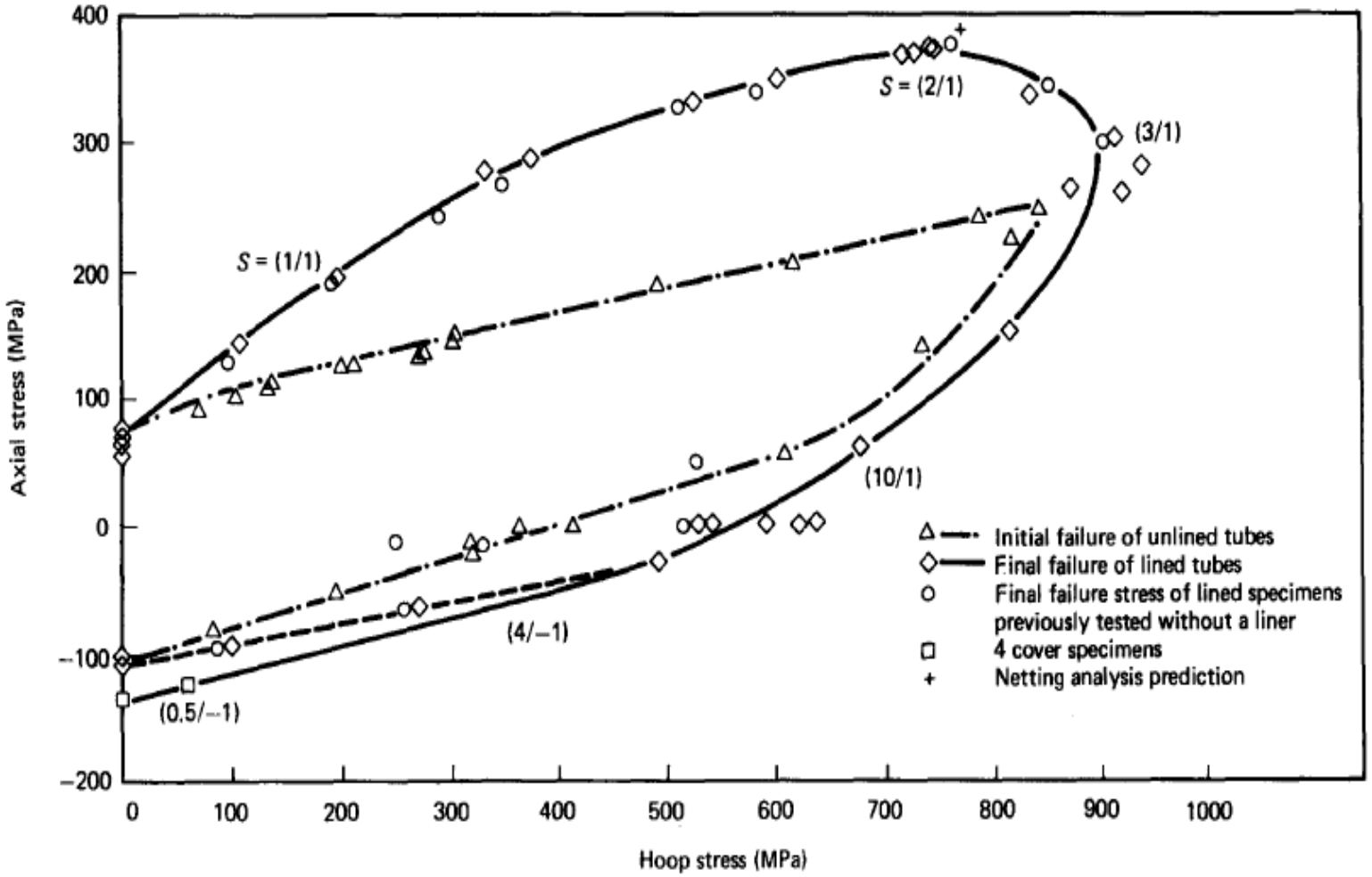

Figure 2.5: Failure envelope from Soden et al. for ±55° filament wound E-glass/epoxy tubes subjected to biaxial loads

2.7. Effect of winding angle on the strength of GRE pipe

The advances in today's modern computer controlled filament winding machines have paved the way for the generation of almost any winding angle in GRE pipes. The most common filament wound pipes normally have fibres wound in helices at angles of ±θ° to the pipe's axial direction. To achieve the optimum design criteria, the winding angle of the fibres is orientated in directions that offer the maximum working loads for particular applications. From numerous experimental analyses [23, 24, 26, 93, 94] it has been shown that the best winding angle for GRE pipes subjected to internal pressure alone (2:1 stress ratio) is ±55°.

The effect of varying the winding angle on the strength performance of helical wound pipes under internal pressure was studied by Spencer and Hull [93] and Soden *et al.* [94]. They concluded that the winding angle and stress ratio have a pronounced effect on the associated deformation and fracture strength of GRE pipe. Three failure envelopes for ±45°, ±55° and ±75° wound pipes produced by Soden show that an increase in winding angle increases uniaxial tensile strength in the hoop direction but decreases tensile strength in the axial direction. Simple validation through 'netting analysis' indicates that the maximum strengths for GRE pipes with winding angles of ±45°, ±55° and ±75° are achieved when loaded at stress ratios of 1:1, 2:1 and 14:1 respectively.

Furthermore, for all winding angles, leakage failures were seen at stress levels much lower than final fracture stresses. For a wound GRE pipe subjected to an internal pressure with a winding angle within a range of 35° to 55°, matrix cracking after initial plastic lengthening was found to dominate and formed throughout the pipe before weepage occurred. After weepage, extensive whitening developed and shortening of the pipe was clearly evident, accompanied by rotation of the fibres [93]. In pure hoop loading, bursting failure was always associated with fibre fracture in the vicinity where fibre bending was pronounced due to bulging and fibre cross-over. For pipes with higher winding angles, transverse matrix cracking is less significant since the stress generated transverse to the fibres is very relatively small.

In 1984, Rosenow [25] used laminate theory to predict the stress strain response of GRE pipes with winding angles varying from 15° to 85°, which he later compared with experimental results. He found that the optimum winding angle very much depends on stress ratio. The results suggest that the pipe should be wound at 54.7° for internal pressure loading, 75° for pure hoop loading and at the lowest possible angle for cases of pure axial loading.

Mistry [111] later continued this work by studying the effect of the same varying winding angles but under combined external pressure and axial compression loads. He showed that failure may result from buckling and material failure, depending on winding angles and stress ratios. Similar failure modes were also observed by Moreno *et al.* [112] but their results suggested no strong influence of winding patterns on the buckling failure of wound GRE pipe.

Previous studies have shown that ±θ° helical wound pipe is strong for an intended stress ratio but prone to transverse matrix crack damage when loaded outside the stress ratio. Recently, Mertiny *et al.* [113] experimentally studied the effect of multiangle filament winding on the strength of filament wound. Their results exhibited good overall performance against initial failure when subjected to various loading conditions, which could provide an advantage in performance over conventional angle ply laminates. The benefits of multiangle wound GRE pipes were also discussed by Lea and Yang [114] with regards to their improved tension and bending characteristics compared to the commonly used ±55° wound pipe. However, predicting the failure strength and modes from available failure criteria is complex and can be very cumbersome.

2.8. Effect of environment on the strength of GRE pipe

One of the major problems in polymer matrix composites concerns durability under natural environmental exposure such as to moisture and temperature. These conditions are generally recognized to cause degradations in strength and mechanical properties. The durability of GRE laminates is strongly influenced by its constituents, and notably

by the matrix properties. This is because it is usually the matrix or the fibre-matrix interface that is most affected by moisture absorption and temperature changes.

A review by Schutte [115] covered the mechanisms that lead to the degradation of properties of the glass fibres, polymer matrix and their interface. The most significant effect of moisture absorption in polymer composites is the plasticization of the matrix. This resulted in a reduction of the glass transition temperature, hence weakening the matrix. The strength of the bonding between the fibre and the matrix has also been revealed to be degraded in the presence of moisture and higher temperature. It has been suggested that the moisture diffuses along the fibres and weakens the bonds at the fibre-matrix interface. The process is very slow and temperature dependent. Without the strong bonds in the fibre-matrix interface, the weakened matrix system then carries all the load, hence precipitating damage in forms of matrix cracks and delamination.

Lundgren and Gudmundson [116] investigated the rate of moisture ingress in cross ply GRE laminates containing transverse matrix cracks. They discovered that the moisture ingress filled up the cracks early in the process and very little difference in moisture absorption was observed between the cracked and uncracked laminates. Kotsikos *et al.* [117] studied the combined effect of an aqueous environment and flexural fatigue on cross ply glass polyester laminates. They observed that the exposed samples exhibited higher crack concentrations of which the damage progressed to the delamination and debonding stages.

Komai [118] reported the influence of water absorption on the mechanical behaviour and fatigue strength of ±45° angle ply carbon reinforced epoxy laminates. They found that water absorption caused damage to the interface bonding, resulting in decreases of tensile and fatigue strengths. The effects of environmental conditions on filament wound GRE pipes were discussed by Perreux and Suri [119]. They stated that the rate of moisture absorption for tubular-shape specimens is much lower compared to coupon specimens, which resulted in longer times being taken for impregnation. They reported that GRE pipes can be very susceptible to damage by stress corrosion cracking due to the combined effects of applied stress and corrosive environments. Furthermore, there is

evidence that cyclic loading causes much more damage than static loading to GRE pipes under moist conditions [120, 121]. The impact of the hygrothermal aging on the fatigue behaviour of glass/epoxy composites has been looked into by Vauthier *et al.* [122]. They reported that immersion in 60°C water caused most damage and led to a drastic decrease in fatigue life.

Ellyin and Rohrbacher [123, 124] studied the effect of moisture and temperature on GRE laminates subjected to monotonic load. They found that the extent of damage strongly depended on immersion temperature. They then broadened their investigation by testing under cyclic loading three types of laminates: cross ply, multiangle and angle ply. They found that fatigue resistance for immersed samples was higher than in those in a dry environment. This is likely to be due to the closure of defects such as cracks and voids from the swelling of the epoxy resin. High temperatures were also shown to have a significant detrimental effect on the behaviour of laminates, yielding reductions in fatigue strength by 35%-65%. Ellyin and Maser [125] studied the same effects on the mechanical properties of GRE pipes and very similar findings were observed. The matrix system in GRE pipe suffered plasticization and a reduction in glass transition temperature, resulting in a decline in pipe stiffness. Further observations implied that the matrix and fibre exhibited more brittle characteristics at higher temperatures.

In 2002, Hale [28] investigated the failure behaviour of GRE pipes subjected to continuous exposure to hot and wet environments at various biaxial loadings. He concluded that the strength of the matrix system was considerably reduced at high temperatures, especially those approaching the resin glass-transition temperature, T_g. The degradation in strength became more critical when hoop to axial stress ratios were further away from 2:1. Chiou and Bradley and Hale *et al.* [126, 127] tried to simulate actual working conditions by studying the effects of sea water on GRE pipes. They concluded that the absorption of seawater caused a significant reduction in the bursting strength of the pipe.

2.9. Effect of filament winding parameters on the strength of GRE pipe

Other factors that could affect the strength and long term performance of GRE pipes are the winding parameters during the manufacture of GRE pipes, such as winding tension, winding time and volume fraction. Mertiny *et al.* [128] investigated the influence of the initial parameters, which are those that can be controlled by operators, on the secondary processing parameters of layer thickness and resulting bandwidth. Lee and Springer [129-131] then developed a model describing the filament wound process which is capable of predicting the physical part properties of the pipe.

Cohen [132] used a design of experiment (DOE) technique to investigate the influence of filament winding parameters on the strength of a composite vessel similar to the GRE pipe used in this work. He identified applied tow tension as the most significant manufacturing parameter. Increasing this parameter resulted in a higher fibre volume fraction, and hence increased strength in the composite structure. He went on to study the effects of fibre volume fraction by establishing its relationship in the hoop layers with the failure strength of filament wound composite vessels. Similar work was also conducted by Mertiny and Ellyin [133] on the impact of filament winding tension on the physical and mechanical properties of reinforced composite tubes. They found that component strength is strongly dependent on the degree of fibre tensioning suggesting that increasing in winding tension improve the component strength in fibre dominated loading whereas reduce in fibre tensioning is preferred for matrix dominated loading. Pre-stressing the fibre has also been found to reduce the thermal residual stress that developed as a result of the cooling process from high curing temperature to working temperature [134].

2.10. Fatigue behaviour of GRE pipes

Many studies have been conducted on the fatigue behaviour of GRE pipes, especially given the need to understand long term performance based on short term testing. Since this investigation involves carrying out a UEWS test which involves of combination of

static and cyclic loading, it is important to understand the fatigue mechanisms of GRE pipes, particularly in comparison with those of metals.

Fatigue is defined as the time dependent failure of a material from repetitive alternating or cyclic stresses of intensity considerably below the static yield strength. In most cases, fatigue mechanisms involve crack initiation followed by progressive propagation of cracks with growth increments taking place during each fatigue cycle before sudden fracture. Hence, the fatigue life of a material is referred to as the total number of stress cycles it can cope with before final fracture. Conventionally, the relationship between fatigue strength and lifetime is presented in the form of S-N curves, where fatigue strength, S, is plotted against the number of cycles to failure, N, both in logarithmic scale. A typical S-N curve is shown in Figure 2.6.

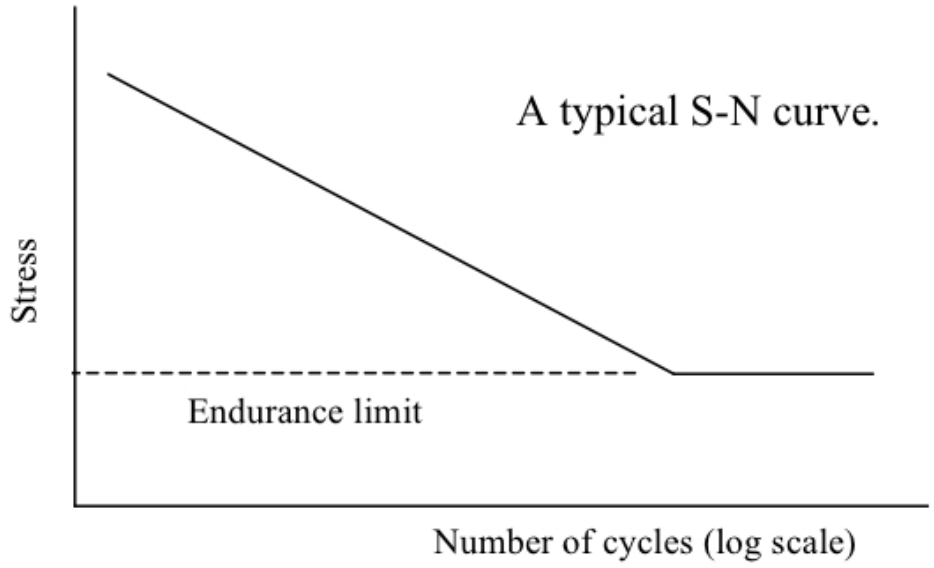

Figure 2.6: Fatigue life (S-N) curve

Both Talreja [135] and Reifsnider [136] conducted comprehensive reviews on the fundamental concepts of fatigue and modelling of fatigue strength. One of the earliest works on the fatigue mechanism was done by Dharan [137], who elucidated the roles of the fibres, the matrix and their interface in causing composite fatigue. He came out with a conceptual framework of explaining fatigue damage known as the fatigue life diagram

as shown in Figure 2.7. Talreja [138] then continued the work and was the first person who interpreted composite fatigue behaviour using the fatigue life diagrams.

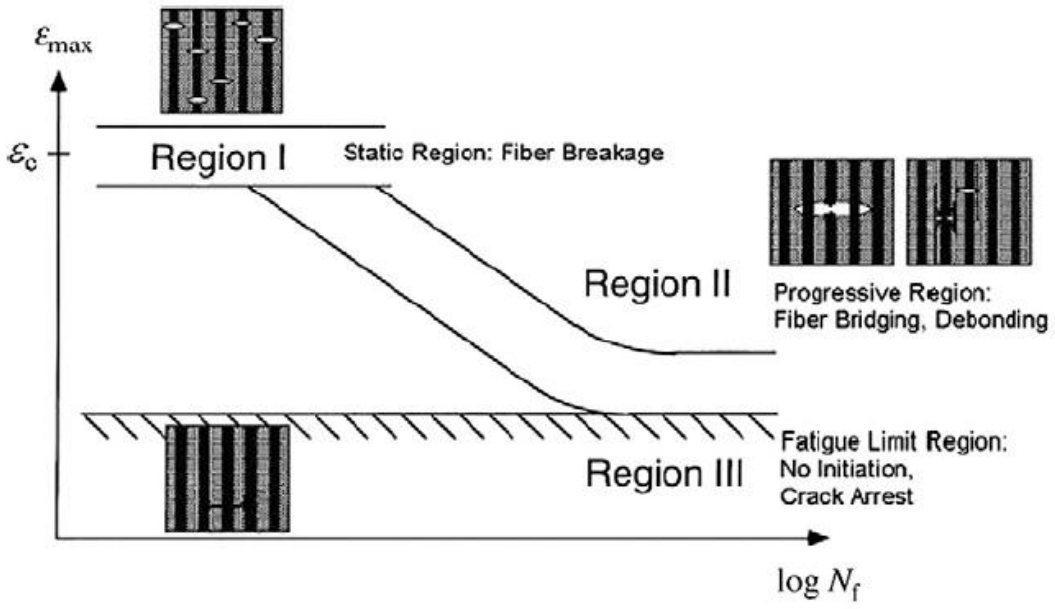

Figure 2.7: Fatigue life diagram for unidirectional composites for axial tension–tension loading.

The fatigue behaviour of composite tubes was studied by Owen *et al.* [139], who conducted a series of fatigue tests of thin walled glass/polyester tubes under a combination of axial loading and internal pressure. Krempl *et al.* [140, 141] compared the effect of uniaxial and biaxial loading on fatigue in composite tubes under completely reversed loading. Bredemo [142] studied the uniaxial fatigue of filament wound GRE pipes, focusing on the initiation and progression of damage mechanisms. He found that damage progressed sequentially from the initiation of matrix cracks to local delamination before failure due to fibre fracture. Matrix cracks were observed to initiate perpendicular to fibre direction within a single ply. Increases in crack density subsequently initiate local delaminations in the fibre-matrix interface where the matrix cracks ended in the ply. These then coalesce with matrix cracks in the next ply and eventually create a pathway for fluids to pass through the pipe wall thickness. Fibre fractures take place once the tensile stress in the fibres exceeds the limiting strength of the glass, whereupon the structure fails completely.

Frost [42, 73] investigated the short and long term performance of GRE pipes under static and cyclic internal pressurization. He concluded that matrix crack propagation in these types of loading, controls failure through a combination of transverse matrix cracking and ply delamination at the fibre-matrix interface. The ply stresses controlling failure were therefore, transverse and shear stress. A second order polynomial criterion based on these two stress components was developed by Frost, which can be expressed as:

$$\left(\frac{\sigma_2}{\sigma_{2\,fail}}\right)^2+\left(\frac{\tau_{12}}{\tau_{12\,fail}}\right)^2-\left(\frac{\sigma_2\tau_{12}}{\sigma_{2\,fail}\tau_{12\,fail}}\right)=\phi \qquad (2.9)$$

where σ_2 and τ_{12} are the transverse and shear ply stresses respectively, and failure will only occur when ϕ is equal to unity. Frost later made a calculated assumption of the crack density in individual plies and correlated this with the equivalent stiffness for the damaged materials by mean of damage mechanics.

Kujawski *et al.* [143, 144] studied the effective stress parameters for long term fatigue strength, particularly under the cyclic fatigue loading of internal pressure. Carroll [40, 75] conducted extensive experiments to investigate the effects of load rate and ratio on the fracture behaviour of ±55° and multiangle filament wound pipes under biaxial loading. It was observed that the failure mode is very much dependent on the stress ratio and the rate of loading. Comprehensive work on filament wound glass/epoxy pipes was also conducted by Perreux and his colleagues, including studying the effect of winding angle [145], biaxial loading [46] and moisture absorption [119] on the fracture behaviour of composite tubes. They then went on to study the fatigue behaviour of GRE pipes under uniaxial cyclic loading, working on the development of a damage model from cumulative damage law and eventually predicting lifetime. They found that fatigue life declines with an increase in stress levels. They then analysed experimentally the impact of load frequency on damage and fatigue lifetime under biaxial loading [45].

Keynak and Mat [146] carried out an investigation to determine the fatigue life of ±55° wound GRE pipes tested at stress levels between 60% and 80% of their ultimate strength, applying three different frequencies for each stress level. Gemi [39, 72] similarly studied the fatigue failure behaviour of ±55° and ±75° filament wound pipe under alternating internal pressure, testing at load levels ranging from 30% to 70% of ultimate strength. Whitening was observed before leakage and final rupture. Both studies concluded that failure is controlled by fibre breakage at high loads while at low loads it is controlled by matrix cracking.

2.11. Cumulative damage rules

As mentioned in earlier section, fatigue damage accumulates in composite laminates with cyclic loading, leading to catastrophic failure once the damage exceeds a critical limit. In order to predict the fatigue life of GRE pipes under this type of loading, a cumulative damage rule is needed. Cumulative damage has been the subject of many recent experimental and analytical investigations [147-151]. Most of the damage models available today are derived from experimental investigations, and may be defined by strength degradation, stiffness degradation or the energy released by the composites.

The first credible form of damage rule was that of Miner's Law. Miner's Law [152] is a damage law generally accepted for predicting the development of cyclic fatigue damage in metals. For fatigue tests, the law states that failure occurs when the following condition is met;

$$\sum \frac{\Delta N_i}{N_{if}} = 1 \tag{2.10}$$

where N_{if} is the number of cycles to failure at stress level σ_i and ΔN_i is the number of cycles applied at each stress level σ_i of the fatigue cycle. The corresponding form under creep conditions is given by;

$$\sum \frac{\Delta t_i}{t_{if}} = 1 \tag{2.11}$$

with t_{if} is the creep rupture lifetime at a stress level σ_i and Δt_i is the time applied at each stress level σ_i. Frost [42] suggested that, for conditions with both cyclic and static elements present, Miner's law can be extended as follows:

$$\sum \frac{\Delta N_i}{N_{if}} + \sum \frac{\Delta t_i}{t_{if}} = 1 \tag{2.12}$$

There are some criticisms of this method since it treats independently the loads applied. However, the method has remained widely used because of its simplicity and ease of use. For example, Owen and Howe [153] found that this law provides reasonable results for FRP laminates subjected to multiaxial load.

Another general approach of describing damage is to understand that cracks under fatigue loading grow according to a power law form, with rate of growth expressed as the stress level to some exponent. This is widely known as Paris's law [154];

$$\frac{da}{dN} = A(K)^m \tag{2.13}$$

where *a* is the crack length, *N* is the number of cycles, *A* is the proportionality constant and *m* is the experimentally determined constant. The power law approach is used to predict the number of load cycles before crack growth becomes unstable. Once it reaches a certain critical limit, service life is considered to be completed. This subject has been discussed in great detail by Suresh [155]. Recently, Christensen [156] formulated a new cumulative damage model which was derived from the basic relationship of crack growth rate as a power law function of a stress intensity factor, similar to that of Paris's law. Further details of these two approaches are given in Chapter 4 as they are used later to model the stress-strain response in the UEWS test conducted in this study.

Other previous studies modelling the deterioration of properties under cyclic loading includes that of Talreja [135]. This model was based on internal variables to predict damage accumulation under fatigue loading. Broutman and Sahu [157] first predicted the lifetime under variable amplitude loading describing two constant amplitudes of loading of glass/epoxy laminates. In their approach, failure was considered to occur when the residual strength decreases to the value of the maximum stress amplitude at the last cycle before failure. Yao and Himmel [150] later presented an extended version of the cumulative damage model for predicting the lifetime of GRP laminates subject to variable amplitudes of fatigue loading. They assumed that deterioration in the strength of GRP is directly proportional to the cumulative fatigue damage caused by cyclic loading.

Fawaz and Ellyin [158] presented a multiaxial model to predict the lifetime of fibre-reinforced composite. The model was based on the modification of a reference fatigue curve to take account of loading ratios and conditions. They claimed that the proposed model significantly reduced the number of calibration parameters which needed to be determined experimentally. Inoue *et al.* [159] utilized stiffness degradation to develop a model predicting the lifetime of glass fabric composites, in which declining modulus ratios in tension and shear were used as damage indicators. An interesting ply-by-ply stiffness reduction approach explaining damage growth under multiaxial fatigue loading was also presented by Adden and Horst [160]. Recently, a thorough analysis of fatigue in composite laminates under multiaxial loading was conducted by Quaresimin and colleagues [161]. They found that the leading factor influencing fatigue strength is the ratio of the shear stress amplitude to the largest normal stress amplitude, which is also referred to as the ply-level biaxiality ratio.

Hashin [162] formulated a cumulative damage theory which can be used with residual life theory as well as residual strength theory. Subramanian *et al.* [148] presented a micromechanics model using the effect of the fibre-matrix interface in a cumulative damage scheme to predict the tensile fatigue behaviour of composite laminates. Reifsneider and Stinchcomb [163] later studied the proposal to use change in stiffness

as the fatigue damage parameter. They claimed that the results showed it to be quantitatively related to the fatigue life and residual strength of the laminates.

2.12. Acoustic emissions (AE)

During the biaxial loading of GRE pipes, Hull [24] reported that minutes before weepage was observed, the formation of white streaks was always accompanied by a creaking noise. This creaking sound is an acoustic emission (AE) indicating the cracking process involved.

Composite materials, as do many other materials, emit acoustic signals under load if elastic stresses are reduced by plastic deformation or the initiation of cracks. These emissions correspond to the strain energy due to micro structural changes. Once these emissions reach a threshold level, they can be detected and converted into a voltage signal by a piezoelectric transducer. The signals can then be amplified and measured to produce data such as frequency, energy release and duration of the signals. Each signal emitted is recorded in real time and associated with a specific event over time. The acoustic emission and detection process is illustrated in Figure 2.8. A typical AE signal or event is shown in Figure 2.9. Each event can be described by several parameters such as amplitude, counts, energy counts, duration and rise time.

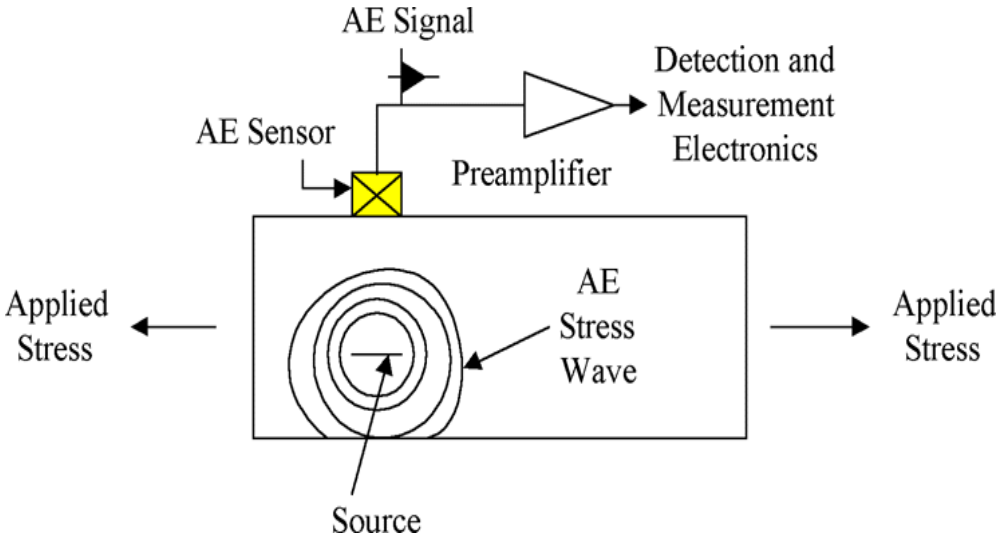

Figure 2.8: Basic principal of acoustic emission

Comprehensive reviews of acoustic emissions as a tool for detecting damage in composite materials were conducted by Reynolds [164] and Scott and Scala [165]. Of late, there has been increasing interest in the prospect of using AE monitoring to detect the fatigue performance of GRE pipes. This is due to the presence of multiple failure mechanisms of matrix cracking, delamination and fibre breakage all of which generate specific distinguishable frequencies. Hence, the technique is not only of potential use in determining the point of failure, but also in determining its nature.

Barre and Benzeggagh [166] tested glass fibre reinforced polyester and concluded that AE amplitudes vary with different failure modes. They found that AE amplitudes in the range of 40-55dB correspond to the matrix cracking, 60-65dB to debonding, 65-85dB to fibre pull out and 85-100dB to fibre fracture. Barnes and Ramirez [167] conducted a study of static and fatigue loading on carbon fibre reinforced pipes and used correlation plots of event duration and amplitude to characterize the damage mechanisms. They reported that low amplitude events are normally characteristic of matrix cracking, high duration low/intermediate amplitude events with debonding and delamination, while high amplitude with short duration is typically attributed to fibre breakage.

Kaiser reported in 1950 [168] that the application of the first load in cyclic loading produced more emissions than subsequent loadings, until the previous maximum load applied is exceeded. This later became known as Kaiser Effect. However, it is expected that in composite materials at higher stress levels, more emissions will be observed at loads lower than the previous maximum load which is thought to correspond to the onset of a defect. This behaviour is known as the felicity effect and its derivative, the felicity ratio can be described as [169]:

$$\text{Felicity Ratio (FR)} = \frac{\text{load at which significant AE observed on reloading}}{\text{previous maximum load}}$$

Given the definition above, Kaiser's effect can be interpreted as FR of 1.0 or greater. Monitoring of the FR can be used to describe damage progression in composite pipes where decreases in FR values suggest the pipe is approaching final failure. This AE

information can then be correlated with the internal pressure that caused the onset of damage in the pipe.

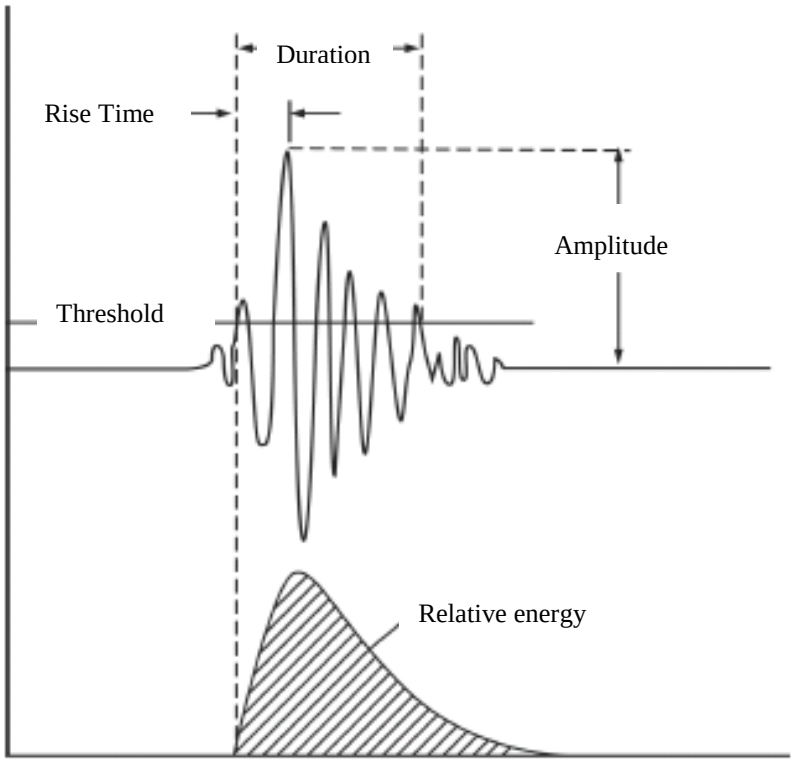

Figure 2.9: Common parameters from acoustic signals [170]

Prevorovsky *et al.* [171] recorded acoustic signals from multiaxial tests on GRE pipes combining internal pressure and axial tensile loading. Highest AE activity was recorded during tension cycles while pressure testing. They went on to identify matrix micro-cracking and delamination as the main damage mechanisms in the test. Later work by Ramirez *et al.* [172] investigated the endurance limits to weepage for GRE pipe under internal pressure using acoustic emission techniques and static pressure tests. Their results suggest that AE monitoring can be used to predict the long term cyclic loading performance of GRE products from a single short term test. If this were proven, it would potentially reduce the amount of fatigue testing required to qualify products. In addition, AE can also be used for a rapid evaluation of the factors that affect fatigue performance, such as changes in raw materials, fabrication processes or fitting design.

2.13. Qualification and testing procedure

Investigations into the performance of GRE pipes have been carried out for many years now, a majority of which emphasise long term design limits, failure modes and associated deformations [19, 24, 26, 38]. The situation is complicated, however by the fact that GRE pipes are not only anisotropic materials, but on the micro scale are also non-homogeneous. As a result, variety failure mechanisms which limit their use can be observed such as matrix micro-cracking, fibre-matrix debonding, delamination and fibre fracture [21, 75]. Therefore, it is very important initially to determine the design parameters of each variant, but also in the context of service life to be able to predict the long term performance of GRP/GRE systems with respect to pressure, temperature, chemical resistance, fire performance and impact load.

2.13.1 International standard ISO 14692

In December 2002, a new ISO 14692 standard was issued, dealing with the qualification, system design and installation of GRE piping systems as well as quality assurance issues [173]. The scope of this document refers to offshore applications, but the standard can also be used as a guide for onshore applications. It specifies how to qualify and manufacture GRP/GRE pipes and fittings, how to conduct system design, and finally it gives guidelines for fabrication, installation and operation. It comprises of four parts;

Part 1: Vocabulary, symbols, applications and materials.

Part 2: Qualification and manufacture.

Part 3: System design.

Part 4: Fabrication, installation and operation.

The advantages of ISO 14692 are that it provides standardizing principles, working methods and clear guidance for everybody involved in the industry to have the same understanding. The main draw for this document is the connection between the properties of specific GRP products and safety in installed pipe systems. Qualification

necessitates a test programme that involves full-scale hydrostatic performance tests, establishing a long-term design basis not only for pipes but also for the entire system including joints and fittings. This section however, focuses on part two of the standard which details the procedures for the qualification and manufacture of GRE products.

2.13.2 Biaxial testing according to ASTM D2992

As mentioned before, part two of ISO 14692 is the standard governing the qualification of fibreglass pipe. According to this part, the procedure by which the fibreglass products are certified is delineated in the ASTM D2992 document, which describes the method used to establish the strength-regression data in obtaining the hydrostatic design basis (HDB) or pressure design basis (PDB) for fibreglass pipes [174]. It outlines the procedures in detail for both cyclic loading pressure and long term constant pressure loading in ASTM D2992a and ASTM D2992b respectively [175]. It is also important to mention that the discussion set forth in ISO 14692 relates solely to GRE pipes that fail by a weepage mechanism.

In the qualification process, the specimen is loaded in the 'closed end' condition where the hoop stress developed is twice the axial stress. With fibreglass pipe, it is usually found that both cyclic and static behaviour exhibit a linear relationship between the logarithm of applied pressure and the logarithm of the lifetime (in cycles or time), as shown in Figures 2.10 and 2.11. For both constant pressure and cyclic loading, a minimum of 18 data points are required in order to establish acceptable regression, with at least one sample providing a point in excess of 10,000 hours and 15,000,000 cycles of internal pressure at 25cycles/minutes respectively. In order to allow for some product variability and inconsistency in manufacturing, which are often likely to happen, it is necessary to compute the lower confidence limit (LCL) of the results. LCL denotes the line above which 97.5% of the newly determined regression data are predicted to lie.

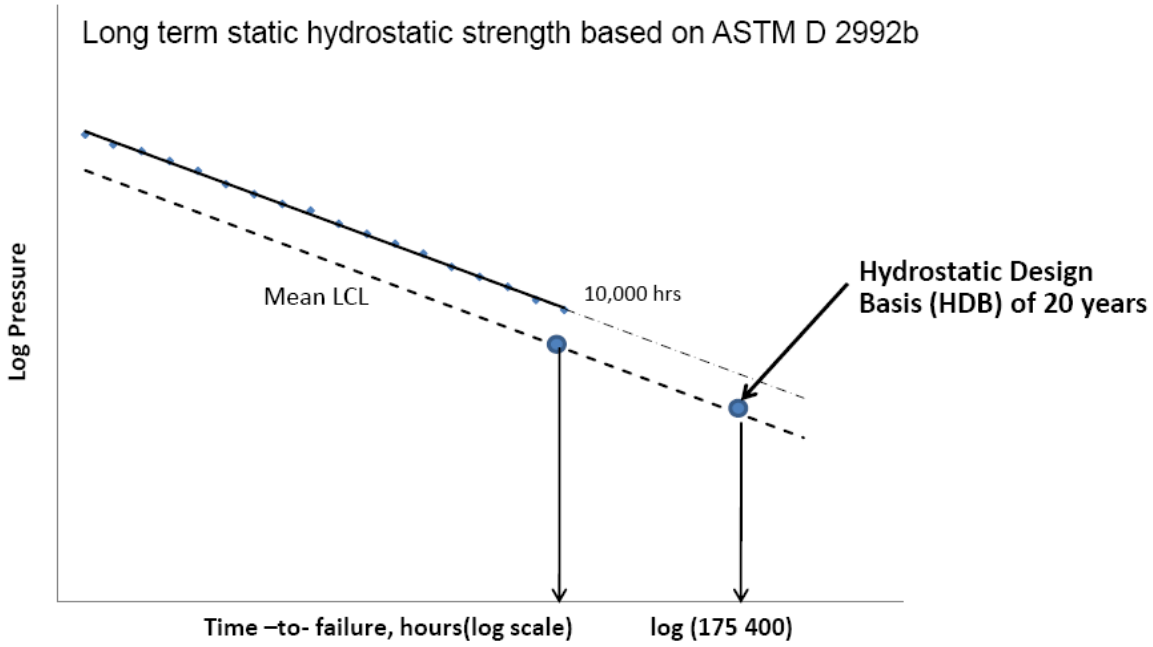

Figure 2.10: Long term static hydrostatic strength based on ASTM D 2992b showing the pressure at design lifetime of 20 years and the pressure at 1000 hours for reconfirmation test [174]

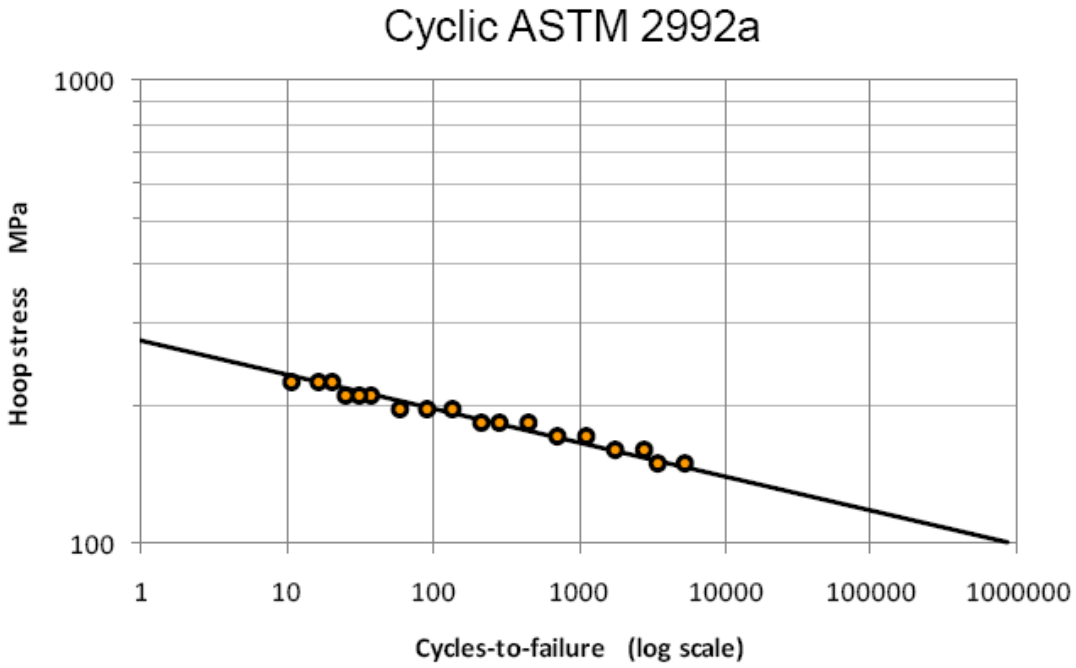

Figure 2.11: Long term cyclic hydrostatic strength based on ASTM D2992a

The pressure rating for the pipe, known as the hydrostatic design basis (HDB), is then determined by extrapolating the LCL line to the design life which is typically 20-50 years for offshore piping products. The HDB, combined with a number of other factors, is used to determine the qualification pressure in the pipe. The manufacturer can carry out qualification testing provided it is witnessed and certified by a recognized independent authority. Alternatively, testing and certification may also be carried out by a third party testing organization.

The regression data obtained from this procedure gives significant information that qualifies the product for manufacturing and defines the pressure rating to be used in the pipe's system design. It is also important when reconfirmation of the HDB is required, performed if there are changes to materials, manufacturing processes, construction or fitting design that might affect the overall performance of the pipe. It would be expensive and time consuming to subject the pipes to a full qualification programme every time small changes were made. According to the procedure, GRE pipe is subjected to 1000 hours of hydrostatic pressure based on the 1,000 hour lower confidence limit (LCL) of the regression line initially acquired from ASTM D2992. Survival of this test strongly implies that the pipe has the same or a better design life than the originally qualified pipe.

Pipe manufacturers have to comply with ISO 14692, to ensure that products delivered are safe and will perform well within the requirements of end users and with manageable reliability. However, while the present method of determining lifetime predictions for GRE pipes is acceptable, many manufacturers feel that the current procedure is too time-consuming and expensive. For every product to be qualified, manufacturers have to undergo a tedious qualification programme as detailed in ASTM D2992, which often exceeds two years. This is rather a long time considering the timeframe within which the products normally have to be delivered. This is because at least one set of the test data must be obtained at a time in excess of 10,000 hours for static fatigue and 15,000,000 cycles for cyclic fatigue. Hence, a single product qualification programme will take over a year to complete with no room for error or premature failure. Such failure would require the product to be retested and yet more

valuable time would be wasted. Difficulties also arise when the tested pipes do not fail within the test period. Current practice treats unfailed specimens as failure points, but this procedure may not be ideal since it gives a rather conservative estimate of the long term behaviour of the pipe. Such uncertainty is not acceptable in such an expensive qualification programme. So although many accept that the procedure delineated by ASTM D2992 does provide some basic indication of the long term durability of fibreglass pipes, it may not be the most appropriate method of achieving this objective.

Figure 2.12: Example of test spool for 1000 hrs HDB reconfirmation testing [176]

Another issue with regard to constant pressure testing arises when the slope obtained from the regression analysis is somewhat shallow. Here, small statistical variations in the product could result in large variations in the time to failure, and hence it will be very difficult to distinguish under what particular pressures the pipes will fail during the testing programme [177]. This is extremely troublesome when establishing long term test data. For instance, a shallower regression line would mean that the product could be subjected to lower 1000-hour test pressures. This allows manufacturers to reduce the overall thickness of the pipes purportedly without compromising on the pipe's rating. On the other hand, subjecting the pipes to a lower 1000-hour test pressure can result in reliability issues which if not known or handled properly and later installed to the piping network can lead to damage of property or even worse, loss of life.

A steeper regression line, on the other hand, provides a better precautionary measure since the products are subjected to higher pressure at the 1000 hour test, and thus the pipe is designed with thicker walls. However, if the regression line is steeper than it should have been, this could result in the pipe to being overly safely designed for a particular application. The pipes are then produced with unnecessarily thick walls which increases the manufacturing costs.

There are also great concerns that each analysis from the regression-based method results in slightly different data even when the test is run on virtually identical products. This means that the HDB reconfirmation test, which is directly related to the regression gradient, will only be applicable to one regression test. The regression gradient is also highly dependent on the resin system used, glass sizing, production technique, process control and test temperature, which vary for different manufacturers and are very difficult to compare. Furthermore, inconsistent failure mechanisms can also significantly influence the gradient of the regression line.

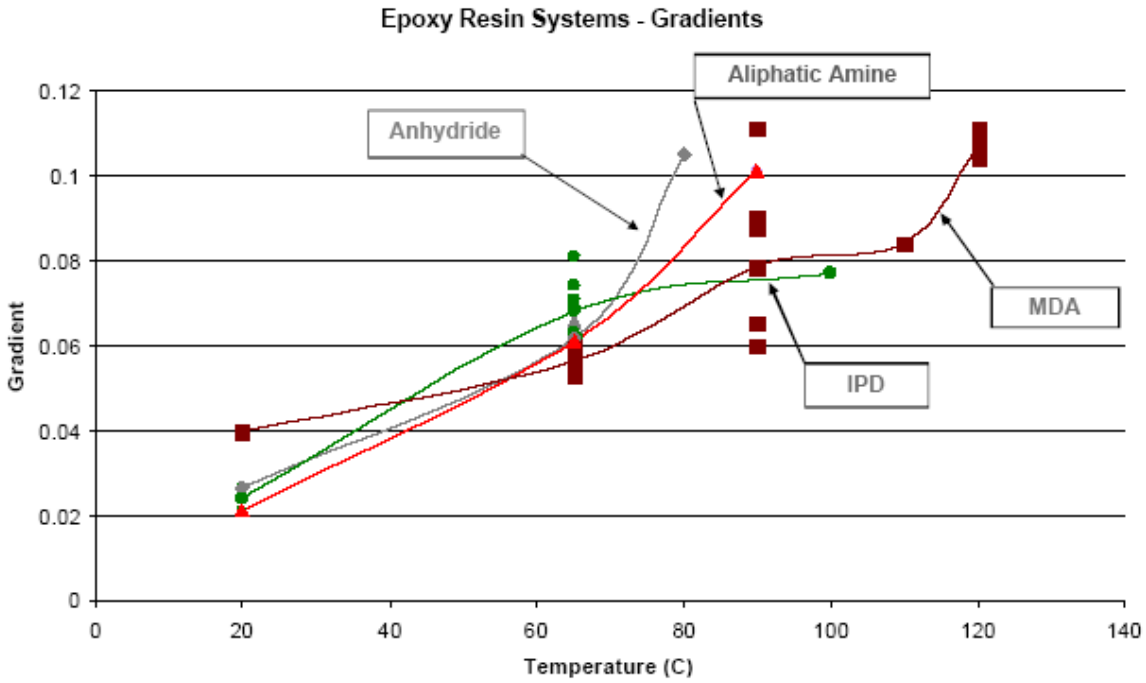

Figure 2.13: Examples of variation in regression line gradients of identical test samples from different manufacturers [178].

Variations in the gradients of regression lines presented by manufacturers are also more problematic when they try to define their regression line to be as shallow as possible. This enables them to conduct reconfirmation tests at lower pressures hence improve their market position by reducing materials costs [178]. Due to competitiveness in the market and the freedom the manufacturers have to interpret the regression line gradients for their products, could lead to manipulations of test data to secure millions of dollars worth of contracts by offering products claimed to have a long design lifetime. Given all the limitations of the existing test procedure including the (time wise) impossibility to execute this test as part of a commercial project for fibreglass piping, there is now an impetus to recognise the need for a better, faster and cheaper test procedure in qualifying GRE pipes.

2.13.3 Determination of ultimate elastic wall stress (UEWS) test

While the current procedure for qualifying GRE pipes based on regression analysis provides very good predictions of the long term behaviour of the pipe, manufacturers are driven by the need for a faster and simpler qualification process. A number of possible short term tests have been examined such as the interlaminar shear stress (ILSS), flexural and UEWS tests. The UEWS test is not yet standardized, but appears to offer an attractive alternative to existing procedures. Its principles were first investigated by Shell Research in 1968 [179]. There are very limited studies that have been reported on this procedure. Hull [24] and Frost [42] have both reported on the UEWS test and observed that matrix cracking is consistently associated with non-linearity in stress strain responses. The marked advantages of the UEWS method compared to those outlined in ASTM D2992 are that the process involved is relatively cheap and it can be repeated as many times as required since one full test can easily be completed within one day.

The intention of the UEWS test is to identify, by examining the stress-strain response, a stress level below which damage growth is either negligible or at least sufficiently low to prevent long term failure at the design life. GRE pipe fails when debonding occurs between the fibres and matrix interface. Once debonding takes place, there will be less

surface area for proper stress distribution. This leads to the development of stress concentrations within the GRE system which, in turn, causes further debonding. The point at which the fibre-matrix interface starts to debond is used as an indication of the borderline between permissible and non-permissible deformation. This point is called the Ultimate Elastic Wall Stress (UEWS).

The UEWS test involves the application of groups of 10 one-minute hydrostatic pressure cycles at increasing pressure levels. The strain at the end of the first and the last cycle of each ten cycle group is measured, and these values are plotted against pressure (or hoop stress). If zero or negligible damage occurs at a particular pressure level, then a linear relationship is observed between strain and hoop stress, and the strain after the tenth cycle in the group is the same as at the first cycle. This can be clearly seen in the early cycle groups. As the UEWS is approached, a deviation in strain can be seen between the first and the last cycle, and the relationship begins to become non-linear. This non-linearity in the stress–strain relationship will then be used to indicate the UEWS point which corresponds to first ply failure in the pipe. Further details on the UEWS test procedure and the calculations involved are given in Chapter 3.

2.13.4 Comparison between ASTM D2992 procedure and UEWS test

Table 2.1 summarizes the differences between the regression-based ISO 14692 and the UEWS procedure. The main advantage claimed for the ASTM procedure based on cyclic and static fatigue is that it provides a realistic statistical approach to establishing a long-term pressure rating when there is a slow deterioration in properties. This makes it attractive in connection with statistically-based design. However there are significant practical issues involved in running experiments over a long period, and the ageing processes operating in the test procedure may differ from those that apply in the field.

The most significant drawback of the long-term tests is the time needed to achieve the full qualification of new products. The ASTM 2992b procedure requires static fatigue data at times in excess of 10,000 hours (~14 months). For new piping products, where

the regression line slope is not identifiable in advance, this requires significant trial and error to determine the pressures to be used, which often results in a qualification period that exceeds two years. Although it is generally agreed that proof of long term durability is desirable, long term static fatigue measurements may not be the best method of achieving this.

Table 2.1: Comparison of regression-based and UEWS test procedures.

	Regression-based procedures	**UEWS tests**
Time, expense and convenience.	Expensive procedure requiring ~2 years to achieve qualification.	Simple procedure, which can be carried out in less than one day.
Ability to define a long-term pressure rating.	Provides the basis for a 20 year design rating.	Identifies a stress level below which the rate of damage progression is very low. This stress corresponds approximately to that determined by long term regression.
Ability to quantify changes due to process and materials.	HDB reconfirmation procedure is adequately sensitive to these effects, but takes a minimum of 1,000 hours to perform and only provides a yes/no answer.	Very sensitive to these effects.
Ability to quantify effects of chemical environment.	Limited.	Limited.
Ability to quantify aging effect	Yes	No, only when pipes are aged e.g. by exposing the pipes for a long term to water.

CHAPTER 3: EXPERIMENTAL PROCEDURE

3.1. Introduction

This chapter describes all the experimental work conducted in this research investigation, particularly in the multiaxial UEWS tests. Prior to that, the test specimen used and the development of the dedicated test rig for conducting UEWS tests are described in detail. The test rig was developed so that it is capable of performing the UEWS test under various combinations of internal pressure and axial load without having to apply an external load. By varying these loading conditions, ratios ranging from pure axial to pure hoop loading can be obtained, thus enabling the construction of a full tensile-tensile biaxial UEWS based failure envelope. The procedures for the determination of the stiffness properties of the test specimen from virgin to failed samples and the microscopy analysis of post UEWS test samples are also explained.

3.2. Pipe specimen

GRE pipes for the UEWS tests conducted in the experiments were provided by Future Pipe Industries (FPI) from their standard range of Wavistrong wound pipes. The pipes were manufactured from glass fibre impregnated with aromatic amine (MDA) cured epoxy resin [180]. Thermosetting epoxy resin is the most widely used resin employed in the construction of GRE pipes due to its superior corrosion resistance and excellent mechanical, physical and thermal properties [16, 23, 181]. The pipes were designed so as to resist the corrosive effects of mixtures of low concentrations of acids, under both internal and external loads at temperatures up to 110°C.

Table 3.1 shows the physical and mechanical properties of the tubes. The pipes were manufactured by a conventional automated winding machine with a winding angle of ±55° for optimum working conditions under internal pressurization. The wall of the pipes is protected on the outer side by the resin topcoat.

Table 3.1: Mechanical and physical properties of the GRE pipes provided for this investigation by Future Pipe Industries [180].

Internal diameter	200 mm
Average wall thickness	6 mm
Length	2000 mm
Liner	n/a
Density	2000 kg/m^3
Number of plies	10
Glass volume fraction	59 %
Axial tensile modulus	11.5 GPa
Hoop tensile modulus	19.0 GPa
Shear modulus	11.0 GPa
Major Poisson's ratio,	0.65
Coefficient of linear thermal expansion	2x10^{-5} mm/mm°C
Thermal conductivity	0.29 W/m.K
Specific heat	921 J/kg.K

Figure 3.1 shows the dimensions of the specimen agreed with FuturePipe Industries (FPI) for this investigation for tests at (a) room temperature (RT) and 65°C, and (b) an elevated temperature of 95°C. The parallel length of the pipe used in the test, not including the fitting region, was about 1,600 mm. The pipes were designed with built-up, tapered end reinforcement in design (a) and were slight tapered with a straight cut built up in design (b).

The main purpose of having tapered reinforcement at the end of the specimen is to reduce the stress concentration effects that might develop when it is subjected to additional axial tensile or compressive loading. In the first design illustrated in Figure 3.1 (a), the reinforced ends were prepared by machining a 2.5° external taper. Steel end fittings then bonded onto the pipe's tapered ends using a FPI EasyFit two-component epoxy adhesive. Bonding length required for the specimen was calculated from the following relationship:

$$\text{Shear stress, } \tau = \frac{P \times ID}{4 \times \text{Bonding length}}$$

where *P* is the maximum working pressure applied and *ID* is the internal diameter of the pipe. By using an allowable shear strength estimation of 10MPa and maximum working pressure of 180bar, the minimum bonding length required was calculated to be about 90mm. To ensure failure would occur in the pipe rather than bonding failure between the pipe and the end cap fittings, a safety factor of 1.5 was applied, and hence the bonding length for the fitting was chosen to be 140mm.

At first, the pipe was designed with the intention of using it with adhesive bonded end fittings throughout the investigation. The design was a success for the UEWS tests at room temperature and an elevated temperature of 65°C. However, the adhesive bonding joint failed at the higher test temperature of 95°C. Hence, the pipe specimens were then redesigned to accommodate new mechanical end fitting to be used at 95°C, as illustrated in Figure 3.1 (b).

3.3. End fitting design

For these UEWS tests, which involved the static and cyclic pressurization of the GRE pipe, it was imperative to design an end-fitting suitable for the task. With such a 'closed end' test setup, the axial load caused by the internal pressure is transferred to the pipe wall through the end fitting. Hence, a strong joint between the pipe end and the fittings is essential. As mentioned in the previous section, two end fittings were designed for the test setup. The design of both, adhesive bonded and mechanical end fittings are shown in Figures 3.2 and 3.3 respectively.

Initially, the adhesive bonded end fitting was intended to cater for all the UEWS tests required in this study. Simple tapered mild steel was designed to be bonded at each end of the pipe specimen with a Wavistrong Easy-Fit epoxy-based adhesive supplied by FPI. To increase the strength of the joint, the fittings were also designed to have a 2mm separated groove carved on the inside surface of the fittings, hence providing not just adhesive joint strength but also the additional 'mechanical' grip between the joint and the fitting. The adhesive joint was then cured at 125°C for two hours using a heater band.

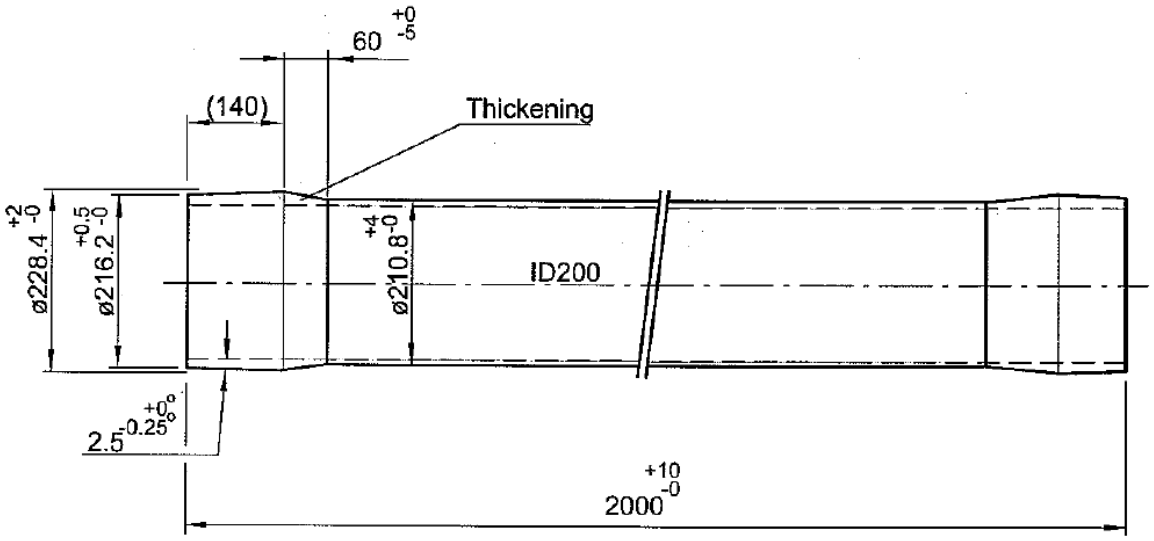

(a)

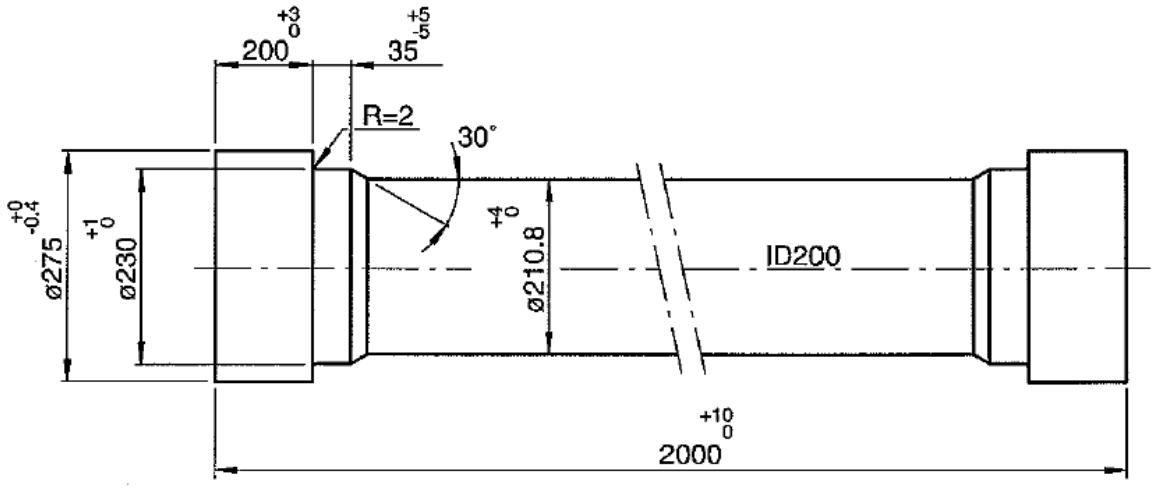

(b)

Figure 3.1: Dimensions of the specimens: (a) for tests at RT and 65°C and (b) for tests at 95°C

However, since the adhesive bonded fitting failed during the 95°C tests, a new mechanical end fitting was designed to enable tests at that temperature. It consists of a steel flange sealed with an o-ring from the inside of the pipe, connected together to a steel collar by twelve high tensile steel bolts. Wedge/taper serrated grips were then placed in between the flange and the collar, sitting on the pipe reinforcement.

During the installation, the flange and the collar were tightened, clamping both onto the serrated grip wedges. This forces the 'wedging action' and the wedges grip onto the pipe reinforcement in proportion to the loads applied during tightening, locking all the parts together to the pipe. During the test, axial load is applied to the end fittings, hence on the serrated grip wedges. As the pressure rises, higher axial force is then transferred to the wedges causing them to tighten further onto the pipe and subsequently create a stronger seal. This set up is proven to be much more convenient, as it is easy to assemble and less time consuming as no curing is required. Any problems encountered, such as leakage from the end fittings during the test, can be easily rectified by merely dismantling the parts for investigation, which is impossible to do with the former adhesive joint end fitting.

3.4. Development of the test rig

Currently, the standard UEWS tests conducted by FPI involve applying internal pressure alone, giving a 2:1 hoop to axial stress ratio which is the optimum design condition for the ±55° filament wound GRE pipe used in this work. However, one of the main objectives of the present study is to conduct UEWS tests at various ratios of hoop to axial stress ranging from pure axial loading to pure hoop loading. Hence, a special test rig was developed capable of applying static and cyclic pressure tests to the Wavistrong piping system to conduct the UEWS tests. In principle, the biaxial strength of composite pipes can be achieved by pressurizing the specimens to failure under a combination of tensile axial force and internal pressure. The test rig basically consisted of three main parts: the pressure system, the control and instrumentation system, and the thermal enclosure.

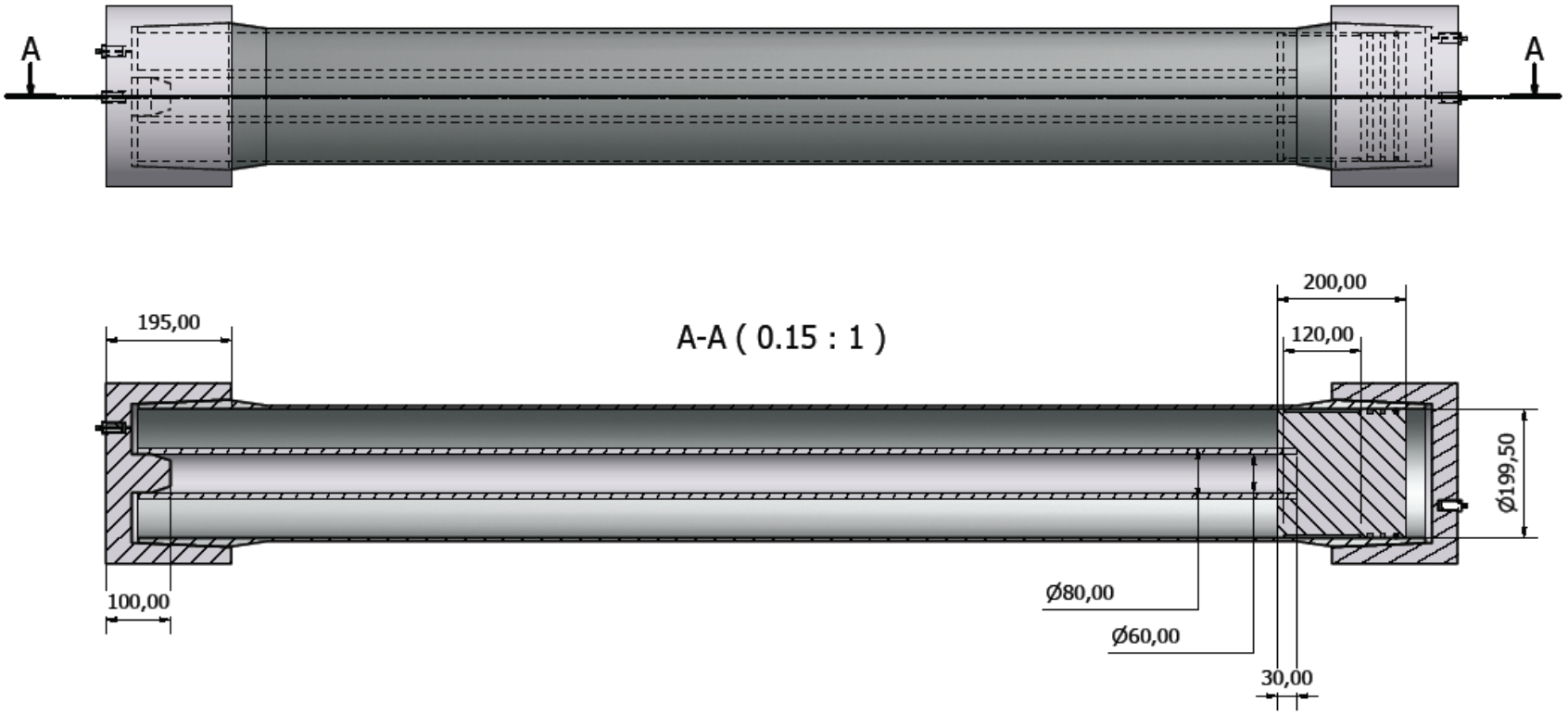

Figure 3.2: Design of the adhesive bonded end fitting used for UEWS tests at RT and 65°C.

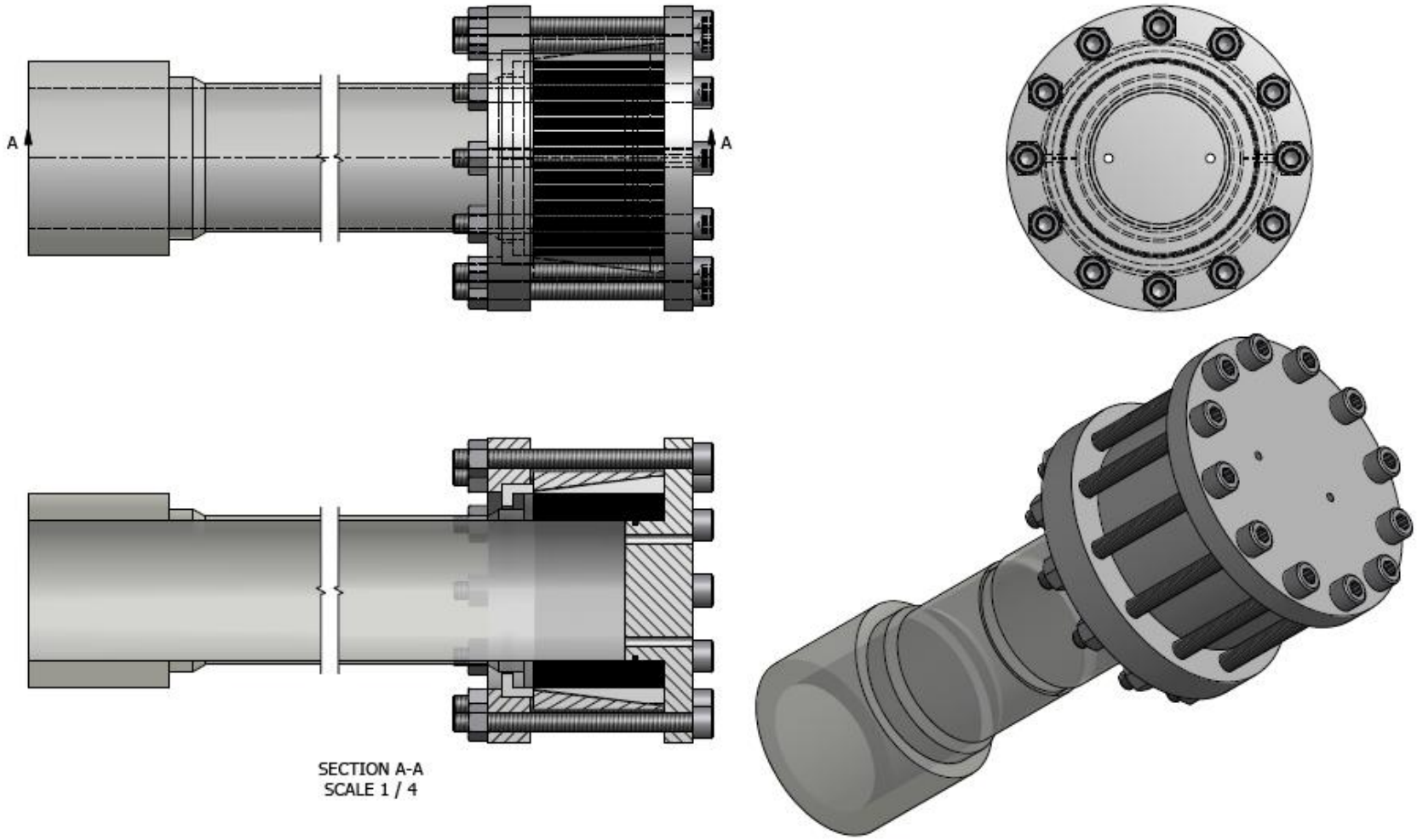

Figure 3.3: Design of the mechanical end fitting used for UEWS tests at 95°C

3.4.1 Pressurization system

The pressure system was designed so that it could facilitate multiple loading conditions in order to produce various hoop-to-axial stress ratios and at the same time withstand a maximum working pressure up to 250-300 bars. A schematic drawing for the hydraulic test rig with a 200mm diameter and 2-meter length test spool is illustrated in Figure 3.4. The test spool was designed with a piston-like configuration installed inside the pipe, creating two separate chambers (Figure 3.2). The two chambers were sealed with the use of an 'o-ring' to prevent the leakage of pressure between chambers during pressurizing. The end fittings were fixed at each end of the test specimen with an adhesive joint for tests at room temperature and at 65°C or with mechanical end fittings via serrated grips for tests at 95°C.

The two chambers were then separately pressurized to create various hoop-to-axial loading conditions. This was achieved by using a differential pump driven by an air compressor via a ball valve. This pump is manufactured by SC Hydraulic Engineering Corp. and operating on the principle of differential working areas can produce up to 350 bars pressure from 6-7 bars supply of compressed air. The pump flow rate is managed by using a pressure regulator installed in the compressed air inlet to the pump. The pressure loading was controlled manually by the opening and closing of the unloading valve. During pressurizing, the valve was kept closed. Once the pressure required was reached and held for the required amount of time, the water in the pipe was released back into the tank by opening the unloading valve. It was noted that a drop in pressure in the pipe occurred almost immediately when the valve was opened.

The ratio of the pressures in the two chambers was controlled by a pressure intensifier to produce additional axial loads within the pipe. This method was chosen rather than using two independent pump sources due to its ease of handling and fabrication. The pressure intensifier consisted of cylinders of different bore diameters with a simple stepped piston. A diagram of the design construction of the intensifier is shown in Figure 3.5. From the basic concept of Pascal's law, the pressurized fluid from the main chamber acted on the larger piston area, enabling the smaller piston to intensify the

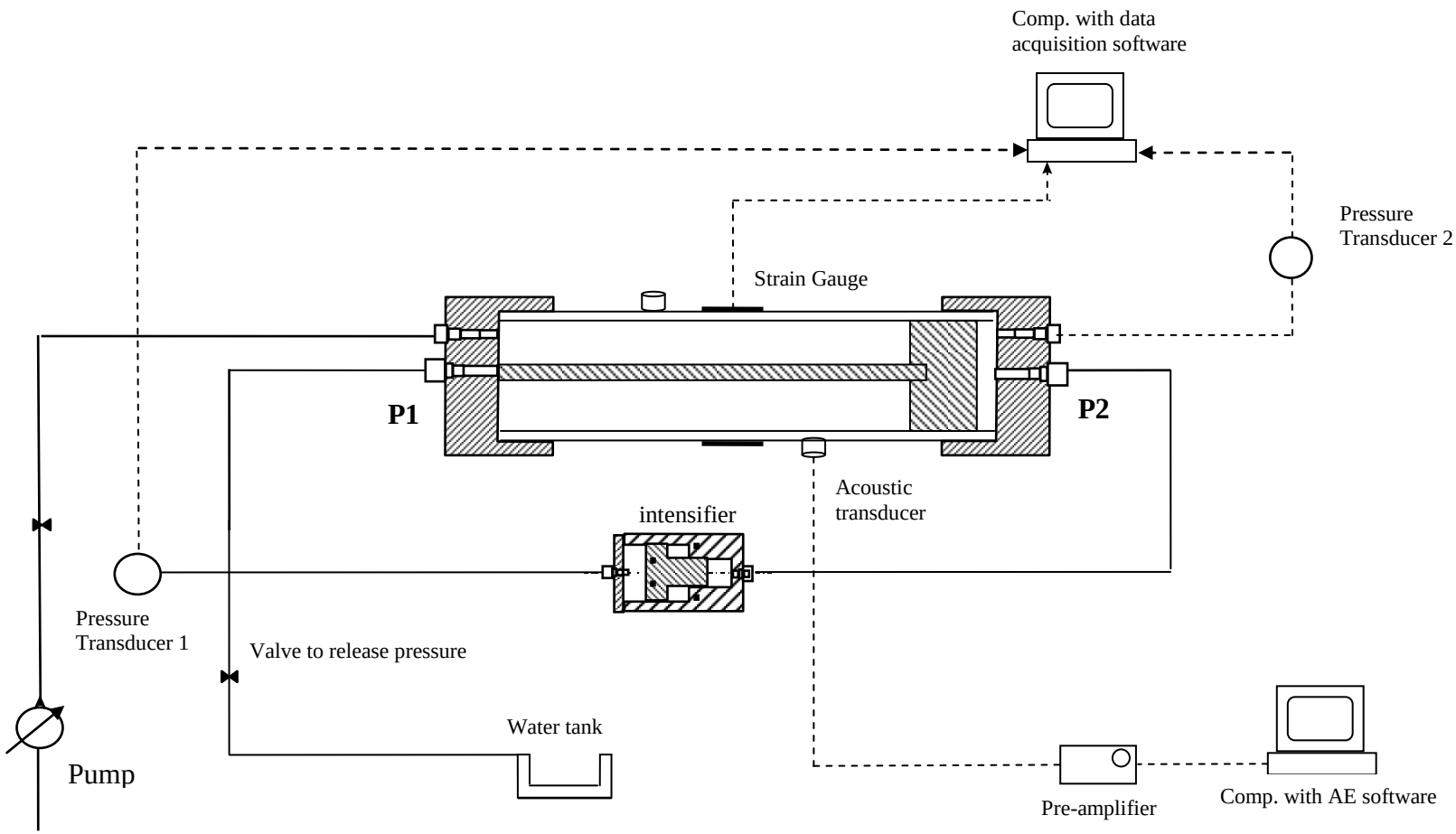

Figure 3.4: Schematic drawing of test rig for conducting UEWS test at various loading conditions with acoustic setup.

pressure in the fluids in its bore. The pressure ratio is proportional to the ratio of the area of the stepped piston or to the ratio of the square of piston diameter as given below;

$$\frac{P_1}{P_2} = \frac{A_1}{A_2} \quad \text{or} \quad \frac{P_1}{P_2} = \frac{{d_1}^2}{{d_2}^2} \tag{3.1}$$

where:

P_1 and P_2 are the low and high pressure in the high and low chambers respectively,

$A_1$and A_2 are the areas of the low and high pressure pistons respectively, and

d_1 and d_2 are the diameters of the low and high pressure pistons respectively.

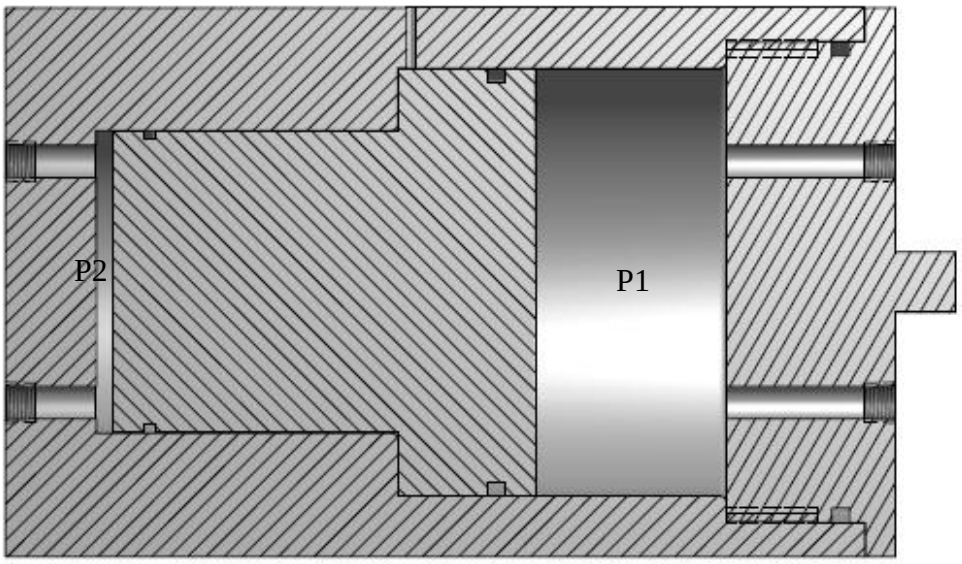

Figure 3.5: Cross-section drawing of the pressure intensifier/reducer used to obtain the intermediate loading conditions for 1:1 and 4:1 hoop to axial stress.

For instance, the 1:1 hoop to axial loading condition was achieved by installing a stepped piston with a 2:1 ratio of the larger to the smaller piston area. The pressure applied to the pipe acted on the intensifier and hence doubled the pressure applied in the small chamber. Since the piston inside the pipe was free to move and was sealed with a high pressure rubber o-ring, the higher pressure inside the small chamber pushed the

piston inside and at the same time exerted additional tensile axial stress to the pipe wall to create the 1:1 hoop to axial stress ratio. Likewise, the 4:1 hoop to axial stress ratio was achieved by inverting the direction of the stepped piston from the intensifier, hence reducing the stress inside the small chamber by half. The pure axial test could be performed by pressurizing only the small chamber, and pure hoop loading was achieved by applying pressure only to the main chamber (the main body of the pipe).

In order to estimate the working pressure to be employed in both chambers inside the test spool for the UEWS tests ranging from pure hoop to pure axial stress, the relationships in equation (2.1) was recalled;

$$\sigma_{Hoop} = \frac{P_1 d}{2t} \text{ and } \sigma_{Axial} = \frac{P_2 d}{4t} \tag{3.1}$$

where P_1 and P_2 correspond to the pressures required in the main and the small chamber respectively to achieve various test ratios. Table 3.2 contains data relating to the previous results [14] at ambient temperature and the estimated working pressures for the two chambers.

Table 3.2: Ambient temperature (25ºC) failure data for glass/GRE pipe [14] and corresponding maximum pressures for the test chambers.

Pressure ratio (hoop:axial)	**Hoop stress (MPa)**	**Axial stress (MPa)**	P_1 **(bar)**	P_2 **(bar)**
Pure Axial (0:1)	0	75	0	75
0.5	41	82	20.5	82
1:1	97	97	48.5	97
2:1	222	111	111	111
4:1	292	73	146	73
Pure hoop (1:0)	390	0	195	0

Assuming the *d/t* ratio for the pipe to be 40, these results can be converted into hydrostatic pressures for the two chambers inside the pipe. For a start, these pressures can be regarded as the maximum working pressures for the chambers. The calculated

pressures are then used for the design and purchase of suitable pumps and fittings for the test rig. Considering the failure envelope at a 25ºC test temperature from [14], the upper boundaries of the pressures to be exerted in the two chambers were calculated to be 195 bar and 111 bar respectively.

3.4.2 Control and instrumentation system

The control and data acquisition system was developed to control the static and cyclic pressure applied, and at the same time to display and store pressure and strain data gathered during the tests. The voltage signals from the pressure transducer and the strain measurements from strain gauges were recorded as a function of time by the CompactDAQ data acquisition system. This system was developed by National Instruments (NI) and is able to integrate sensor measurements with voltage, current, and digital signals to create customized, mixed-measurement systems with a single, easy USB cable back to the computer using LabVIEW software.

LabVIEW is a software programming environment used to build sophisticated measurement, test, and control systems using intuitive graphical icons and wires that resemble a flowchart. It was chosen as the platform for the visual programming language due to its built-in functionality in data acquisition, instrument control and measurement analysis. Figure 3.6, shows the front panel and block diagram of the interface developed from the LabVIEW environment for the UEWS test.

The two sensors used to collect data were a pressure transducer and a strain gauge to measure the pressure applied and corresponding strains respectively. The pressure transducer allows for the electronic monitoring of pressure during the UEWS test via the LabVIEW interface. An industrial pressure transducer from Swagelok was chosen for this purpose which has the capability to monitor the pressure applied during testing up to 400 bars.

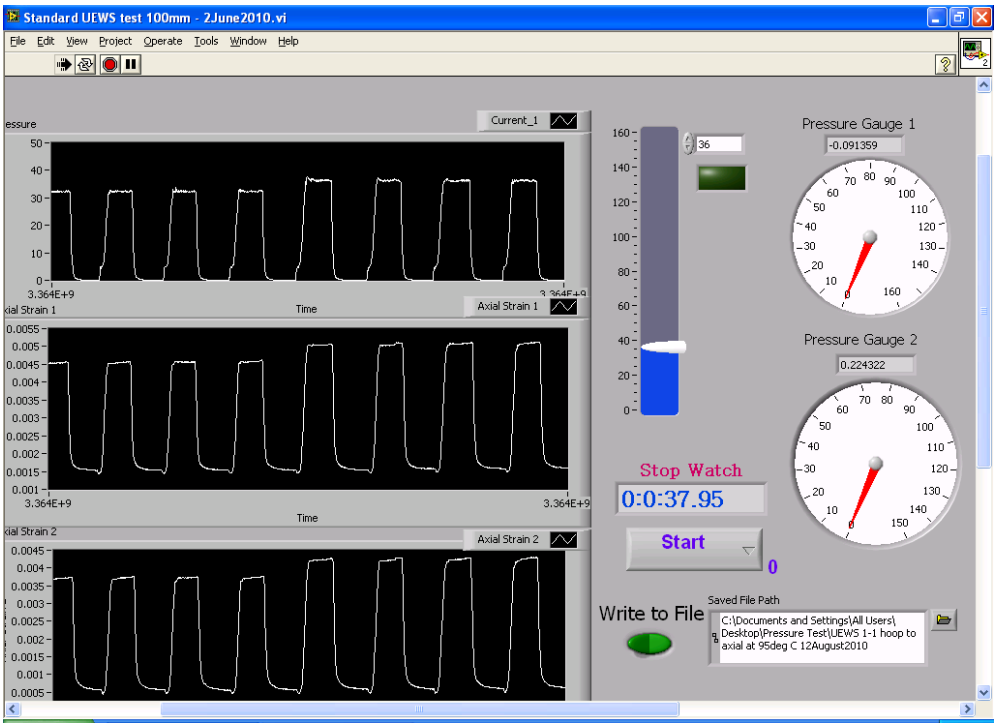

(a)

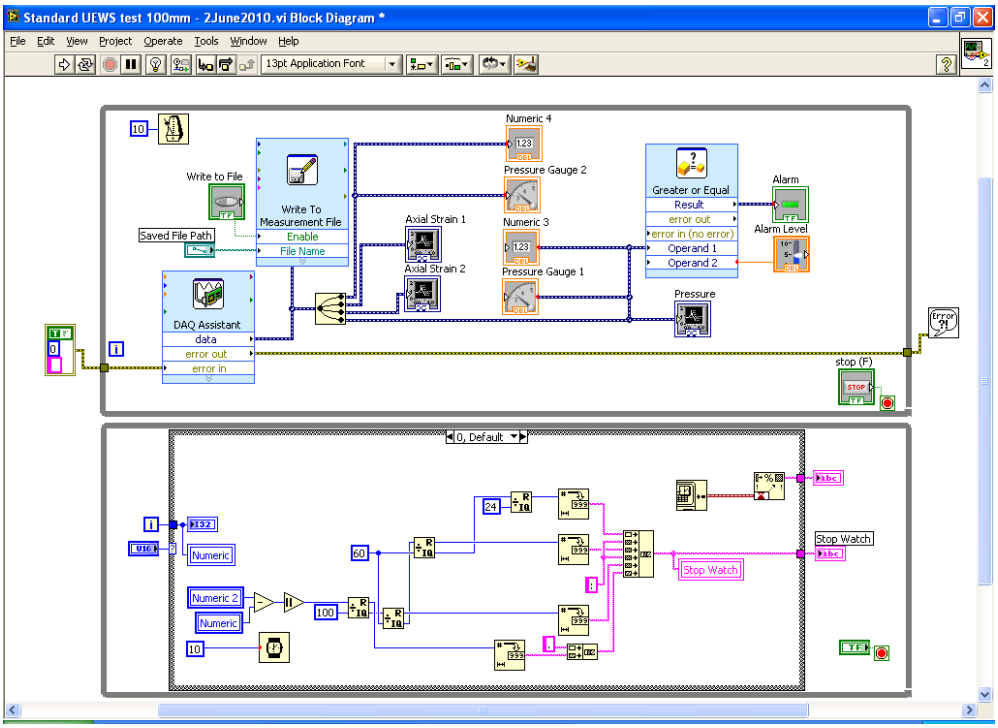

(b)

Figure 3.6: Front panel (a) and block diagram (b) of the LabVIEW interface for strain and pressure measurement during UEWS test.

Meanwhile, strain gauges were used to measure the hoop and axial strains induced during the UEWS tests. Since a strain gauge fulfils its intended functions only when attached to specimens, it was imperative to select the most appropriate type of gauge for the specimen's material type, operating temperature, measurement environment and installation dimensions. For measuring the strain in GRE pipes in the UEWS tests, a special type of strain gauge was chosen, which is 60mm in length utilizing a transparent plastic backing impregnated with a polyester resin. The strain gauge was provided by Feteris Components, and it is the same type as used by FPI in their engineering and evaluation tests. It is supplied with a $0.11mm^2$ pre-attached 3 meters long PVC lead wire and has a 2.12 gauge factor with 120Ω resistance. It is important to ensure that the strain output provided by the strain gauges during the latter stages of the test is in check. This is because in situations where the pipe undergoes considerable deformation prior to rupture, the strain gauge may become detached from the body of the pipe hence causing error in strain readings. However, in this case, it was observed that during testing and near to failure the strain gauges used remained strongly bonded to the surface of the pipe and the strain readings remained smooth and continuous.

3.4.3 Thermal enclosure

Since elevated temperature performance is of interest here, a special custom-made thermal enclosure was designed and fabricated. It was specifically designed to enable the testing of modified spools at temperatures of 65°C and 95°C, maintaining these test temperatures with a maximum variation of 3°C. The unit was designed so that the heater and the blower were separated from the oven space and placed at the back of the oven to achieve much better and more uniform control of test temperature, as well as to avoid any possible damage to the side of the wall during testing which would halt the operation of the oven. The closure was constructed with three holes. One in the centre of the oven flooring, allowed any water leakage from the pipes during testing to drain, and two on one of the side walls (at mid-height and 0.5m apart) gave access for pressure tubing and instrumentation wiring. A schematic diagram and photograph of the thermal enclosure used are given in Figures 3.7 and 3.8 respectively.

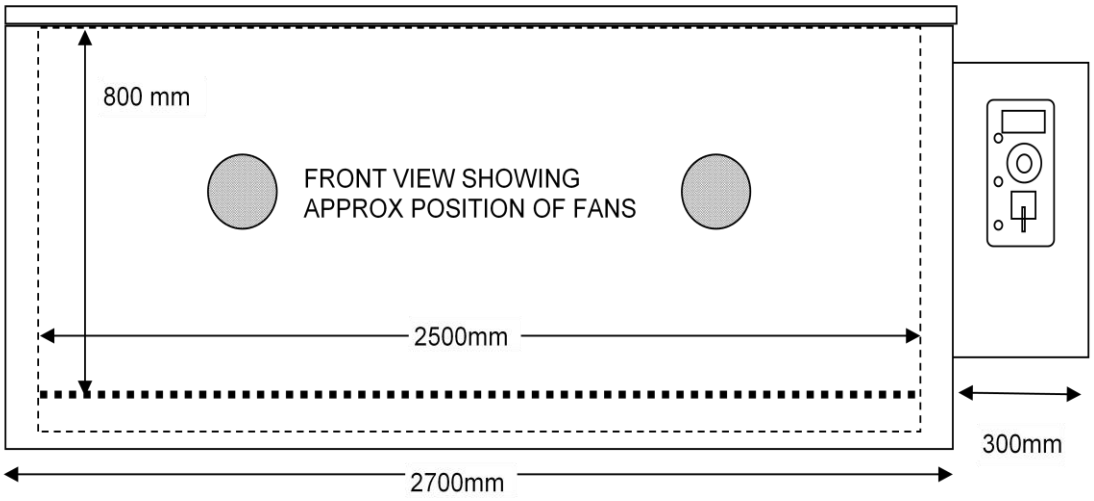

(a)

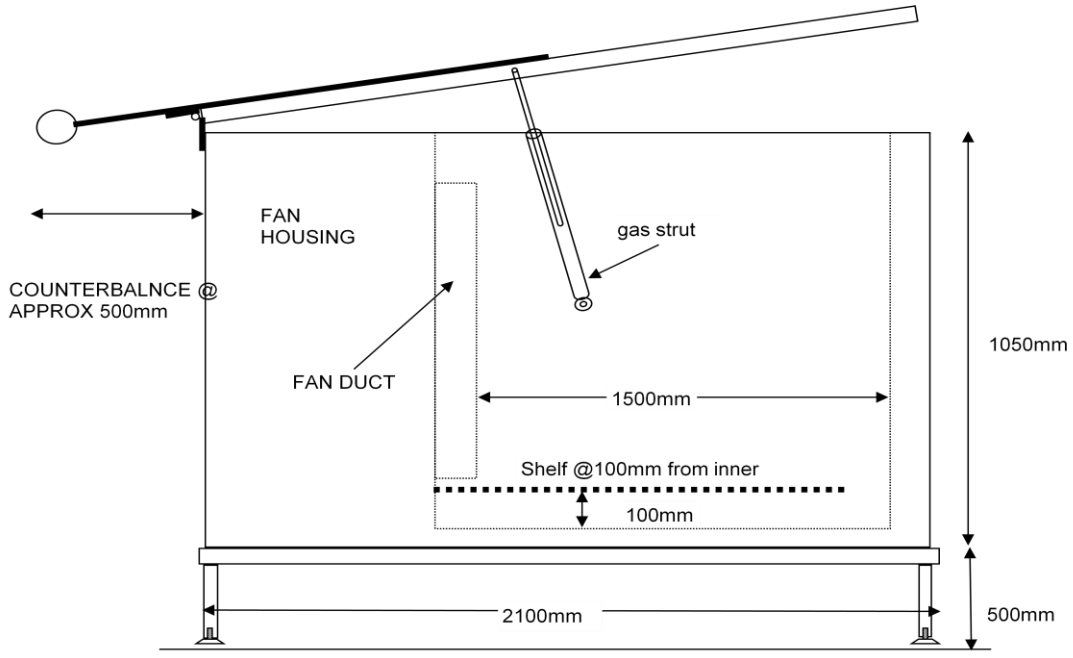

(b)

Figure 3.7: Front (a) and side (b) view of the thermal enclosure.

Figure 3.8: Thermal enclosure used for the UEWS tests.

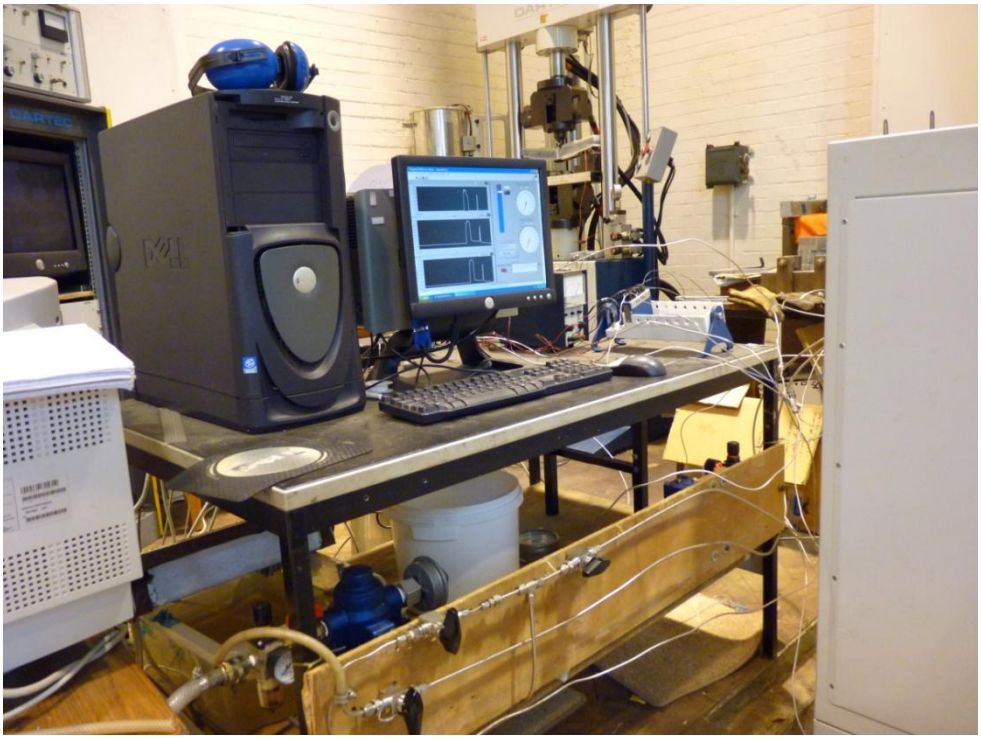

Figure 3.9: The rig consisting of the pressurizing system, control and instrumentation system and thermal enclosure.

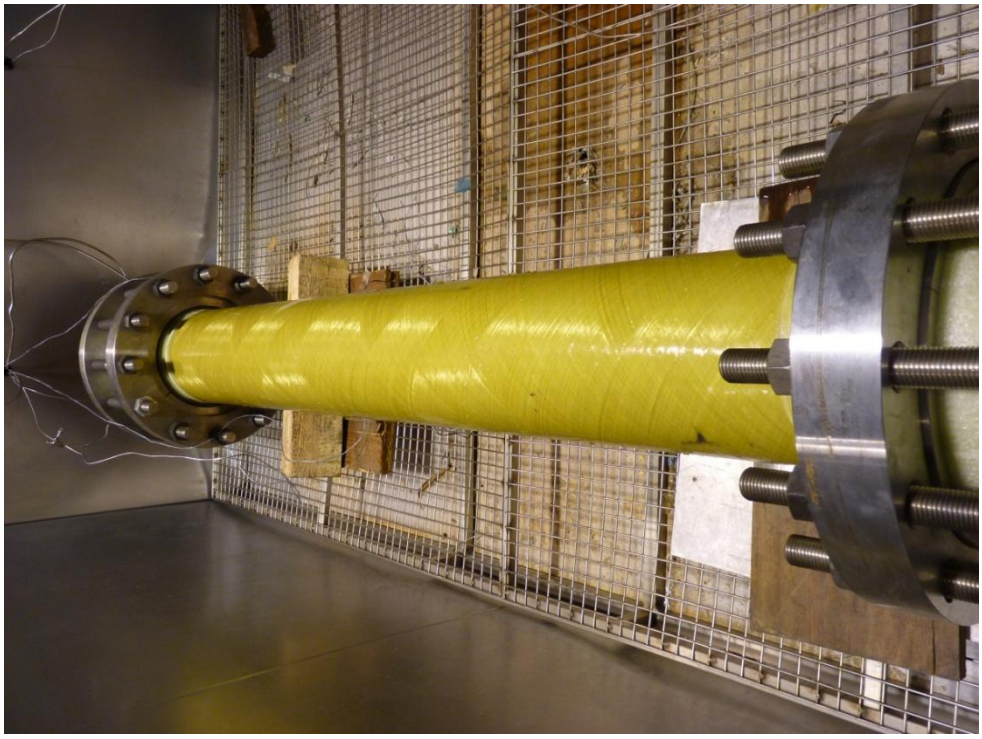

Figure 3.10: Test spool setup inside the thermal enclosure ready for testing

3.5. UEWS test procedure

3.5.1 UEWS test preparation

Prior to each test, the specimen was visually inspected to identify any obvious defects that may have occurred during manufacturing or transportation to the lab. The pipe was then carefully placed on the workbench and the end fittings were installed. For UEWS tests other than the 2:1 loading condition (hydrostatic pressure only) that is for 0:1, 0.5:1, 1:1, 4:1 and 1:0 hoop to axial loadings, the piston-like arrangement was fitted inside the test spool before end fitting installation.

Next, the strain gauges to measure the strain on the pipe during the test were placed in the middle of the pipe, diametrically opposite to one another. Before placing the strain gauges, the top coating from the pipe surface was removed using sandpaper in order to obtain direct contact with the pipe wall. However, this task needed to be conducted with care to avoid damage to the reinforced pipe wall. The sanded surface was rendered as flat, clean and dust free as possible. Acetone was used to clean the surface and remove dust and small particles.

After the attachment of the strain gauges, the test pipe was then moved into the thermal enclosure and filled with water using the inlet of one of the end fittings. It is particularly important that the whole system was ‘bled’ (at no pressure) for approximately 3-5 minutes before the test began in order to ensure that no air was trapped within the test system. Inside the thermal enclosure, the test pipe was positioned on a simple support at one end with another end positioned on a free-to-move roller. This was to prevent any influence of the support on the measured strain. It also ensured that the end supports did not restrain the specimen in the longitudinal or circumferential directions. For safety reasons, all tests were conducted with pipes placed inside the thermal enclosure, including those at room temperature, so that the test setup was isolated from the operators and the surroundings.

Finally, the strain gauges and pressure transducers were connected to the CompaqDAQ data acquisition systems for monitoring and data collection. After attaching the test rig to the pressurizing source, the UEWS test was ready to commence.

3.5.2 UEWS test procedure

In the UEWS test, the pipe filled with water was loaded in a prescribed time versus pressure schedule which consisted of a number of cycle groups. Each group consisted of ten one-minute cycles at pressure and ten one-minute cycles at no pressure, as illustrated in Figure 3.11. The pressure was increased uniformly until the first cyclic test pressure (CTP) was reached. This first CTP was taken to be 10% of the estimated pressure at UEWS. For each subsequent cycle group, the CTP was further increased by another 10% of the pressure corresponding to the expected UEWS (MPa) pressure.

During the procedure, either axial or hoop strain was measured, where axial strain was preferred for axial dominated loading and hoop strain measurement was a better choice for hoop dominated loading. The strain at the end of the first and the last cycle of each group of ten cycles was measured. The UEWS point is considered to be exceeded when either of the following is reached:

a) The difference in strain, $\Delta\varepsilon_c$ between the first and the tenth cycle is more than 5%

$$\Delta\varepsilon_c = \left(\frac{\varepsilon_{10} - \varepsilon_1}{\varepsilon_{10}} \right) \times 100 \tag{3.2}$$

where ε_1 and ε_{10} are the strains at first and tenth cycle respectively, or

b) The difference in strain $\Delta\varepsilon_p$ between the maximum strain at the end of the tenth cycle of a given cycle group and the predicted strain is more than 5%

$$\Delta\varepsilon_p = \left(\frac{\varepsilon_{10,m} - \varepsilon_{10,p}}{\varepsilon_{10,m}} \right) \times 100 \tag{3.3}$$

where ε_p is the difference between the measured strain at the tenth cycle and the predicted strain from linear behaviour and ε_{10m} and ε_{10p} are the measured strain and predicted strain at the 10^{th} cycle respectively. The predicted strain was calculated from earlier points by linear regression.

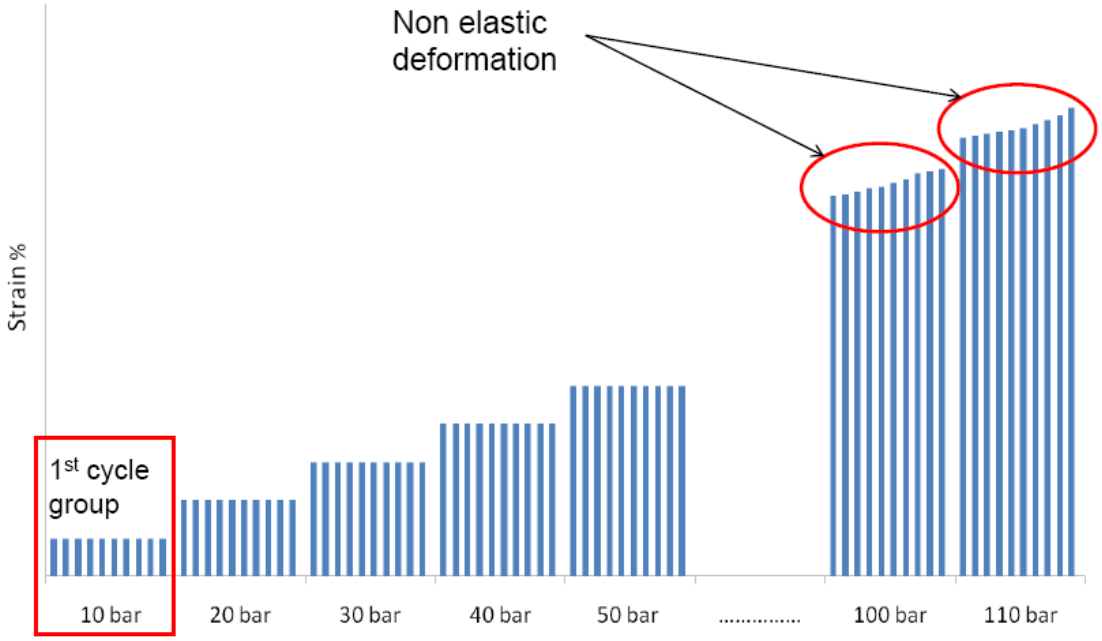

Figure 3.11: Pressure versus time during UEWS test

Once the UEWS point was reached, the test was continued until one of the following criteria was met:

a) weeping or leakage failure of the pipe was visually observed; or
b) two further cycle groups were performed after the onset of non-linear behaviour in the strain response.

It is important to note that the above mentioned definition of the UEWS point is derived from many years of rigorous study of the stress-strain response of GRE pipes subjected to pure hydrostatic loading with a 2:1 hoop to axial loading condition. For non-hydrostatic loading ratios, where the initial stress strain response may not be linear due

to viscoelasticity property of the pipe or the effects of residual stress, a more refined definition of UEWS point may be required. This current investigation into various loading ratios for UEWS tests hence provides the basis for improving this definition and producing a UEWS-based strength limit of the pipe for all loading conditions.

3.5.3 Post UEWS test

Once weepage was observed, or the final two cycle groups after the UEWS point was reached had been completed, the test specimen was detached from the pressurizing source. It is crucial to make sure that the pressure within the systems is released before detaching the specimen, for safety reasons. The pipe was then removed from the thermal enclosure for closer inspection. Any obvious damage or deformation observed was photographed and recorded.

Then, the specimen was cut in the middle section through the strain gauges for measurement of the inner diameter, reinforced wall thickness, and topcoat thickness of the specimen. This was conducted in accordance with the ASTM D3567 standard [182]. The topcoat resin-rich layer was found to be in the range of 0.3 mm with marginal variation arising from the manufacture of the pipe. The hoop stress was calculated from the following formula:

$$\text{Hoop Stress, } \sigma_{\text{H}} = P\left(\frac{ID_{sg} + TE_{sg}}{2TE_{sg}}\right) \tag{3.4}$$

where;

P = pressure (MPa),

ID_{sg} = inner diameter at the location of the strain gauge,

TE_{sg} = reinforced wall at the location of the strain gauge.

The raw data of pressure applied and the corresponding strains measured were then analysed. The strain values at the end of the first and last cycles of each ten cycle groups were measured. These values were plotted against the hoop stress calculated

from equation (3.4). The plot produces two lines representing the linear and non-linear behaviour of the tested pipes under such loading conditions. The two lines are then extended and their interception was drawn and taken as the UEWS point, which indicates the onset of damage to the pipe. An example of this plot is illustrated in Figure 3.12.

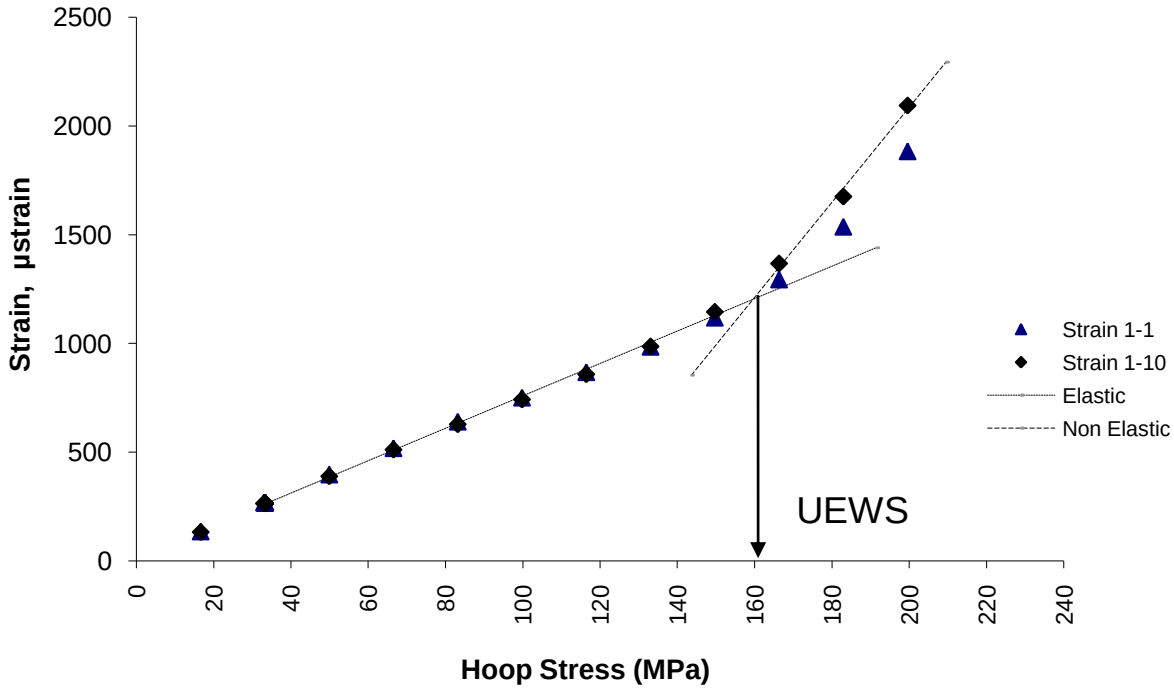

Figure 3.12: General UEWS test results showing strain response

3.6 Acoustic emission set-up

In hydrostatic (2:1), pure axial (0:1) and pure hoop (1:0) loadings of UEWS tests at RT, the acoustic emissions (AEs) were monitored and recorded using an AE instrument manufactured by the Physical Acoustics Corporation (PAC) with 150 kHz resonant sensors. Two sensors were placed on the outer surface of the pipe with a layer of silicone grease and secured using sellotape. The signals picked up by the sensors were strengthened to higher voltage using a preamplifier, which was placed close to the sensors in order to minimize electromagnetic interference. The AE set up used is shown in Figures 3.4 and 3.13.

After the sensor was fixed and connected to the acoustic software, simple 'lead break' calibration was carried out to ensure that the signal received was consistent and the sensor properly secured to the pipe surface. The process involved breaking a lead pencil near the sensor to verify the response from the acoustic sensors. If the latter were properly attached, the lead breaks should give a reproducible signal throughout. To eliminate background noise and unrelated signals from the data, the acoustic signal threshold was set at 40dB, which meant that only events with hits above 40dB were recorded. The AE data was continuously recorded throughout the UEWS test and line marks were made to differentiate the cycle groups of increasing pressure. AE monitoring was continued until weepage failure was observed.

Figure 3.13: Acoustic setup showing the location of the sensor and the pre-amplifier.

3.7. Determination of the stiffness property of GRE pipes tested

In order to examine the effects of the UEWS test on the degradation of axial and hoop modulus of the pipes, several samples of GRE pipes from an undamaged pipe to

intermediate stages of UEWS and to failure were needed. As a result, four samples in different conditions were prepared for this investigation: a virgin pipe, one at 50% of UEWS, 100% of UEWS and a pipe at weepage failure. Two types of tests were carried out to determine the axial and hoop stiffness as detailed below.

3.7.1 Determination of axial stiffness

Simple pull tests were carried out on the pipe specimens to determine the axial modulus of the pipe. Figure 3.14 shows a photograph of the test setup. Samples were pinned-supported at each end and subjected to a pull test using an Instron 4505 testing machine with gauge length set at 0.6m. A strain gauge was attached at the middle of the gauge length in the same manner as described above to measure the strain response during testing.

The test procedure was started by placing the sample pipe on the testing machine and the strain gauge was connected to the CompaqDAQ data acquisition system. The set up was left for several minutes to ensure stability before strain measurement. A constant load was then applied. After 100 seconds, a strain measurement was taken. The load was then increased and again held for another 100 seconds before strain was measured. This procedure was repeated several times. The applied load, however, was maintained at a low enough level to ensure a proportional relationship between load and displacement without causing permanent deformation or damage to the pipe. The whole test was then repeated for other specimens in different conditions as specified earlier. The axial modulus was then calculated using the linear stress-strain relationship in the axial direction.

3.7.2 Determination of hoop stiffness

In order to carry out the creep hoop Young's modulus tests, a number of ring specimens (20mm width) were cut from the conditioned samples tested in previous procedure. A specimen was then placed in the Instron tensile machine as shown in Figure 3.15. Similar to the test procedure for axial modulus measurement, step loading was again

applied with each load held for 100 seconds, whereupon the corresponding vertical displacements were recorded. It was very important that the load applied was maintained to give a linear relationship to displacement.

From Castigliano's strain energy method, the creep hoop modulus was then calculated [183] from the relationship below:

$$E_H = \frac{0.1484\ W\ R^3}{I\ \delta} \tag{3.5}$$

where W is the applied load (N); *R* is the radius of the sample (m); *I* is the moment of inertia. (m^4) and δ is the vertical displacement (m).

Figure 3.14: Test setup for the pull test to determine the axial Young's modulus of the pipe.

Figure 3.15: Test setup for the ring test to determine the hoop Young's modulus of the pipe.

3.8. Microscopic study

For closer inspection of the damage that occurred, an optical microscopy technique was used to examine the post test microstructure of the pipe wall. The main investigation looked at the distribution of matrix cracks as a result of the UEWS test and subsequently to define the crack density at the point of weepage failure. This was carried out simply by cutting out a piece from the failed tested pipe and analysing it under a light microscope. This section describes in detail the sectioning, polishing and microscopic analysis of the GRE pipe samples.

3.8.1 Sample preparation

In preparing the samples for microscopic analysis, 15mm x 30mm samples were cut from the failed pipe samples provided by FPI, targeting the areas at which weepage was observed. This was to increase the probability of observing matrix cracks in the plies. As reported earlier, weepage failure usually takes place when a network of cracks

parallel to the fibre coalesces, which eventually creates a continuous path for the fluid to pass through the pipe wall. In order to observe cracks within plies, the samples were cut along the direction of the fibres. A diamond cutting wheel was used to cut the pipe in order to minimize further damage to the surface of interest. Afterwards, the surface was thoroughly cleaned using acetone to remove dust and debris resulting from the cutting process, and the sample was dried so as to be ready for the encapsulating process.

The sectioned samples were then mounted inside a polymer block of mixed epoxy and hardener. The mounting process, also known as 'cold mounting', requires a simple cylindrical ring mould with a removable bottom flat surface. Next, the specimen was placed inside the mould with the surface of interest facing downwards. Epoxy resin and hardener were mixed accordingly to the manufacturer's instructions then poured into the mould and allowed to set. The curing process took about 5-6 hours. Once cured the specimen which was now transparent and in a cylindrical block as shown in Figure 3.16 was removed from the mould and labelled for identification. The sample was later ground and polished as described in the next section.

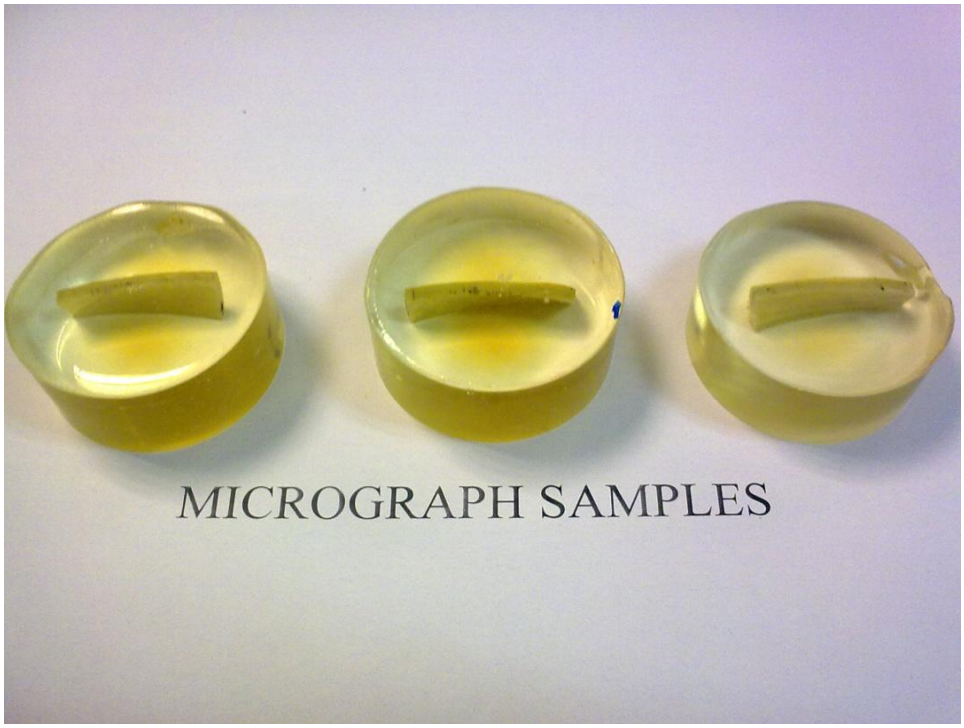

Figure 3.16: Micrograph samples of the pieces from failed tested GRE pipes.

3.8.2 Procedures for grinding and polishing GRE pipe sample

In order to observe micro cracks in the microscopy study, the mounted specimen had now to be polished to a micro fine finish. This was achieved using an EcoMet grinder-polisher machine manufactured by Buehler. There are two main stages in preparing the samples; planar grinding and stepped polishing. The programme for the planar grinding and polishing process is given in Table 3.3.

To start with, the specimen was subjected to planar grinding to flatten the surface and to eliminate any damage or rough surfaces due to the cutting process. For this purpose, samples were attached to a rotating disc and ground with coarse silicon carbide paper of 240μm grit size. A slight pressure was applied during the grinding process and water was occasionally added. The procedure was continued until all the blemishes had been removed and the specimen was absolutely flat. The samples were then washed with water followed by acetone and dried before moving on to the polishing process.

The next stage was stepped polishing, which is vital in producing the deformation-free surface that is flat, scratch-free and mirror-like in appearance necessary in studying the microstructure of the specimen. At this stage the samples were polished with a soft cloth impregnated with diamond particles and oil-based diamond suspensions. Starting with 6μm grade cloth, the specimens were polished until the scratches from the previous grinding process had been removed. Then, the samples were removed from the machine and washed with acetone before being left in the ultrasonic bath for 2 minutes to remove fine particles from the polishing process. Finally the samples were again washed with water and dried. Rapid drying of the ground/polished surface can also be achieved by applying a stream of compressed air to the polished surface. The procedure was then repeated with a smaller grade cloth of 3μm, and followed by 1μm cloth. The final polishing with 1μm-diamond particle grade cloth removed all the fine scratches from previous polishing and subsequently produced a very smooth surface finish with good contrast between the fibre, resin and cracks.

It is crucial that the sample was thoroughly cleaned as described, before moving to a smaller size grade cloth (3μm and 1μm) for subsequent polishing. This is because unclean samples can cause contamination to the polishing cloth and hence result in an unsatisfactory surface finish of the sample.

3.8.3 Microscopic analysis of the samples

The degree of damage within the plies through matrix micro cracking and delamination from failed UEWS test samples were carefully examined using a light microscope. The main objective was to examine the nature of matrix microcracks and if possible to measure the crack spacing, before hence calculating the critical crack density at which weepage/failure occurred. Matrix cracks were clearly apparent in the sectioned samples using the optical light microscope. The microscope also provided wide views for clearer and easier examination of the samples. The findings are discussed in detail in Chapter 5.

Table 3.3: The details of the grinding and polishing programme used in preparing the specimens for microscopic study

Surface	Abrasive/Size	Load (N)/Specimen	Base Speed (rpm)/Direction	Time (min:sec)
Planar grinding				
CarbiMet® 2 Abrasive Discs (Waterproof Paper)	240 grit SiC with water cooled	18	150-240 Comp.	Until Plane
Stepped polishing				
UltraPol™, UltraPad™ Cloth	6um MetaDi® Supreme Diamond Suspension*	18	120-150 Comp.	4:00
TriDent™ Cloth , TexMet® Pad or Nylon Cloth	3um MetaDi Supreme Diamond Suspension*	22	120-150 Comp.	4:00
MIcroCloth® Cloth, or ChemoMet® Pad	1um MasterMet® Colloidal Silica or MasterPrep® Alumina Suspensions	27	120-150 Comp.	2:00-4:00
*Plus MetaDi® Fluid extender as desired Comp. = Complementary (platen and specimen holder both rotate in the same direction)				

CHAPTER 4: MODELLING OF UEWS TESTING AND DAMAGE DEVELOPMENT

In this chapter a model based on Miner's law is developed to demonstrate the damage accumulation caused by cyclic and static fatigue loading in UEWS tests, using the input from the long term test data provided by FPI. The model is extended to simulate the stress-strain behaviour of GRE pipe during UEWS testing, which is directly linked to the progressive nucleation of matrix micro cracks using a crack growth model analogous to Paris Law. A general lifetime damage model for GRE pipes is then developed from a modified interactive failure criterion similar to the Tsai Hill criterion. The model is applied to produce failure envelopes for GRE pipes under various combinations of hoop to axial stress as well as at different temperatures. However, prior to this modelling, laminate theory is used to model the elastic constants of the GRE pipe used in this study.

4.1. Laminate theory

For the purpose of the modelling, it is assumed that the pipe wall is analogous to an angle ply laminate comprising of a number of even unidirectional plies, as shown in Figure 4.1. Firstly, the elastic properties of a unidirectional ply are calculated using the micromechanics theory of composite structures from the principal axes for those constituent laminae [16]. Equal strain treatment and the Halpin-Tsai simplification [23] are then used to determine the elastic behaviour of the unidirectional ply in the principle axes of the laminates from the following equations.

From the rule of mixtures:

$$E_1 = E_f V_f + E_m V_m \qquad \nu_{12} = \nu_f V_f + \nu_m V_m \tag{4.1}$$

and from the Halpin-Tsai simplification:

$$E_2 = \frac{1+\xi\eta_e V_f}{1-\eta_e V_f} \quad \text{where } \eta_e = \frac{E_f/E_m - 1}{E_f/E_m + \xi} \tag{4.2}$$

$$G_{12} = \frac{1+\xi\eta_g V_f}{1-\eta_g V_f} \quad \text{where } \eta_e = \frac{G_f/G_m - 1}{G_f/G_m + \xi} \tag{4.3}$$

In the above equations, E_1 and E_2 are the longitudinal and transverse modulus of the ply respectively, while G_{12} and v_{12} are the shear modulus and the Poisson's ratio in the 1-2 plane, as indicated in Figure 4.1. According to Halpin-Tsai [16], ξ is suggested to be equal to 2 for predicting the transverse modulus, and equal to 1 when predicting the shear modulus. The volume fractions, modulus of elasticity and shear modulus of the fibre (f) and matrix (m) in the laminates are represented by V_f, V_m, E_f, E_m, G_f and G_m respectively. The in-plane shear moduli for fibre G_f and matrix G_m can be estimated from:

$$G_f = \frac{E_f}{2(1+v_f)} \qquad \text{and} \qquad G_m = \frac{E_m}{2(1+v_m)} \tag{4.4}$$

Since the pipe wall is an angle ply laminate, the lamina can be considered to have orthotropic elastic properties, which are highly dependent on the winding angle θ. Thus, the stress-strain response of the lamina can be expressed as:

$$\begin{pmatrix} \sigma_1 \\ \sigma_2 \\ \tau_{12} \end{pmatrix} = \begin{pmatrix} Q_{11} & Q_{12} & 0 \\ Q_{12} & Q_{22} & 0 \\ 0 & 0 & Q_{66} \end{pmatrix} \begin{pmatrix} \varepsilon_1 \\ \varepsilon_1 \\ \gamma_{12} \end{pmatrix} \tag{4.5}$$

where Q_{11}, Q_{12} *and etc.* are the stiffness matrices, which can be expressed in engineering terms as:

$$Q_{11} = \frac{E_1}{1-\nu_{12}\nu_{21}}; \qquad Q_{12} = \frac{\nu_{12}E_1}{1-\nu_{12}\nu_{21}} = \frac{\nu_{21}E_2}{1-\nu_{12}\nu_{21}}$$
$$Q_{22} = \frac{E_2}{1-\nu_{12}\nu_{21}}; \qquad Q_{66} = G_{12} \tag{4.6}$$

E_1 and E_2 are the modulus of elasticity in the lamina's principal axes. However, in the case of angle ply laminates, the unidirectional lamina is now loaded at some arbitrary angle θ (Figure 4.1) relative to the principal axes. A transformation matrix is used to transform the applied stresses and strains in the axial-hoop axes into the directions of principal axes 1-2 from the relationship below:

$$\begin{pmatrix}\sigma_1\\ \sigma_2\\ \tau_{12}\end{pmatrix} = \begin{pmatrix}\cos^2\theta & \sin^2\theta & 2\sin\theta\cos\theta\\ \sin^2\theta & \cos^2\theta & -2\sin\theta\cos\theta\\ -\sin\theta\cos\theta & \sin\theta\cos\theta & \cos^2\theta-\sin^2\theta\end{pmatrix}\begin{pmatrix}\sigma_{axial}\\ \sigma_{hoop}\\ \tau_{ax/hp}\end{pmatrix} = [T]\begin{pmatrix}\sigma_{axial}\\ \sigma_{hoop}\\ \tau_{ax/hp}\end{pmatrix} \tag{4.7}$$

hence,

$$\begin{pmatrix}\sigma_{axial}\\ \sigma_{hoop}\\ \tau_{ax/hp}\end{pmatrix} = [T]^{-1}\begin{pmatrix}\sigma_1\\ \sigma_2\\ \tau_{12}\end{pmatrix} = [T]^{-1}[Q]\begin{pmatrix}\varepsilon_1\\ \varepsilon_2\\ \frac{1}{2}\gamma_{12}\end{pmatrix} = [T]^{-1}[Q][T]\begin{pmatrix}\varepsilon_{axial}\\ \varepsilon_{hoop}\\ \frac{1}{2}\gamma_{ax/hp}\end{pmatrix} = \left[\overline{Q}\right]\begin{pmatrix}\varepsilon_{axial}\\ \varepsilon_{hoop}\\ \gamma_{ax/hp}\end{pmatrix} \tag{4.8}$$

where $\left[\overline{Q}\right]$ is the transformed stiffness matrix, which relates the engineering strains to the stresses developed in the ply when loaded at an arbitrary angle θ. Thus, from algebraic manipulation, the relation between the $\left[\overline{Q}\right]$ and $[Q]$ matrices can be expressed in the form of:

$$\begin{aligned}
\overline{Q}_{11} &= Q_{11}\cos^4\theta + Q_{22}\sin^4\theta + 2(Q_{12}+2Q_{66})\sin^2\theta\cos^2\theta\\
\overline{Q}_{22} &= Q_{11}\sin^4\theta + Q_{22}\cos^4\theta + 2(Q_{12}+2Q_{66})\sin^2\theta\cos^2\theta\\
\overline{Q}_{12} &= (Q_{11}+Q_{22}-4Q_{66})\sin^2\theta\cos^2\theta + Q_{12}(\cos^4\theta+\sin^4\theta)\\
\overline{Q}_{16} &= (Q_{11}-Q_{12}-2Q_{66})\sin\theta\cos^3\theta - (Q_{22}-Q_{12}-2Q_{66})\sin^3\theta\cos\theta\\
\overline{Q}_{26} &= (Q_{11}-Q_{12}-2Q_{66})\sin^3\theta\cos\theta - (Q_{22}-Q_{12}-2Q_{66})\sin\theta\cos^3\theta\\
\overline{Q}_{66} &= (Q_{11}+Q_{22}-2Q_{12}-2Q_{66})\sin^2\theta\cos^2\theta + Q_{66}(\cos^4\theta+\sin^4\theta)
\end{aligned} \tag{4.9}$$

where θ is the magnitude of the angle between the lamina's principal axes and the *axial*-axis. An early assumption that each lamina is homogenously orthotropic and perfectly bonded eliminates the coupling between direct stress and shear strain that could have developed. Therefore, the constants $\left[\overline{Q_{16}}\right]$ and $\left[\overline{Q_{26}}\right]$ can be set to zero [23, 184]. By using the transformed stiffness matrix calculated above, the elastic properties of the pipe wall in the axial and hoop directions are then evaluated using the following equation:

$$E_{axial} = \overline{Q}_{11}(1-\nu_{axial} * \nu_{hoop}); \qquad E_{hoop} = \overline{Q}_{22}(1-\nu_{axial} * \nu_{hoop})$$

$$\nu_{axial} = \frac{\overline{Q}_{12}}{\overline{Q}_{22}}; \qquad \nu_{hoop} = \frac{\overline{Q}_{12}}{\overline{Q}_{11}}; \qquad G_{ax/hp} = \overline{Q}_{66} \tag{4.10}$$

The inverse stress-strain relations for orthotropic lamina can also be written as:

$$\begin{pmatrix} \varepsilon_{axial} \\ \varepsilon_{hoop} \\ \gamma_{ax/hp} \end{pmatrix} = \begin{bmatrix} \overline{S_{11}} & \overline{S_{12}} & \overline{S_{16}} \\ \overline{S_{12}} & \overline{S_{22}} & \overline{S_{26}} \\ \overline{S_{16}} & \overline{S_{26}} & \overline{S_{66}} \end{bmatrix} \begin{pmatrix} \sigma_{axial} \\ \sigma_{hoop} \\ \tau_{ax/hp} \end{pmatrix} \tag{4.11}$$

Since the filament wound GRE pipe is treated as an angle ply laminate with orthotropic elastic properties, the strains produced by the general state of stress in equation (4.11) can be derived to form the following relations [16]:

$$\varepsilon_{axial} = \frac{\sigma_{axial}}{E_{axial}} - \nu_{hp/ax} \frac{\sigma_{hoop}}{E_{hoop}}$$

$$\varepsilon_{hoop} = \frac{\sigma_{hoop}}{E_{hoop}} - \nu_{ax/hp} \frac{\sigma_{axial}}{E_{axial}}$$

$$\gamma_{ax/hp} = \frac{\tau_{ax/hp}}{G_{ax/hp}} \tag{4.12}$$

where E_{axial}, E_{hoop}, $G_{ax/hp}$, and $\upsilon_{ax/hp}$ are the modulus of elasticity in the longitudinal and transverse directions, and the shear modulus and Poisson's ratio respectively, which can be determined from equation (4.10).

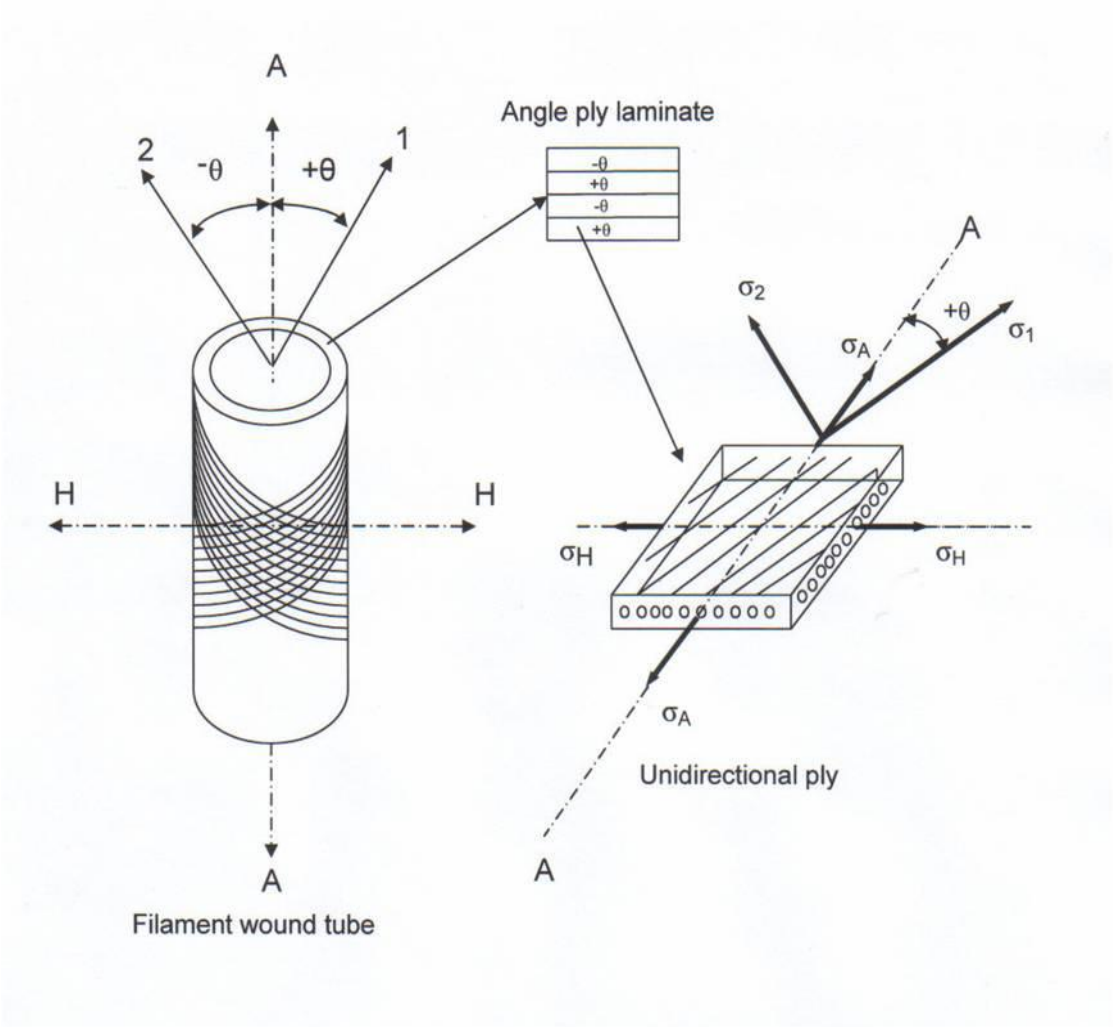

Figure 4.1: Schematic diagram of GRE filament wound pipe showing its coordinate system and the principal axes of the unidirectional lamina [14]. The pipe wall is essentially an angle ply laminate built-up from unidirectional plies. In these plies, all the fibres are aligned in the 1-direction, where the 2-direction is the transverse direction of the fibre.

4.2. Modelling of reduction in elastic properties during UEWS testing.

As discussed in detail in the literature review, transverse matrix cracking is the most common failure mode under uniaxial or biaxial loading in composite pipes. In this section, the effects of matrix cracking on the degradation of elastic properties during the UEWS tests are modelled. General expressions of longitudinal and hoop moduli against crack density are obtained and compared with the values measured during the tests. The finite element results from Sun and Tao [70] were used in establishing the relationship between the effective transverse and shear moduli, and crack density.

The biaxial stress induced during the UEWS tests is calculated by recalling equation (2.1) and given below:

$$\sigma_H = \frac{P\,d}{2t}$$

$$\sigma_A = \frac{P\,d}{4t} \tag{4.13}$$

The corresponding strains produced by the stresses generated in the tubes are then worked out from the following relations:

$$\varepsilon_H = \frac{\sigma_H}{E_H} - \nu_{AH}\frac{\sigma_A}{E_A}$$

$$\varepsilon_A = \frac{\sigma_A}{E_A} - \nu_{HA}\frac{\sigma_H}{E_H} \tag{4.14}$$

These strains were then transformed to the ply coordinate system by multiplying with the transformation matrix. Hence,

$$\begin{aligned}\varepsilon_1 &= \varepsilon_A \cos^2\theta + \varepsilon_H \sin^2\theta \\ \varepsilon_2 &= \varepsilon_A \sin^2\theta + \varepsilon_H \cos^2\theta \\ \gamma_{12} &= 2\sin\theta\cos\theta(\varepsilon_H - \varepsilon_A)\end{aligned} \tag{4.15}$$

Thus, at a low stress level where the stress-strain behaviour can be considered to be linear, the stresses in the unidirectional ply can be calculated from equation (4.5). The elastic moduli E_1 and E_2 are determined from the stiffness matrices given in equation (4.6).

However, due to the significant differences in thermal expansion in the reinforcement materials and matrix, residual stress is often generated prior to actual loading on the pipe. So, it is imperative that any such thermal stress generated is taken into account when modelling the stress-strain response. In order to calculate the thermal stresses generated, the coefficient of thermal expansion of the ply is calculated. First, from the literature available, the coefficient of expansion for the fibre, α_f, and epoxy matrix, α_m, are found to be $5x10^{-6}/^oC$ and $5.5x10^{-5}/^oC$ respectively. The thermal expansion of the ply in the longitudinal and transverse directions is then calculated from the formula derived by Schapery [16] as stated below:

$$\alpha_1 = \frac{1}{E_1} E_f \alpha_f V_f + E_m \alpha_m (1 - V_f)$$

$$\alpha_2 = \alpha_f V_f (1 + \upsilon_f) + \alpha_m (1 - V_f)(1 + \upsilon_m) - \upsilon_{12} \alpha_1 \qquad (4.16)$$

The ply coefficient estimated above was later used in the laminate theory calculation to determine the coefficient of thermal expansion for the GRE pipe provided by FPI. The resulting thermal expansion for the ply and laminate are given in Table 4.1.

Table 4.1: Coefficients of thermal expansion of the ply and angle ply laminate used in GRE pipe

Ply	
α_1, $(x10^{-6}/^0C)$	α_2, $(x10^{-6}/^0C)$
6.66	33.2
±55° laminate	
α_{axial}, $(x10^{-6}/^0C)$	α_{hoop}, $(x10^{-6}/^0C)$
24.5	7.3

Residual stress occurs because of the thermal mismatch between the fibre and the matrix and also the constraints which exist within laminates. This happens as a result of temperature changes during the manufacturing of the pipe when it was cooled to working temperature after curing. Due to the differences in the thermal coefficient, the matrix material shrinks significantly more than does the reinforcement fibre. This induces tensile stress in the matrix component and compressive stress in the fibre reinforcement. For modelling purposes, 120°C was adopted as the curing temperature for Wavistrong pipes before they are cooled to a working temperature of 20°C. Hence, thermal stresses were generated due to this 100°C temperature drop, which acted like a preload prior to the actual loading.

The thermal stresses induced in the angle ply layup were then calculated by transforming the thermal expansion coefficient to the laminates axes using the following relationships:

$$\begin{aligned} \alpha_{ax} &= \alpha_1 \cos^2\theta + \alpha_2 \sin^2\theta \\ \alpha_{hp} &= \alpha_1 \sin^2\theta + \alpha_2 \cos^2\theta \\ \alpha_{ax/hp} &= 2\sin\theta\cos\theta(\alpha_1 - \alpha_2) \end{aligned} \qquad (4.17)$$

The corresponding strains due to this 100°C temperature drop in the pipe and the ply at the laminate axes were calculated and are given in Table 4.2.

Table 4.2: Computed thermal strains of the ply and angle ply laminate used in GRE pipe

	$\varepsilon_{axial}^{Therm}$	$\varepsilon_{hoop}^{Therm}$	$\gamma_{ax/hp}^{Therm}$
GRE pipe	-0.002450	-0.00073	0
Ply ±55°	-0.002449	-0.00154	0.0025
Difference	-0.000001	0.0008724	-0.0025

From the calculated values shown in Table 4.2, there were clear differences in the resulting thermal strains in the laminate and in the ply of the same axes. However, this change in temperature in the pipe does not induce shear strain in the laminate. Only

after the ply strains were transformed into the laminate principal axes at ±55° were significant shear strains induced. The constraint on the ply within the laminates generates the thermal stresses. This is computed by working out the difference in strain between the laminate and ply, before multiplying this with the transformed matrix in order to determine the ply strains in the original ply axes. The thermal stress induced is then calculated by multiplying these strains with the ply stiffness matrix.

It was found that the stresses generated due to temperature changes from curing to the working state in a ±55° laminate were, σ_1 = -23.6MPa, σ_2 = 15.7MPa and γ_{12} = 6.9MPa. These stresses acted like a pre-loading and must be taken into account when carrying out the modelling to determine the reduction in elastic properties. Finally, these values were then added to the principal stresses generated from the applied pressure. It is also worth pointing out that the calculation conducted here used linear elastic laminate theory with constant thermal expansion and stiffness properties throughout the temperature change.

From the finite element model developed by Sun and Tao [70], the deterioration in the transverse and shear moduli of composite laminates due to the increasing presence of matrix cracks can be estimated in the form of:

$$\frac{E_2}{E_2^{o}} = \exp(-\alpha_{E_2}\rho^*)$$

$$\frac{G_2}{G_2^{o}} = \exp(-\alpha_G\rho^*) \qquad (4.18)$$

where;

E_2 and E_2^{o} are effective and initial transverse Young's modulus of ply respectively.

G_2 and G_2^{o} are effective and initial shear modulus of ply respectively.

α_{E2} and α_G are curve fitting constants determined by the finite element analysis.

ρ is the normalized crack density function.

The relationship between crack density and applied stress was derived by Roberts [49] and is given below;

$$\rho = \kappa\left[\frac{\sigma_2 - \sigma_m^{fail}}{\sigma_m^{fail}}\right] \tag{4.19}$$

where;

σ_2 is the limiting transverse stress in unidirectional ply,

σ_m^{fail} is the failure strength of the matrix material, and

$\kappa = \sqrt{\frac{(E_1 + E_2)G_{12}}{E_1 E_2}}$, where κ involves only the ply modulus constants.

The estimation of the effective transverse and shear modulus of the ply at every pressure group increment can then be computed from equation (4.18). This effective modulus is later used together with laminate theory to determine the new corresponding axial and hoop modulus of the pipe after taking into account the effects of increasing crack density.

4.3. Damage cumulative model of UEWS test

As mentioned before, the ASTM D2992 document outlines the procedures for carrying out hydrostatic pressure tests under cyclic or long term static loading. From the regression line shown in Figures 2.10 and 2.11 for static and cyclic procedures, both types of failure can be described by the following power law expressions for cyclic and static behaviour respectively:

$$\sigma = HN_f^{-J} \tag{4.20}$$

$$\sigma = Ft_f^{-G} \tag{4.21}$$

where t_i is time in hours and N_i is the number of cycles to failure. These expressions can be re-arranged to give the time or number of cycles to failure, so:

$$t_f = \left(\frac{\sigma}{F}\right)^{-\frac{1}{G}} \tag{4.22}$$

for static fatigue conditions, and

$$N_f = \left(\frac{\sigma}{H}\right)^{-\frac{1}{J}} \tag{4.23}$$

for cyclic fatigue. In both conditions, constants F, G, H, and J were determined from the regression analysis of the long term static rupture and cyclic tests. These tests were conducted by FPI in accordance with ASTM D2992 for the design and qualification of GRE pressure pipes and fittings.

In order to model the damage accumulation in the GRE pipe during the UEWS test procedure, which is expected to be dominated by cyclic loading, a cumulative damage rule was used. A number of damage models have been employed in recent decades to describe the development of damage in composite materials [148, 151, 177, 185, 186]. For modelling UEWS procedures, a widely used Miner's Law [152] has been employed. This empirical law provides a simple way of accounting for damage accumulation due to different stress levels in cyclic loading, such as that applied in UEWS tests. Recalling equation 2.10 given in Chapter 2, the law states that, for cyclic fatigue, failure occurs when:

$$\sum \frac{\Delta N_i}{N_{if}} = 1 \tag{4.24}$$

where N_{if} is the number of cycles to failure at stress level σ_i and ΔN_i is the number of cycles applied at each stress level σ_i of the fatigue cycle. This provides a method of summing the damage produced by fatigue cycles of different magnitude, which can be extended to model and sum the effects of other types of damage in composite structures. In the case of UEWS testing where cycle groups of different stress magnitudes are present, the end of life is reached when:

$$\frac{N_1}{N_{1f}}+\frac{N_2}{N_{2f}}+\frac{N_3}{N_{3f}}+.....\frac{N_i}{N_{if}}+.....=\sum\frac{\Delta N_i}{N_{if}}=1 \tag{4.25}$$

This expression applies where N_1 stress cycles occur at stress σ_1; N_2 cycles occur at stress σ_2 and, in general, N_i cycles occur at stress, σ_i. N_{1f}, $N_{2f}...N_{if}$ are then the corresponding numbers of cycles that would cause failure in a cyclic fatigue test at a constant repeated stress of, σ_1, $\sigma_2...\sigma_i$.. Using the expression derived, it is now possible to model the damage accumulation which occurs during the cyclic loading of increased pressure in the UEWS test. The same can now be generalized to include static as well as cyclic fatigue loading. The analogous static creep conditions can now be expressed as:

$$\sum\frac{\Delta t_i}{t_{cf}}=1 \tag{4.26}$$

where t_{cf} is the creep failure at stress level σ_i and Δt_i is the time applied at each stress level σ_i. Hence, for a UEWS test where static loading at different stresses is present:

$$\frac{t_1}{t_{1f}}+\frac{t_2}{t_{2f}}+\frac{t_3}{t_{3f}}+.....\frac{t_i}{t_{cf}}+.....=\sum\frac{\Delta t_i}{t_{cf}}=1 \tag{4.27}$$

In this case, t_1, $t_2...t_i$ are the times at a specific stress level, while t_{1f}, $t_{2f}..t_{cf}$ are the corresponding times to creep failure at constant values of these stresses. However, few studies have reported the combined effect of cyclic and static fatigue at the same time. One of these by Frost [42], concluded that both static and cyclic fatigue contribute to matrix crack growth, with one or the other usually seen to dominate the total damage induced. Frost then went on to propose that, for a GRE system subjected to combined static and cyclic loading, similar to the UEWS test, failure is predicted to occur when;

$$\sum\frac{\Delta t_i}{t_{cf}}+\sum\frac{\Delta N_i}{N_{if}}=1 \tag{4.28}$$

It would be very interesting to find out if the damage accumulation model derived above can be related to the design lifetime of GRE pipes obtained from the regression-based procedure as described previously. Rearranging equations (4.22) and (4.23) and integrating them with equation (4.28) allows the failure state to be predicted for loading histories containing both static and fatigue loading. Thus, the total Miner's law sum can now be rewritten as the following;

$$\sum\left(\frac{\sigma_i}{F}\right)^{\frac{1}{G}} t_i + \sum\left(\frac{\sigma_i}{H}\right)^{\frac{1}{J}} N_i = 1 \tag{4.29}$$

Since the UEWS test involves the application of groups of 10 one minute cycles with pressure and one minute cycles without pressure, the simplified approach above can be used to predict the design life of GRE pipes. In a UEWS test with a stress increment, $\Delta\sigma$, the usual conditions of a cyclic loading period of one minute and groups of 10 cycles, this is given by:

$$\frac{10}{60} F^{-\frac{1}{G}} \left(\sigma^{\frac{1}{G}} + (2\sigma)^{\frac{1}{G}} + (3\sigma)^{\frac{1}{G}} + \ldots\ldots \right) + 10H^{-\frac{1}{J}} \left(\sigma^{\frac{1}{J}} + (2\sigma)^{\frac{1}{J}} + (3\sigma)^{\frac{1}{J}} + \ldots\ldots \right) = \Phi \tag{4.30}$$

where the first term represents the static loading effect and the second term denotes cyclic fatigue. Using the constants values acquired from the regression analysis of the FPI fibreglass product, damage accumulation based on the modified Miner's law can be computed for each stress level during the UEWS test. Figure 4.2 below shows damage accumulation from the static and cyclic loadings of the UEWS test.

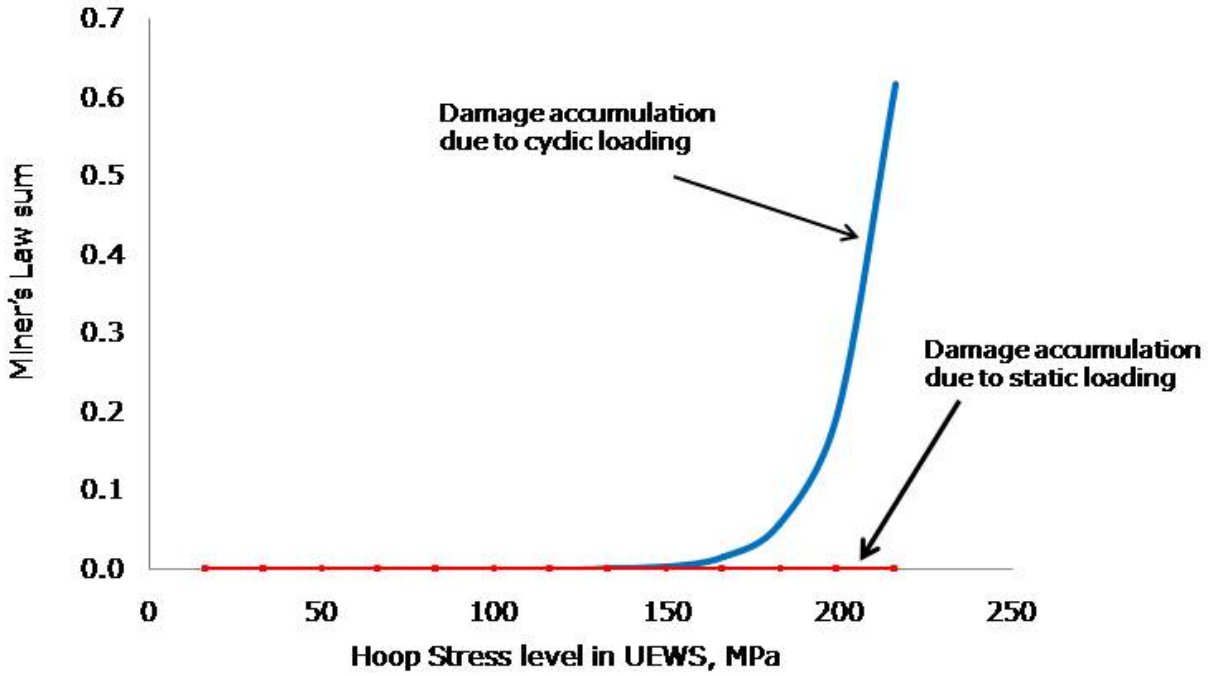

Figure 4.2: Miner's Law sum at each hoop stress level showing static and cyclic element in UEWS test.

As can be seen in Figure 4.2, damage accumulations due to the cyclic element during the UEWS test clearly predominate over the contribution from static loading. This suggests that the development of matrix micro cracks in GRE pipe is governed by cyclic loading, as more time would be required for the static condition to cause the same degree of damage accumulation. It should be borne in mind, however, that the static loading applied in the UEWS test was very low. In effect, it is only applied for ten one-minute periods per cycle group for over ten cycle groups, whilst the regression-based procedure requires more than a year of constant pressure loading to be completed.

On a positive note, this approach does enable the whole test to be completed within one day. Still, since the UEWS has been shown to be governed by cyclic loading, in order for the procedure to be fully employed for qualification purposes, additional information would be needed regarding the relationship or equivalency between the damage caused by cyclic loading and that produced statically.

Further significant information can be deduced from Figure 4.2 is that, the stress value at which the Miner's law sum begins to deviate from zero, at say, approximately 1%, shows very good conformity with the UEWS value provided by FPI. For new GRE pipes where the CTP value for the first cycle is unknown, the Miner's law sum model could now be used to predict the onset of damage, which corresponds to the UEWS value, hence avoiding trial and error in determining the first CTP value.

In order to predict the lifetime pressure rating for the GRE pipe, the effect crack density must be considered in the constitutive law which defines the stress-strain relationship. In addition, a growth damage law is also needed to relate stiffness reduction to loading history. The parameter normally used to define the state of damage is crack density, $\boldsymbol{\rho}$, measured in the ply transverse direction. $\boldsymbol{\rho}$ is dimensionless, being defined as the ratio between ply thickness and average distance between micro cracks [49]. This provides a means of taking into account the well-known effect of ply thickness on crack growth. It is assumed that weepage takes place at a critical value of crack density, $\boldsymbol{\rho}_{\text{weepage}}$, and that this value is the same irrespective of how the weepage state is reached (whether by different combinations of static and cyclic loading or different combinations of internal pressure and axial load).

As mentioned previously, transverse matrix micro cracking would be the first observed damage mode in GRE pipes. Although not crucial in causing abrupt structural failure, many agree that matrix cracking results in degradation in elastic properties, and therefore it can be the initiator of more severe damage such as delamination, fibre matrix debonding and fibre fracture [149, 187, 188]. Gudmundson and Zhang [189, 190] and Roberts *et al.* [49] examined the effects of matrix cracks on the behaviour of angle ply laminates as used in the pipes studied here. They demonstrated an analytical model for predicting the thermoelastic properties of angle ply laminates containing transverse matrix micro cracks parallel to fibre direction. Their findings suggested that the elastic properties and especially the axial and hoop modulus varied significantly with crack density.

In this section, Gudmundson's formulation is used to calculate the elastic constants of ±55° glass epoxy cracked laminates. These are then used to simulate the stress-strain response in the UEWS test. However, to make this applicable to the present work, their model's results have been normalized by dividing each elastic constant by its original value in the undamaged state. This is necessary because the elastic constants of the GRE pipe used in the present UEWS tests are different from those adopted by Gudmundson in his model. Figure 4.3 shows the dimensionless plot of the elastic constants against crack density. It can be observed that axial modulus elasticity shows the most sensitive reaction, exhibiting a rapid decline with increase in crack density. The hoop modulus, on the other hand, declined rather less with increase in crack. The in-plane shear modulus and major Poisson's ratio $\upsilon_{ah,}$ meanwhile were scarcely influenced by the presence of matrix cracks, although the minor Poisson's ratio $\upsilon_{ah,}$ was highly affected. It is thought that weepage is very likely to occur at a low value of crack density of approximately 0.5.

As mentioned before, GRE pipe failure is always governed by cracks propagating through the matrix phase. Once initiated, matrix cracking grows rapidly in the direction of the fibres, since there is fairly little resistance to crack growth to slow down crack propagation. Therefore, the major factor governing damage development in GRE pipes is in fact crack initiation rather than growth. Frost and Cervenka [42] suggested a damage growth model for GRE pipe using a relationship analogous to Paris Law as used for crack growth in metals. The modified Paris Law describes the rate of change of crack density, rather than the increase of a single crack. So, for cases of cyclic fatigue:

$$\frac{d\rho}{dN} = A\sigma^n \tag{4.31}$$

where A is the proportionality constant, N is the number of cycles and n is the experimentally determined exponent. The above expression can then be generalized to consider the effects of combined static loading and cyclic loading, hence:

$$d\rho = A\sigma^n dt + B\sigma^m dN \tag{4.32}$$

where t is the time to failure for static loading.

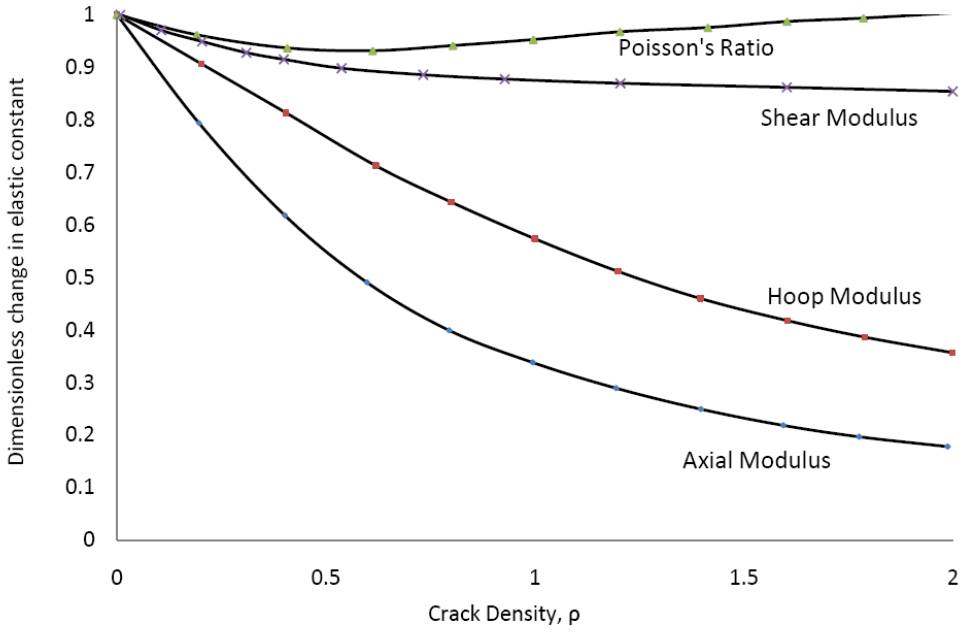

Figure 4.3: Dimensionless change in elastic constants against crack density for an angle ply pipe laminate, calculated from the model of Gudmundson and Zhang.

Interestingly, the form of crack growth law in equation (4.32) is similar and can be treated as analogous to the Miner's law sum in equation (4.29). This can now be used to relate crack growth to the damage accumulation rule previously derived from the modified Miner's law. Comparing the two power law equations, the *m* and *n* exponent constants in equation (4.32) are now equivalent to 1/J and 1/G in equation (4.29). It is now possible to model the stress-strain response in the UEWS test from the degradation of elastic properties caused by progressive matrix cracking. As mentioned before, it is usual in the UEWS test to measure either axial or hoop strain during the application of the hydrostatic pressure cycles. For cases in which axial strain are measured:

$$\varepsilon_A = \frac{\sigma_H}{2E_A} - \nu_{HA}\frac{\sigma_H}{E_H} = \frac{\sigma_H}{E_A}\left(0.5 - \nu_{AH}\right) \tag{4.33}$$

and when hoop strain is measured;

$$\varepsilon_H = \frac{\sigma_H}{E_H} - \nu_{AH}\frac{\sigma_H}{2E_A} = \frac{\sigma_H}{E_H}\left(1 - 0.5\nu_{HA}\right) \tag{4.34}$$

Rearranging equations (4.33) and (4.34) gives:

$$E_A^{UEWS} = \sigma_H / \varepsilon_A = \frac{E_A}{0.5 - \nu_{AH}} \tag{4.35}$$

and

$$E_H^{UEWS} = \sigma_H / \varepsilon_H = \frac{E_H}{1 - 0.5\,\nu_{HA}} \tag{4.36}$$

where E_A^{UEWS} and E_H^{UEWS} are defined as the UEWS effective modulus of elasticity. Using the actual data received from FPI for their Wavistrong GRE pipe range, the above UEWS quantities in the undamaged state are calculated to be 95.8GPa and 28.2GPa respectively.

Again, by using the results from Gudmundson and Zhang, the dimensionless change in the 'hydrostatic/axial modulus' (the hoop stress divided by the axial strain) and the 'hydrostatic/ hoop modulus' (the hoop stress divided by the hoop strain) with increasing crack density were calculated and these are plotted in Figure 4.4. According to the plot, E_A^{UEWS} is shown to be the most responsive to an increase in crack density, declining almost linearly at first before becoming non-linear after crack density reaches about 0.5. This is probably the main rationale for axial strain measurement being preferable to hoop strain measurement during UEWS tests, since axial strain is more sensitive to increments in crack density. E_H^{UEWS}, on the other hand, although affected, declined merely in a linear fashion with increases in crack density. From the plot, provided that the critical value of crack density is taken to be less than 0.5, both quantities can be described by the following linear approximations:

$$\frac{E_A^{UEWS}}{E_{A_0}^{UEWS}} = 1 - 1.66\rho \tag{4.37}$$

and

$$\frac{E_H^{UEWS}}{E_{H_0}^{UEWS}} = 1 - 0.16\rho \tag{4.38}$$

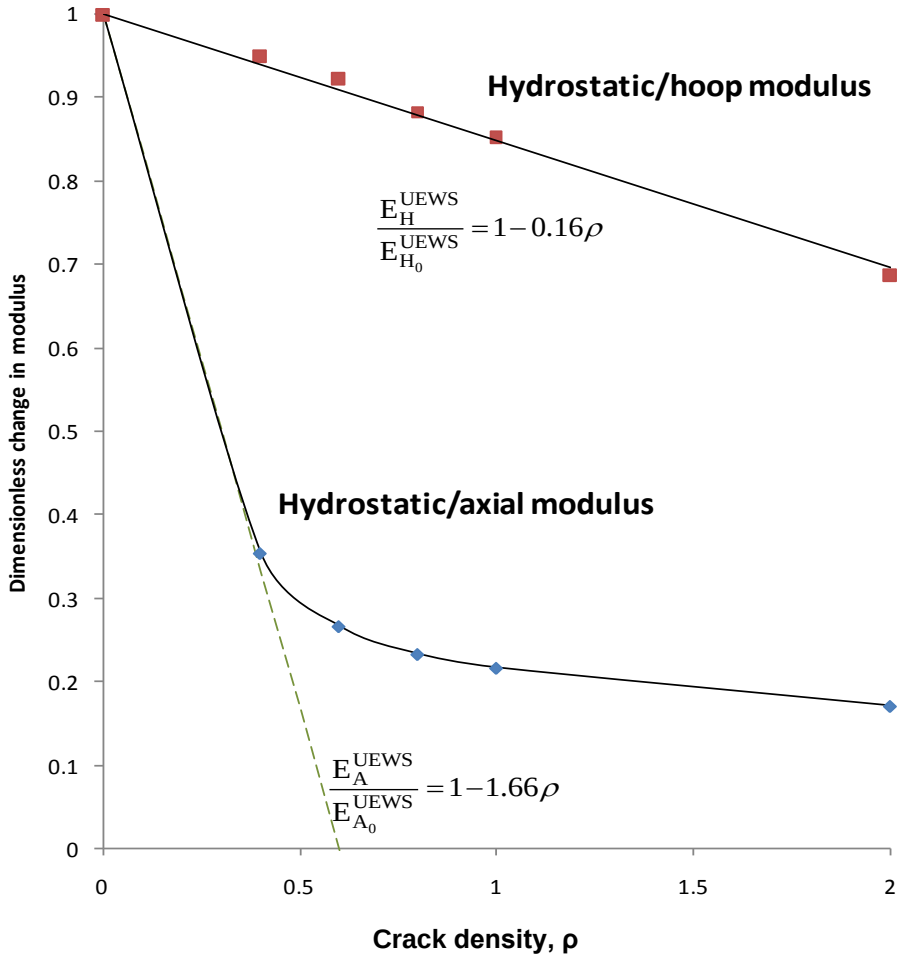

Figure 4.4: Dimensionless change in the 'hydrostatic/axial modulus' (the hoop stress divided by the axial strain) and the 'hydrostatic/hoop modulus' (the hoop stress divided by the hoop strain) with increasing crack density.

To relate the crack density growth to the damage accumulation law from Miner's law in the UEWS test, equation (4.30) can now be expressed in the following form:

$$\Phi = k\rho \tag{4.39}$$

Hence, substituting equation (4.39) into equation (4.37) provides the expression for the change in elastic properties which can now be directly related to the Miner's Law sum, so that:

$$\frac{E_A^{UEWS}}{E_{A_0}^{UEWS}} = 1 - 1.66\frac{\Phi}{k} \tag{4.40}$$

By varying the *k* value to fit the UEWS experimental results, the Miner's Law-based stress-strain response in the UEWS test can be plotted as shown in Figure 4.5. This is then repeated for the 65°C and 95°C tests using the regression constants from FPI's qualification tests at those temperatures. The plots at elevated temperatures are expected to give similar curves as shown below, showing an almost initial linear strain response but starting to deviate from linearity at different points. Figure 4.6 gives the flow diagram for the UEWS strain response modelling described.

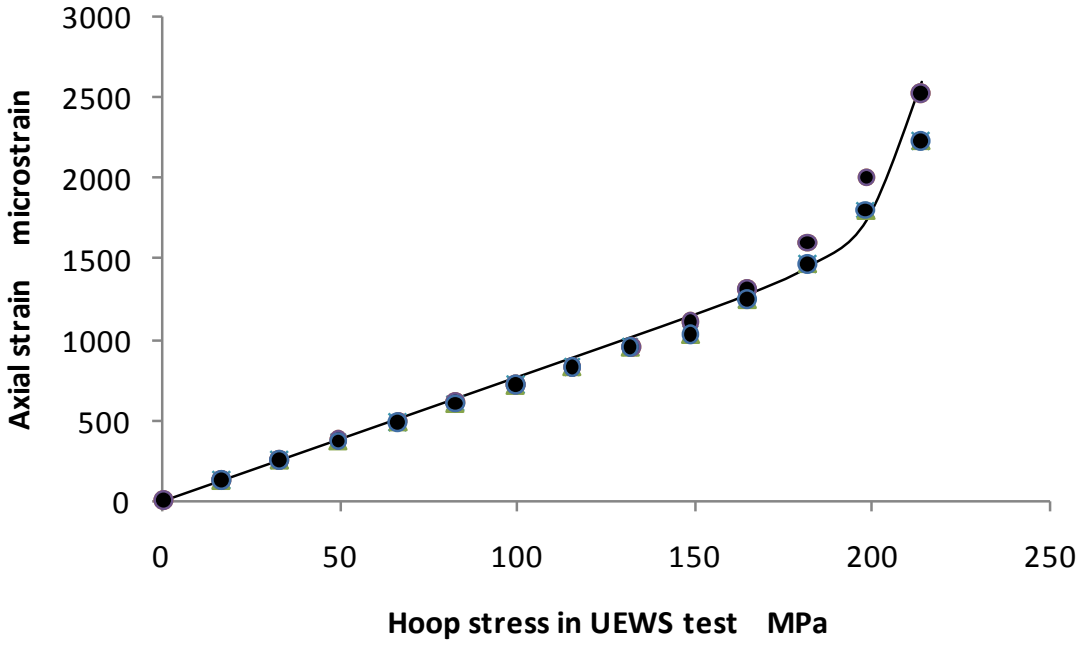

Figure 4.5: Miner's Law-based simulation of the strain response in UEWS testing.

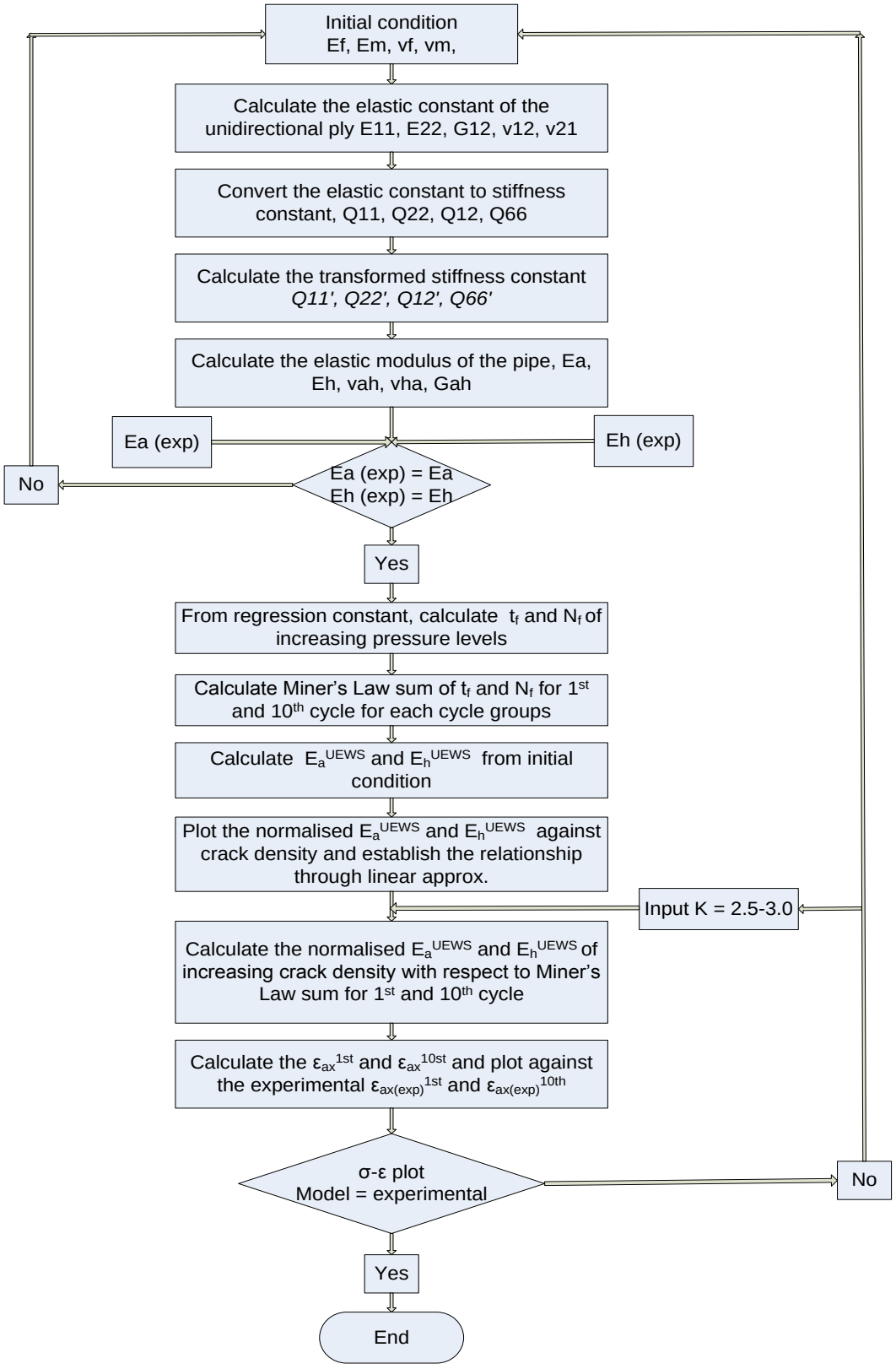

Figure 4.6: Flowchart of the Miner's law modelling for predicting the strain response in UEWS testing

4.4. General lifetime damage model for GRE pipe

During the initial period of cyclic fatigue in the UEWS test, many non-interactive cracks occur in the matrix phase of the laminate. Since the ply is restricted by plies of different orientations above and beneath it, cracks once initiated would at first start to propagate within each ply, before reaching the adjacent plies. This implies that the initiation of these cracks governed by the stress state in the ply.

In order to model the interactive combination of stresses in the ply that cause microcracking damage, a polynomial expression similar to the well known Tsai Hill criterion is used. Tsai Hill's criterion [191] is based on the Von Mises distortional energy criterion which was modified by Hill so as to satisfy anisotropic materials and was subsequently applied to composite materials by Tsai. For orthotropic materials similar to GRE pipes, the criterion may be expressed as:

$$\sqrt{\left(\frac{\sigma_1^2}{\sigma_1^{*2}}\right)+\left(\frac{\sigma_2^2}{\sigma_2^{*2}}\right)+k_1\sigma_1\sigma_2+k_2\sigma_2\tau_{12}+\left(\frac{\tau_{12}^2}{\tau_{12}^{*2}}\right)}=\Phi \tag{4.41}$$

where the subscripts, 1, 2, and 12 indicate, respectively, tensile stresses parallel and transverse to the direction of the composite ply, and shear stress. The starred terms refer to stresses at failure. k_1 and k_2 are parameters appointed that describe the importance of the interactions between the two tensile stresses and between σ_2 and τ_{12} respectively. According to this criterion, no failure will occur provided that Φ is less than unity. This particular failure criterion was chosen due to its ease of use and most importantly take into account the effects of interactions between the stress components.

The effect of the stress developed in each ply can then be expressed in terms of the axial and hoop pipe wall stresses. This can be achieved by substituting the general transformation matrix from equation (4.7) into equation (4.41):

$$\begin{pmatrix}\sigma_1\\ \sigma_2\\ \tau_{12}\end{pmatrix}=[T]\begin{pmatrix}\sigma_{axial}\\ \sigma_{hoop}\\ \tau_{ax/hp}\end{pmatrix}=\begin{pmatrix}\cos^2\theta & \sin^2\theta & 2\sin\theta\cos\theta\\ \sin^2\theta & \cos^2\theta & -2\sin\theta\cos\theta\\ -\sin\theta\cos\theta & \sin\theta\cos\theta & \cos^2\theta-\sin^2\theta\end{pmatrix}\begin{pmatrix}\sigma_{axial}\\ \sigma_{hoop}\\ \tau_{ax/hp}\end{pmatrix} \quad (4.42)$$

As a result, the detrimental effects of all stresses can be expressed in a single quadratic relationship. Since the original equation (4.41) included all the stresses acting on the ply that could govern the initial damage to the system, a lifetime behaviour model for GRE pipes under various combinations of axial to hoop stress can be developed. The quadratic relationship is then solved to produce limits in terms of axial and hoop stress which can then be presented in the form of a failure envelope.

CHAPTER 5: TEST RESULTS AND DISCUSSION

Experimental and modelling findings throughout the investigation are reported and discussed in this chapter. In Section 5.1, the laminate elastic properties of GRE pipes are calculated using laminate theory and are compared with the engineering data provided by the manufacturer. The experimentally determined degradation in elastic properties of the pipes taken from different stages of the UEWS tests and the model's predictions are discussed in Section 5.2. The results of UEWS tests under various ratios of hoop to axial stress ranging from pure axial loading to intermediate, 2:1 loading, to pure hoop loading are described and discussed in Section 5.3. Here, the current definition of UEWS employed by FPI is reviewed. In Section 5.4, the failure modes observed are categorised and discussed at length. The UEWS and weepage based failure envelopes are presented in Section 5.5 and the importance of these envelopes for judging the long term performance of GRE pipes are discussed. Section 5.6 presents the acoustic data gathered and interpretations of the failure mechanisms involved, whilst Section 5.7 analyzes the results of the microscopic study. Finally, the modelled stress-strain responses of UEWS tests and the general lifetime model are presented and compared with the experimental findings in Section 5.8.

5.1. Determination of the pipe's properties

The properties of the isotropic glass fibre reinforcement and epoxy matrix provided by FPI for their Wavistrong product are given below:

E_{glass} =73 GPa, E_{matrix} =3.6 GPa,
V_{glass} =0.59, V_{matrix} =0.41

Based on these values, the ply properties were calculated using the rules of mixture and the Halpin Tsai simplification from equations (4.1) to (4.4). The results are as follows:

$$E_1 = 44.55 \text{ GPa}$$
$$E_2 = 12.20 \text{ GPa}$$
$$\nu_{12} = 0.28$$
$$G_{12} = 4.33 \text{ GPa}$$

The elastic properties of the pipe wall in the axial and hoop directions of the pipes were then computed using laminate theory, as detailed in chapter four using equations (4.5) to (4.10). Hence:

$$E_{axial} = 11.52 \text{ GPa}$$
$$E_{hoop} = 19.70 \text{ GPa}$$
$$\nu_{axial} = 0.40$$
$$\nu_{hoop} = 0.69$$
$$G_{12} = 11.76 \text{ GPa}$$

Similar to findings in previous work in the literature, the radial component is much lower than the axial and hoop components, and is therefore ignored. For simplification, the resin-rich top coating of the pipes was ignored as a structural element during calculation. Although it may carry a load and adds to the structure its role is, however, thought to be minimal. Table 5.1 shows the comparison between the mechanical properties obtained analytically above, and the experimental values provided by FPI. Overall, the results show acceptable agreement. This indicates that the top coating on the outer surface of the pipe could have only a very minimal effect on the total stiffness of the pipe. Nevertheless, it should be noted that these values are very much dependent on the laminates volume fractions and its constituent's properties. Thus, these properties must be determined experimentally prior to the UEWS tests and after weepage failure as described in the next section.

Table 5.1: Comparison between the measured mechanical properties of the GRE pipes provided for this investigation and the predicted values from laminate theory.

Property	Value from laminate theory	Experimental value by FPI	Difference (%)
Axial modulus, E_{ax}	11.52GPa	11.5GPa	0.2%
Hoop modulus, E_{hp}	19.70GPa	19.0GPa	3.7%
Poisson's ratio, υ_{ah}	0.40	0.38	5.3%
Poisson's ratio, υ_{ha}	0.69	0.65	6.2%
Shear modulus, G_{ah}	11.76GPa	11.0GPa	6.9%

5.2. Determination of the elastic property of tested GRE pipes

The elastic properties of GRE pipes were determined from simple pull and ring tests of the UEWS tested samples as described in Sections 3.7.1 and 3.7.2. The axial and hoop modulus of virgin samples were determined to be 12.7GPa and 18.2GPa respectively. These values showed good agreement with the predicted values computed using laminate theory as indicated in Table 5.1. Figure 5.1 shows the reduction in elastic properties of the ±55º filament wound GRE pipes taken during different stages of the hydrostatic UEWS test at 2:1 hoop to axial loading. It can be seen from the plot that both the axial and hoop modulus of pipe samples taken during the test at 50% and 100% of UEWS and finally after weepage failure was observed, were significantly lower than those in the virgin pipe. The axial modulus appeared to be affected slightly more than the hoop modulus, resulting in a total reduction of over 26% from virgin to weepage samples. The hoop modulus, on the other hand, declined from 18.2GPa for the virgin sample to 14.2GPa at weepage, representing a 22% reduction. As discussed in the literature review, these reductions are largely claimed to be the result of the state of matrix cracking in the laminates.

In Figure 5.2, the test results were then plotted against crack density at the same stages of the UEWS test in order to illustrate the effect of crack density on the degradation of elastic modulus. The crack density was computed from the modelling work described in Section 4.2, which was later correlated with the condition of the samples tested. The plot shows that the axial modulus deteriorates in an almost linear relationship with increments of crack density initially up to the 100% UEWS condition before declines at

higher rates up to weepage. The hoop modulus, on the other hand, declines linearly at first, before the rate of deterioration slows down to reach close to saturation as crack density increases from 100% UEWS condition toward weepage failure. It seems appropriate to conclude that the axial modulus is more sensitive than the hoop modulus to the effects of crack density. This is because the elastic properties in this direction are more strongly influenced by the matrix resin. It was also noted that, with both moduli, the crack density is more than twice as much at the 100% UEWS condition compared to that of the value at 50% UEWS. Critical crack density at which weepage occurred is about 10% higher of the crack density at 100% UEWS. From the model, this was found to be about 0.95. This was then compared with crack density measured through micrograph analysis in Section 5.7.

Figure 5.3 shows the modelled changes in elastic modulus against crack density in GRE pipes subjected to UEWS tests at three different test temperatures: room temperature (RT), 65°C and 95°C. The results were obtained from the crack density modelling based on the work of Roberts [49] as detailed in Section 4.2. For comparison, the experimental results are also included. According to the modelling computation, the axial modulus declined almost linearly for all test temperature conditions, which is in reasonably good agreement with the experimental data obtained earlier. However, somewhat poorer agreement was observed between the predictions and experimentally determined degradations of hoop modulus. From the modelling, the hoop modulus for all test temperatures showed linear degradation with increased crack density. But from experimental finding, the deterioration is slightly exponential with the rate of reduction observed being lower after the UEWS point is reached. The plot also shows that both the axial and hoop modulus at all three test temperatures declined at about the same rate and ceased to deteriorate further once the crack density reached its critical value, at which weepage failure was observed. This implies that, although elevated temperatures may have weakened the pipes leading to a lower magnitude of loads needed to initiate cracks, the critical crack density for 2:1 loading at which first failure was observed remained unchanged.

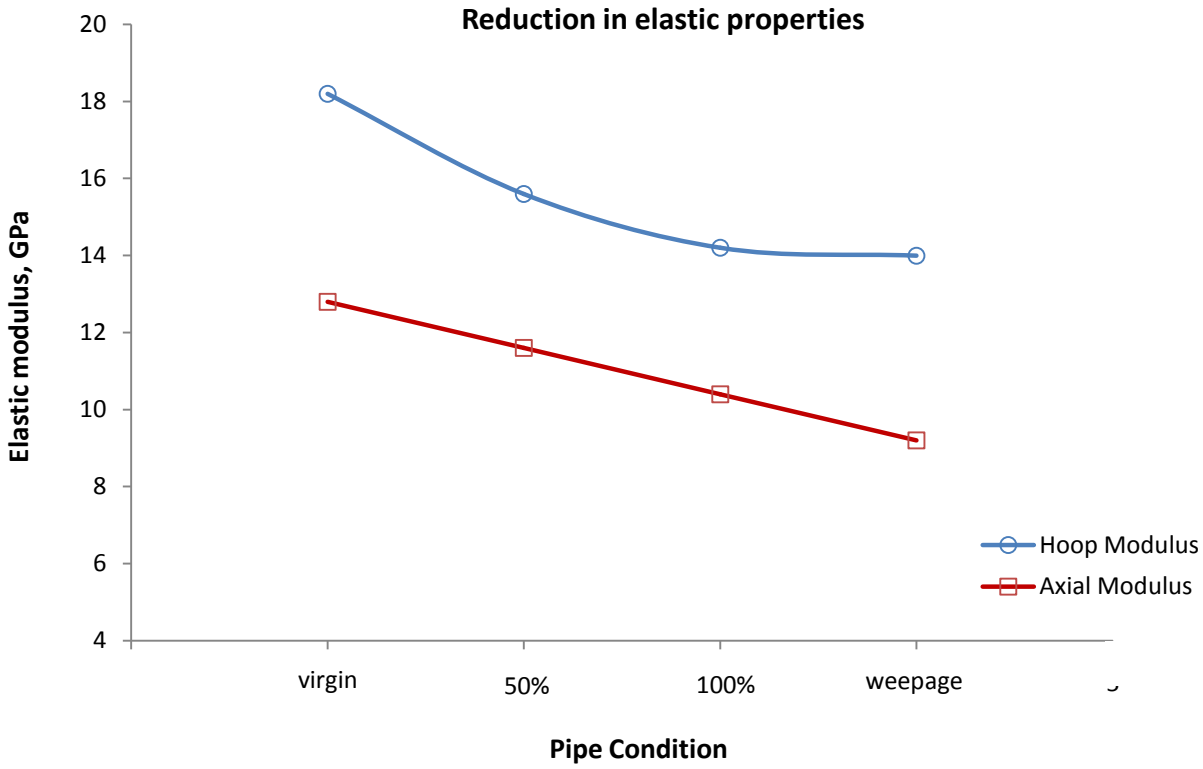

Figure 5.1: Reduction in axial and hoop modulus at different stages of UEWS test.

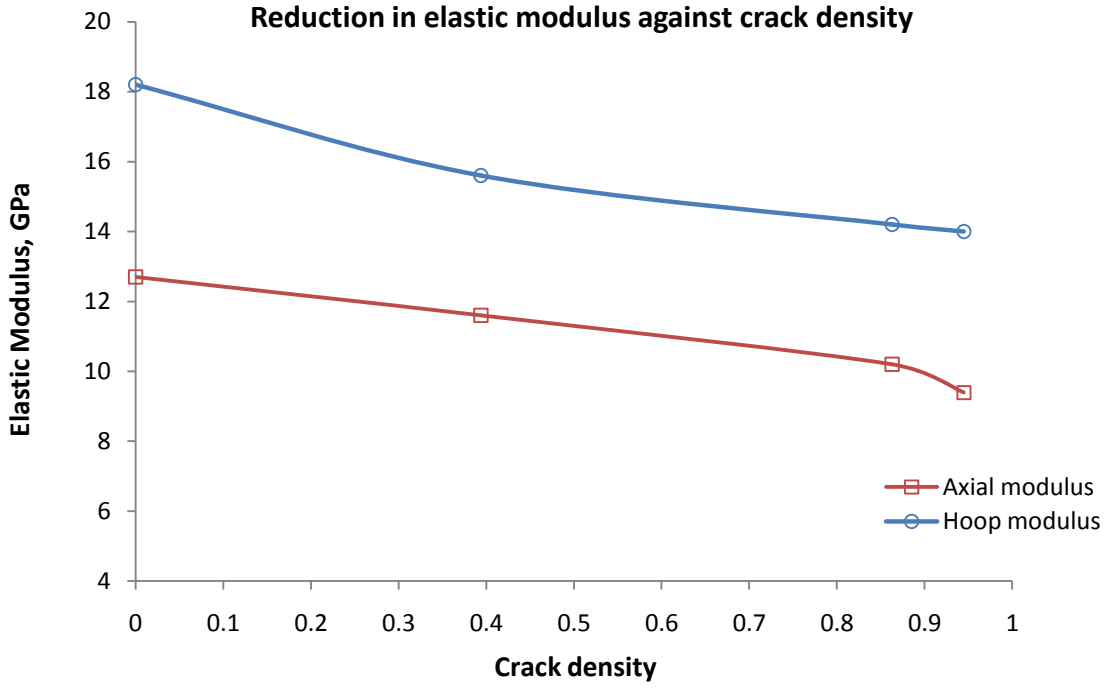

Figure 5.2: Reduction in axial and hoop modulus against crack density

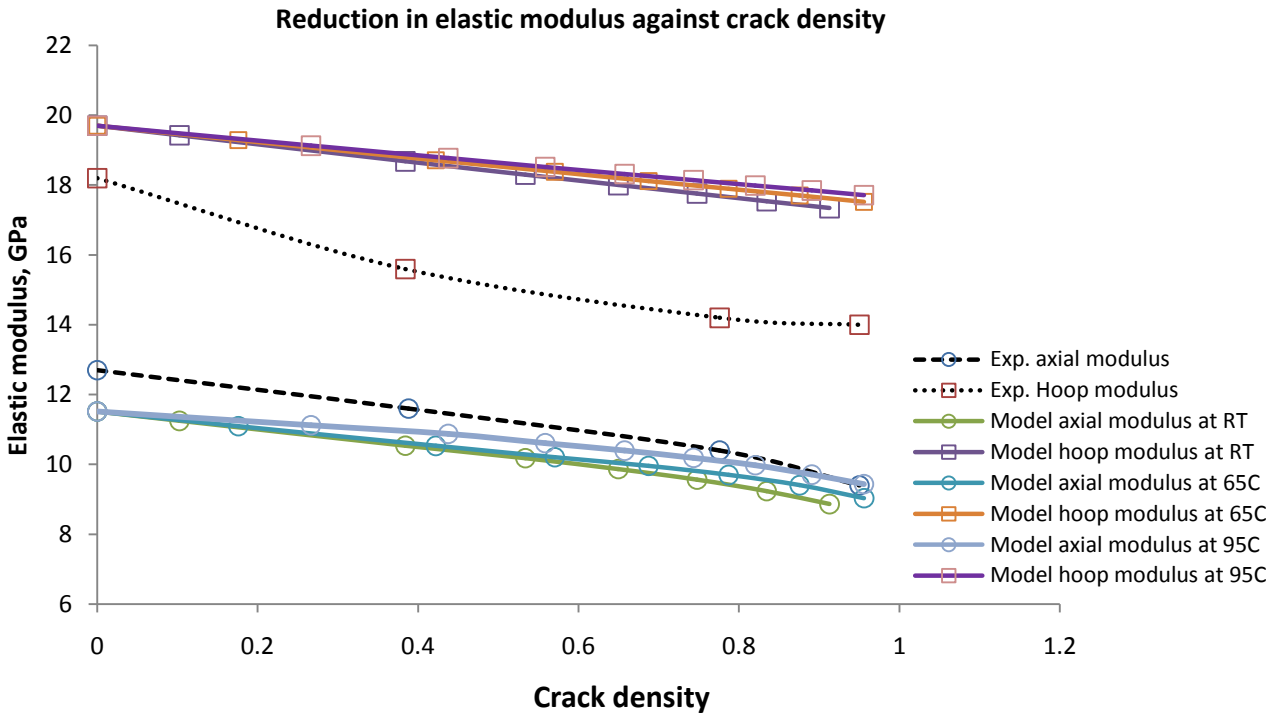

Figure 5.3: Modelling and experimental results showing reduction in elastic modulus against crack density at RT, 65°C and 95°C.

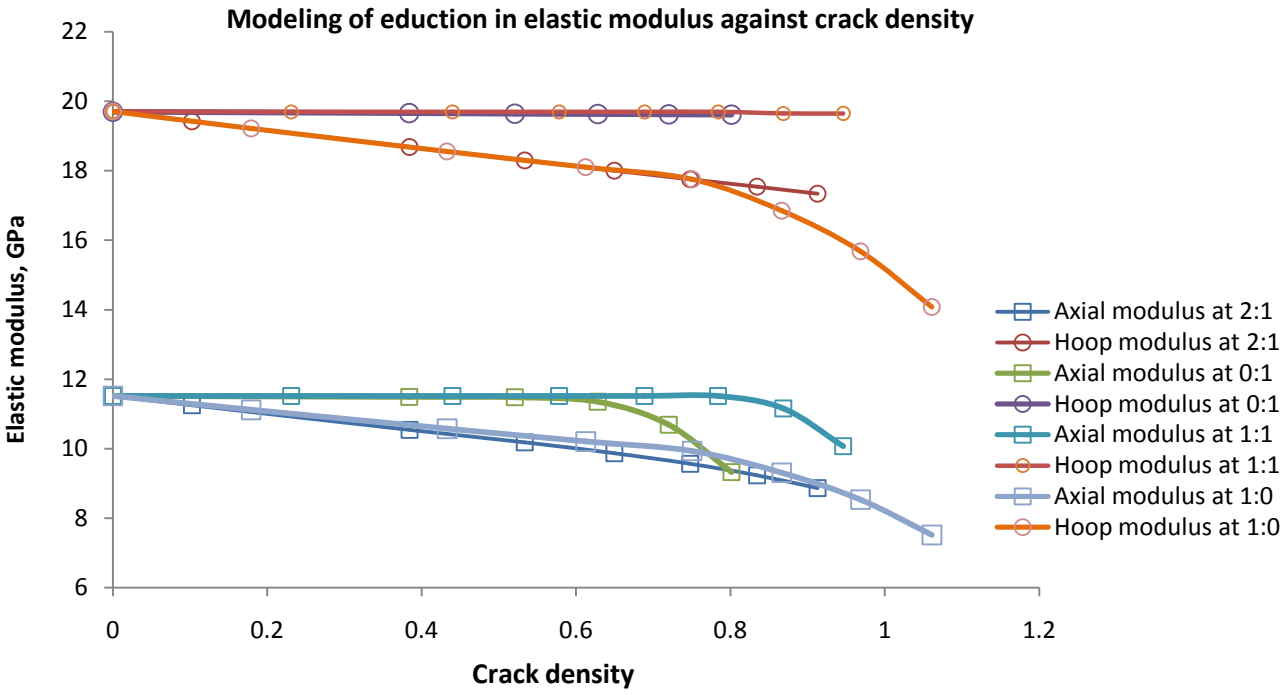

Figure 5.4: Modelling of UEWS tests under various loading conditions showing respective reduction in elastic modulus against crack density.

Figure 5.4 shows the modelled results for the reduction in elastic modulus in UEWS tests under various loading conditions ranging from pure axial loading (0:1) to intermediate 1:1 and 2:1 loadings, to pure hoop loading (1:0) at RT. It can be seen that the moduli decrease at different rates in different test conditions with increases in crack density. Since the degradation in properties is due to matrix cracks, this strongly implies that loading conditions very much influence the initiation of cracks and subsequently rates of deterioration.

The plot indicates that, in hydrostatic loading of 2:1 stress ratio, the hoop modulus degraded linearly with increases in crack density but almost unaffected in the axial dominated loadings of 0:1 and 1:1. The axial modulus on the other hand, declined almost at a similar rate initially before exhibiting a rapid decline at different rates with only small increments of crack density. This is because in these types of loading the load is strongly dominated by the resin matrix. Once transverse matrix cracking is initiated, it propagates through the pipe wall rapidly, and shortly after series of cracks coalesce, weepage failure occurs. Furthermore, it is interesting to note that the weepage failure in pure axial loading was observed at much lower levels of crack density than in any other test conditions. The reason for this is that in this loading most of the load now acts transversely to the direction of the fibres, hence rapidly precipitating the initiation and propagation of cracks up to the critical value of crack density.

Pure hoop loading exhibited the largest decline in the axial and hoop modulus from 11.52GPa to 7.52GPa and 19.70GPa to 14.10GPa respectively. This corresponds to a reduction of 35% in axial modulus and over 28% in hoop modulus. In this loading condition, the hoop modulus shows similar trends to the deterioration in axial modulus, indicating a sharp decline after small increments in crack density. In fact, this is the only loading condition where such decline in hoop modulus is observed compared to other loadings, which declined linearly with increases in crack density. This is because crack density in other loading conditions is controlled by transverse stress. However, in pure hoop loading, relatively low transverse stress was generated to cause fibre-resin debonding. In contrast, higher shear stress developed between adjacent plies. This is

believed to have caused delamination and hence cracks between the plies due to the shear deformation of the matrix material.

5.3. UEWS stress-strain response

In this section, the results of the UEWS tests conducted at various hoop to axial loading ratios are presented and discussed. The stress-strain responses of each loading condition are plotted in the manner detailed in Section 3.5.3. All tests also showed similar plot trends with an initially almost linear response followed by very distinctly non-linear responses at higher strains, particularly in the last two or three cycle groups. It was observed that stress-strain response is strongly dependent on the stress ratios and test temperatures applied.

However, before continuing with the analysis of the stress-strain data to identify the UEWS point, one has to make sure that the original definition provided by FPI is applicable to all stress ratio conditions. This is because, as mentioned before, the current procedure for identifying the UEWS point seems to apply only in pure hydrostatic loading creating 2:1 hoop to the axial stress ratio. It has been shown that, for this loading condition, the stress-strain response in the early cycle groups is very linear and the onset of damage or the UEWS point is considered to be reached once it starts to deviate and become non-linear. A similar response was recorded in the 2:1 loading tests conducted in this investigation, and hence the original definition can be applied in these circumstances.

However, general observations of other stress ratio loadings have indicated that stress-strain responses in the early stages of UEWS testing may not be so linear, and instead suggest a slightly curved profile. This could be due to the viscoelastic properties of the pipe or the effects of either residual stress or the non-linearity of properties of the matrix material [96]. This implies that the original definition of the UEWS point, taken from the interception of the linear and non-linear line in the stress-strain curve, may now not be suitable. Furthermore, there have been some criticisms of this method since

the non-linear line drawn in the original definition is never actually a straight line even for the 2:1 loading condition.

Another issue is raised in the hoop dominated loadings (4:1 and 1:0). In addition to the early non-linearity observed, the strain response history illustrated in Figures 5.9(d) and 5.10(d) also indicates that the pipes had been permanently deformed from the early stage of the tests and not only after the UEWS had been reached. The critical question, however, remains whether or not this deformation induced the growth of damage causing the failure of the pipe. The original definition of the UEWS used for hydrostatic loading, may now be inapplicable in this case. It is of great importance that the current definition used for identifying the exact UEWS point is adequately redefined for application at various stress ratios. After a number of brainstorming sessions with FPI engineers, a consensus was reached that the UEWS point in this investigation should now be redefined as the point at which the difference in strain between the first and the tenth cycle from a cycle group exceeded 3%, as given below:

$$\left(\frac{\varepsilon_{10_i}}{\varepsilon_{1_i}} \right) \geq 1.03 \tag{5.1}$$

where ε_{1i} and ε_{10i} are the maximum strains at the end of the first and the last cycle of cycle group i respectively.

5.3.1. UEWS test at 2:1 hoop to axial stress ratio

Figure 5.5 (a-c) shows the 1st and 10th stress-strain responses for the pressure cycle groups of the UEWS tests conducted under 2:1 hoop to axial loading at RT, 65°C and 95°C. All three sets of test results exhibited initial linear relationship between the measured axial strain and hoop stress. The strain measurements at the first and tenth cycles in each pressure group were virtually the same, which indicates that the deformation up to this point was elastic and no creep was involved. However, as the UEWS point was approached, deviations in strain can be seen between the first and

tenth cycles of the group and hence its relationship with hoop stress became non-linear. This non-linearity in the stress–strain relationship indicates the onset of ply damage in the pipe believed to result from transverse matrix cracks developing within the ply, thus causing a reduction in pipe stiffness. As the load is further increased, the non-linearity in the stress-strain relationship becomes more pronounced. This signifies the growth of damage which subsequently reaches the threshold level leading to weepage failure. A creaking sound of increasing frequency was clearly audible during this stage of testing, which corresponds to the cracking process that was taking place.

Using the new definition, the UEWS points were identified as 200MPa at RT and 210-215MPa at 65°C and 95°C. Weepage failure, on the other hand, was recorded at 220MPa for RT and 240MPa for the tests at elevated temperatures. The UEWS strain at RT was observed to be approximately 0.16%, whereas for elevated temperatures the strain was slightly higher at 0.2%. Maximum axial strain to failure for all three temperature conditions was found to be in the range between 0.22-0.26%. The 2:1 hoop to axial loading is considered to be the ideal loading condition for ±55° wound pipe, since the loads in the principal direction of the laminates are fibre dominated. At higher temperatures, it is suspected that the matrix material become more ductile, hence resulting in increases in strength and UEWS strain.

Figure 5.5(d) shows the axial and hoop strain responses throughout the 2:1 loading of UEWS test at RT. Both showed positive strain responses, with recorded hoop strains being significantly greater in magnitude. Similar responses were also obtained for the tests at 65°C and 95°C. From the plot, a non-linear response of axial strain was observed from the 8^{th} cycle group onwards, whereas an almost unnoticeable change was noted in the hoop strain measurement. A clearer tendency was noted in the 9^{th} cycle group, where axial strains showed a pronounced non-linear response between the 1^{st} and 10^{th} cycle compared to that in the hoop direction. This is due to the orthotropic nature of the pipe, which resulted in a varying strength threshold in the different directions in the pipe. For this reason, the measurement of axial strain is always preferable to hoop strain, especially in axial dominated UEWS tests.

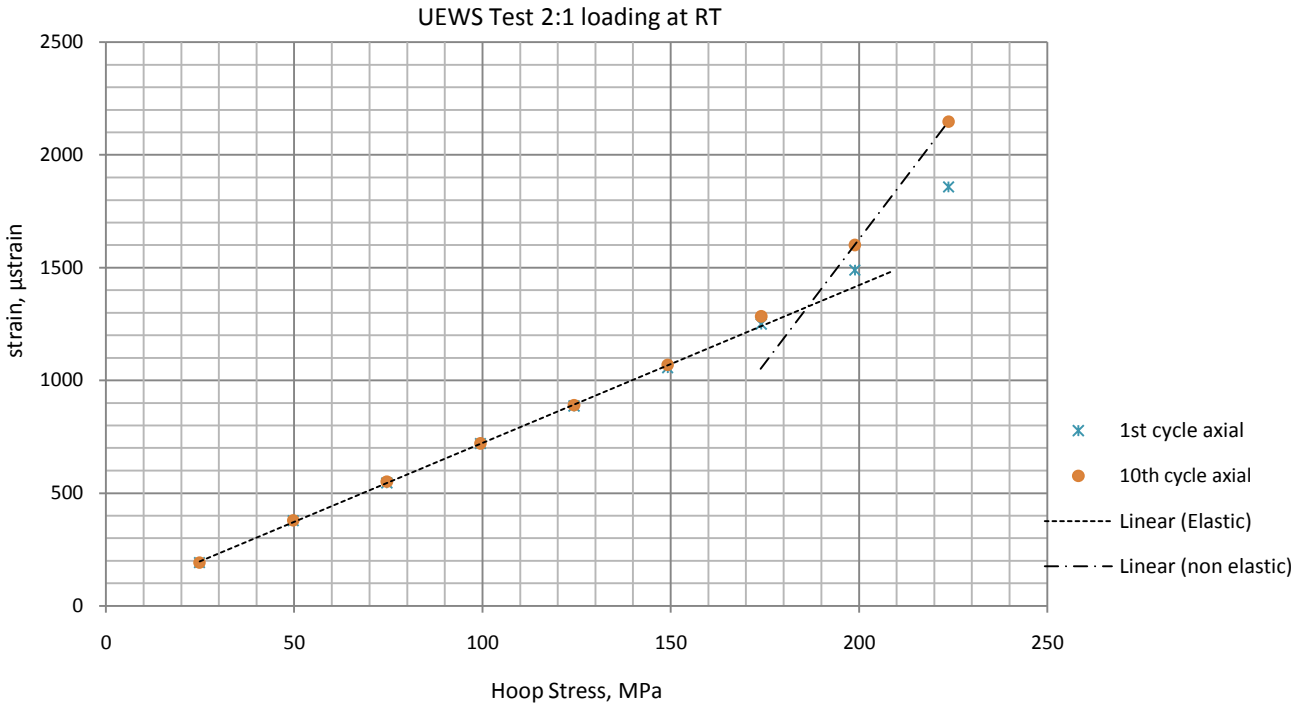
UEWS Test 2:1 loading at RT
strain, µstrain
Hoop Stress, MPa
0
500
1000
1500
2000
2500
0
50
100
150
200
250
1st cycle axial
10th cycle axial
Linear (Elastic)
Linear (non elastic)

(a)

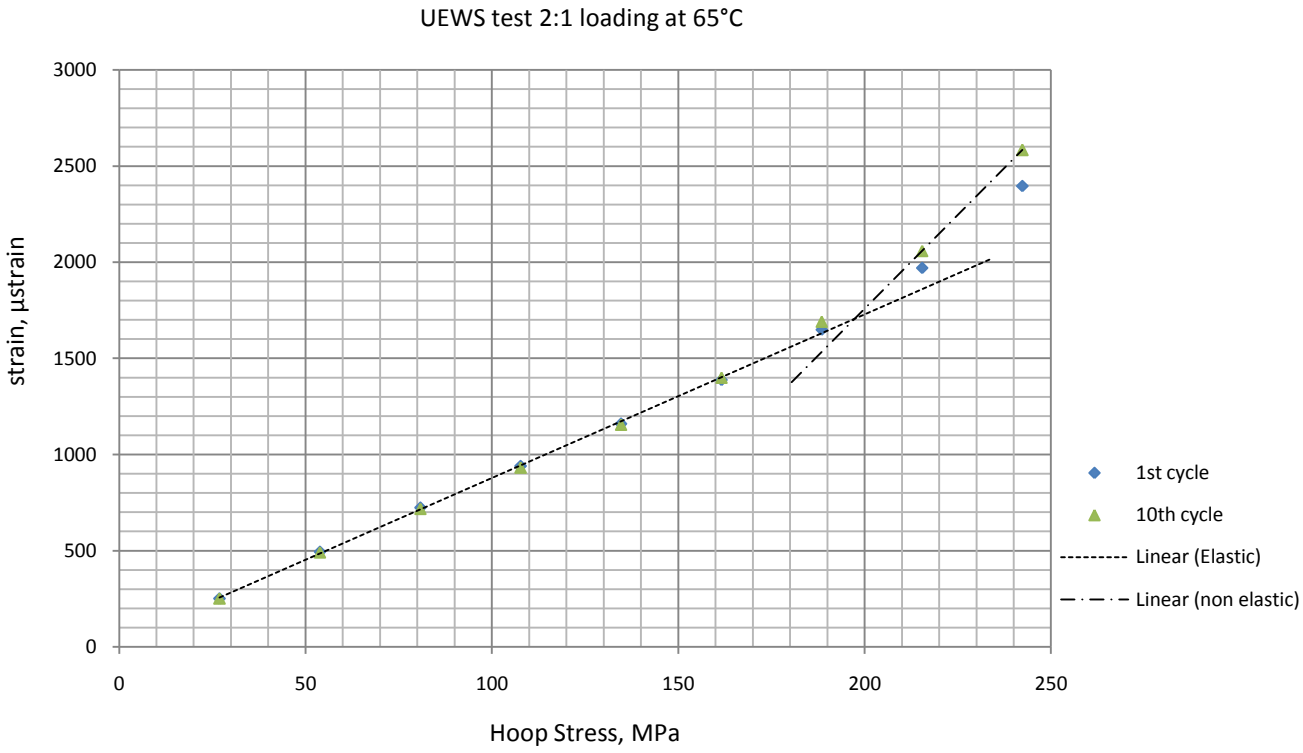
UEWS test 2:1 loading at 65°C
strain, µstrain
Hoop Stress, MPa
0
500
1000
1500
2000
2500
3000
0
50
100
150
200
250
1st cycle
10th cycle
Linear (Elastic)
Linear (non elastic)

(b)

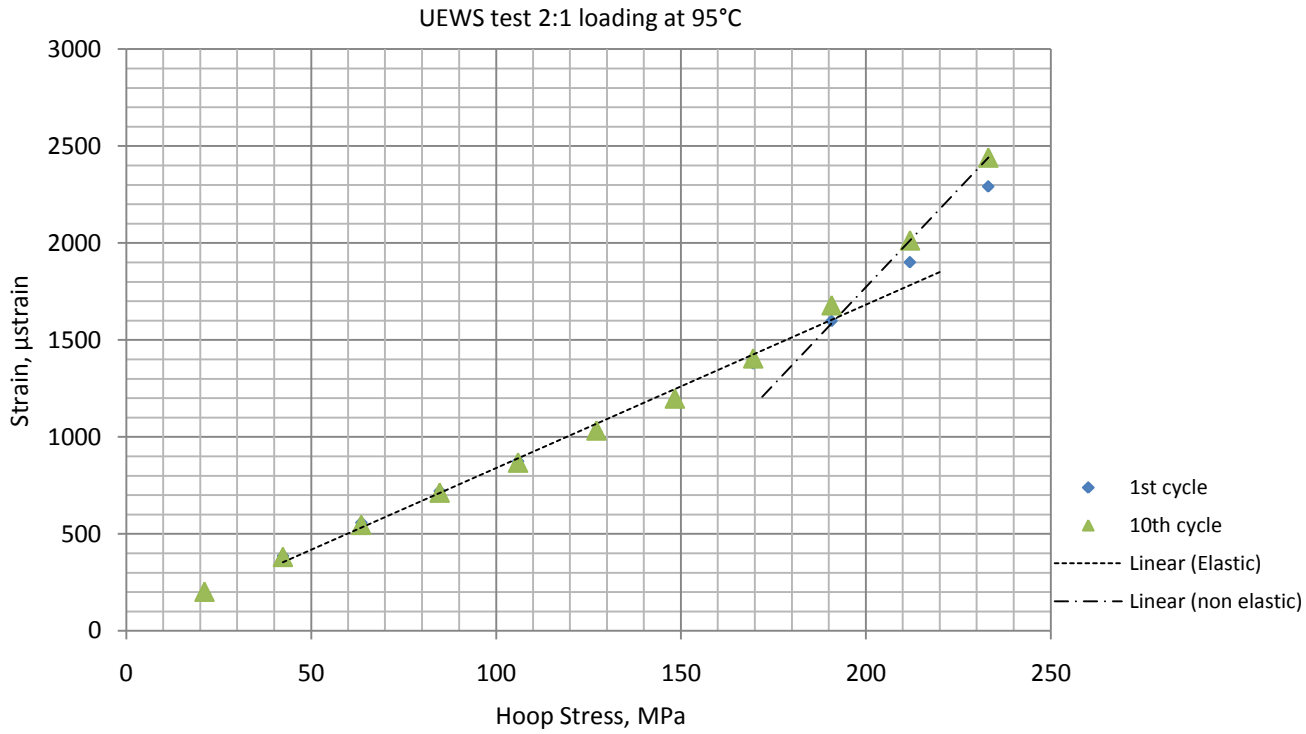

(c)

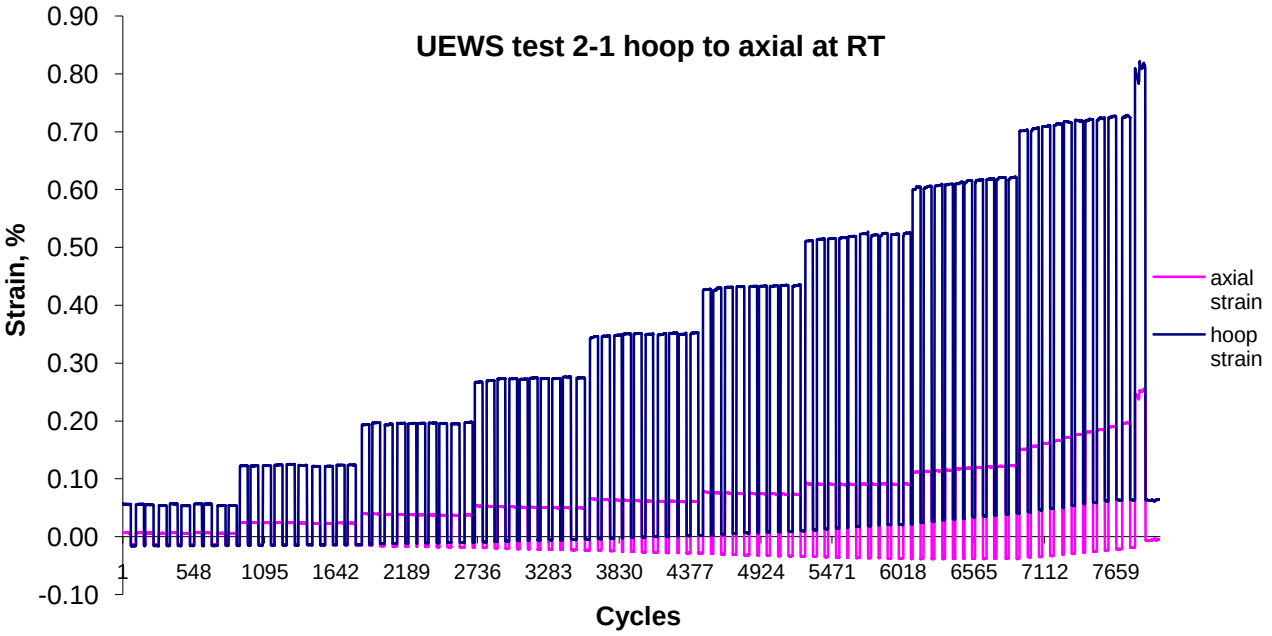

(d)

Figure 5.5: 1st and 10th cycle stress-strain plots of 2:1 UEWS tests at (a) RT, (b) 65°C, (c) 95°C and (d) strain history responses for test at RT.

5.3.2. UEWS test at 1:1 hoop to axial stress ratio

Figure 5.6(a-c) shows the UEWS plots for 1:1 hoop to axial loadings tested at RT, 65°C and 95°C, and Figure 5.6(d) exhibits the axial strain history throughout the 95°C test. Similar trends to those in the 2:1 tests were observed, with the stress–strain responses tending to be almost linear in the early stages of the test followed by very distinct non-linear behaviour once the UEWS had been reached.

In this loading condition, the UEWS points were identified at 88MPa, 78MPa and 74MPa of hoop stress for RT, 65°C and 95°C respectively. These results were much lower than those observed in the 2:1 tests, yielding over 50% reduction at all three test temperatures. This is because in this loading condition, the load was highly dominated by the matrix with less transformation along the direction of the fibres. This subsequently induced much higher strains in the weaker matrix, and hence the lower UEWS point can be attributed to the initiation of transverse matrix cracks in the pipe wall. Weepage failure for the test at RT was observed close to 100MPa, whereas at elevated temperatures failure was recorded at reduced strength between 82-85MPa.

Contrary to the results obtained for 2:1 loadings, where the strength increased at higher temperatures, the pipes at 1:1 loadings exhibited considerable reductions in the UEWS and failure strength. Previous work by Hale *et al* [28] suggested that the strength of the epoxy matrix, which was the same as used in GRE pipes tested here, suffered significant degradation in high temperature environments. Since this load is matrix dominated, the critical limiting strength at which matrix cracks started to initiate was reduced at higher temperatures, resulting in the reduced UEWS and failure strength.

The effects of high temperature also included reductions in the UEWS strain and the maximum strain to weepage failure. The UEWS strain was recorded at roughly 0.48% for the test at RT, 0.46% at 65°C and 0.42% at 95°C, representing a total reduction of about 12%. Strain to failure in the 10^{th} cycle showed a significant decrease, from 0.62% at RT to 0.58% and 0.5% respectively at the elevated temperatures of 65°C and 95°C due to the softened and hence weakened matrix.

Figure 5.6 (d) shows the strain history responses taken from the 1:1 loading UEWS test at 95°C. Only axial strain was measured for this loading and a positive response was recorded throughout. According to the plot, the UEWS clearly occurred in the 10th cycle group where non-linearity was clearly observed between the 1st and the 10th cycle. Permanent deformation was observed once the UEWS was surpassed, indicating the rapid progressive damage that occurred immediately before weepage failure. The strain history responses recorded for the UEWS tests at RT and 65°C yielded similar trends.

5.3.3. UEWS test at 0.5:1 hoop to axial stress ratio

Figure 5.7(a-c) shows the stress-strain response of UEWS tests conducted at the 0.5:1 loading ratio for RT, 65°C and 95°C respectively, and Figure 5.7(d) demonstrate the axial strain history plot for the 95°C test. All three test plots registered almost linear responses in early cycle groups followed by evident non-linearity after the 8th or 9th cycle group after which the UEWS was identified. The UEWS points for this loading were noted at 38MPa, 32MPa and 28MPa of hoop stress for RT, 65°C and 95°C respectively whilst the failure strengths were recorded at 42MPa, 35MPa and 31MPa. The results indicate a huge reduction in the UEWS and failure strength with less than one-fifth of the strength of the ideal 2:1 loading. Similar to the situation in the 1:1 UEWS tests, this is because the loading is highly matrix dominated. A higher strain was hence generated in the matrix leading to the initiation of transverse matrix cracking in the pipe wall which resulted in the reduced UEWS and failure strength. With regards to the effects of elevated temperatures up to 95°C, the results show that both the UEWS and failure strength decreased by more than 26%. The UEWS strain, on the other hand, was found to decrease from 0.53% at RT to 0.5% at 65°C and 0.46% at 95°C.

Figure 5.7(d) shows the axial strain history for the 95°C tests. Little difference in strain responses between the 1st and the 10th cycle was observed during the early cycle groups, indicating almost linear behaviour. However, a considerable difference was noted in the 9th cycle group between the strains in the 1st and the 10th cycle, suggesting the onset of non-linearity here, which is in good agreement with the UEWS point identified earlier. Plastic deformation was observed from the 10th cycle group onwards after the UEWS point had been reached. The strain histories for RT and 65°C exhibited similar trends.

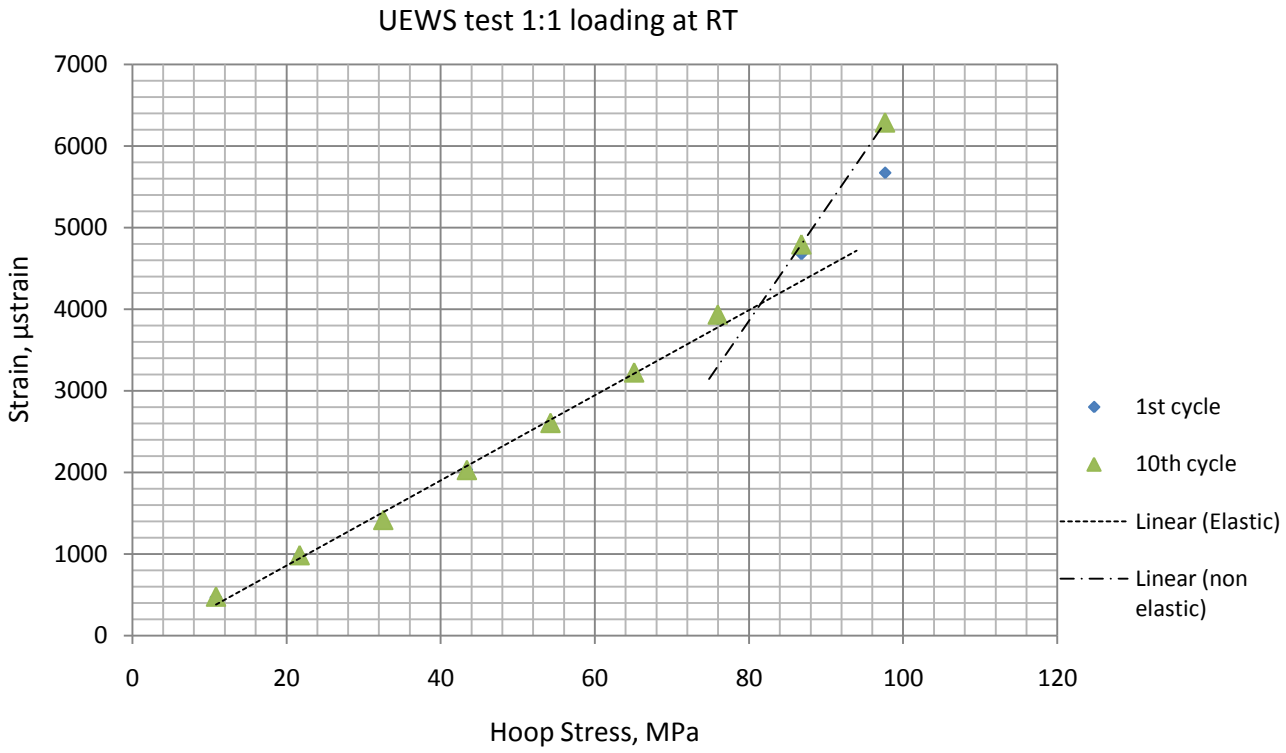
UEWS test 1:1 loading at RT
Strain, µstrain
Hoop Stress, MPa
0
1000
2000
3000
4000
5000
6000
7000
0
20
40
60
80
100
120
1st cycle
10th cycle
Linear (Elastic)
Linear (non elastic)

(a)

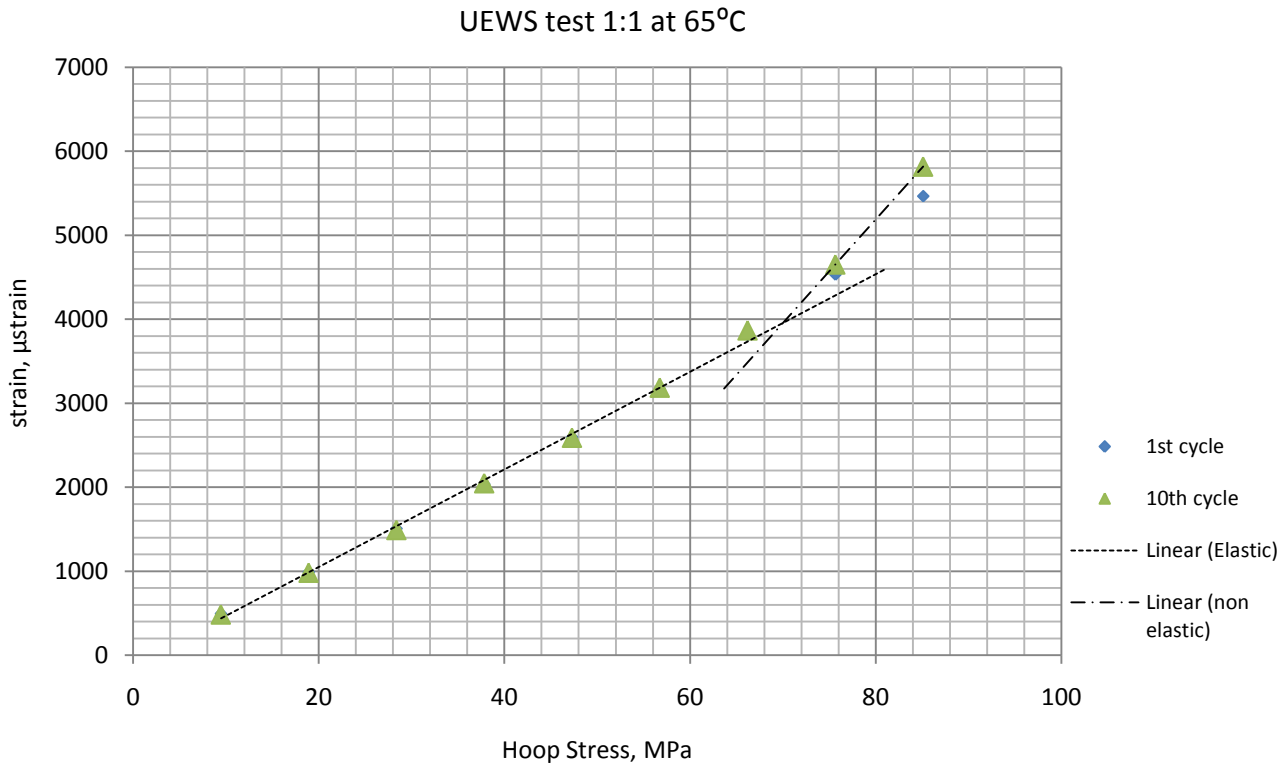
UEWS test 1:1 at 65°C
strain, µstrain
Hoop Stress, MPa
0
1000
2000
3000
4000
5000
6000
7000
0
20
40
60
80
100
1st cycle
10th cycle
Linear (Elastic)
Linear (non elastic)

(b)

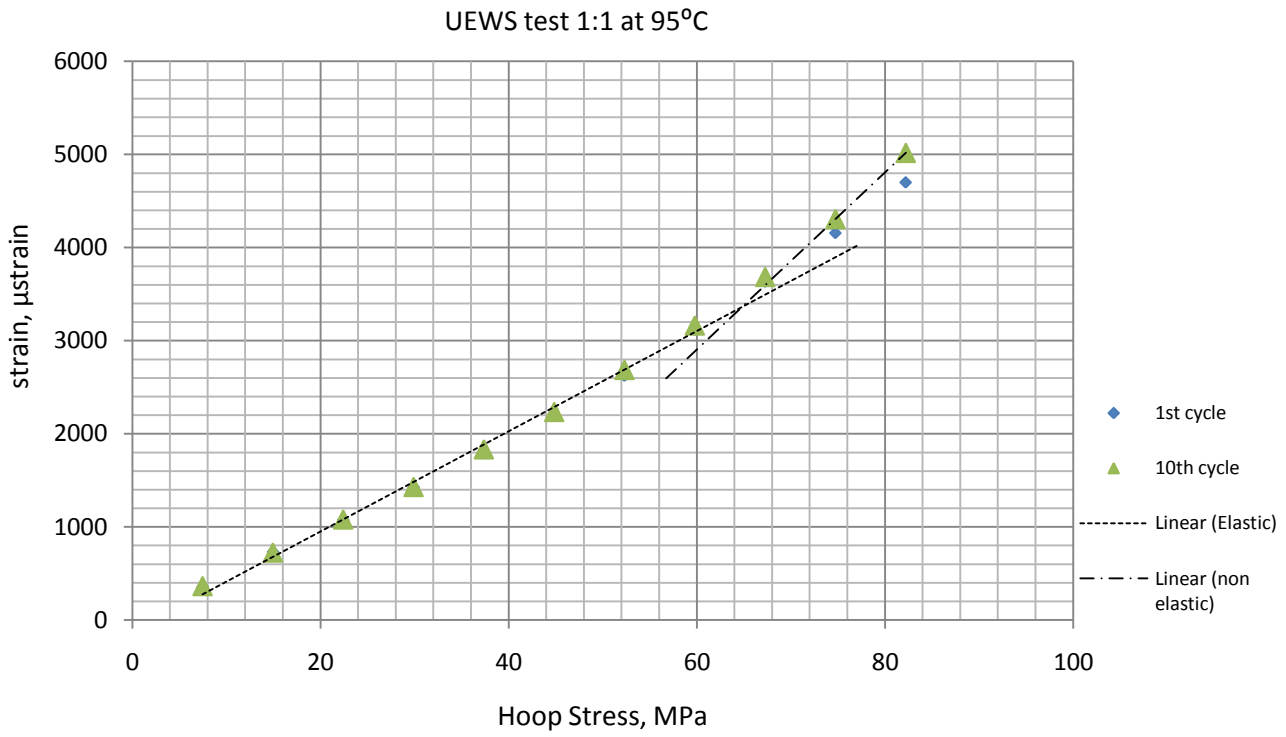

(c)

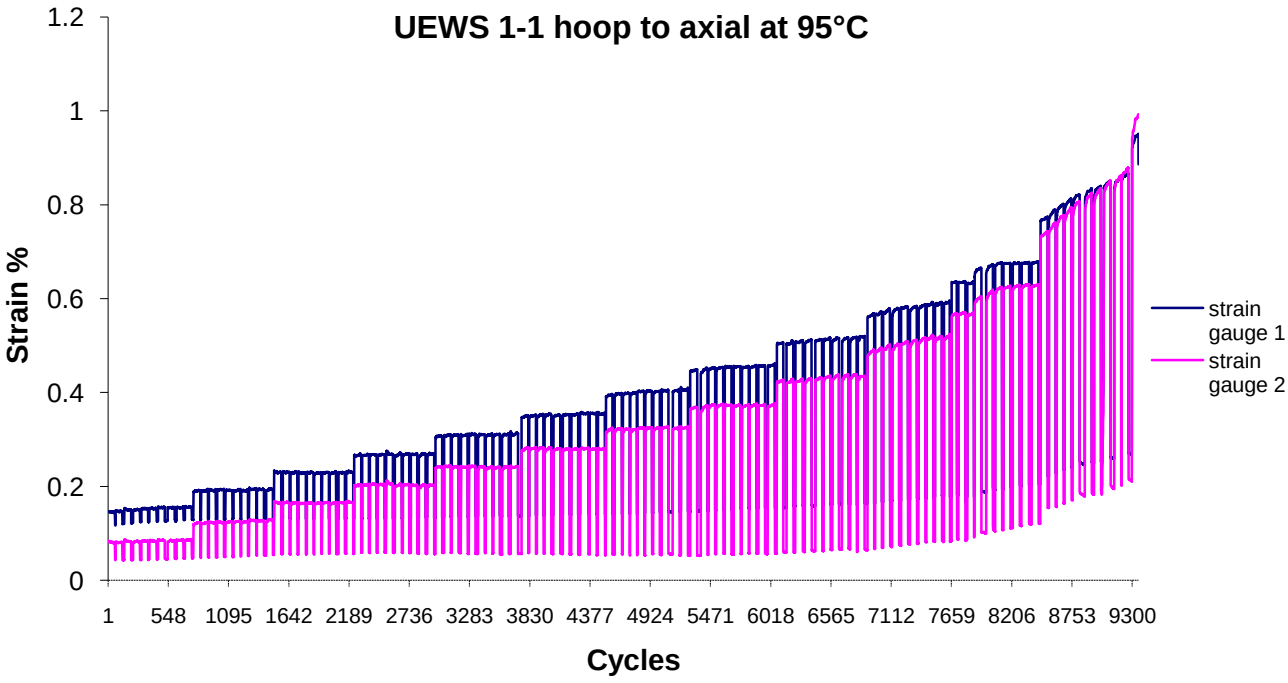

(d)

Figure 5.6: 1st and 10th cycle stress-strain plots of 1:1 UEWS tests at (a) RT, (b) 65°C, (c) 95°C and (d) strain history responses for test at 95°C.

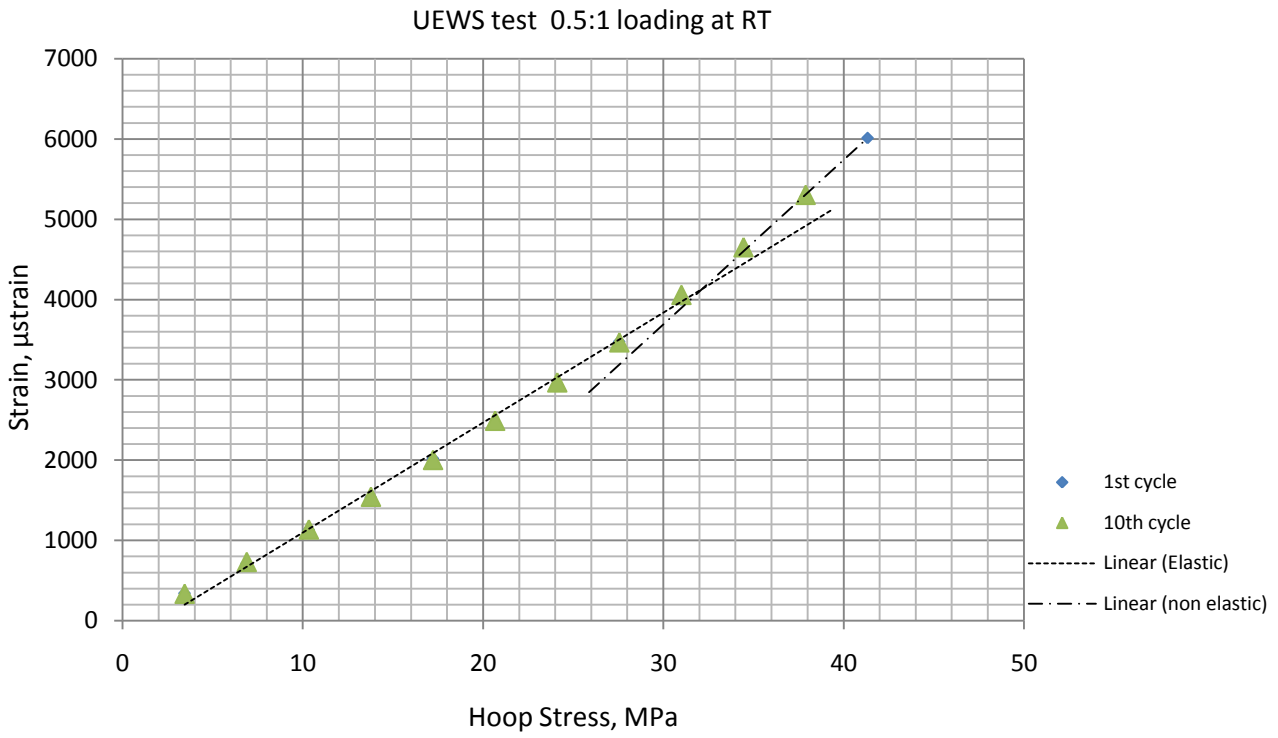
UEWS test 0.5:1 loading at RT
Strain, µstrain
Hoop Stress, MPa
0
1000
2000
3000
4000
5000
6000
7000
0
10
20
30
40
50
1st cycle
10th cycle
Linear (Elastic)
Linear (non elastic)

(a)

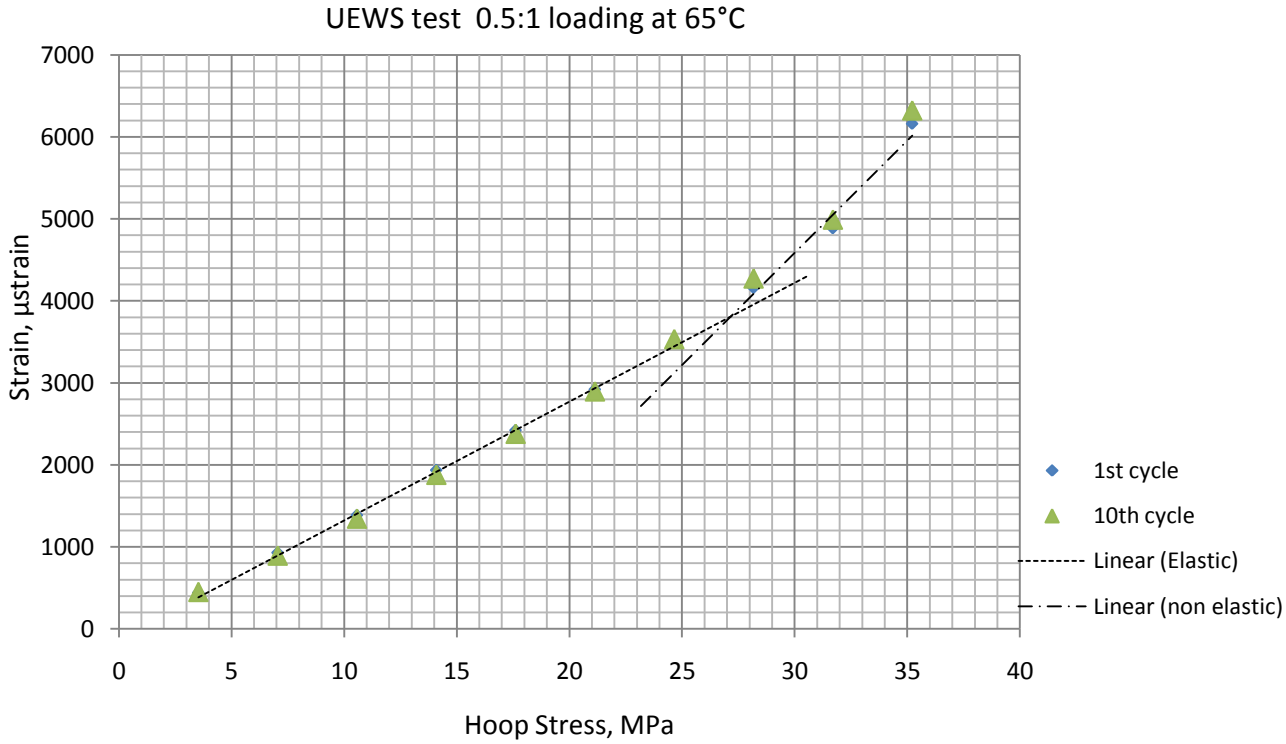
UEWS test 0.5:1 loading at 65°C
Strain, µstrain
Hoop Stress, MPa
0
1000
2000
3000
4000
5000
6000
7000
0
5
10
15
20
25
30
35
40
1st cycle
10th cycle
Linear (Elastic)
Linear (non elastic)

(b)

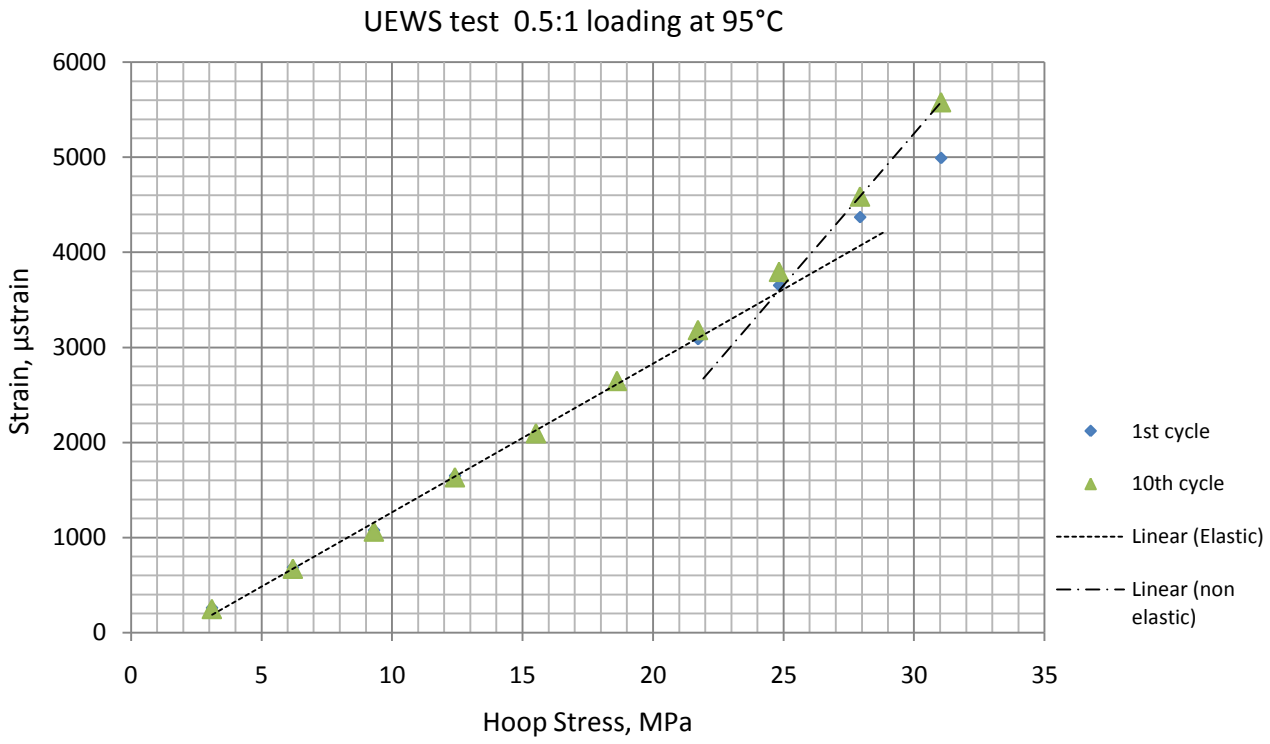

(c)

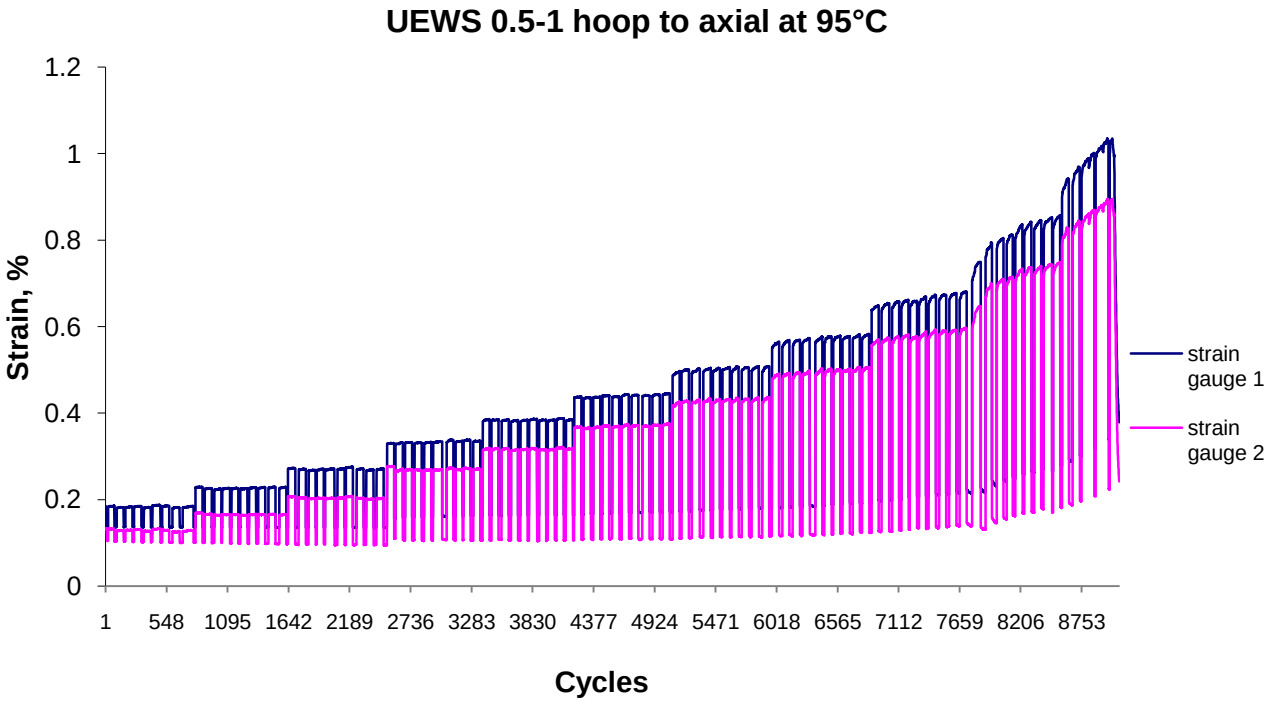

(d)

Figure 5.7: 1st and 10th cycle stress-strain plots of 1:1 UEWS tests at (a) RT, (b) 65°C, (c) 95°C and (d) strain history responses for test at 95°C.

5.3.4. UEWS test at 0:1 hoop to axial stress ratio (pure axial loading)

Figure 5.8 (a-c) presents the stress-strain plots for pure axial loading (0:1) of the UEWS tests conducted at RT, 65°C and 95°C. Similar trends to those in the previous test results were obtained, with the effects of axial loading becoming more pronounced since no hoop stress was applied to the pipe wall. All plots registered fairly linear responses in the early cycle groups, followed by tangible non-linear behaviour later. The UEWS points for the test at RT, 65°C and 95°C were identified as 63MPa, 48MPa and 43MPa of axial stress respectively, whereas failure strengths were recorded at 68MPa, 55MPa and 48MPa. As with the results for 1:1 and 0.5:1 loadings, the UEWS points and failure strengths exhibited significant reductions with increases in temperature. The test at 65°C registered a decline in UEWS strength of almost 24%, whereas at 95°C it was more substantial at 32%. The results were also comparatively much lower than those observed in the previous loading conditions, especially in the 2:1 loading at RT, where UEWS axial strength was now 37% lower. This was very much to be expected, since the load in this test was so strongly dominated by the weaker matrix.

The plots also show that the values of maximum strain to failure in the tests at RT, 65°C and 95°C were 0.87%, 0.82% and 0.76% respectively, yielding a total reduction of nearly 13%. However, it is important to note that the failure strains registered in these plots refer to strains at final rupture rather than the weepage failure as seen in previous loadings. Since there was no pressure applied in the main chamber of the pipe to achieve pure axial loading, the pipe was loaded until it ruptured. This explains the considerable increase in the failure strain recorded compared to those observed in the 2:1 and 1:1 loadings. Figure 5.8(d), shows the axial strain history response of the test at 95°C. Although small differences in strain exist in the earlier cycle groups, more significant increases in strain between the 1st cycle and 10th cycle were observed in the 9th cycle group. The difference in strain then becomes much more pronounced in the following two cycle groups, suggesting the rapid progression of damage. Furthermore, plastic deformation was also noted in the plot in the final stages of the test, which confirms the damage progression process. The strain histories recorded at RT and 65°C also yielded similar responses.

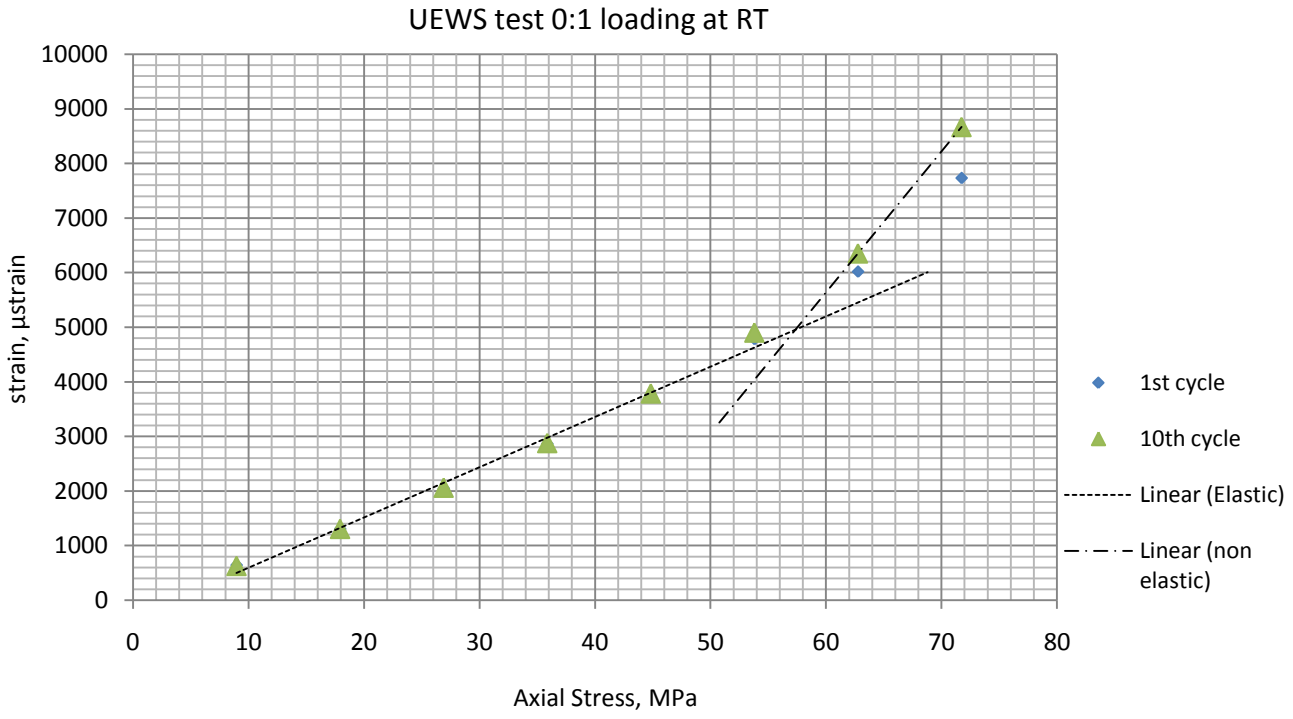
UEWS test 0:1 loading at RT
strain, µstrain
Axial Stress, MPa
1st cycle
10th cycle
Linear (Elastic)
Linear (non elastic)

(a)

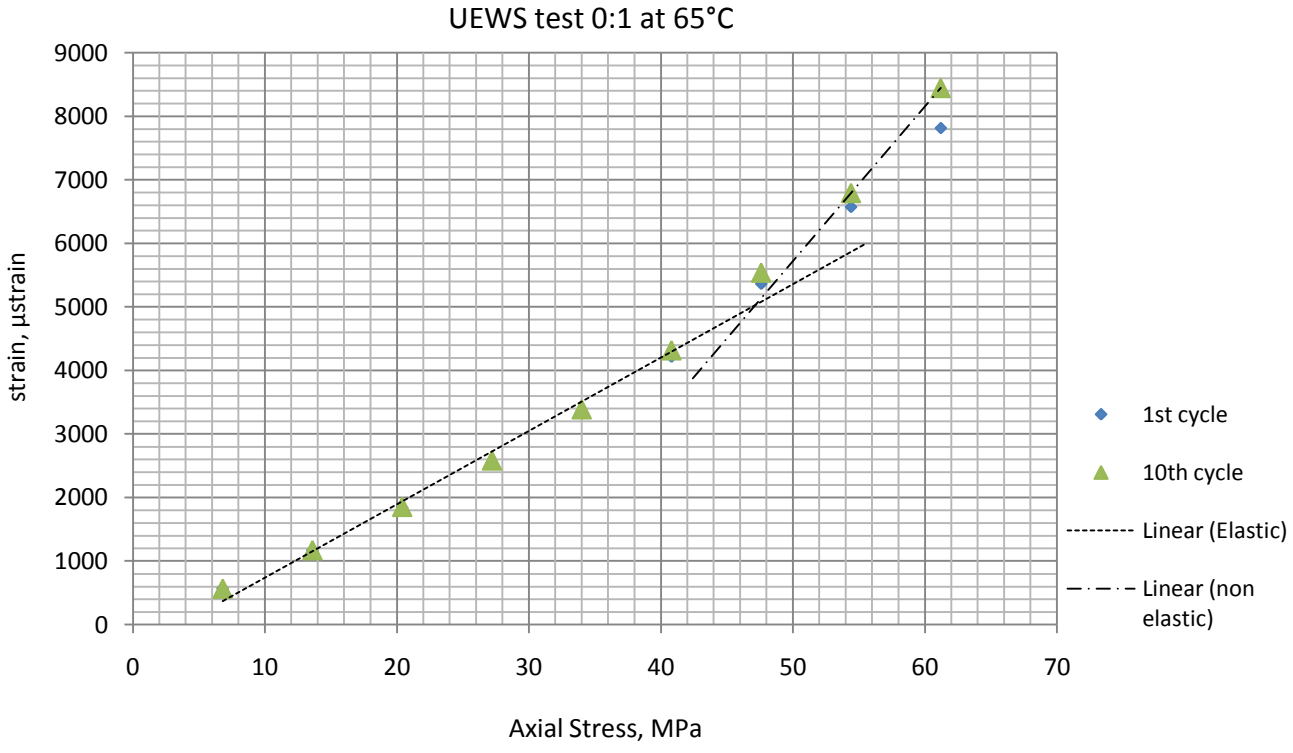
UEWS test 0:1 at 65°C
strain, µstrain
Axial Stress, MPa
1st cycle
10th cycle
Linear (Elastic)
Linear (non elastic)

(b)

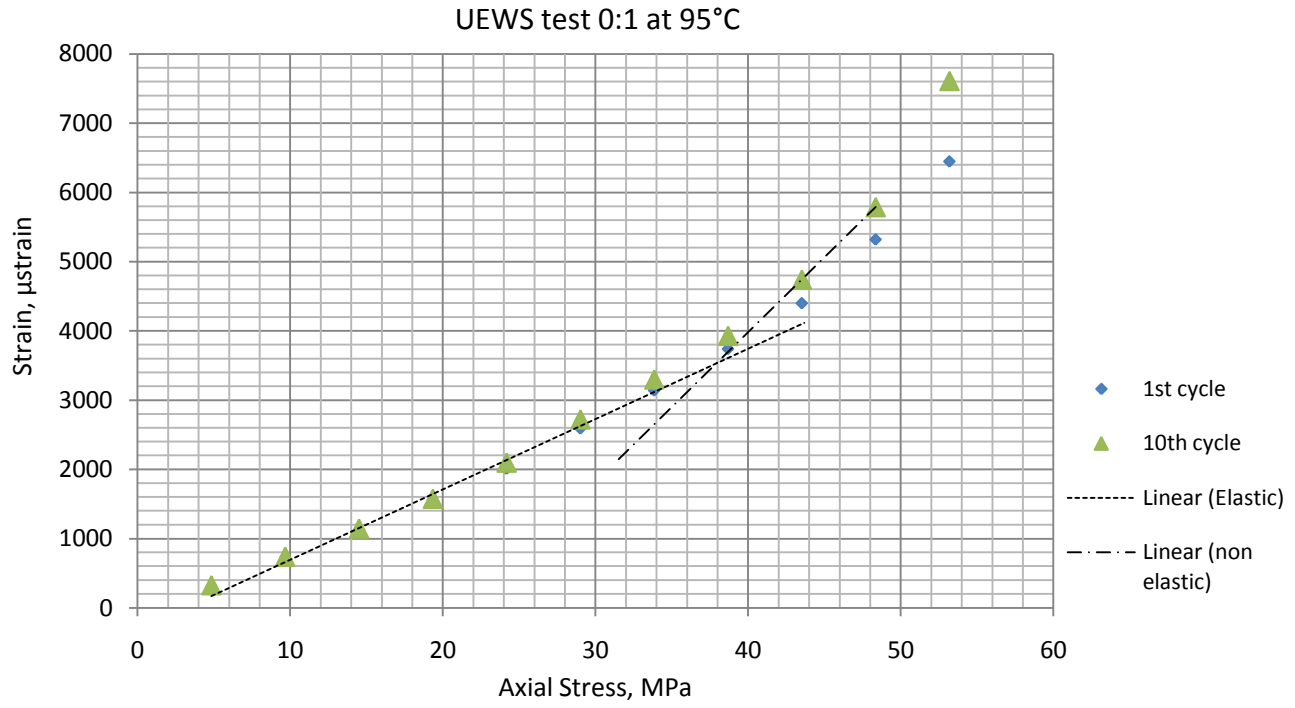

(c)

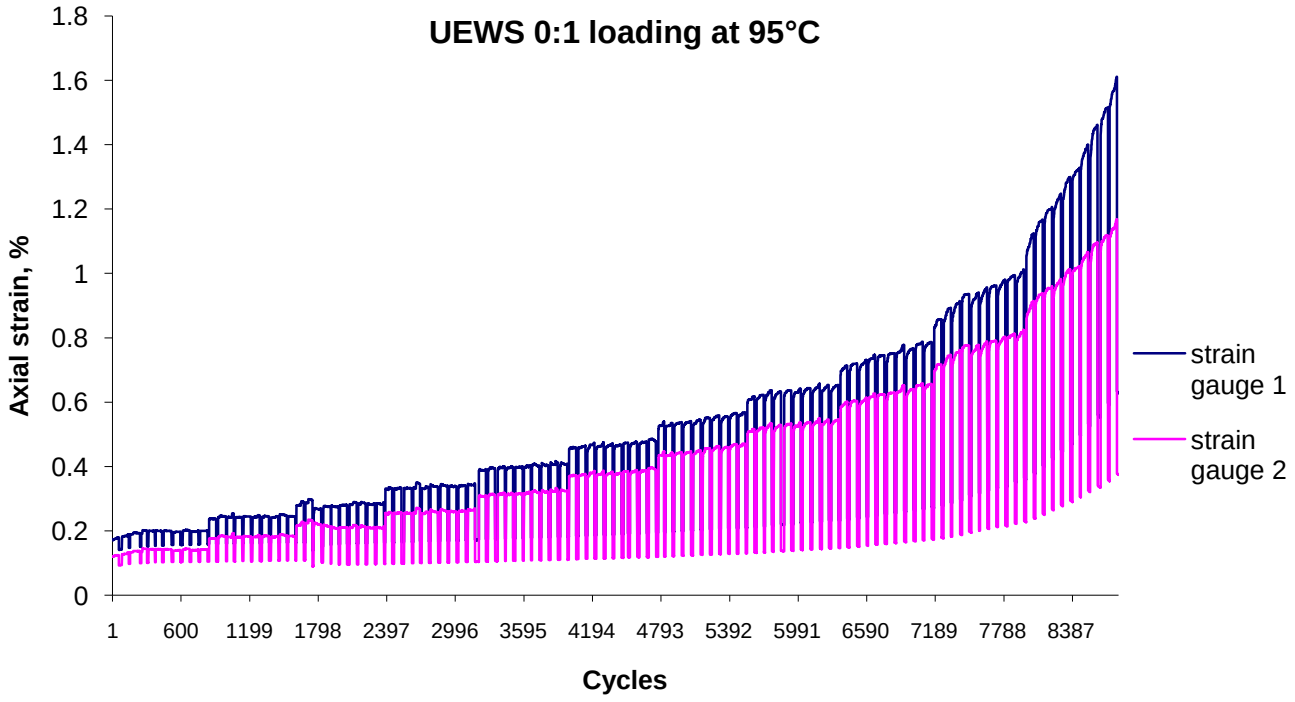

(d)

Figure 5.8: 1st and 10th cycle stress-strain plots of 0:1 UEWS tests at (a) RT, (b) 65°C, (c) 95°C and (d) strain history responses for test at 95°C.

5.3.5. UEWS test at 4:1 hoop to axial stress ratio

The stress-strain plots for the UEWS tests under the 4:1 hoop to axial loading ratio conducted at RT, 65°C and 95°C are shown in Figure 5.9 (a-c). Although showing similar trends as those in the axial dominated loadings, the UEWS points and failure strengths were observed at a considerably higher hoop stress levels. From the plots, the UEWS points at RT, 65°C and 95°C were identified at 375MPa, 345MPa and 290MPa respectively, with failure strengths at 410MPa, 380MPa and 320MPa. This finding indicates that a ±55° wound GRE pipe can support much larger internal pressures in hoop dominated loadings.

Analysis of the effects of increased temperature on UEWS and failure strength shows massive reductions in both, yielding a decline of approximately 22% from the RT to 95°C tests. Furthermore, the failure strains for all tests were registered at nearly 2%. This indicates that, although the UEWS was reached at a lower stress level in the high temperature tests, the strain to failure remained unaffected. This is because, in hoop dominated loadings, leakage failure is due to the combined effects of transverse cracks and shear deformations in the resin matrix. At higher temperatures however, the resin matrix becomes softened, and hence is able to withstand larger shear strains before cracking takes place.

Figure 5.9(d) illustrates the strain history response of the UEWS test at 95°C, showing a positive hoop strain response and a negative response for axial strain. Significant increases in the strain readings between the 1^{st} and 10^{th} cycles were noted in the 9^{th} cycle group for both axial and hoop strain, which can be considered to represent the onset of permanent damage. Unexpectedly however, the plot also indicates that plastic deformation occurred long before the UEWS point. Although there were minimal differences in strain between the 1^{st} and 10^{th} cycles in the early cycle groups to indicate that permanent damage had occurred, the plot implies that the pipe suffered plastic deformation. This was clearly evident in the 5^{th} cycle group onwards, where the 10^{th} cycle strain recorded became progressively higher compared to the 10^{th} cycle strain of the 1^{st} cycle group. It is suspected that this behaviour is due to the non-linearity in the

matrix material, particularly in the shear response. Similar responses were observed in these tests at RT and 65°C. Further study to elucidate this finding was carried out and is discussed in Section 5.3.7.

5.3.6. UEWS test at 1:0 hoop to axial stress ratio (pure hoop loading)

Figure 5.10 (a-c) shows the UEWS plots under pure hoop loading (1:0) conducted at RT, 65°C and 95°C respectively. Higher hoop loading was applied compared to the axial-dominated loadings, but slightly less than that applied in the 4:1 UEWS tests. In this loading, the UEWS points were identified as 265MPa at RT, 220MPa at 65°C and 190MPa at temperature of 95°C. The failure strengths, on the other hand, were observed at 300MPa, 250MPa and 215MPa. These results were considerably lower than those obtained for the 4:1 loadings because no axial loading restrained hoop deformation, and hence less hoop stress was required to cause damage and subsequently failure. Similar to previous results, apart from those for the 2:1 loading condition, the UEWS and the failure strength showed evident degradation with increases in test temperature. In this case, both declined by nearly 30% from RT to 95°C. The axial strains to failure were recorded at approximately 1.7-2.0% for all test temperatures. This again showed a similar pattern to the results of the 4:1 loadings. Final failure was dominated by shear deformations of the resin matrix, which softened and became more resistance to cracking at high test temperatures, hence resulting in almost unaffected strains to failure, although strengths were degraded.

Figure 5.10 (d), shows the axial and hoop strain history responses for the test at 95°C, which were similar to those recorded for the 4:1 loadings. Significant differences in the first and final strains were noted in the 8^{th} cycle group, indicating the onset of permanent damage which corresponds to the UEWS point of 190MPa as indicated in Figure 5.10(c). Again, as in the 4:1 loadings, obvious plastic behaviour was observed in the plot starting from the 5^{th} cycle group. This indicates that the pipe was permanently deformed even though the UEWS point had not yet been reached. Similar responses were also observed in the RT and 65°C tests. It is interesting to note that this behaviour was only obvious in the hoop dominated loadings.

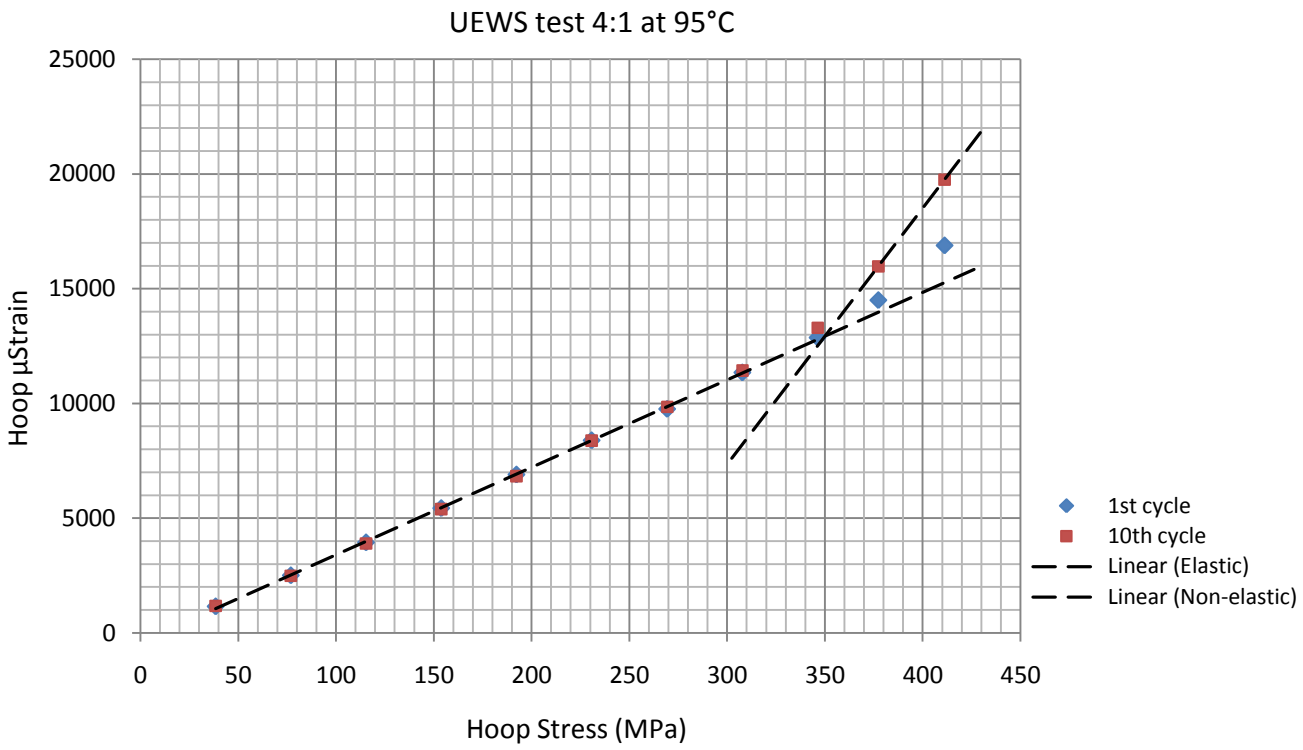
UEWS test 4:1 at 95°C
Hoop µStrain
Hoop Stress (MPa)
0
5000
10000
15000
20000
25000
0
50
100
150
200
250
300
350
400
450
1st cycle
10th cycle
Linear (Elastic)
Linear (Non-elastic)

(a)

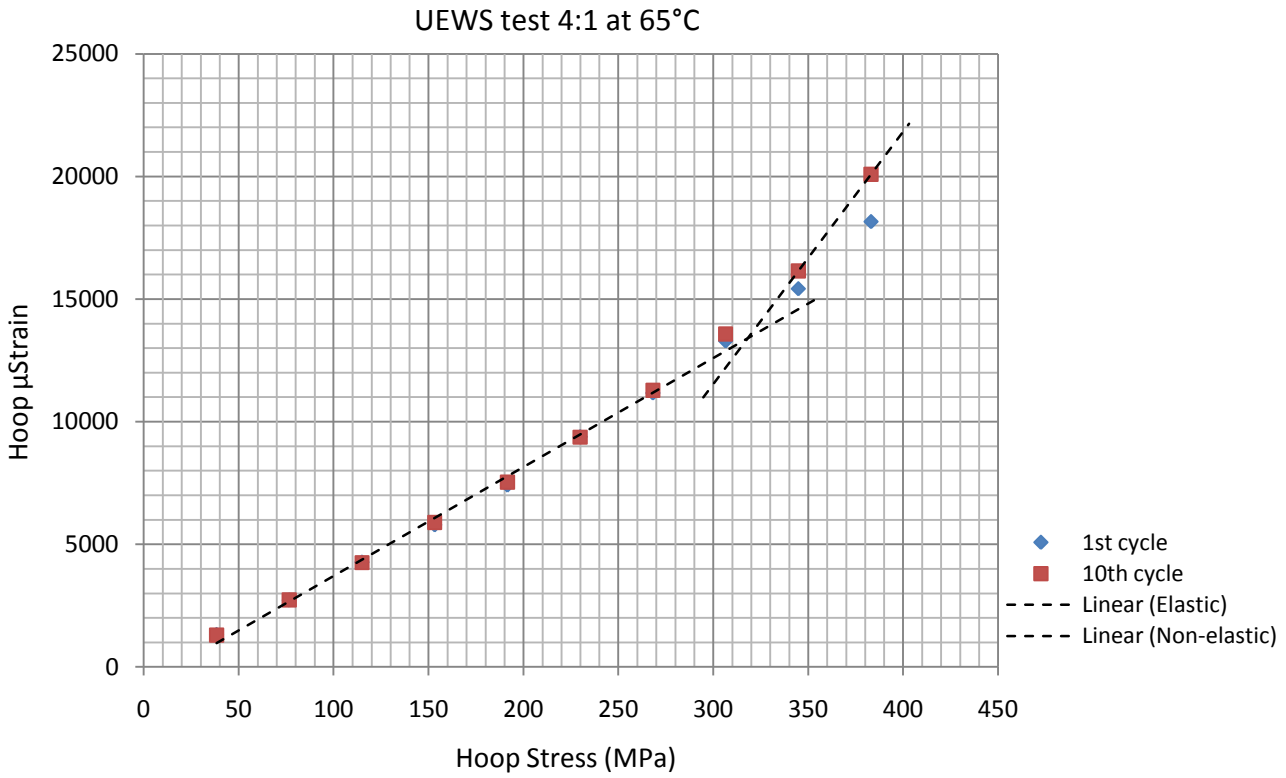
UEWS test 4:1 at 65°C
Hoop µStrain
Hoop Stress (MPa)
0
5000
10000
15000
20000
25000
0
50
100
150
200
250
300
350
400
450
1st cycle
10th cycle
Linear (Elastic)
Linear (Non-elastic)

(b)

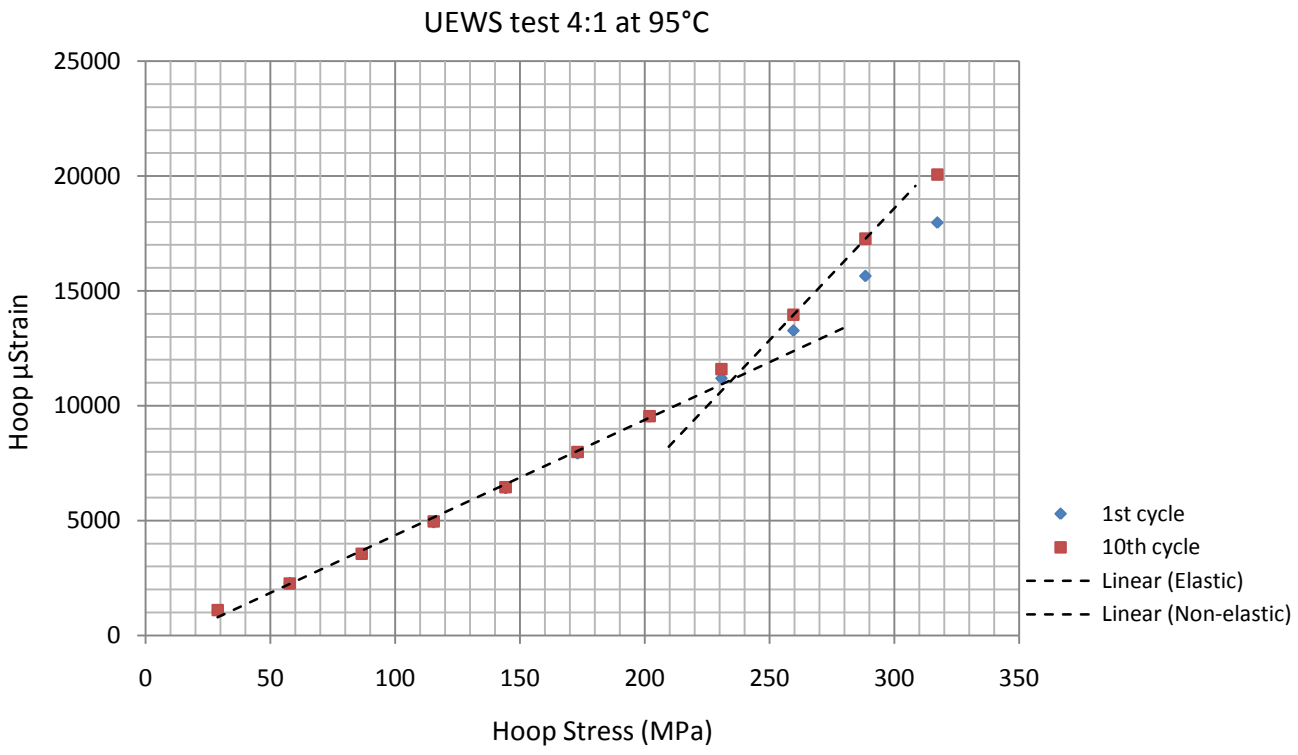

(c)

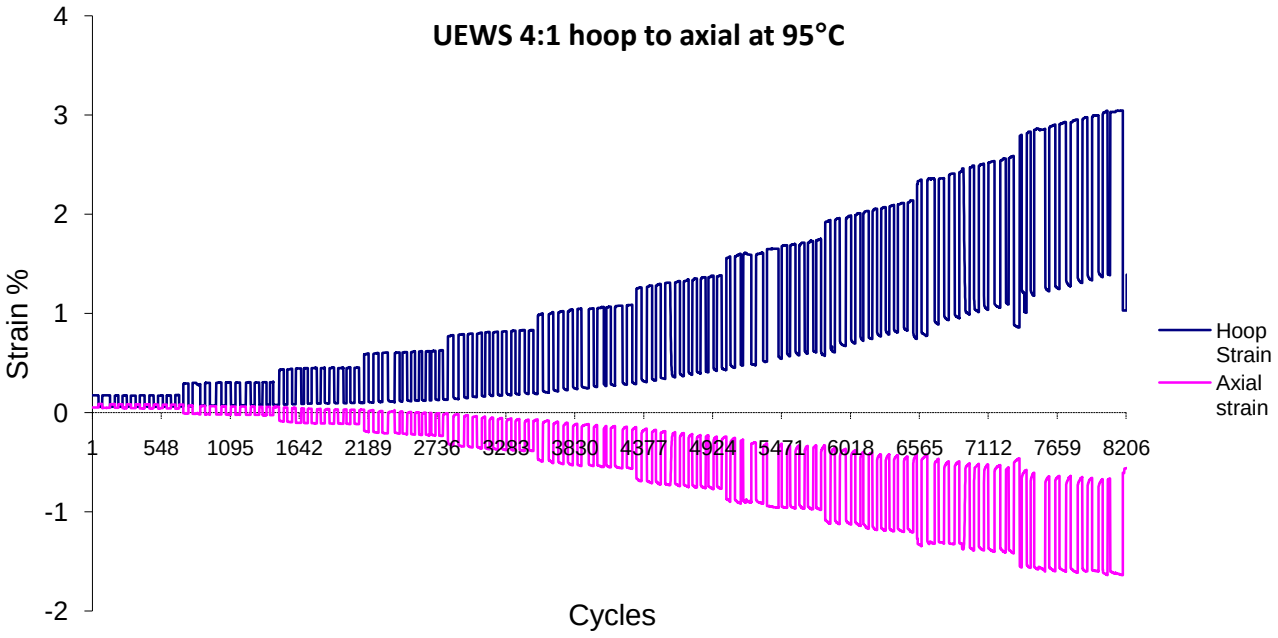

(d)

Figure 5.9: 1st and 10th cycle stress-strain plots of 4:1 UEWS tests at (a) RT, (b) 65°C, (c) 95°C and (d) strain history responses for test at 95°C.

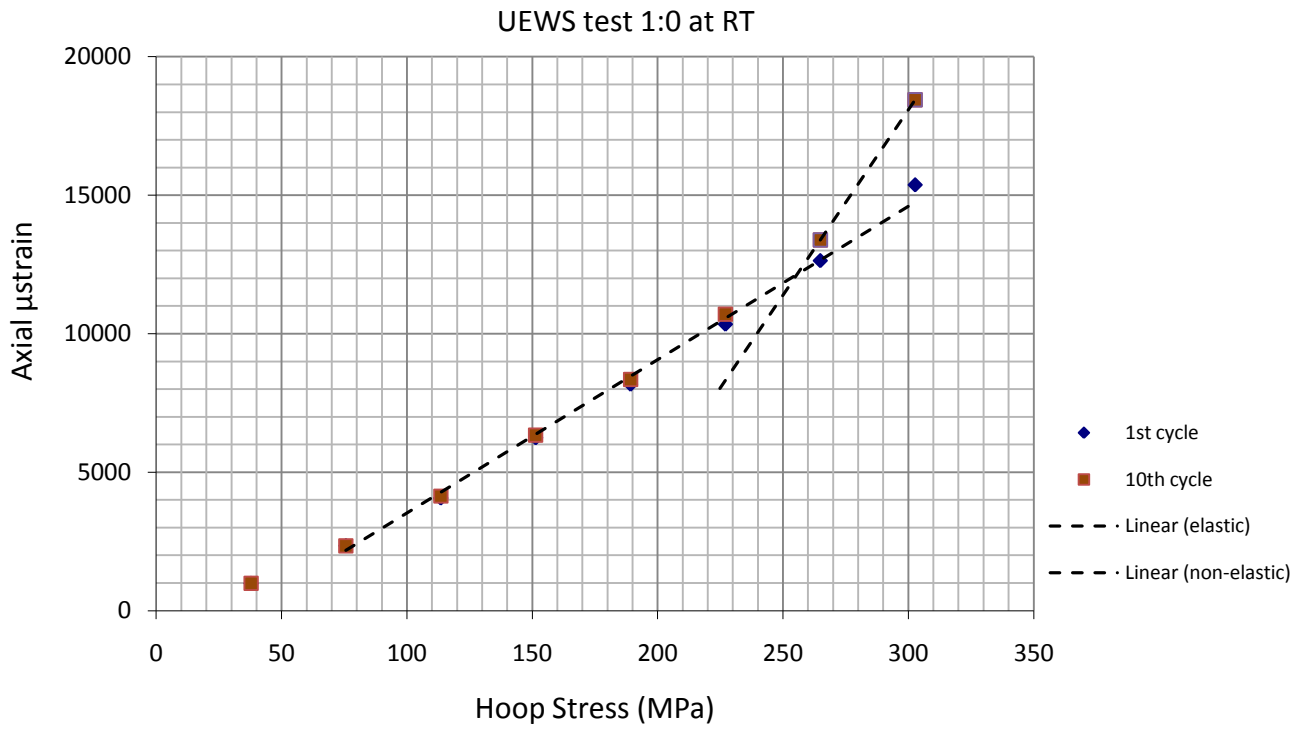
UEWS test 1:0 at RT
Axial µstrain
Hoop Stress (MPa)
0
5000
10000
15000
20000
0
50
100
150
200
250
300
350
1st cycle
10th cycle
Linear (elastic)
Linear (non-elastic)

(a)

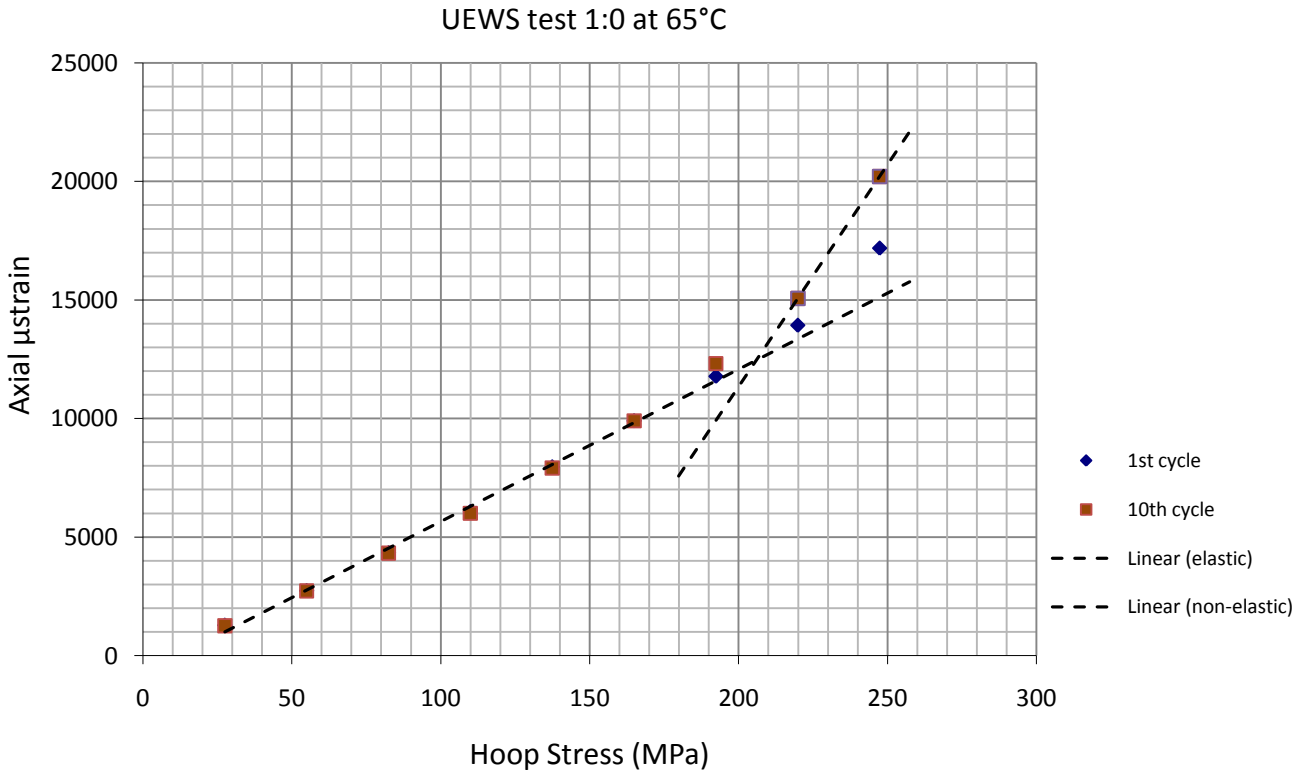
UEWS test 1:0 at 65°C
Axial µstrain
Hoop Stress (MPa)
0
5000
10000
15000
20000
25000
0
50
100
150
200
250
300
1st cycle
10th cycle
Linear (elastic)
Linear (non-elastic)

(b)

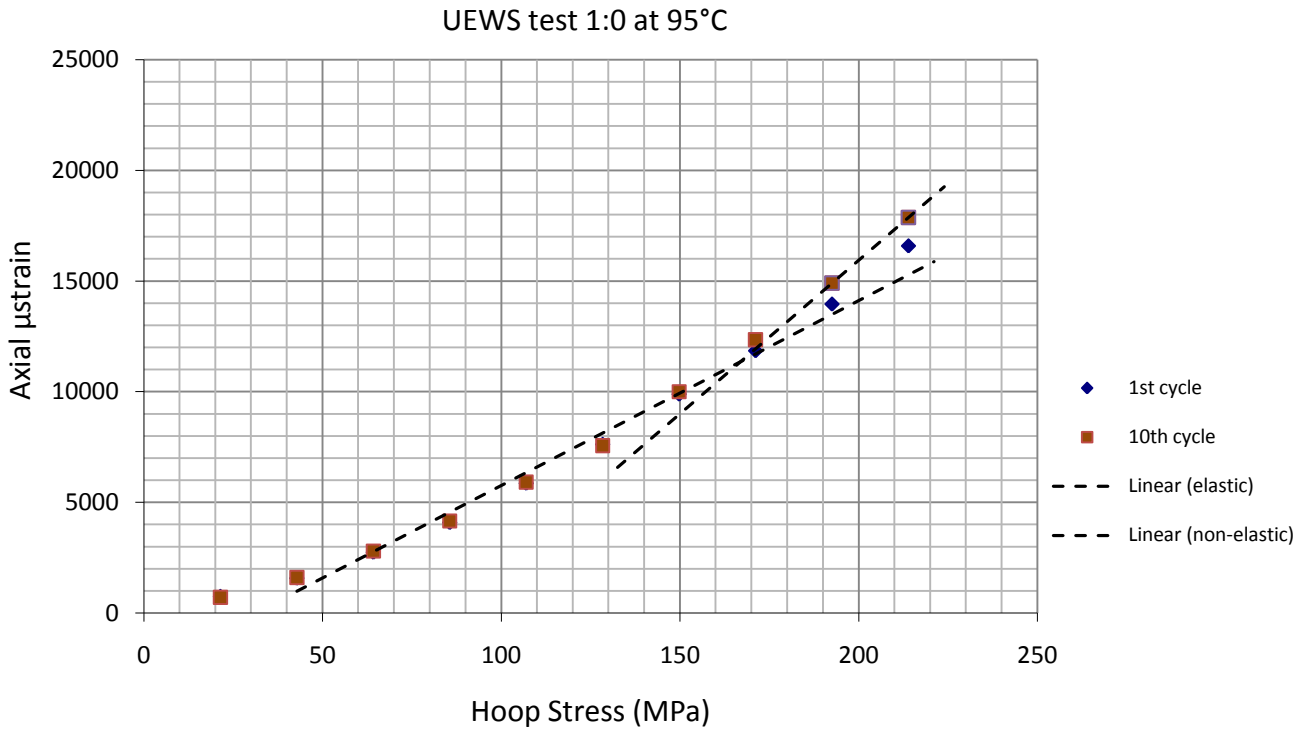

(c)

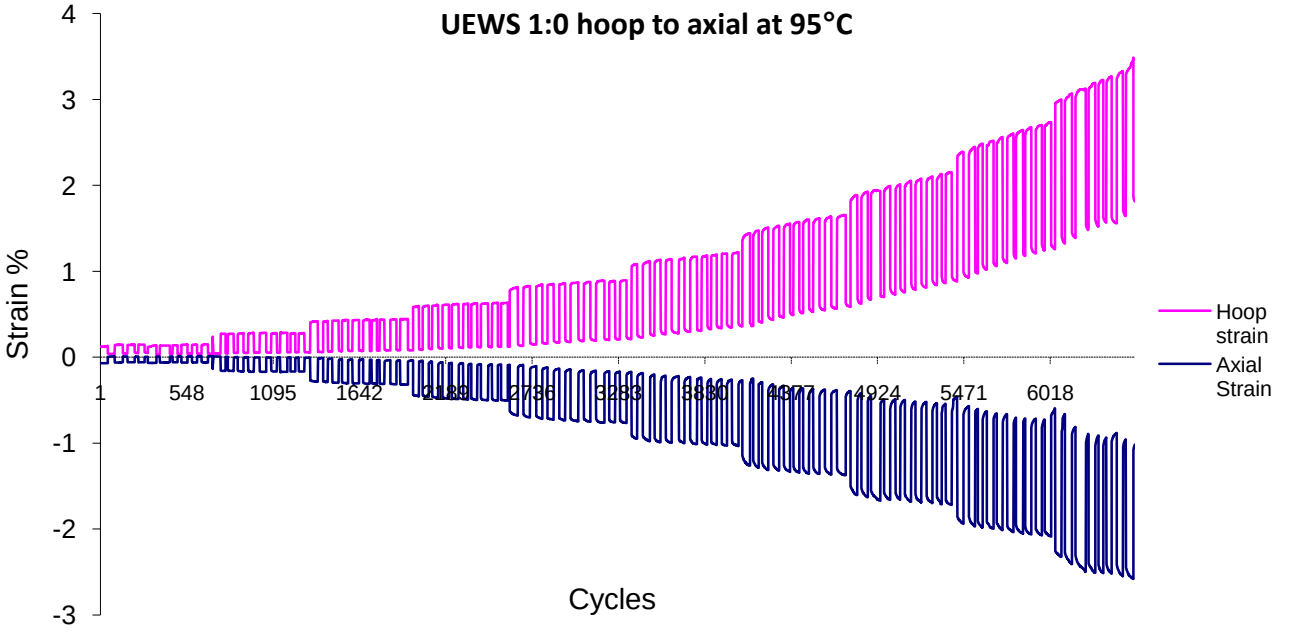

(d)

Figure 5.10: 1st and 10th cycle stress-strain plots of 1:0 UEWS tests at (a) RT, (b) 65°C, (c) 95°C and (d) strain history responses for test at 95°C.

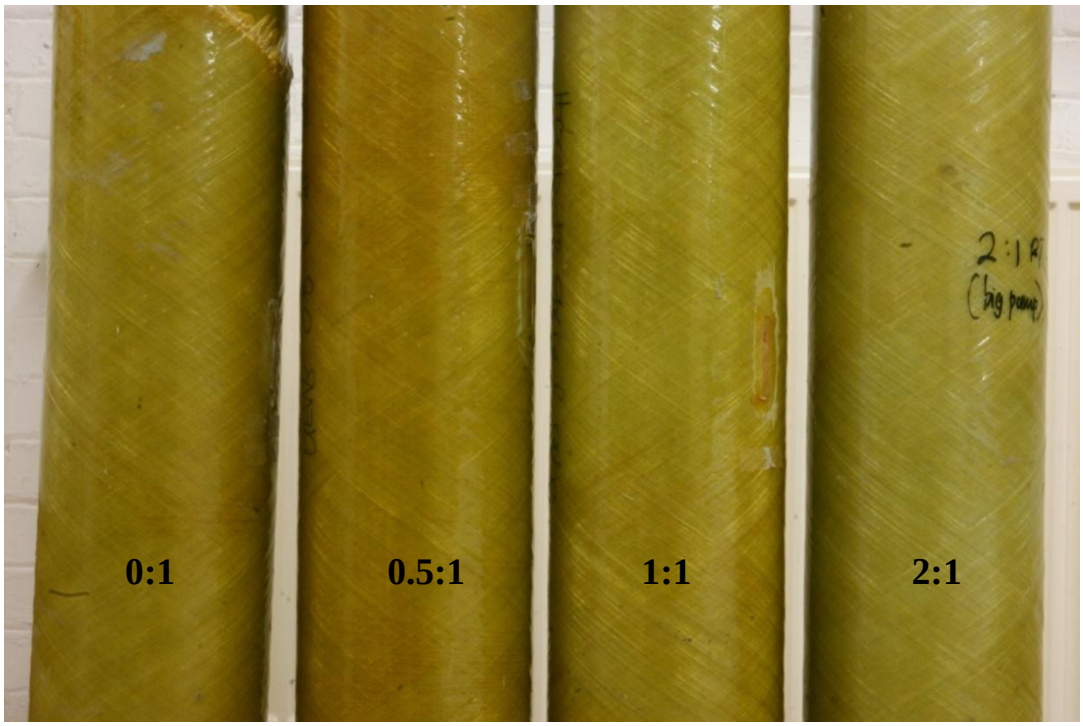

Figure 5.11: Pipe condition after UEWS test under pure axial to 2:1 hoop to axial loading

5.3.7. Comments on the plastic deformation in hoop dominated loading

One distinct characteristic observed in the strain history plots of the hoop dominated (4:1 and 1:0) compared to axial dominated loading was the plastic deformation that occurred considerably before the UEWS point had been reached. In both the pure hoop and 4:1 UEWS tests, deformations were observed as early as in the 5^{th} cycle group, while the UEWS point was only identified later in the 9^{th} cycle group. This was suspected to be due to the non-linear behaviour of the matrix material, particularly in its shear response. To explain this finding, a simple collaborative study with Future Pipe Industries (FPI) involved a neat resin cast similar to the sort used in the manufacture of the pipe was conducted. The cast was subjected to a tensile elastic loading (TEL) test at FPI lab, where the specimen was cyclically loaded to increasing load levels until failure occurred. The TEL could then be defined as the point at which continuous increasing elongation was noted. This test effectively represent a UEWS test under pure axial loading (0:1) but conducted on the resin cast strip. Figure 5.12 shows the 'dog-bone' machined resin casting strip used in the test before and post test failure.

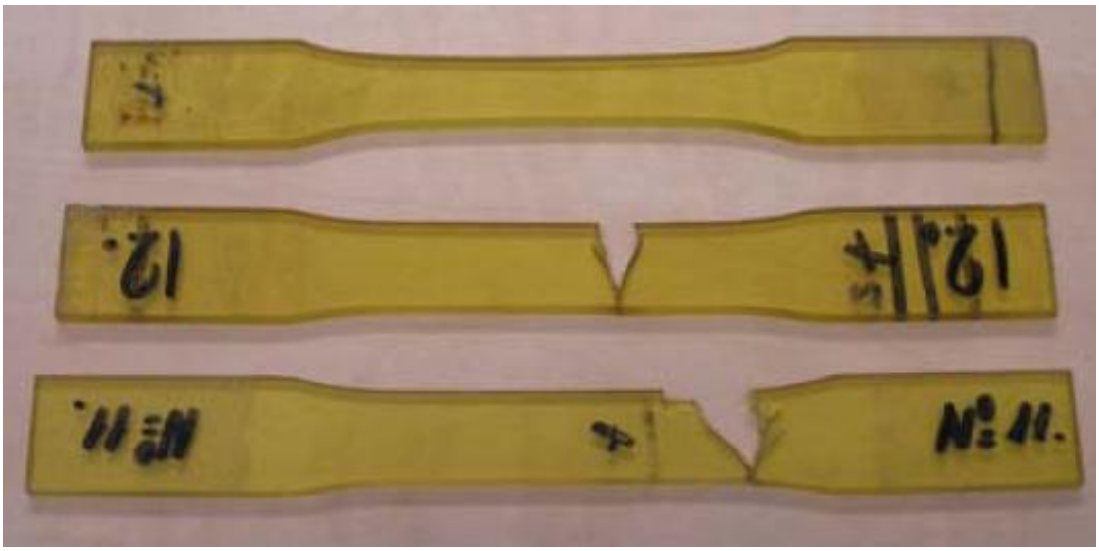

Figure 5.12: Machined and polished resin casting strip, before and after failure

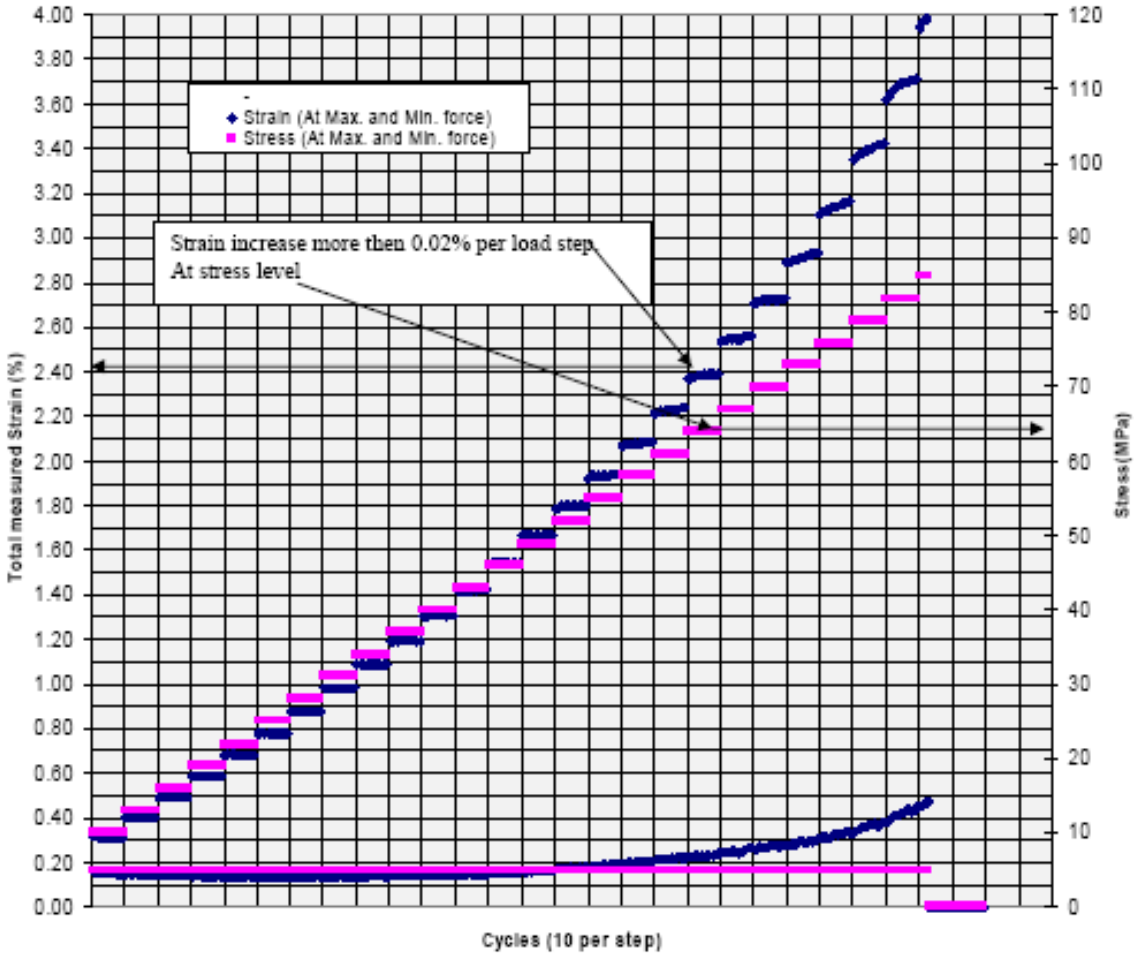

Figure 5.13: The stress strain plot against cycles of the TEL test conducted by FPI.

Figure 5.13 shows the plot of stress-strain against cycle from the TEL test. An increase in strain of 0.02% was measured during the step-loading which corresponds to 64MPa, where no cracking of the resin was observed. This was then identified as the tensile elastic limit. Beyond this stress level, continuous increases in strain were measured. The test sample then failed in the 3rd cycle of the 85MPa cycle group, with a maximum strain at failure recorded at 4%. This indicates that the plastic deformation of the resin cast was already taking place much earlier than this, at about 75% of the tensile axial strength. This corresponds well with the plastic phenomenon observed during the hoop dominated loading in the UEWS tests. The results obtained in this study suggest that although plastic deformation was observed before the UEWS point had been reached, there seemed to be no permanent damage induced to the pipe wall which would cause the long term failure of the pipe. It is suspected that the plastic deformation observed is due to the matrix material's non-linearity. In addition, lower levels of this plastic strain were observed with axial dominated loading because the pipe had only been subjected to low strains as the highest maximum physical strain to failure was noted in pure axial loading at 1.5%. In contrast, a much higher strain was subjected to the pipes in the case of hoop dominated loadings, with both tests (4:1 and 1:0) recording final failure strains of over 3%, which is close to the TEL strain observed for the resin strip.

5.4. Post-UEWS failure modes

This section describes the nature of the failure modes observed in the UEWS tests under complex stress states. The pipes tested were visually inspected and carefully examined noting details such as changes in the appearance of the surface of the pipe, fracture orientation or matrix failure. Three different types of failure mode were observed: tensile axial failure, weepage failure, and localized leakage failure.

5.4.1. Tensile axial failure

This failure mode was observed under pure axial loading (0:1) in UEWS tests where the pipe was subjected to considerable axial strain before a sudden and rapid elongation occurred due to the formation of large helical cracks. This took place after the non-

linear behaviour illustrated in the previous section could be seen in the stress-strain plots. No pressure was applied to the main pipe chamber, and hence no weepage failure was observed. As shown in Figure 5.14 (a-b), a helical crack is evident along the fibre direction, extending along the middle section of the pipe. This is because the loading in this condition is highly dominated by the resin matrix. Since the matrix strength is significantly lower than that of the fibre, the pipe failed at comparatively low stresses due to the formation of matrix cracks normal to the fibres. Further pressurizing caused the cracks to propagate parallel to the winding angle, and the pipe then subsequently fractured. The test results also show that rupture failure happens once the axial strain approaches 1%.

Observations made of the failed pipe samples show that the fibres parallel to the crack stayed intact, but the complementary fibres in the opposite orientation ruptured in a severe brush-like manner. Since only axial loading was acting on the pipe, the ruptured fibres exhibited marked realignment. The interior surface of the pipe was found to be crinkled, which is consistent with the findings of a previous study [35]. Closer inspection of the pipe surface away from the crack also revealed fine white striations parallel to the fibres. This could be attributed to tensile stress normal to the fibres, which cause debonding between the fibre-matrix boundary and matrix cracking transverse to the fibres.

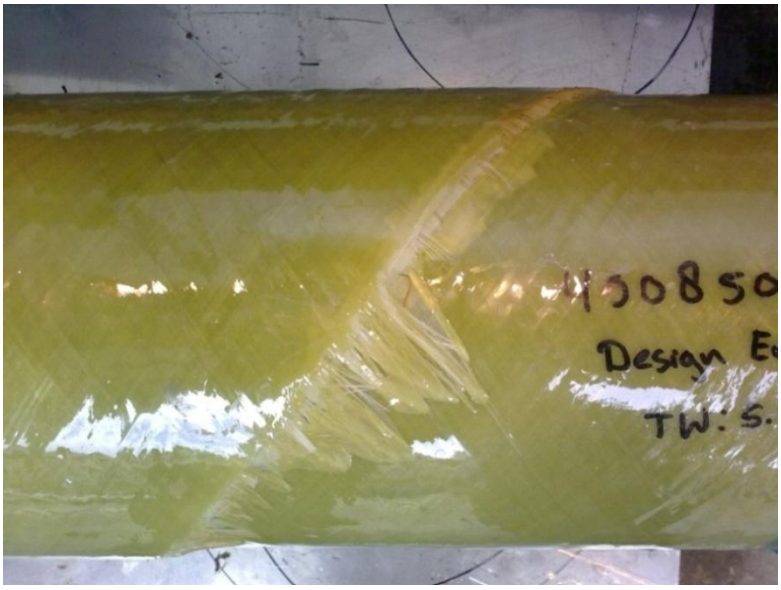

(a)

(b)

Figure 5.14: Tensile axial failure of GRE pipe under pure axial loading showing large helical macro cracks running parallel to the direction of the fibres.

5.4.2. Weepage failure

In this UEWS test investigation the weepage observed in the 0.5:1, 1:1 and 2:1 hoop to axial loading conditions was due to transverse matrix cracking. This can be clearly seen from the uniform formation of water droplets on the outer surface of the pipe. As the internal pressure increased, the numbers of water droplets increased and, after a significant build-up, the surface of the pipe became covered with water which could be seen to be dripping out of the test set-up. All weepage failures were observed long after the UEWS point had been reached. Figure 5.15 illustrates weepage failure in a test under the 2:1 loading condition at room temperature.

After cleaning, the post-test examination of the tested pipes found very little evidence of structural damage. The only visible signs were fine white striations over the entire surface of the pipe parallel to the direction of the fibres. These lines were seen to grow in length and number towards the end of the test as pressure increased. This was later

accompanied by an audible cracking sound immediately before the first formations of water droplets were observed. These white striations are illustrated in Figure 5.16 for 2:1 and 1:1 loadings. A close-up image of white striations is shown in Figure 5.17.

These striations across the surface of the pipe were actually due to transverse matrix cracking and the subsequent damage it caused. The same failure mode has also been reported by other researchers [14, 19, 28, 35, 94]. It is suspected that relatively high transverse tensile stress acting normal to the fibres, which have a higher strain to failure than that of the matrix resin, resulted in the fibre-matrix interface starting to debond. This results in less surface area for ideal stress distribution, and therefore induces stress concentrations within the laminates which cause further debonding. Ultimately, the debonds coalesce to form a crack parallel to the fibres which then grow in the plane parallel to the fibres. Weepage occurs once the crack density has built up to a critical level so that a fluid path is possible through the pipe wall.

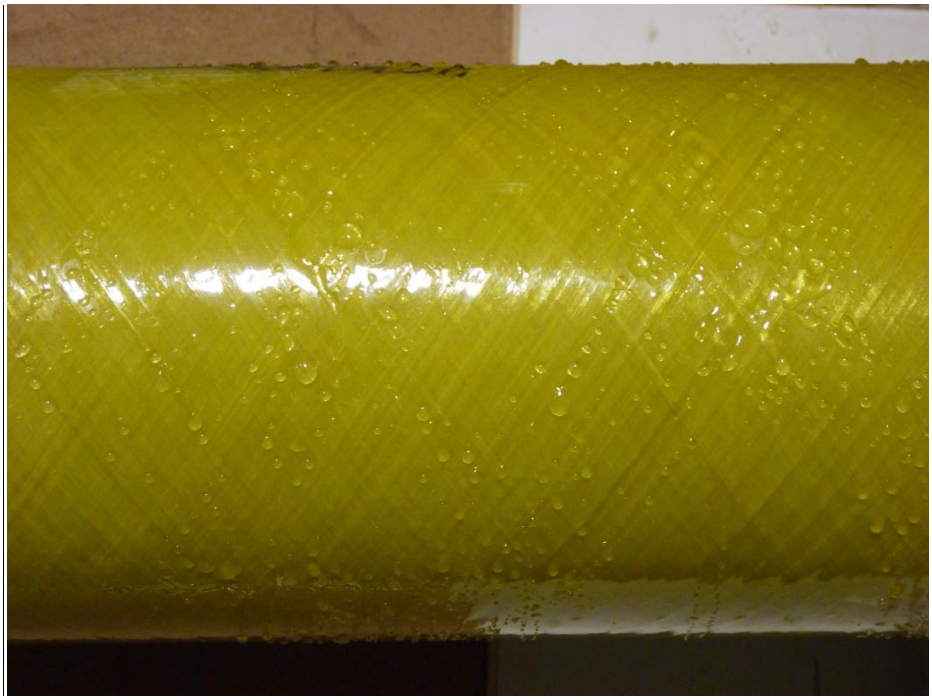

Figure 5.15: Weepage failure of GRE pipe

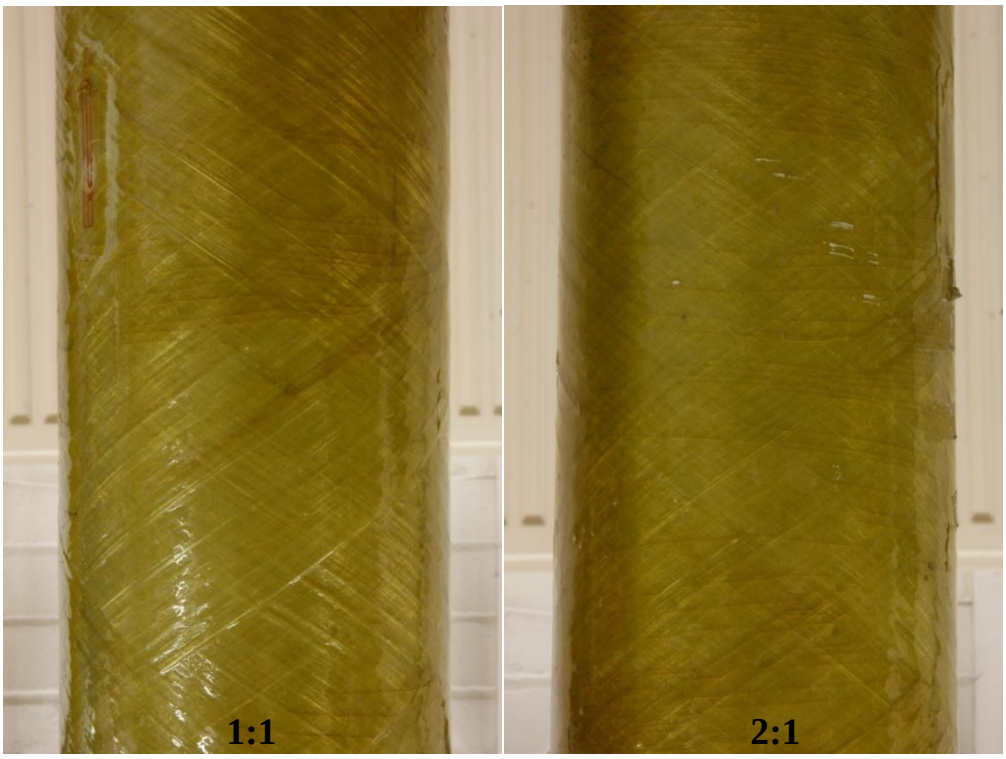

Figure 5.16: Post inspection of the pipes after UEWS test under 1:1 and 2:1 loadings. Visible white striations clearly observed on the surface of the pipes indicating matrix crack damage.

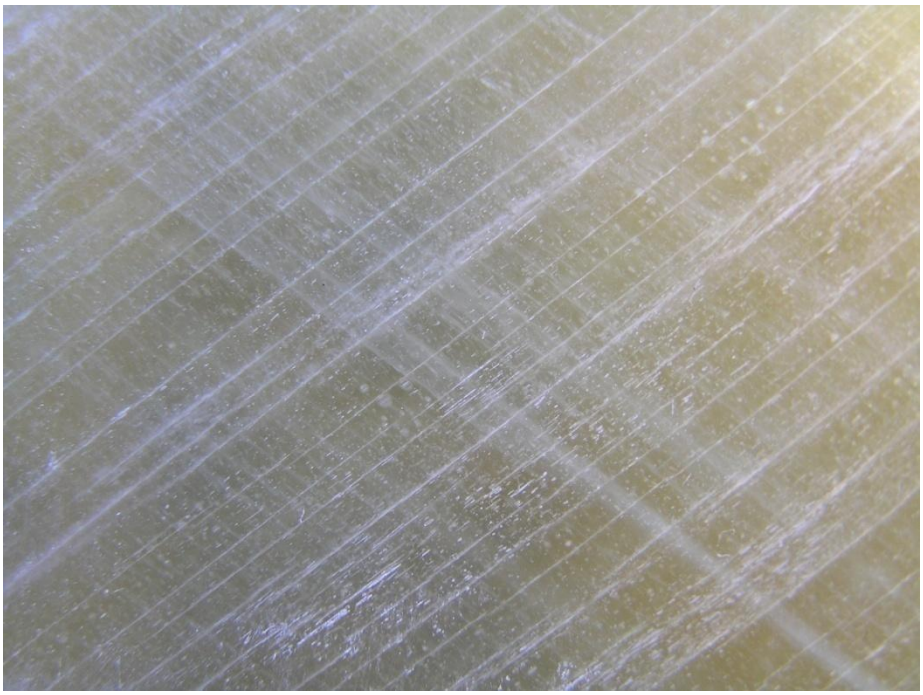

Figure 5.17: Closer look at the white striation observed which is due to transverse matrix crack.

5.4.3. Localized leakage failure

This mode of failure was observed for hoop dominating UEWS tests conditions under 4:1 and 1:0 hoop to axial stress ratios. Leakage behaviour in these cases was significantly different from that observed previously with other stress ratios. In all tests, a localized leakage occurred approximately 30-50mm from the end fittings close to the reinforcement area with obvious peeled-off surface damage showing ragged fibre strands (Figure 5.18 (a)). This type of failure is thought to have been caused by the bending of the pipe during the test, which induced additional tensile stresses on one side of the pipe and compressive stresses on the other. This bending can be clearly seen in the image in Figure 5.18(b) which was taken during the test just before leakage occurred. The overall exterior surface of the pipe also showed a slight opacity, due to coarse striations formed parallel to the direction of the fibre reinforcement. This was reported by Jones [19] to be associated with delamination between layers of fibre wound in different orientations taking place on the compressive side of the bent pipe.

Hoop dominated loading results in significant tensile hoop strains. This leads to an increase in compressive axial strain due to the movement of the inner piston installed inside the pipe. These strains cause large deformations in pipe diameter and decreases in the length of the pipe, followed by a significant rotation of fibres with respect to the pipe axis which leads to the increase in the winding angle. This formation resulted in large interlaminar shear stress in the matrix material, notably near the end fittings on the compressive side of the pipe bends. Such shear stress would have caused severe cracking in the resin matrix, allowing water to penetrate the pipe wall and subsequently causing leakage failure. Once this had occurred, obvious flows of water could be seen running down the pipe surface near the damaged area, rather than the slow droplet formation as seen in weepage failure.

As the load further increased, an increasingly aggressive flow of water was observed from the fractures, and this was reflected in the rapid drops in the pressure contained by the pipe. However, no obvious whitening was observed during the pressurizing of the pipe. The observation of this failure mode is consistent with the findings of previous

work by Hull [24] and Jones and Hull [19], which found that such local leakage is a sign of interlaminar cracking taking place in the laminate due to high shear stress.

(a) (b)

Figure 5.18: (a) The end rupture of the pipe causing localized leakage failure and (b) Bending of the pipe during high hoop dominating loading UEWS tests.

5.5. Failure envelopes

Figure 5.19 shows the UEWS and weepage based biaxial failure envelopes for ±55° GRE pipes tested at RT. Given that the UEWS point is defined as the point at which permanent damage is considered to start, it also can be referred to as the initial failure stress. Weepage failure on the other hand, is referred to as the functional failure since the design function of the pipe has been compromised and it can no longer contain pressurized fluids.

Overall, the failure envelopes generated from the UEWS tests show strong dependence on stress ratio and test temperatures. The weepage based failure envelope indicated by the dotted line in the plot, is approximately 8%-12% higher stress level to the UEWS strength. This is because further loading needs to be applied to cause the initial damage at the UEWS point to propagate and accumulate before reaching the specific threshold level at which leakage or weepage was observed. At high axial dominated loadings of 0.5:1 and 0:1, the UEWS and weepage failure strengths are very close. This implies that, at these loading ratios, damage progressed rapidly from initiation to functional failure.

The envelope also shows that pure hoop UEWS strength (~265MPa) is over four times greater than axial UEWS strength (~63MPa). This is mainly because in pure axial loading the load is strongly matrix dominated. As the stress ratio increases, the axial and hoop UEWS and weepage failure strengths also increased due to the greater loads now being taken up by the stronger fibre. It is shown that under what is regarded as the optimal pipe design loading condition for ±55° wound GRE pipe, which is at 2:1 hoop to axial stress, the UEWS point is at a hoop stress of 200MPa. However, the highest UEWS point was recorded in 4:1 hoop to axial loading ratio at 375MPa hoop stress, although here, the axial failure strength is slightly lower than that for the 2:1 loading ratio, at 93.75MPa.

The UEWS results at RT also registered almost constant axial failure stresses from 0.5:1 to 4:1 loading ratios. This range is thought to correspond to the change in failure mechanisms from transverse matrix failure dominating at pure axial loading to failure controlled by shear deformation of the matrix in pure hoop loading. Weepage failure was observed during this range of biaxial loading. In the hoop dominated loading region, from the 4:1 stress ratio, the axial strength began to decrease until pure hoop loading was reached. UEWS and weepage hoop strength decreased from 375MPa to 265MPa and 410MPa to 300MPa respectively from 4:1 to pure hoop loading, registering reductions of nearly 30% and 26%. This is possibly due to the bending of the pipe observed in this loading condition, inducing relatively high shear stresses especially near the end fittings of the pipe's compressive side.

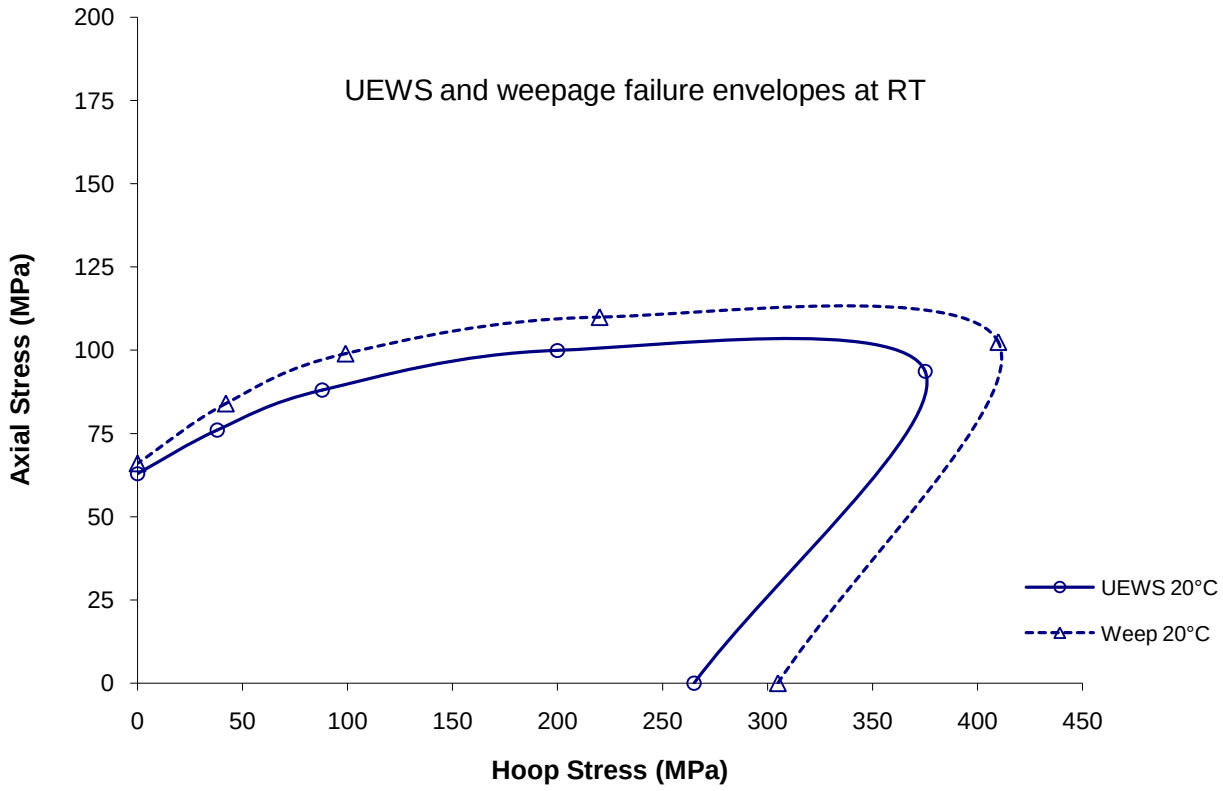

Figure 5.19: UEWS and weepage based failure envelopes at different test temperatures of RT.

An ingenious way of looking at the stress component responses and the changes in damage mechanisms of GRE pipes is to plot the dimensionless change of principal stress components in the ply against the arctangent of hoop stress over axial stress, which corresponds to the stress ratio applied in the UEWS tests. Again, by applying equation (4.7), the principal stresses acting on the ply were first calculated. These values were then divided by their corresponding failure strengths, assuming that σ_1^* = 1000MPa, σ_2^*=75MPa and τ_{12}^*=45MPa to reflect the true responses.

Figure 5.20 illustrates the variation in the principal stresses of the plies from axial dominated to hoop dominated loadings. In pure axial loading, stress in the direction transverse to the fibres clearly governed the failure of the pipe. The same can also be said for the case of 0.5:1 and 1:1 hoop to axial loading conditions. At the 2:1 loading

condition, which is regarded as the optimum working condition for ±55° wound pipe, failure was caused by the combined effect of transverse and shear stresses with the former still dominating. At 4:1 hoop to axial loading, the shear stress component increased rapidly and, although failure governed by both transverse and shear stresses, the latter is now the controlling stress component. However, from 4:1 to more hoop dominating loading ratios, the transverse stress component decreases and, especially at pure hoop loading, shear stress becomes the most dominant stress component which thus governs pipe failure.

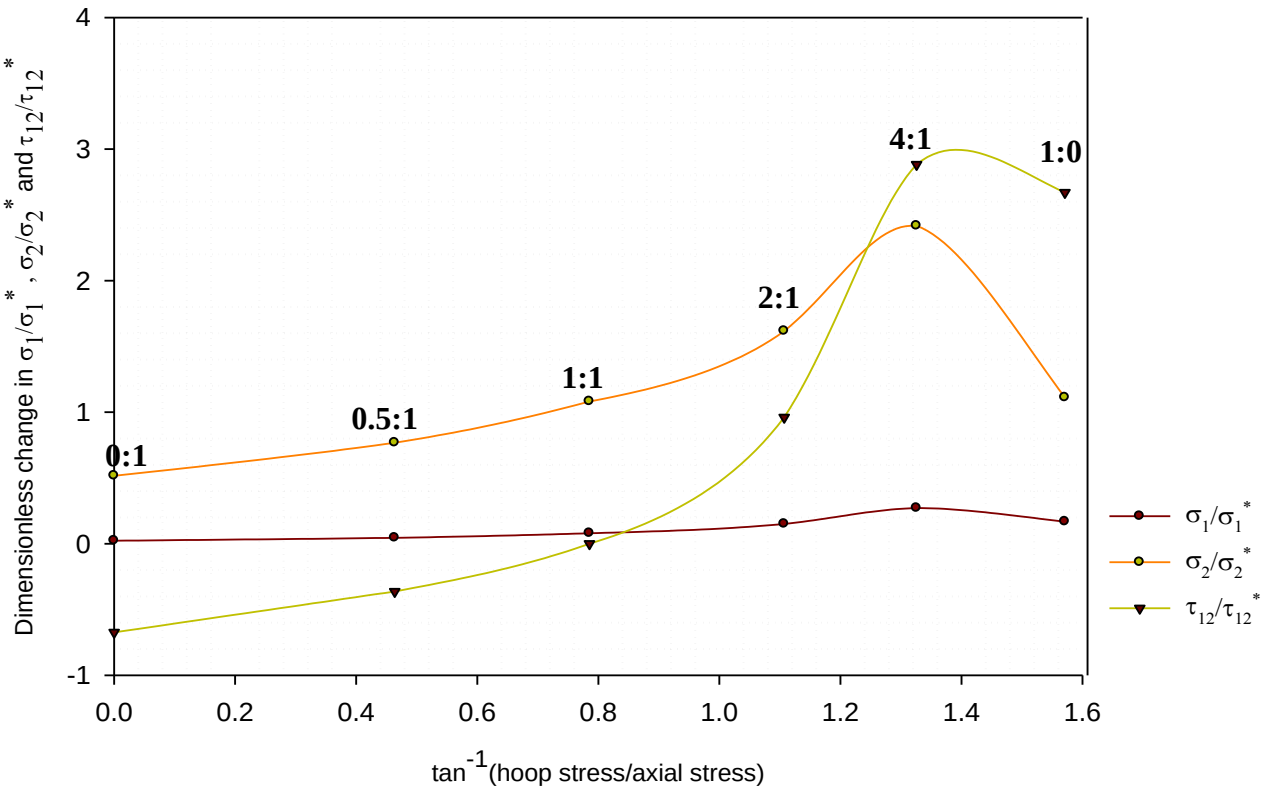

Figure 5.20: Variation in principal stress components relative to the various biaxial loading ratios.

Figure 5.21 (a) and (b) show the UEWS and weepage/leakage failure envelopes for elevated test temperatures of 65°C and 95°C respectively. These give similar shapes of envelope to the RT environment, although clearly indicating significant effects of

temperature on UEWS and weepage strength. UEWS strength is generally reduced, except in the 2:1 loading condition.

Highly noticeable reductions were observed for the pure axial and pure hoop loading conditions, where the failure mode is matrix dominated. The UEWS results for pure axial loading decreased from 63MPa at room temperature to 48MPa at 65°C and only 43MPa at 95°C, which represents an almost one-third reduction in axial strength. The hoop UEWS strength also registered a substantial decline with nearly 30% reduction from 265MPa at RT to a low 190MPa at 95°C. This finding is in good agreement with work by Hale [28, 192], who suggested that the resin matrix becomes softened at high temperatures, which significantly reduces its strength. Since the failures at stress conditions other than the 2:1 ratio are matrix dominated, this resulted in the greatly reduced UEWS strength especially under pure hoop loading and pure axial loading.

In only one condition, at 2:1 hoop to axial loading, did the UEWS points show an increase in strength at room temperature from 200MPa to 215MPa for both 65°C and 95°C tests. Similarly, weepage strengths also increased from 220MPa at RT to 240MPa at elevated temperatures. This is because the 2:1 loading is considered as the optimum loading condition for ±55° wound pipe, where most of the load is carried by the glass fibres and little by the resin matrix. At high temperatures, the matrix system becomes more ductile due to the softened matrix and hence resulted in the increase of strain to failure. This improved failure strain is believed to outweigh the effects of temperature on the elastic modulus which results in the 8% and 9% increments of UEWS and weepage strength respectively. This characteristic of temperature dependence leads the failure envelopes to shrink towards the origin and to become slight narrower to accommodate the increase in strength for the 2:1 loading condition.

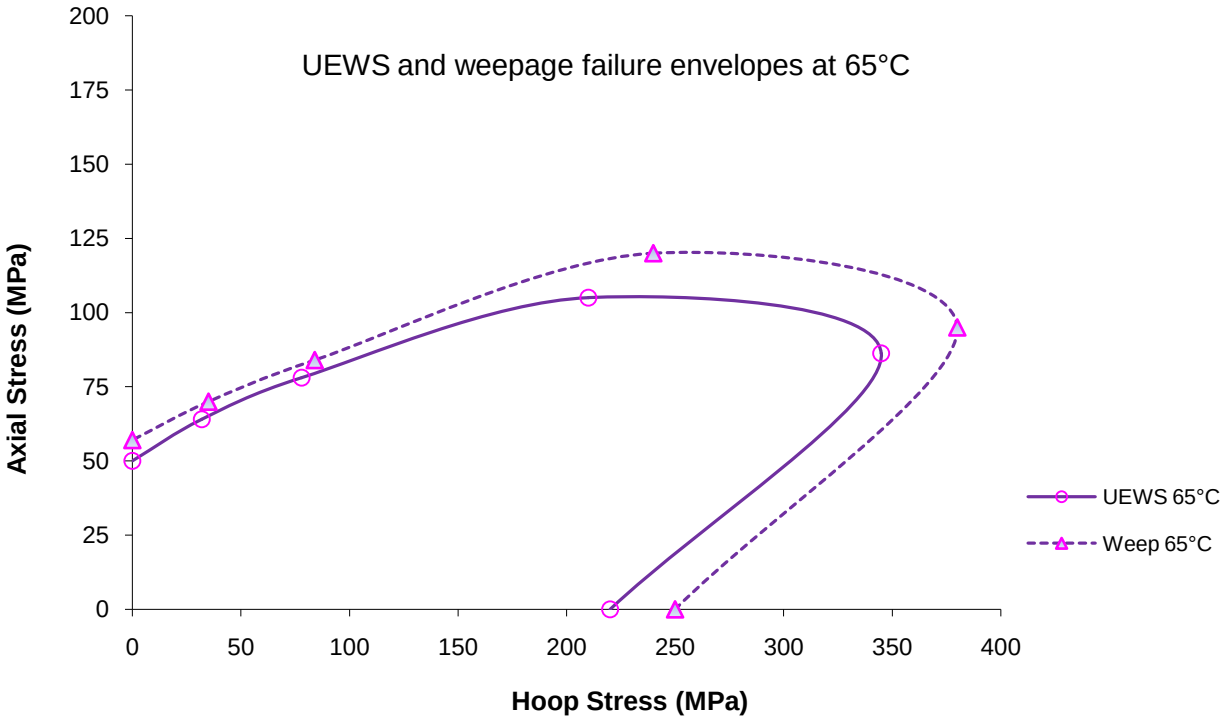

(a)

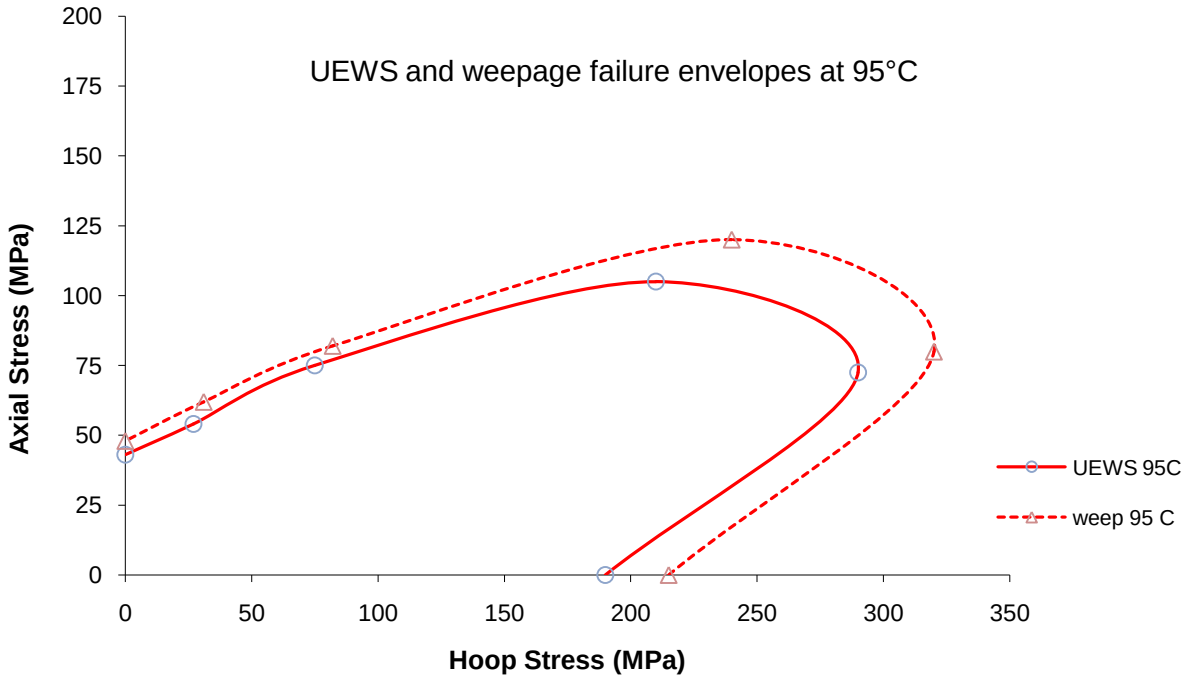

(b)

Figure 5.21: UEWS and weepage based failure envelopes at different test temperatures of (a) 65°C and (b) 95°C.

This particular finding is very interesting because the UEWS procedure employed in this investigation is intended to offer an alternative to the current qualification procedure described in the ASTM D2992. However, the finding does not support the regression lines produced as the 2:1 test shows a degraded LCL value at 65°C and 95°C compared to the RT. The only explanation to this would be that the current regression based procedure is long term where the test sample is exposed to water for a long time causing ageing to laminate. The water ageing effect can have a big impact on the life properties of the pipe. As mentioned in the literature, Ellyin and Rohrbacher [123, 124] studied the behaviour of GRE laminates immersed in distilled water, at RT and 90°C. They found that immersed samples at high temperatures suffer serious degradation in the mechanical strength of the matrix by plasticization and reduction of the matrix-fibre interface strength resulting in a decreased threshold crack initiation strain. Since the UEWS is a short term test, samples were not affected by water ageing, hence the difference noted in this study. Further investigation on the effects of water ageing is needed in order to complete the comparison. This can be achieved by exposing pipes in a water bath for a predetermined time and temperature.

Figure 5.22 gives the single UEWS and weepage based failure envelopes for ±55° wound GRE pipes incorporating the results at all the test temperatures. All the envelopes clearly demonstrate the anisotropic nature of the composite pipe, which can be seen from the much greater hoop UEWS and failure strength compared to strength in the axial direction.

Comparisons of the failure envelopes produced in this investigation with those of previous studies reveal some very interesting contrasts. Most of the envelopes from earlier studies consider weepage as the initial failure point, whereas in this investigation, it is defined as the final failure point. For example, a failure envelope of a similar shape was reported by Soden *et al* [26], although much higher stress levels for pure hoop loading were observed. However, the initial failure envelope in that work was taken at the point of weepage failure whilst final failure in the form of bursting or pipe rupture was obtained through the use of a rubber liner to prevent weeping of fluid.

The present investigation hence suggests a very attractive feature of UEWS based failure envelopes, since it provides engineers with more realistic design limits which consider the initiation and progression of permanent damage in the laminates rather than merely being based on leakage points.

From the failure envelopes produced, the limit in hoop strength was found to be roughly four times greater than the axial tensile strength. Using manual extrapolation, axial strength under compression was predicted to be at least twice as much as axial tensile strength. In order to validate this estimation, a simple compression test on similar GRE pipes, 100mm in diameter was conducted in accordance with British Standard, BS EN ISO 604:2003 [193]. The compressive failure strength obtained was then integrated with the current weepage/leakage based failure envelopes from the UEWS tests. Figure 5.23 shows the resulting prediction of failure envelopes ranging from pure axial tensile to pure hoop loading to pure axial compression. The results confirm the anisotropic response of the pipe under axial tensile/compression loadings. In the UEWS test with pure axial tensile loading, failure strengths were determined at 68MPa, 55MPa and 48MPa for test at RT, 65°C and 95°C respectively, while under pure axial compression the failure strengths of the same test temperatures were determined to be 148MPa, 122MPa and 104MPa, respectively. The compressive failure strength also gives an indication that the UEWS results and failure envelopes produced seem to naturally align with the compression test results, hence implying a satisfactory correlation between the two test sets of results.

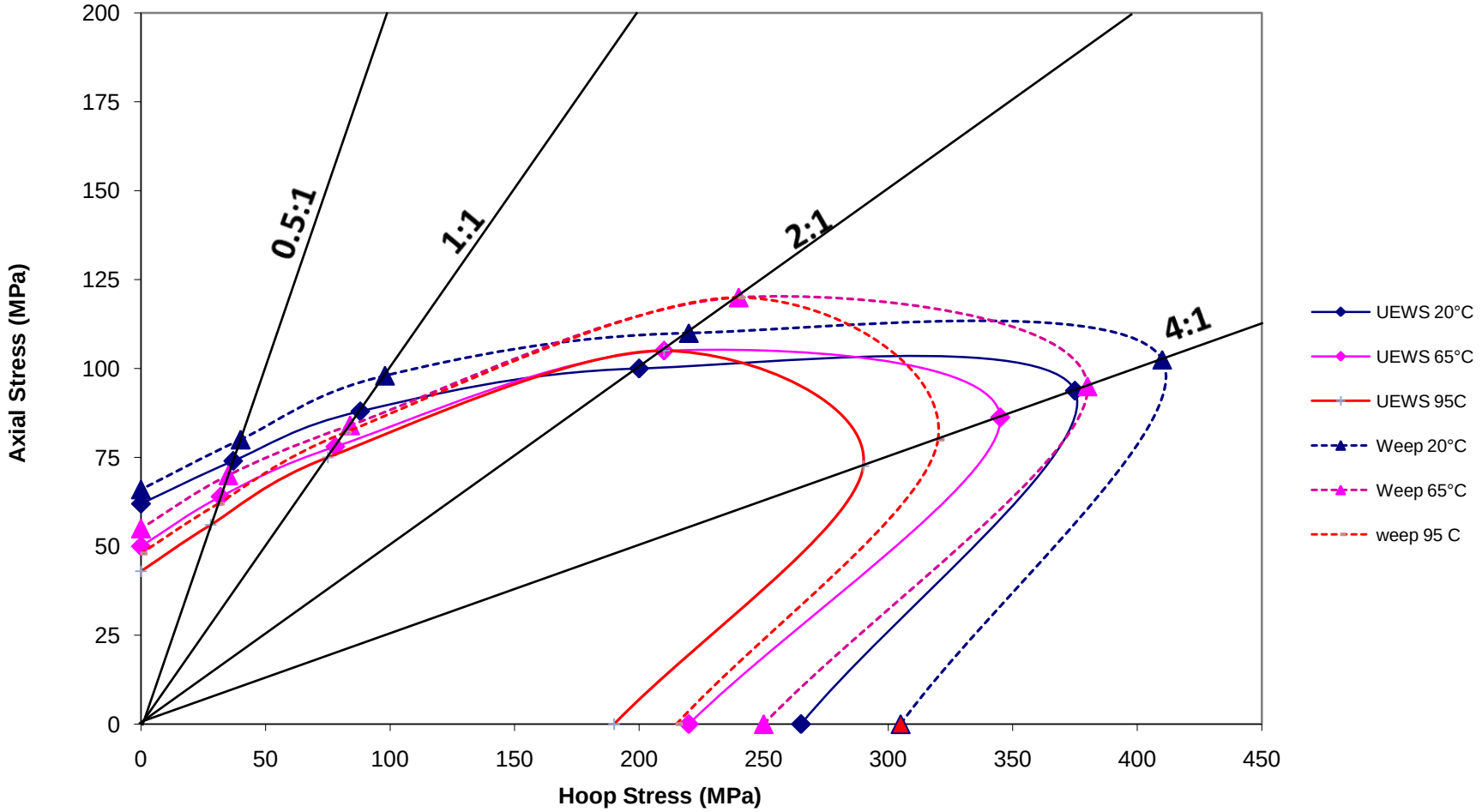

Figure 5.22: UEWS and weepage based failure envelopes of different test temperatures at RT, 65°C and 95°C.

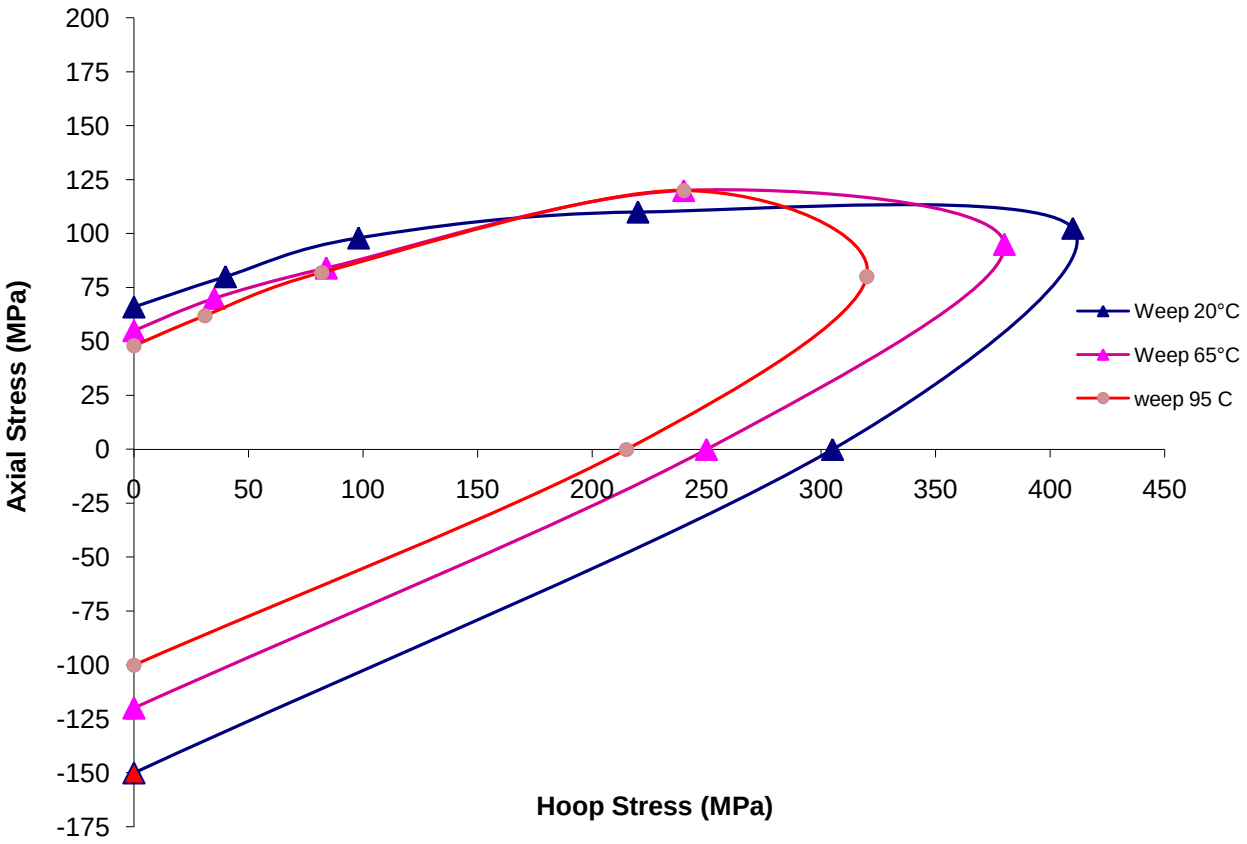

Figure 5.23: Weepage/leakage based failure envelopes at RT, 65C and 95C plotted with failure points of axial compression tests (0:-1).

5.6. Acoustic emissions results

In this section, the acoustic emissions (AEs) observed during the UEWS tests are presented. The purpose of monitoring AE is to quantitatively determine damage initiation and progression leading to different failure mechanisms via an analysis of AE parameters. However, the more important aim is that this analysis is also intended to provide further additional information to confirm the UEWS results by correlating changes in AE activity with the onset of permanent damage as recorded in the UEWS tests. In order to produce a full service condition at RT, acoustic data were recorded from three UEWS tests: pure axial loading (0:1), giving a negative transverse to shear stress ratio; hydrostatic pressure (2:1) which results in a high transverse to shear stress ratio; and finally pure hoop loading (1:0) which yields a high shear to transverse stress ratio.

5.6.1. Pure hydrostatic pressure (2:1 loading)

Figures 5.24 and 5.25 show the recorded AE counts and cumulative energy against time (in seconds) during the UEWS test at the 2:1 loading ratio. The wall stress (MPa) applied in each cycle group is indicated at the top of the plots. As illustrated in Figure 5.24, the AE counts started very early in the low pressure cycle groups. Activity then slowly increased as the pipe was loaded in the next cycle group with increased pressure. A small gap between the 3rd and 4th cycle groups where no AE was recorded was due to the AE system operation being suspended by the operator. Upon resumption, notable increases in AE counts were observed in the 4th cycle group with pressure at 48 bars, which corresponds to 74MPa indicating the first significant change in AE activity. This is believed to be the result of the initiation of matrix cracking. In the next three cycle groups, AE counts more or less stabilized, which suggests a constant rate of damage progression. Another significant increase in AE counts was noted in the 7th cycle group with a wall stress of 130MPa. This sudden change in AE count is likely to correspond to substantial transverse matrix cracking and the progression of interface debonding, which then possibly led to a change in damage mechanism from matrix cracking to delamination.

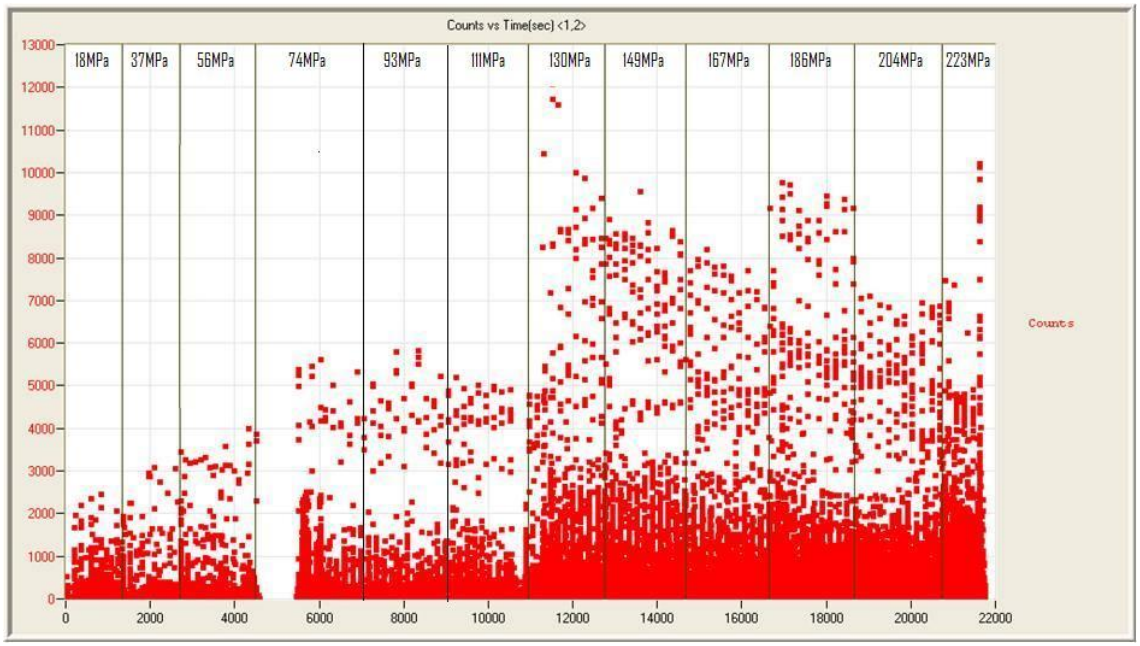

Figure 5.24: Change in AE counts throughout the UEWS test under hydrostatic loading (2:1) at RT

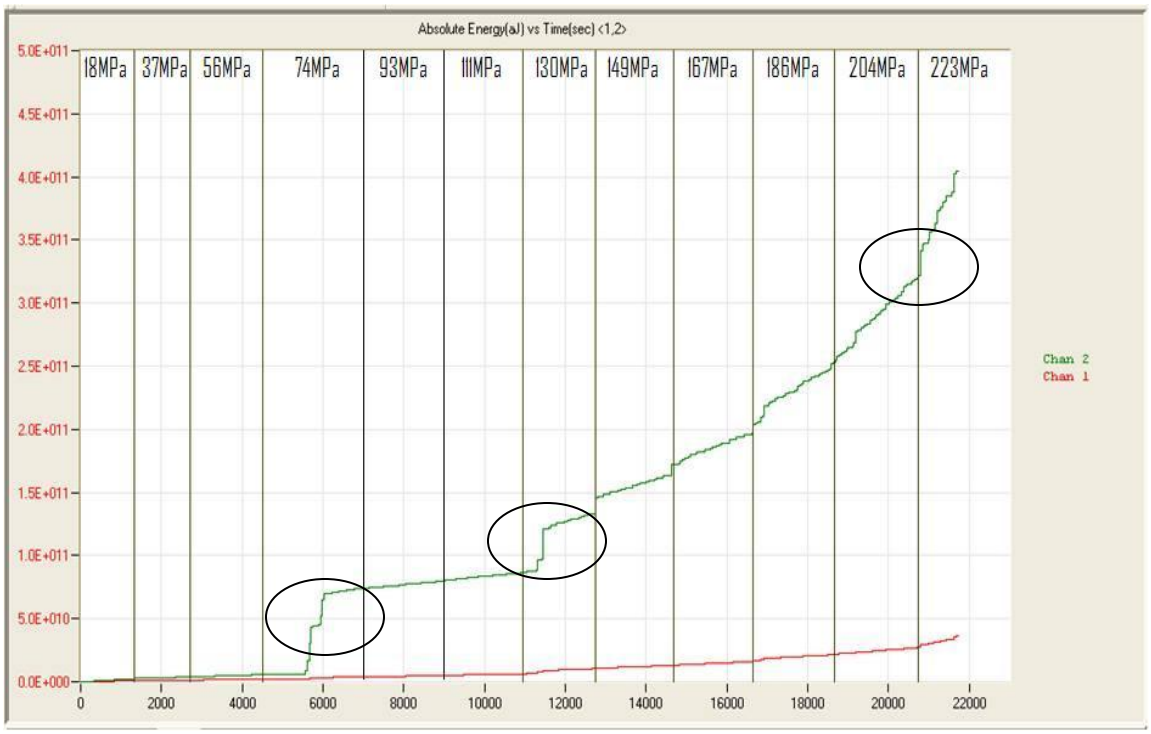

Figure 5.25: Cumulative energy counts throughout the UEWS test under hydrostatic loading (2:1) at RT.

Figure 5.25 shows the cumulative energy plot against time with the corresponding wall stress indicated at the top of the plot. The AE activities recorded suggest that damage initiation and progression were taking place in close proximity to transducer 2. Closer observation of the plot indicates that there are three sharp rises in cumulative energy, firstly in the 4th cycle group at 74MPa wall stress, secondly at 130MPa wall stress, and finally at the start of the 12th cycle group with a wall stress of 223MPa. These correspond well with the previous AE count plot, confirming the onset and progression of damage.

However, in order to characterize the damage mechanisms involved, the AE signal durations from transducer 2 were plotted against the signal amplitude which afterwards generated into a 3D plot against time as given in Figure 5.26 and 5.27 respectively. From Figure 5.26 most of the AE events were of low duration and low/intermediate amplitude ranging from 45dB to 85dB as indicated in zone 1. This was attributed to the combination of matrix cracking and matrix-fibre debonding, and a 3D plot of these AE

parameters against time suggests that these damage mechanisms were acting throughout the test. Small numbers of higher duration AE events were noted with amplitudes from 55dB to 80dB, as shown in zone 2. These events were suspected to be associated with friction between crack surface or resulting from fibre pullout [167]. The 3D plot illustrated in Figure 5.27 indicates that, toward the latter stages of the test, events of low/intermediate duration were observed at high amplitudes between 90dB and 120dB (zone 3), which is likely to be associated with delamination failure. All of these events were noted prior to weepage failure. The 3D plot also suggests the possibility that fibre breakage might have taken place in zone 3, indicated by the low duration of high amplitude AE events (115-120dB) [166], although this would have to be to a limited extent otherwise bursting would have happened instead of weepage. These failure mechanisms deduced from the AE data correspond well with the failure sequence prior to weepage discussed in the literature review earlier.

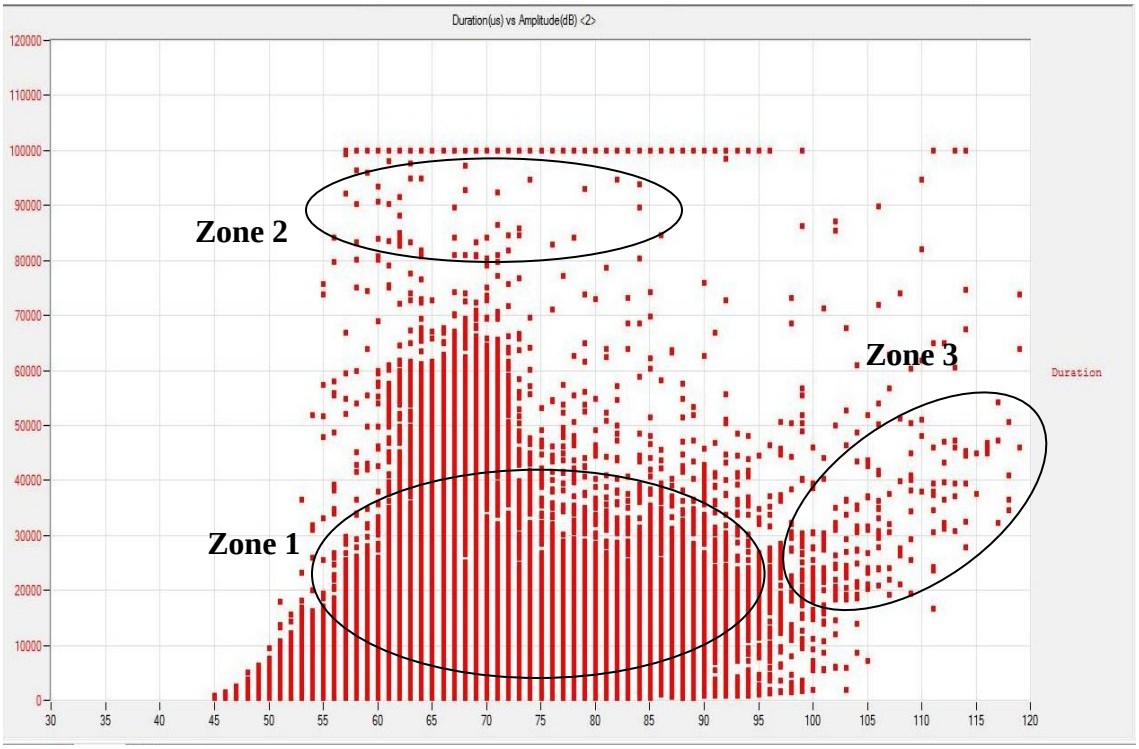

Figure 5.26: Plot of AE duration against AE amplitude for UEWS test under hydrostatic loading (2:1) at RT.

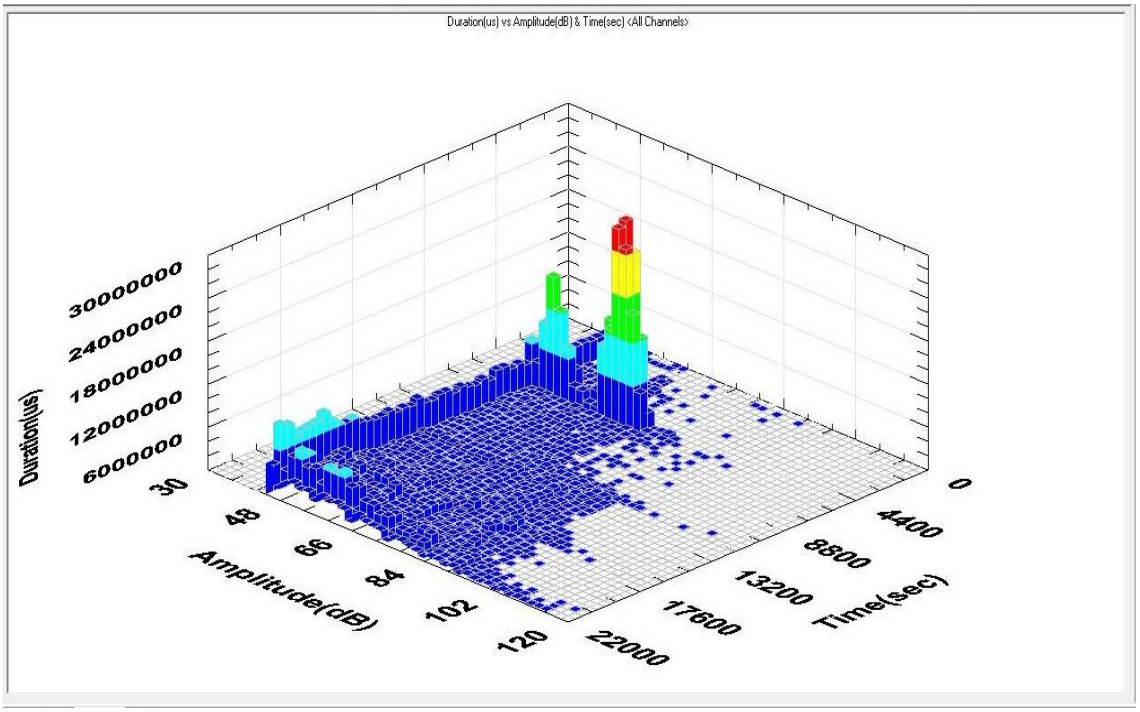

Figure 5.27: 3D plot of AE duration versus amplitude versus time for UEWS test under hydrostatic loading (2:1) at RT.

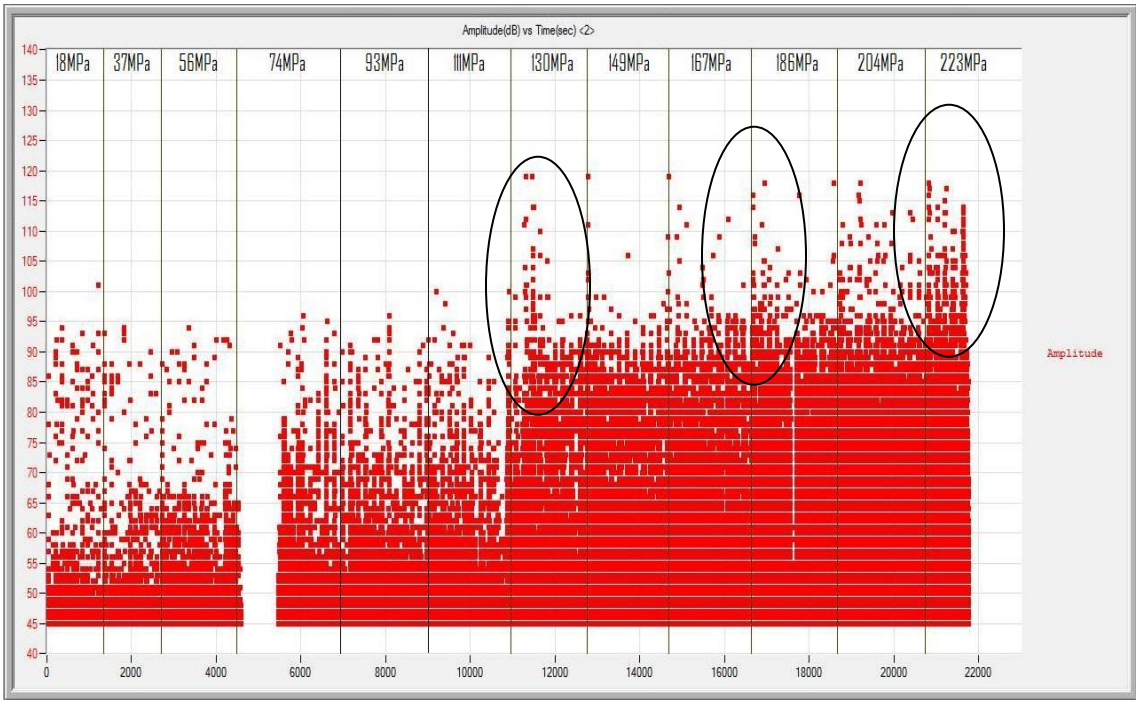

Figure 5.28: Plot of AE amplitudes versus time for UEWS test under hydrostatic loading (2:1) at RT.

Figure 5.28 shows the AE amplitude against time, with the wall stress applied indicated at the top of the plot. Low amplitude events were observed from the very early stages of the test, and the amplitude gradually increased until debonding failure was suspected to have developed at a wall stress of 130MPa. This is illustrated by the surge in AE amplitude in the 7th cycle group in the plot. Amplitude then stabilized before a second sudden rise up to 120dB was observed at the start of the 10th cycle group (186MPa), which could be attributed to the onset of delamination failure within plies. A final surge in amplitude was observed in the 12th cycle group just before weepage failure occurred. This is suspected to be due to further delamination processes and fibre breakage, which would explain the high-amplitude signal. Overall, the AE results in this loading condition imply that matrix cracks were initiated and had progressed to delamination before the UEWS point was reached at 200MPa.

5.6.2. Pure axial loading (0:1)

Figure 5.29 shows the AE counts for the UEWS test under pure axial loading (0:1) tested at RT. Similar to the results for hydrostatic loading, AE counts were observed from the first cycle group at a wall stress of 9MPa, and these gradually increased with increasing pressure up to the 3rd cycle group of 27MPa wall stress. A significant increase in AE counts was noted from the 4th cycle group at 36MPa and this stabilized until the next cycle group at 45MPa. This change in AE activity is believed to correspond to the onset of matrix-fibre debonds and matrix cracking. The AE counts then increased considerably between the 6th and 7th cycle groups indicating the evolution of damage. Finally, the highest peak of AE counts was observed in the 8th cycle group as a result of tensile axial failure.

Figure 5.30 demonstrates the cumulative energy recorded from the two probes. Most AE signals were captured by probe 1, suggesting that damage initiation and evolution were taking place closer to this probe. The plot indicates two distinct rises in cumulative energy, first at a wall stress of 36MPa and second in the final cycle group corresponding to final tensile axial failure. The change in cumulative AE energy showed a similar trend to the previous AE plot, confirming the onset of damage and its progression in pure axial loading.

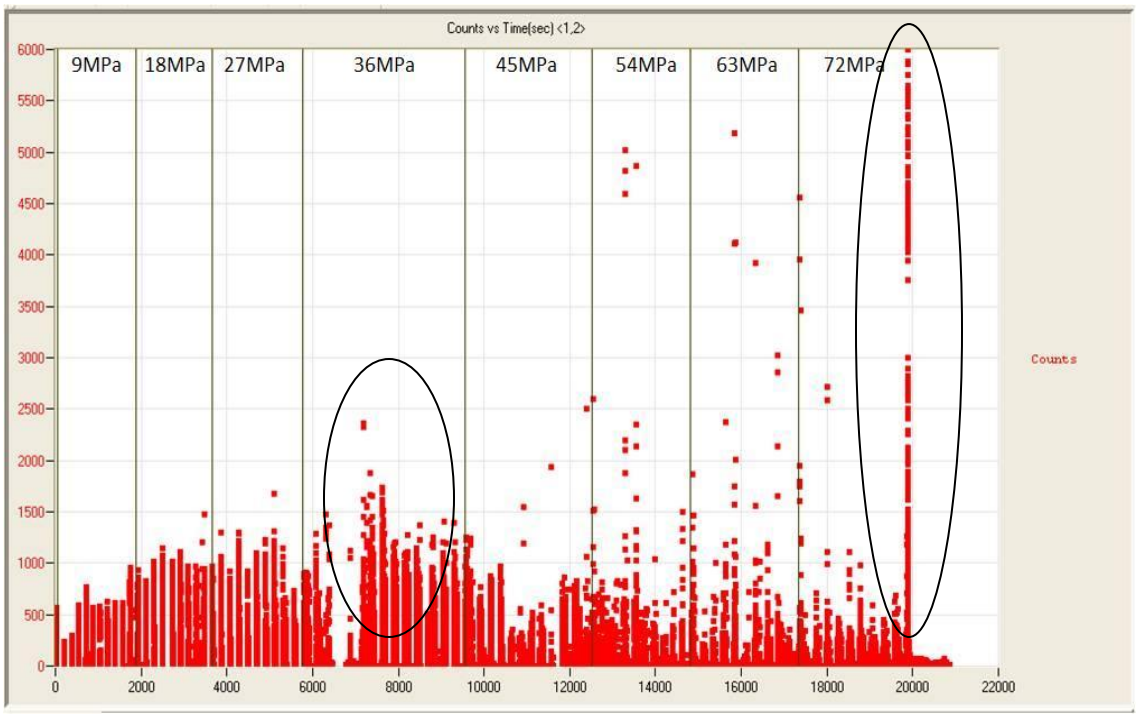

Figure 5.29: Change in AE counts throughout the UEWS test under pure axial loading (0:1) at RT

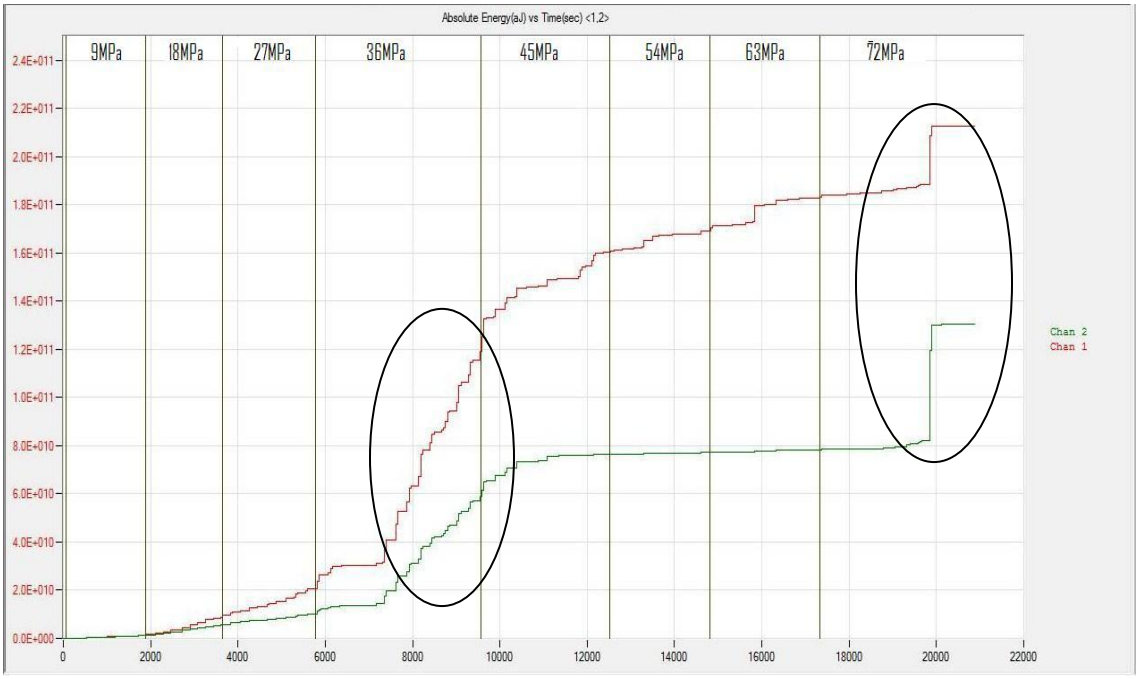

Figure 5.30: Cumulative energy counts throughout the UEWS test under pure axial loading (0:1) at RT.

Plots of AE event durations against amplitude and the 3D plot of these parameters against time are given in Figures 5.31 and 5.32 respectively. Since most AE events were detected near to transducer 1, these plots were generated from the signals gathered by this transducer. As shown in Figure 5.31, most of the AE events were of low duration and low amplitude in the range of 45dB–80dB similar to those observed with pure hydrostatic loading. These events can be seen in zone 1 and were normally associated with matrix cracking and matrix-fibre debonding.

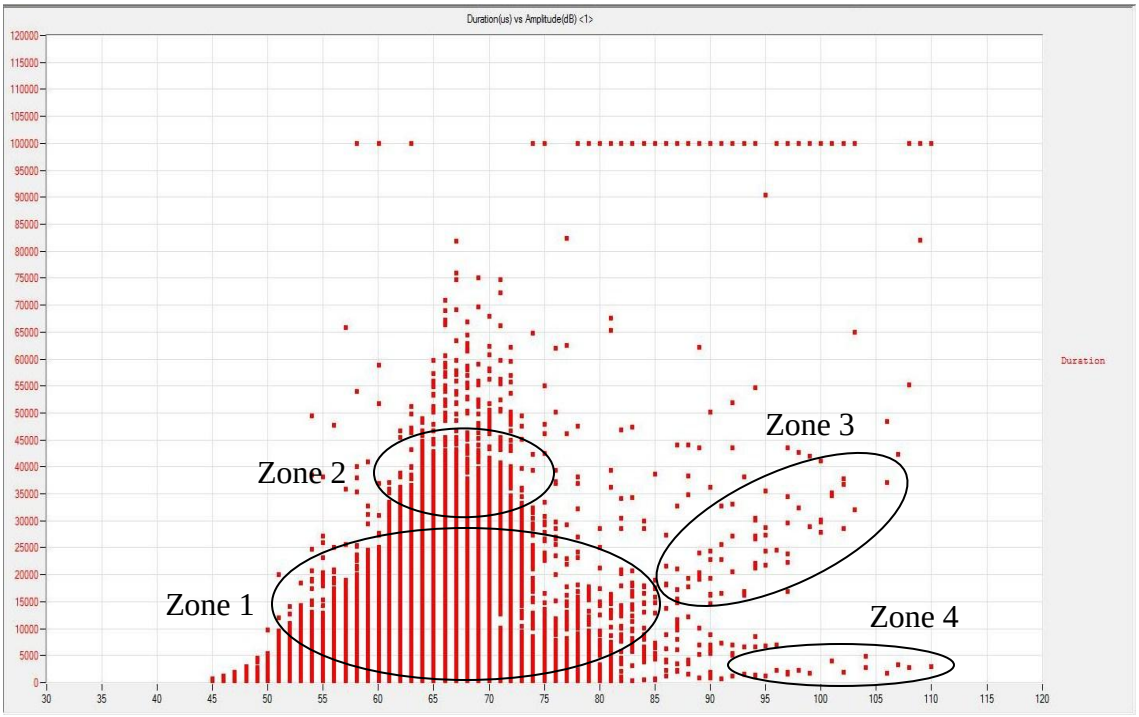

Figure 5.31: Plot of AE duration against AE amplitude for UEWS test under pure axial loading (0:1) at RT.

Intermediate/high duration events from 60dB-75dB in zone 2 correspond to further debonding process and the rapid progression of matrix cracking which, according to the 3D plot in Figure 5.32, were taking place between 6000 and 13000 seconds. This means that the surge observed in the cumulative energy plot during this period can now be attributed to this debonding process. Some of the low amplitude events of higher duration recorded here might also result from friction effects at the crack surfaces [170]. As indicated before, the final failure observed in this type of loading was tensile axial failure in the form of macro helical cracks, where obvious fibre breakage had taken

place. Hence, high amplitude events between 85dB-110dB of low/intermediate duration indicated in zone 3 and 4 can now be attributed to delamination failure and fibre breakage respectively. The 3D plot generated was also in conformity, indicating that these events occurred right at the end of the test just before final failure.

Finally, Figure 5.33 demonstrates the AE amplitude from transducer 1 against time. The first significant increase in amplitude was observed in the 4th cycle group at 36MPa, which occurred at around 6000 seconds and is associated with matrix-fibre debonding and matrix cracking. The second noteworthy increase in AE amplitude was noted around 13,000 seconds at the start of the 6th cycle group. This is suspected to be associated with the rapid progression of matrix cracking and the inception of delamination failure. The final rise in AE amplitude was observed immediately before tensile axial failure at 72MPa wall stress and is due to fibre breakage. According to the experimental findings under this loading condition, the UEWS point was identified at 63MPa, which suggests that matrix cracking has now initiated and progressed into delamination failure.

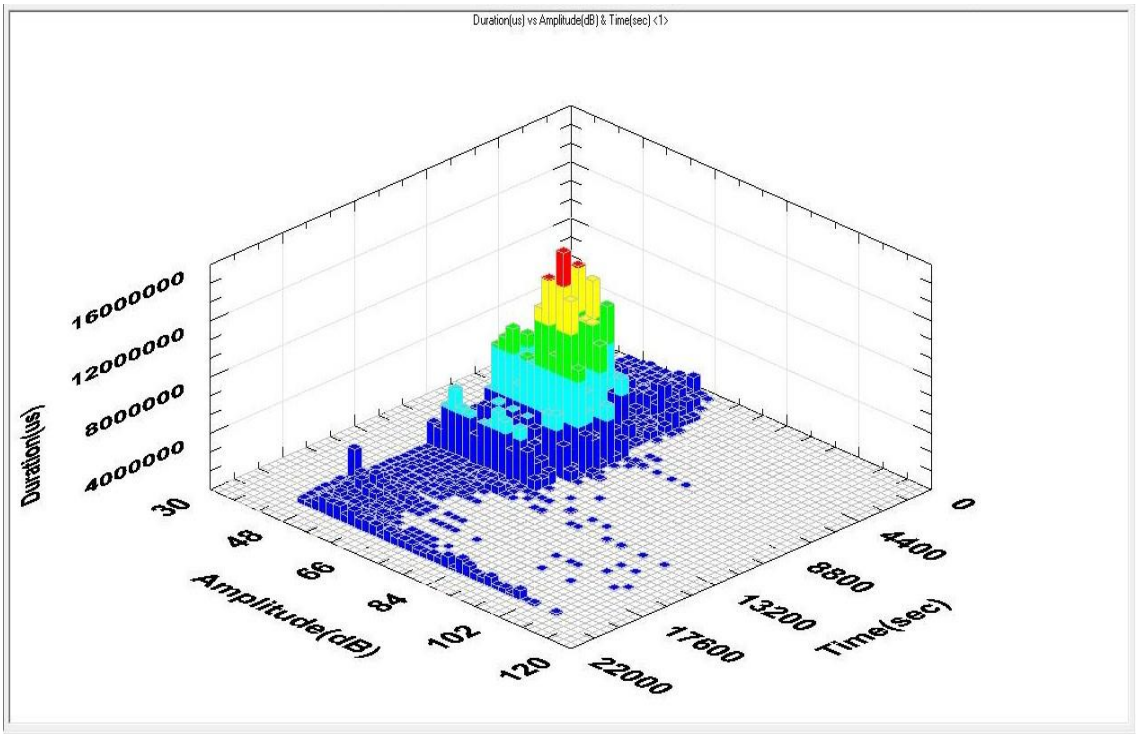

Figure 5.32: 3D plot of AE duration versus amplitude versus time for UEWS test under pure axial loading (0:1) at RT.

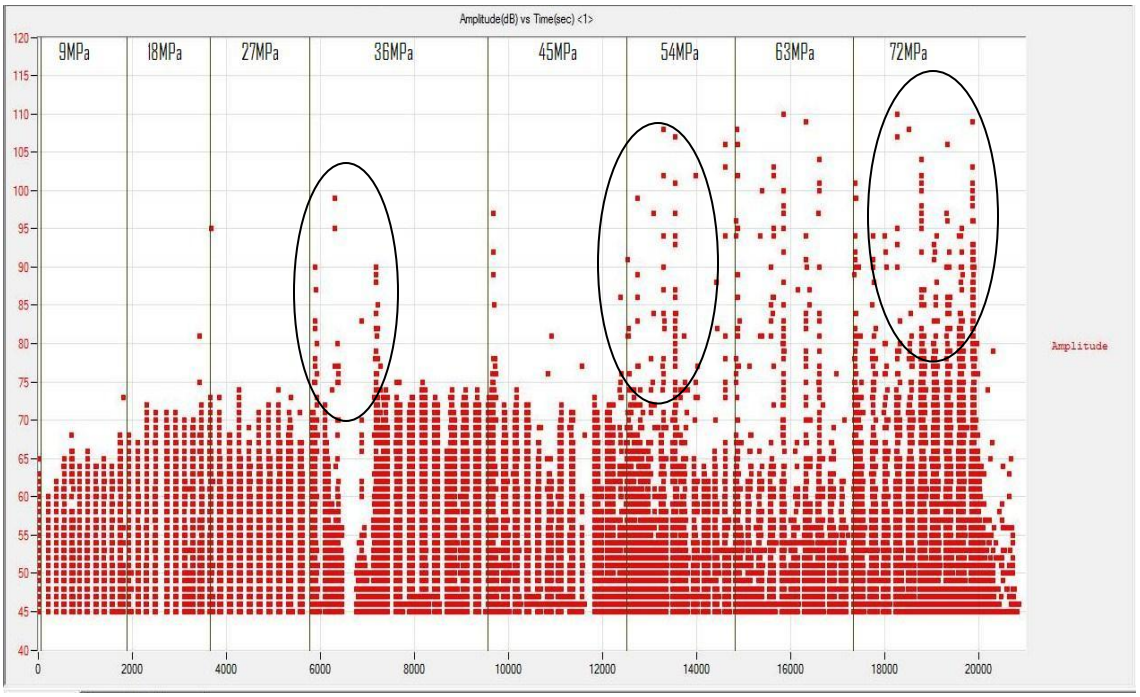

Figure 5.33: Plot of AE amplitudes versus time for UEWS test under pure axial loading (0:1) at RT.

5.6.3. Pure hoop loading (1:0)

Figure 5.34 illustrates the changes in AE counts against time for pure hoop loading (1:0) in the UEWS test at RT. The plot shows that AE activity started very early in the test. However, one distinct difference compared to the previous AE plots for hydrostatic and pure axial loading is that the number of counts did not gradually increase but instead remained fairly stable in distribution with no clear indication of damage initiation and progression. This implies that the sequence of damage mechanisms involved was somewhat different from those seen with 2:1 and 0:1 loadings. The AE counts remained stable until the start of the 7^{th} cycle group at 251MPa wall stress when a sudden increase in activity was noted, suggesting that significant events had occurred. This is believed to correspond to the buckling of the pipe after serious bending had taken place, especially near the reinforcement ends where stress concentrations were at their highest.

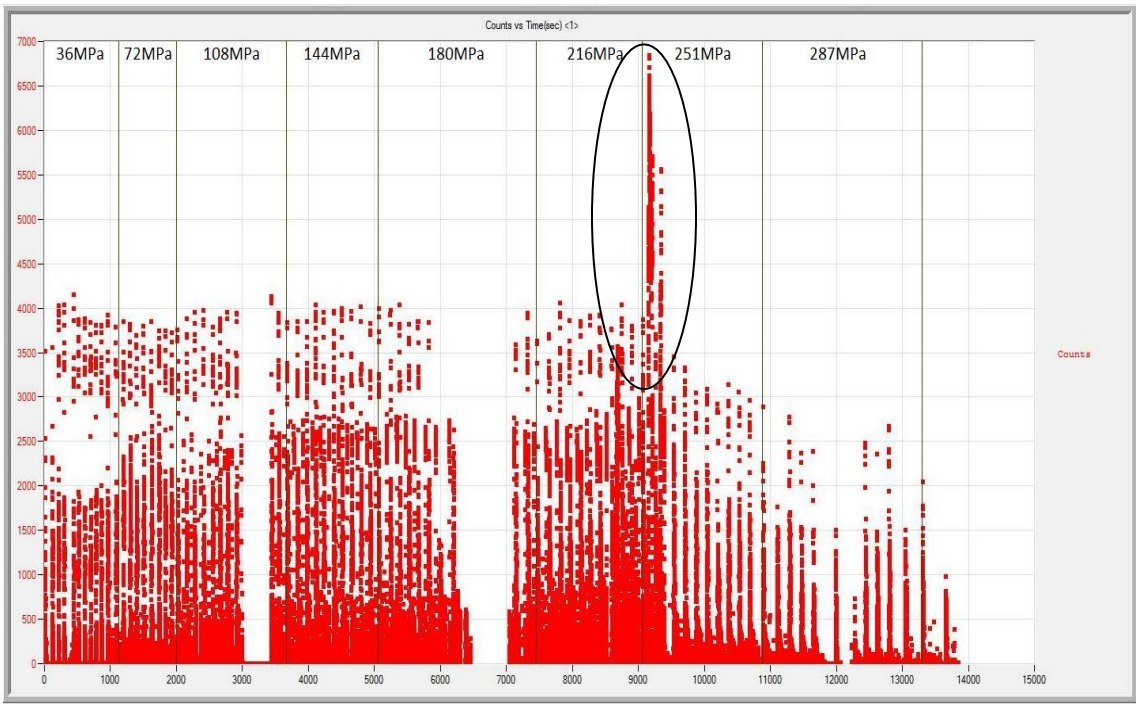

Figure 5.34: Change in AE counts throughout the UEWS test under pure hoop loading (1:0) at RT.

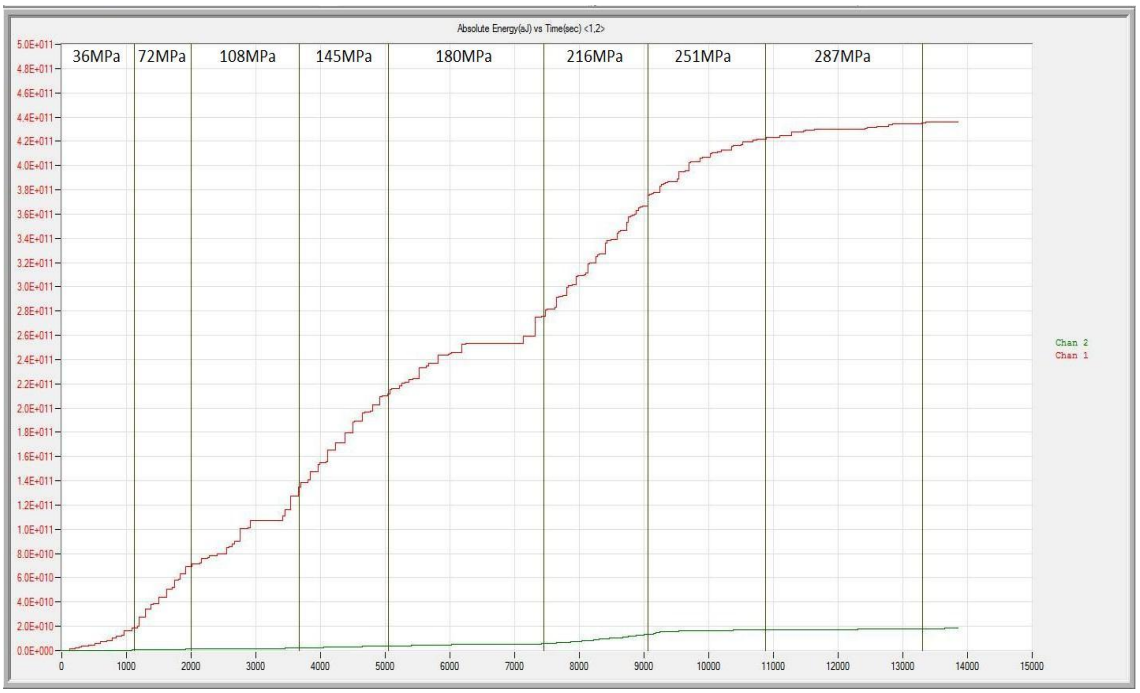

Figure 5.35: Cumulative energy counts throughout the UEWS test under pure hoop loading (1:0) at RT.

The cumulative energy plot against time in Figure 5.35 indicates that failure was taking place close to probe 1. The plot shows continuous rapid increments in energy released, with no clear 'knees' observed. Higher cumulative energy was also released compared to the hydrostatic and pure axial loading conditions, especially in the early cycle groups. Once buckling failure took place in the 7^{th} cycle group, fewer counts and lower energy releases were observed. This is because, after buckling failure, the continuing relatively high shear stress component caused shear deformation of the resin, which then resulted in secondary failure mechanisms such as matrix cracking.

Figures 5.36 and 5.37 show AE duration versus amplitude and a 3D plot of these parameters against time respectively. The plots show that most of the AE events were of intermediate/high duration with intermediate/high amplitude ranging from 60-100dB. These are likely to correspond to the relatively high shear deformation of the resin matrix (zone 2). This is in a good agreement with the plot in Figure 5.20, from which it was established that the shear stress response was the most dominant stress component that governed delamination failure in this loading ratio.

At about 9000 seconds into the test, massive delamination and debonding were generated near the end reinforcement, due to the pipe bending. This was quickly followed by buckling failure accompanied by the audible sound of fibre fracture on the outer surface of the pipe. This can be seen from the 3D plot in Figure 5.37, indicated by the peak of highest duration (due to friction) with a broad range of amplitudes up to 100dB. The bending of the pipe just before buckling failure induced fibre breakage and this is represented by the low duration, high amplitude AE events [166]. The plot also shows that, once buckling failure occurred, secondary failure mechanisms followed represented by events of low amplitude and low/intermediate duration, which can be attributed to matrix cracking (zone 1), and events of high duration, low/intermediate amplitude (zone 3) which are normally associated with friction between crack surfaces [170].

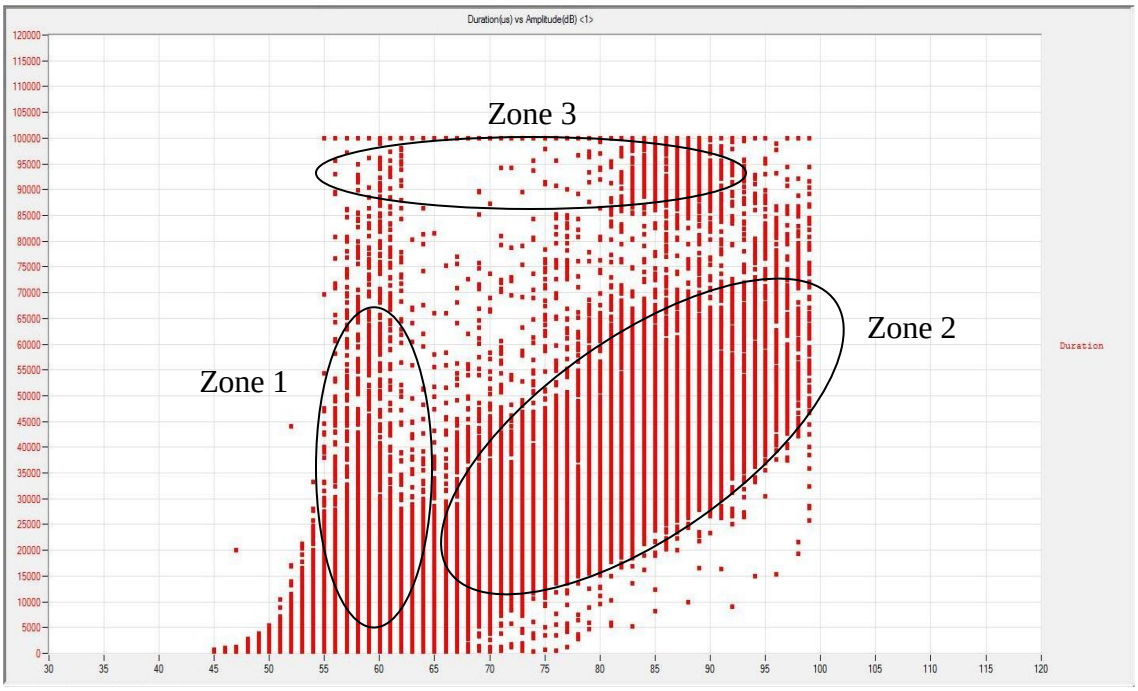

Figure 5.36: Plot of AE duration against AE amplitude for UEWS test under pure hoop loading (1:0) at RT.

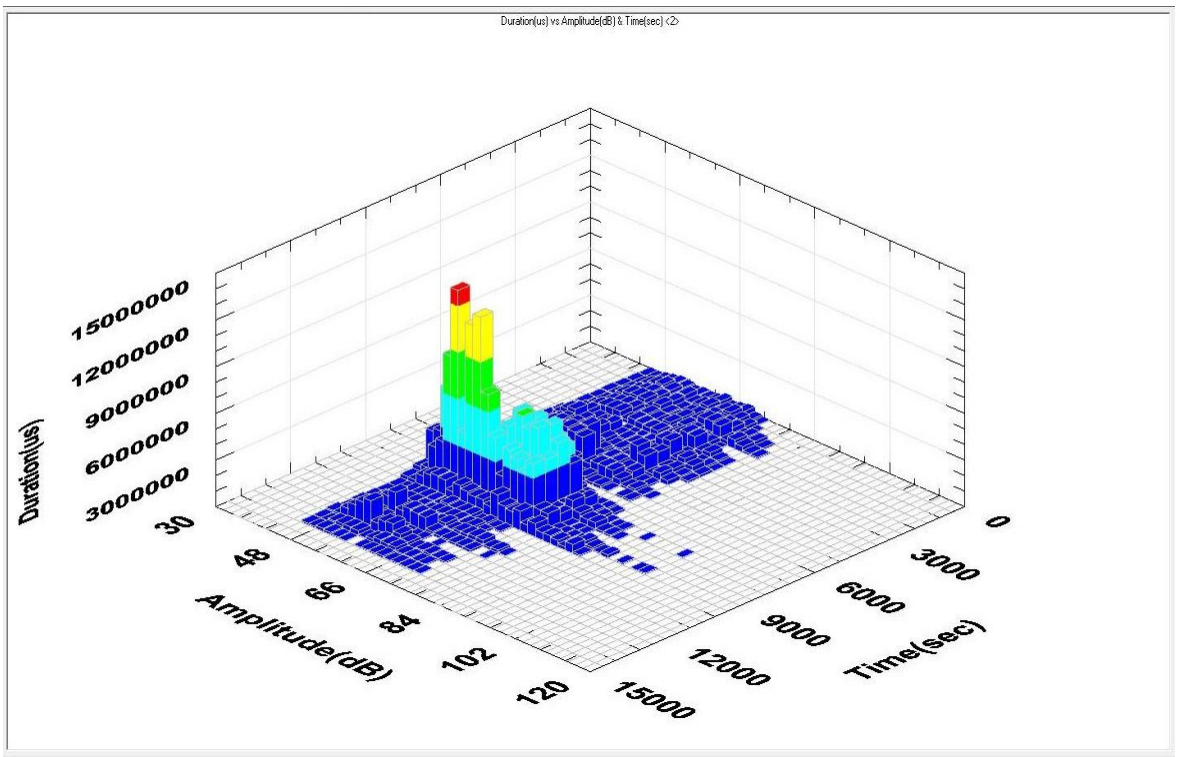

Figure 5.37: 3D plot of AE duration versus amplitude versus time for UEWS test under pure hoop loading (1:0) at RT.

5.7. Microscopic analysis

Samples were cut from the previously marked areas of the tested pipes where weepage had been observed in the UEWS test under hydrostatic loading at the 2:1 stress ratio. The samples were then ground and polished as detailed in Section 3.8 before a micrograph of the sample's cross-section was carefully examined. Figure 5.38 shows a typical micrograph of a polished sample taken using an optical microscope under 25x magnification. Since the sample was cut in the direction of the fibres, a distinct banded structure of +55 and -55 plies is clearly visible. The micrograph image shows that the laminate was less well consolidated in the outer layers compared to the inner layers. It was also apparent that the outer layers have a lower volume fraction of fibres than the inner. The black spots are micro-voids, which are imperfections resulting from entrapped gasses, which may have occurred during the curing process of the epoxy. The black lines are matrix cracks, which appear to have travelled through the ply thickness before ceasing at the nearest interface. Figure 5.39 showing a micrograph sample under 50x magnification, shows the network of transverse matrix cracks spaced almost equidistantly.

Figure 5.40 (a) and (b) shows the matrix cracking under 100x and 200x magnification respectively. The micrograph images confirmed that the matrix cracks propagated transversely in the resin matrix between fibre reinforcements. Figure 5.40(a) shows a matrix crack induced by a void in the middle of the ply which propagated in two opposite directions before reaching the next adjacent ply which at a different angle to the propagating crack plane. This initiation of cracks resulted from the stress concentration developed near the void which acted as a weak point for nucleation. Figure 5.40(b) illustrates the matrix cracks in the regions of high fibre content where cracking took place near the fibre-matrix interface. According to Jones [19], these regions contain many long continuous interface paths. Due to the considerable difference in the modulus of fibre and matrix, the strain distribution is hence not uniform and stressed laminates in the transverse direction cause large strain magnifications in the matrix regions between fibres allowing the initiation of matrix cracks. Once initiated, the matrix cracks propagate through the best fibre packing by coalesces of matrix-fibre debonding.

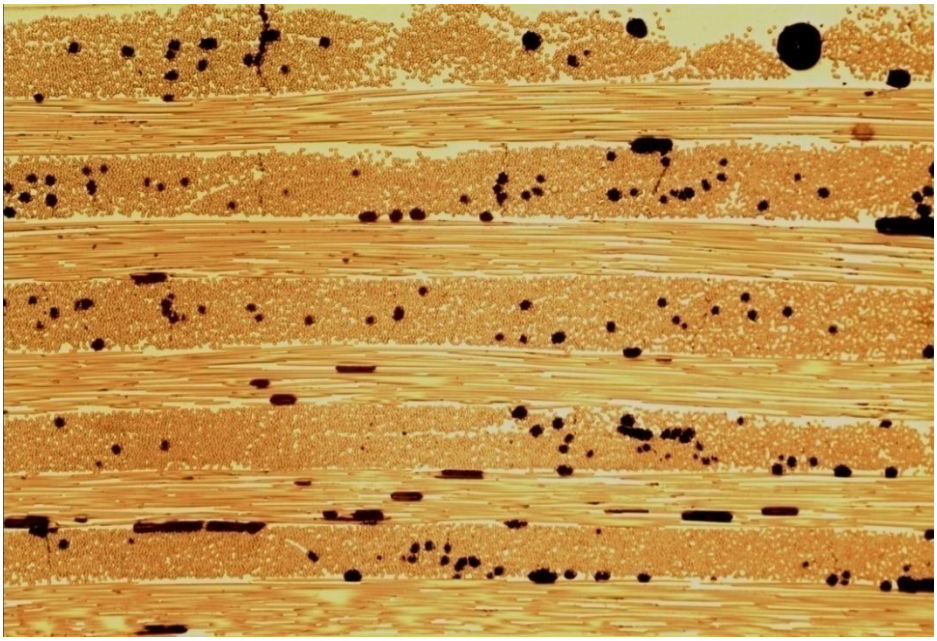

Figure 5.38: Optical micrograph of a polished weepage failure sample under x25 magnification, showing a distinct two banded structure at +55° and -55°. Voids and matrix cracks are clearly visible.

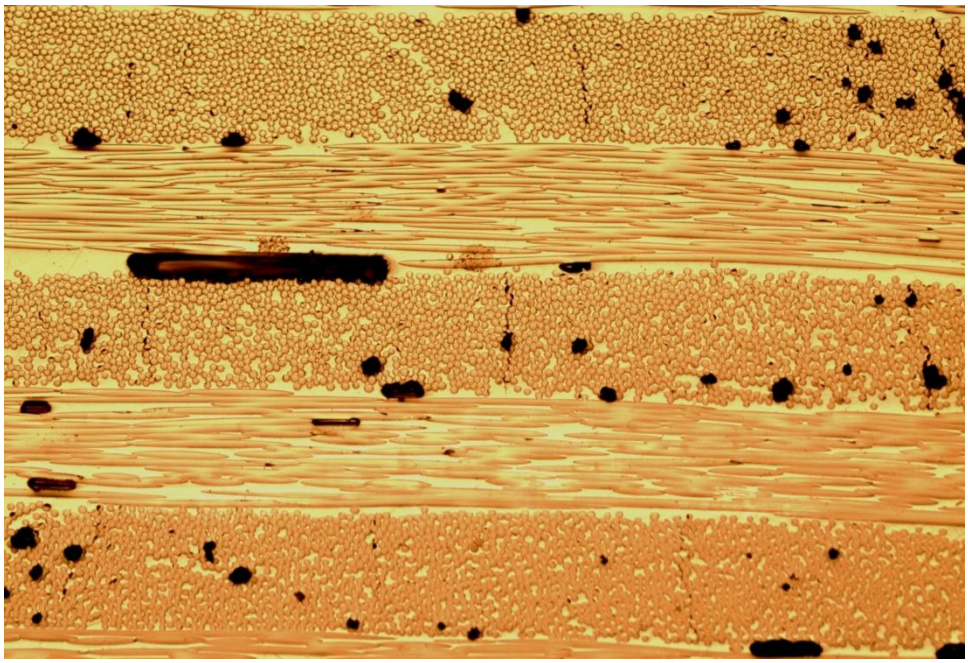

Figure 5.39: Optical micrograph of a polished sample under x50 magnification. Networks of cracks can be seen showing an almost equidistance spacing between cracks.

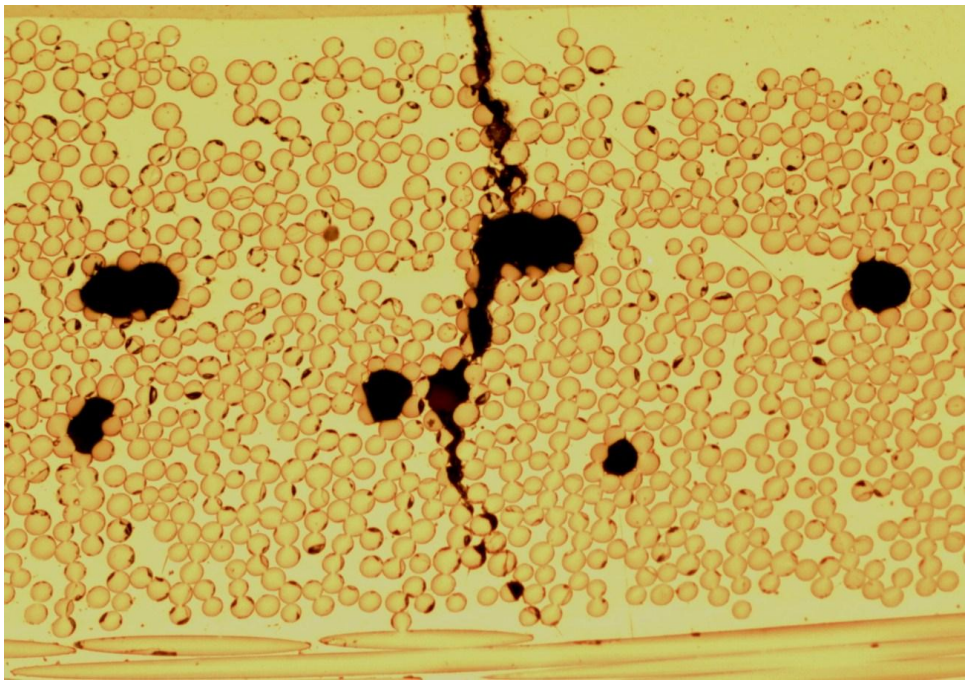

(a)

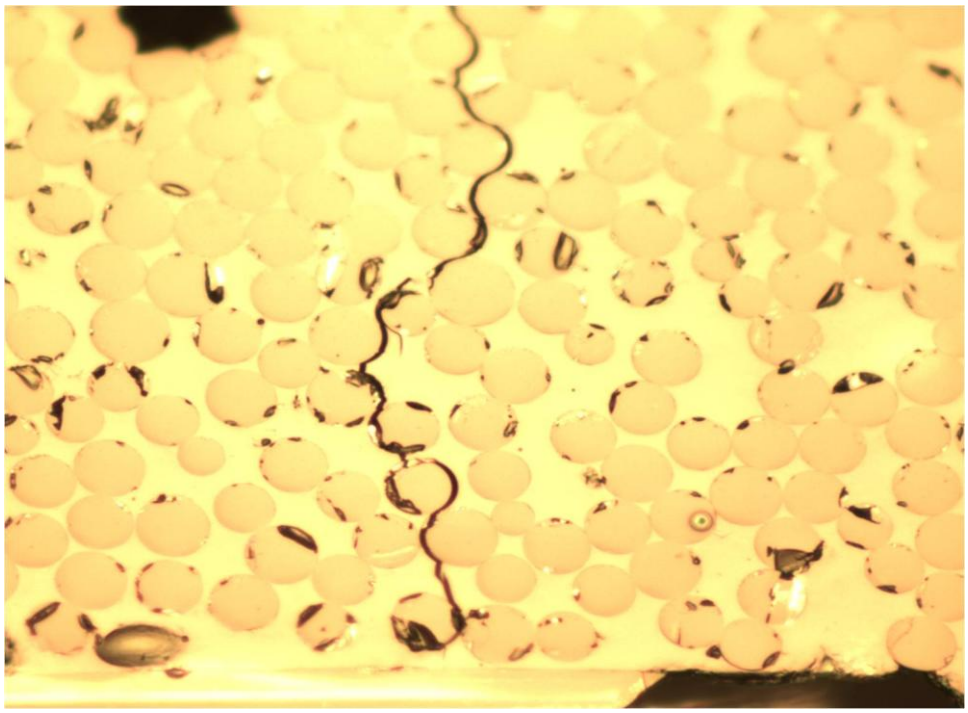

(b)

Figure 5.40: Optical micrograph of a polished sample under (a) x100 and (b) x200 magnification showing types of matrix cracks observed. In (a) cracking was initiated near the micro-void whereas in (b) cracking took place in high density fibre regions between fibre matrix interfaces.

In all samples examined, the main damage mechanism observed was matrix cracking. Thus, the most important parameter used in the modelling of the UEWS tests, and its influence in determining the stress which corresponds to damage growth, is crack density. Crack density is defined as the ratio of ply thickness and crack spacing. Figure 5.41 (a-d) shows micrographs of polished samples with visible crack density distribution and measurements of crack spacing and ply thickness. As observed previously (in Figure 5.39), the cracks are spaced almost equidistantly, implying a specific critical value of crack density at which weepage takes place.

From the measurements acquired, the average crack density at weepage for 2:1 loading was calculated to be in the range 0.60-0.65 depending on the volume fraction and quality of laminate consolidation. This is in close agreement with the assumed value used at the onset of non-linearity response in the E_a^{UEWS} during Miner's law modelling. This value, however was found to be lower than that predicted which was approximately at 0.95. This could be due to the existence of other types of secondary damages such as delamination or fibre breakage that may have precipitated the progression of matrix cracking, but were never accounted for in the modelling process.

As discussed before, weepage failure takes place once a pathway for water through the pipe wall is established. This can only be achieved when the transverse cracks from the inner layer have intersected with the transverse cracks from the next successive layers, thus creating a continuous crack path. However, according to Jones and Hull [19], the existence of interlaminar cracks near ply interfaces, which link up the normally equally distanced transverse cracks, could speed up the onset of weepage failure. These types of cracks are formed due to the interlaminar shear strains developed between plies. However, from the micrograph samples produced, the detection of interlaminar cracks has proven to be very difficult. This is probably because the coalescence of transverse cracks with interlaminar cracks can occur anywhere along the plane parallel to the fibres. Polishing the micrograph samples to the exact point at which these two types of crack meet is almost impossible.

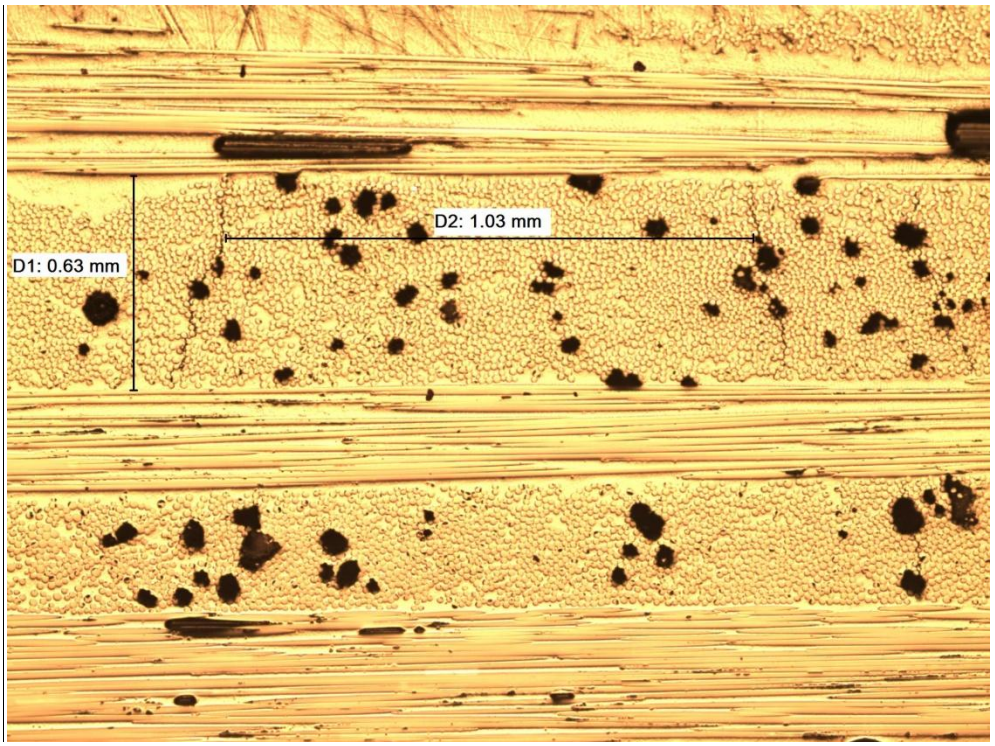

(a)

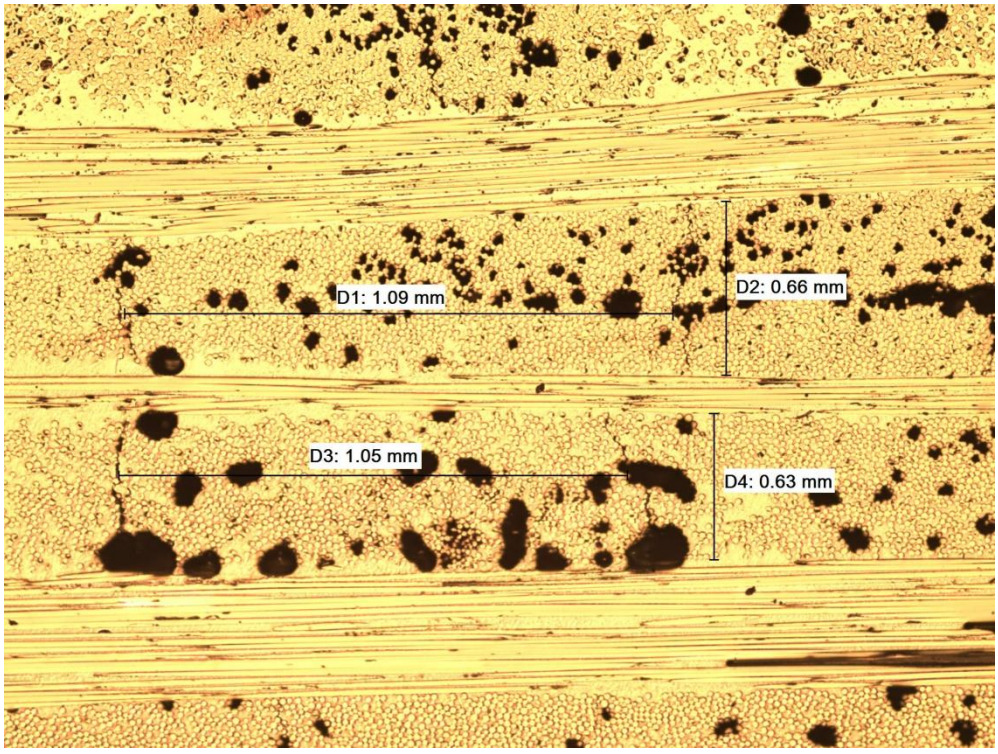

(b)

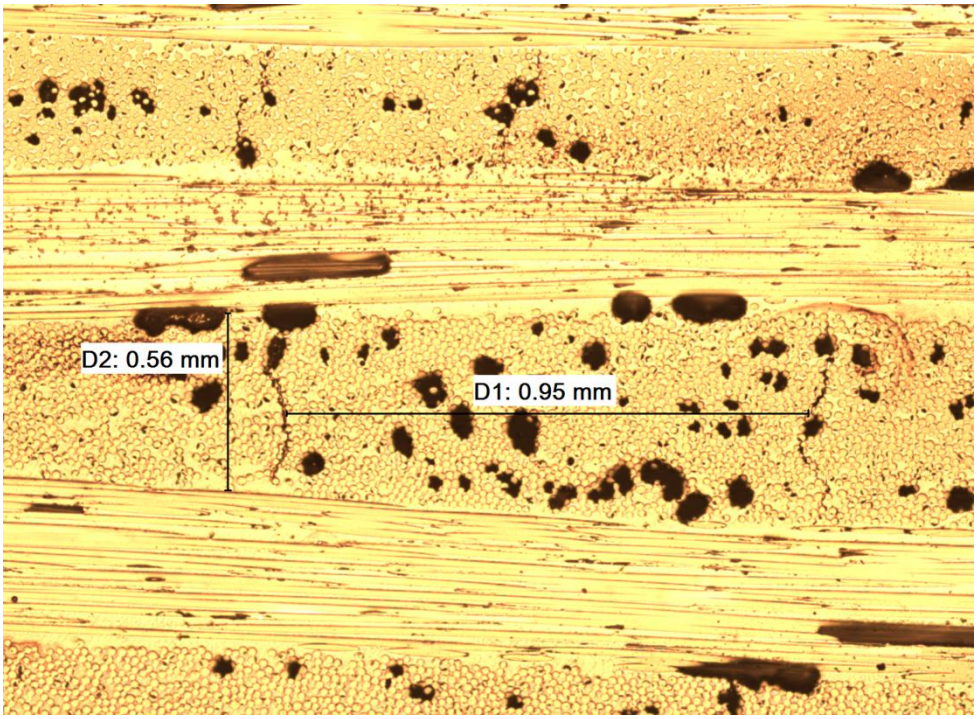

(c)

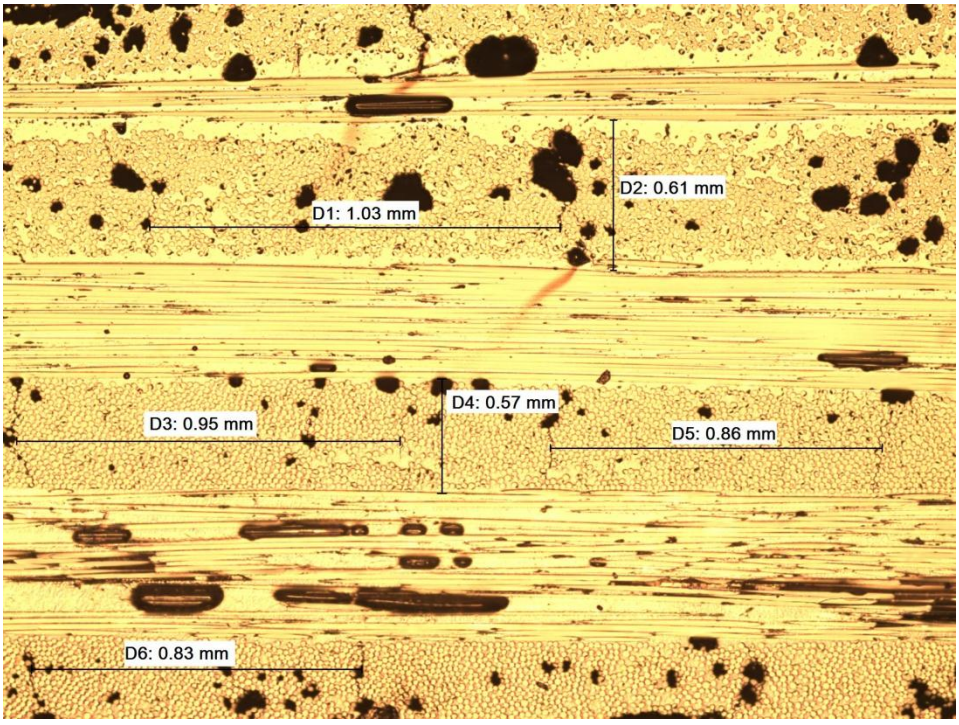

(d)

Figure 5.41: Optical micrograph of a polished sample under x50 magnification showing crack density distribution and measurements of crack spacing and ply thickness. From the measurements, cracks density at weepage is estimated to be in the range of 0.6-0.65.

5.8. Results of damage and general lifetime modelling of UEWS

5.8.1. Miner's Law modelling of UEWS test

The Miner's law modelling of the UEWS test was derived earlier in detail in Chapter 4. Table 5.2 below gives the regression line constants for static and cyclic test methods as described in the ASTM D2992 document, which were provided by FPI for their Wavistrong product used in this investigation. Figures 5.42 to 5.44 demonstrate the modelled stress-strain response of the UEWS tests for the hydrostatic case at RT, 65°C and 95°C respectively. The *k* value that relates the Miner's law expression to the growth of crack density within the laminates was found to vary between 2.5 - 3.0 if the closest fitting to the experimental results, was to be achieved.

Table 5.2: Static and cyclic fatigue constants for GRE pipe at RT, 65°C and 95°C. (Units of *F* correspond to hoop stress in MPa and time-to-failure in hours and unit *H* is in MPa)

	Static loading		Cyclic loading	
Test temp/Const	F	G	H	J
RT	322	0.0395	392	0.099
65°C	392	0.0634	273	0.074
95°C	379	0.0778	305	0.079

All three plots show good agreement with the experimental results, especially in the early cycle groups showing a linear stress-strain response up until the UEWS. Slight discrepancies between the modelled and experimental results were noted at high strains, particularly after the UEWS point had been identified. However, these are suspected to be a consequence of subsequent secondary damages that may have taken place such as delamination or fibre breakage which was not accounted for in the derivation of the model. Furthermore, the linear approximation of the relationship between axial modulus and crack density in the model could have also contributed to the discrepancies noted. Overall, these results indicate that the proposed model successfully offers the possibility of modelling the reductions in strength and elastic properties during the UEWS tests with regards to both crack growth and Miner's Law. This can be observed to agree well with the measured UEWS results for the 2:1 hoop to axial stress ratio reported earlier.

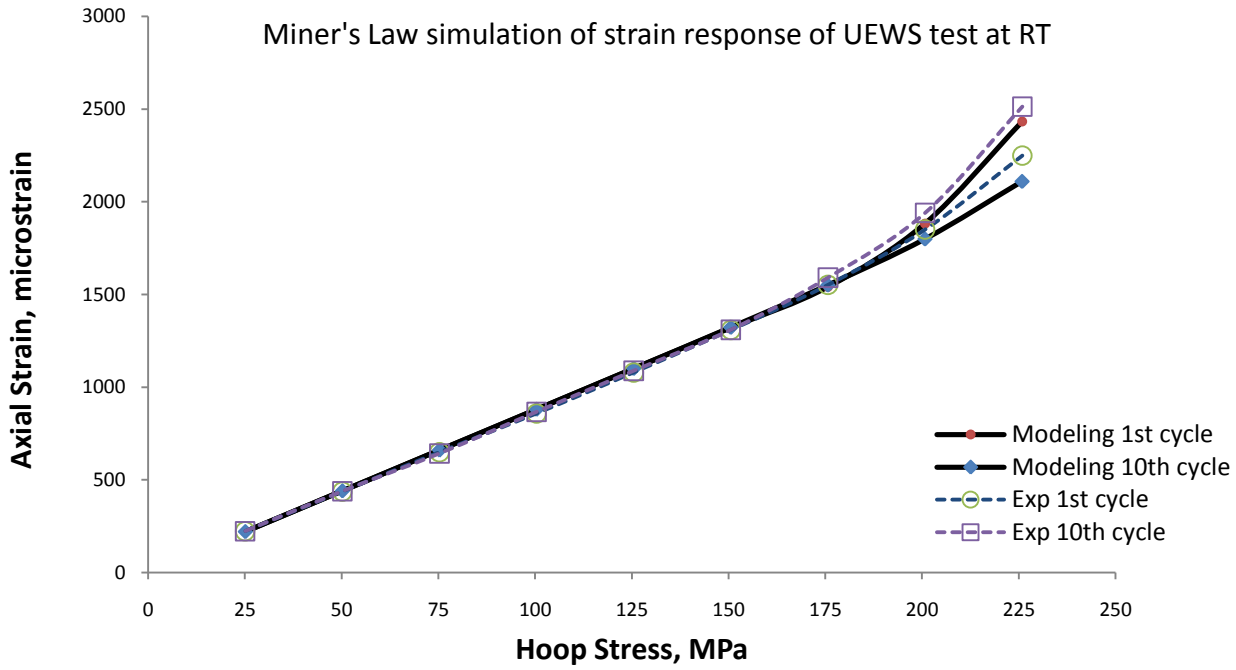

Figure 5.42: Miner's law modelling of UEWS stress strain response for hydrostatic case with 2:1 hoop to axial loading at RT.

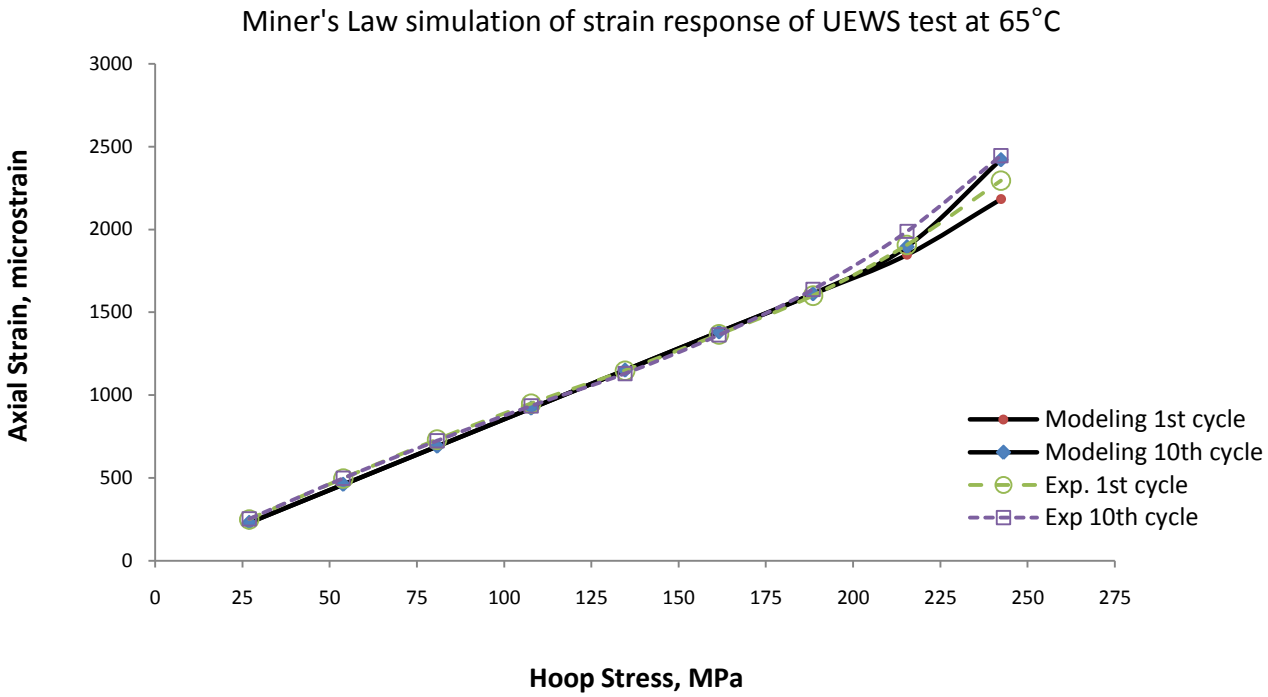

Figure 5.43: Miner's law modelling of UEWS stress strain response for hydrostatic case with 2:1 hoop to axial loading at 65°C.

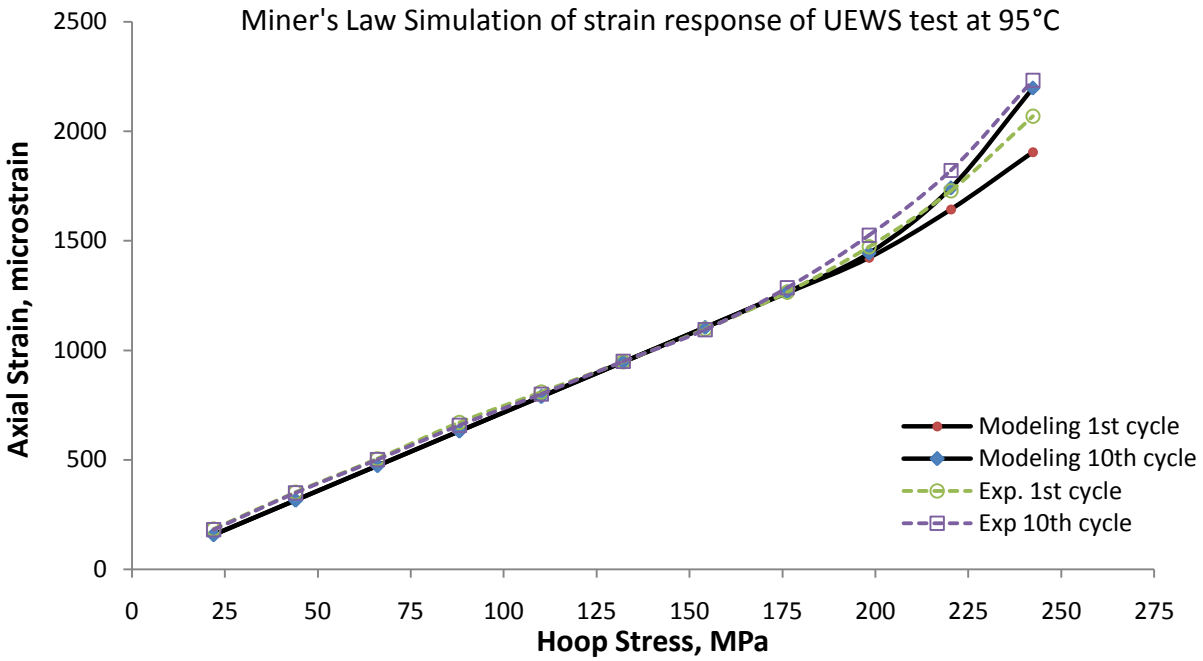

Figure 5.44: Miner's law modelling of UEWS stress strain response for hydrostatic case with 2:1 hoop to axial loading at 95°C.

5.8.2. General lifetime damage model

As been established from the test results, the failure of GRE pipes was governed by either transverse or shear stress, or a combination of both, acting in the ply depending on the loading ratio applied. The test results indicate that transverse stress controlled the failure of pipes in axial dominated loading, whereas high shear stress tends to dominate in hoop dominated loading. In the light of these findings, modelling the failure envelopes from the empirical equation (4.41) described in Section 4.4 was conducted in two sections, each describing these mechanisms of failure. This allows for better fittings of the curves since here the interaction constants between stress components can be adjusted separately according to the dominant stress component. The two sections were then plotted, and lines are expected to intersect at the 4:1 loading ratio as the failure mechanisms changed from being caused by high transverse stress in axial dominated loadings to high shear stress in hoop dominated loadings, as illustrated in Figure 5.20.

Figure 5.45(a-c) shows the failure envelopes generated from this model for the UEWS tests at room temperature (20°C) and elevated temperatures of 65°C and 95°C. For each

envelope, two sets of constants, k_1 and k_2 were determined by fitting the model to the experimental UEWS based failure envelope. The values of the tensile strength in the longitudinal and transverse directions of the ply, the shear strength and the k_1 and k_2 of interaction constants determined are given in Table 5.3.

Table 5.3: Strength of the ply in longitudinal, σ_1* and transverse, σ_2*, shear, τ_{12}*, and interaction constant k_1 and k_2.

Loading conditions	Test temp.	σ_1*, MPa	σ_2*, MPa	τ_{12}*, MPa	k_1	k_2
Axial dominated loading	RT	1000	74	43.75	0.000070	0.000310
Hoop dominated loading		1000	73	44	0.000180	0.000525
Axial dominated loading	65°C	1000	74	43.75	0.000045	0.00048
Hoop dominated loading		1000	73	44	0.000215	0.00043
Axial dominated loading	95°C	1000	73	44	0.000015	0.001
Hoop dominated loading		1000	73	44	0.000250	0.00033

These values tabulated in Table 5.3 were found to give the closest overall fit to the experimental failure envelope based on the UEWS tests. The strength properties were found to be about the same for all test temperatures in order to achieve a satisfactory fit. However, the interaction constants, k_1 and k_2 varied significantly for all three test temperatures and loading conditions. The value of k_1 which is the interactive constant between σ_1 and σ_2 was found to decrease with increases in test temperature for axial loading conditions, but increased for hoop dominated loading. The k_2 value on the other hand, which describes the interaction between σ_2 and τ_{12}, increased markedly from RT to 95°C in the axial dominated loading region, but decreased in hoop dominated loading.

Figure 5.46 shows comparisons between the modelled and the experimental UEWS based failure envelopes. Overall, reasonably good agreement was achieved although slight discrepancies were noted at high axial dominated loadings of 65°C and 95°C, particularly at pure axial loading, 0:1. This is probably because at elevated temperatures the strength of the matrix material degraded, hence resulting in lower UEWS failure points. However, this effect was not accounted for in determining the interaction constants of k_1 and k_2, thus yielding the discrepancies.

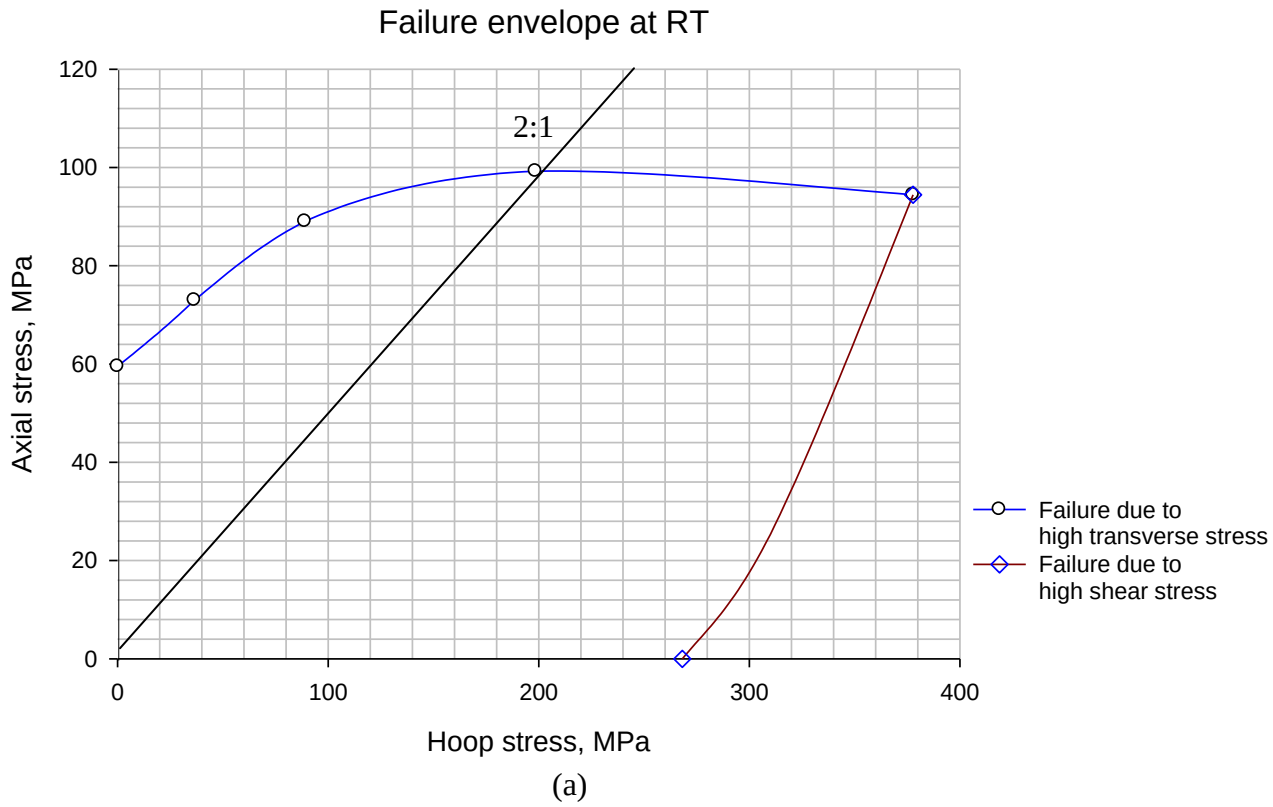
Failure envelope at RT
2:1
Axial stress, MPa
Hoop stress, MPa
0
20
40
60
80
100
120
0
100
200
300
400
Failure due to high transverse stress
Failure due to high shear stress

(a)

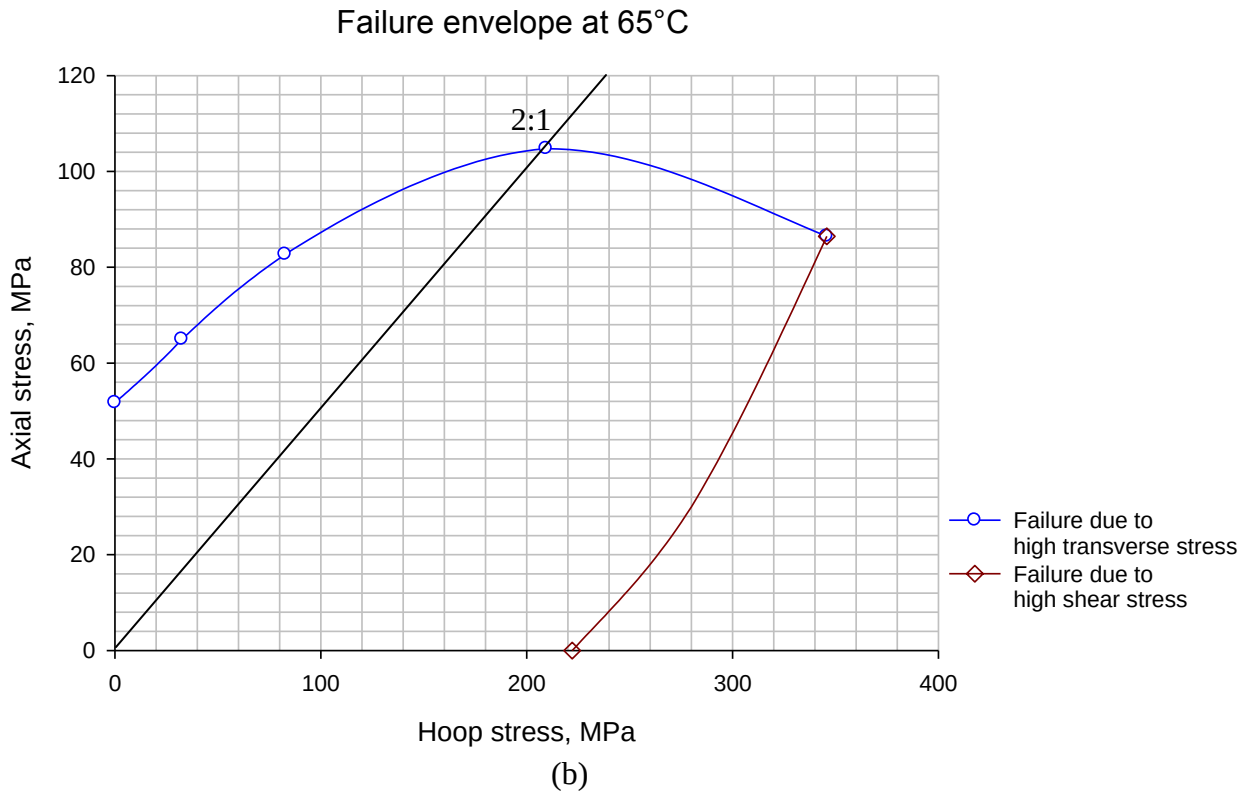
Failure envelope at 65°C
2:1
Axial stress, MPa
Hoop stress, MPa
0
20
40
60
80
100
120
0
100
200
300
400
Failure due to high transverse stress
Failure due to high shear stress

(b)

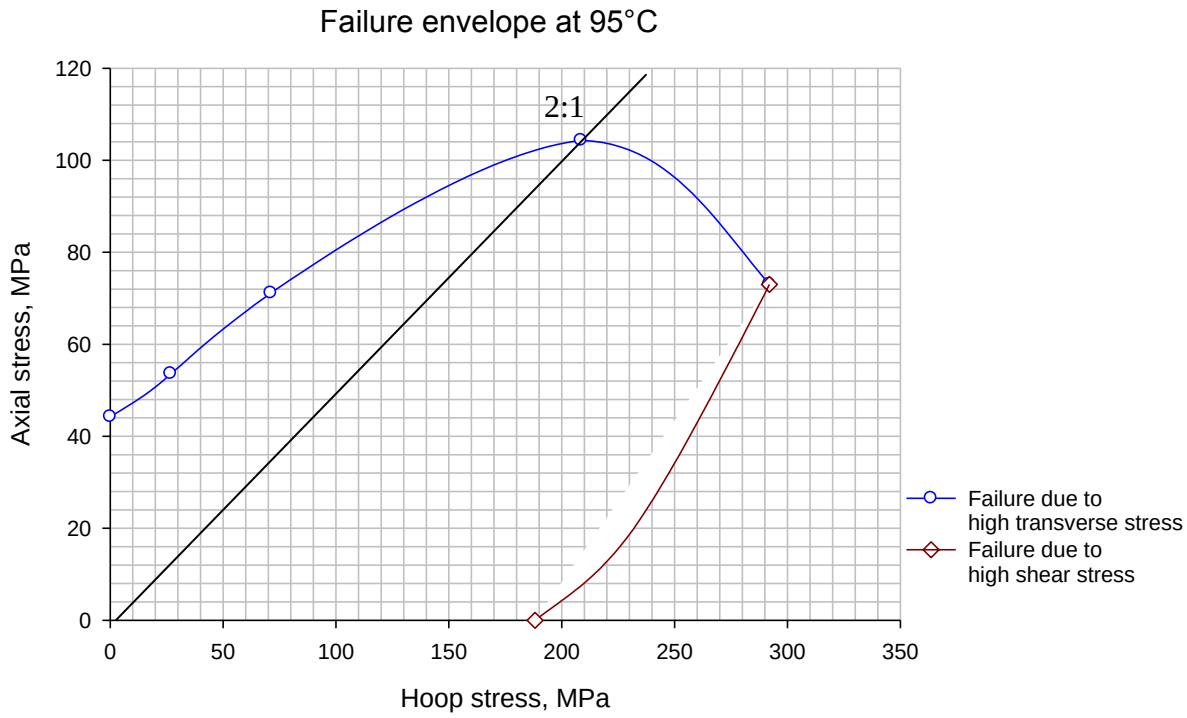

(c)

Figure 5.45: Predicted failure envelopes at (a) RT, (b) 65°C and (c) 95°C generated from two sections representing the dominant failure mechanisms caused by high transverse stress (blue line) and high shear stress (brown line).

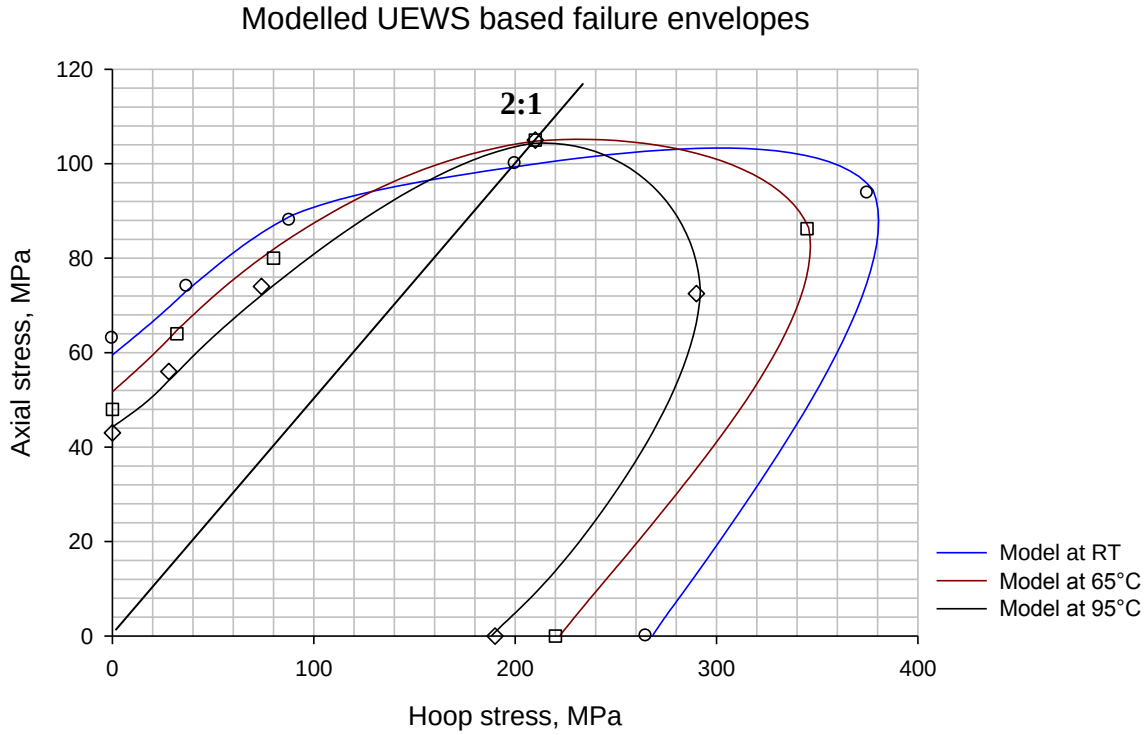

Figure 5.46: Comparison between the experimental (symbols) and predicted (lines) failure envelopes at RT, 65°C and 95°C.

CHAPTER 6: CONCLUSIONS AND FUTURE WORK

6.1. Conclusions

This investigation looks at the UEWS test as a possible alternative for the requalification of GRE pipes instead of those described in the ASTM D2992 document. GRE pipe of 2 metres long and 200mm in diameter were subjected to multiaxial UEWS tests at different temperatures, yielding numbers of interesting findings. In this study, the ply properties of GRE pipes were carefully calculated using the modified Halpin-Tsai and laminate theory was then applied to predict the mechanical properties of the pipes. The results were then compared with engineering values provided by the pipe manufacturer and were found to be in close agreement.

A novel UEWS testing rig capable of independently applying static and cyclic pressure tests under various combinations of hoop to axial stress ratio at temperatures up to 95^0C was developed. The UEWS tests were then conducted under combinations of internal pressure and axial load to produce six different stress ratios, ranging from pure axial loading to pure hoop loading at room temperature. The tests were later repeated at elevated temperatures of 65^0C and 95^0C to investigate the effects of high temperature on the performance of GRE pipe.

The degradations in the axial and hoop moduli of the pipes during the hydrostatic UEWS tests was investigated using simple pull and ring tests on a range of UEWS samples from an undamaged (virgin) pipe to intermediate stages of damage (50% and 100% UEWS) to weepage sample. The results indicate that the axial modulus was reduced by a total of over 26% from virgin to weepage sample, whereas the hoop modulus declined by 22%. It was therefore concluded that the axial modulus is more sensitive than the hoop modulus to the effects of crack density.

From the UEWS results plotted, all test results demonstrated a linear elastic range at low stress levels. The UEWS was then identified when the deviation in strain between the first and the last cycle became more severe, at which point the stress-strain relationship became non-linear. As the load further increased, the non-linearity became more pronounced. This suggests the growth of damage which subsequently reaches a critical level leading to weepage/leakage failure. It was also observed that the UEWS stress-strain response is strongly dependent on the stress ratio and test temperature applied. The early non-linearity noted in hoop dominated loading was established as the result of the nonlinear behaviour of matrix material at high strain.

Three distinct failure modes were observed: tensile axial failure in pure axial loading, weepage failure in 0.5:1, 1:1 and 2:1 loadings, and localized leakage in high hoop dominated loadings (4:1 and 1:0). Transverse matrix cracks govern the failure observed at pure axial, 0.5:1, 1:1 and 2:1 loading, while the shear deformation of the matrix control failure at high hoop dominated loading. The failure modes observed are in good agreement with those reported in earlier studies.

Full tensile-tensile UEWS and leakage based failure envelopes were developed at a range of temperatures from 20°C (RT) to 95°C. Both show a strong dependence on stress ratio and test temperature. The UEWS hoop strength was over four times greater than that of pure axial strength. The UEWS failure strength at elevated temperatures was generally reduced except for the optimum loading condition of 2:1 where strength increased. Considerable reductions were noted in pure axial and pure hoop loading where failure is matrix dominated. This is due to the resin matrix becoming softened at high temperatures, which considerably reduces its strength. In 2:1 loading on the other hand, where load is fibre dominated, the UEWS and weepage strength were enhanced by 7% and 8% respectively due to the improved ductility and hence the strain to failure of the matrix material.

The weepage failure envelopes were noticeably higher by about 8-12% than the UEWS failure strength. The UEWS based failure envelope suggests a very attractive feature, since it provides pipe engineers with more realistic design limits which consider the initiation and progression of permanent damage in the laminates rather than merely being based on leakage points as presented in previous studies.

Acoustic emission measurements were conducted during the UEWS tests under hydrostatic, pure axial and pure hoop loadings at room temperature (RT). The results for both hydrostatic and pure axial loadings indicate that matrix cracks were initiated and possibly had progressed to delamination immediately before the UEWS point was reached at 200MPa of hoop stress and 63MPa of axial stress respectively. However, no clear damage initiation and progression was observed for pure hoop loading. Almost stable AE measurements were recorded, which is thought to be due to relatively high shear stress. Significant AE events were only noted when the bending of the pipe just before buckling induced massive delamination and debonding failure followed by fibre fracture on the outer surface of the pipe.

As specified earlier, the objectives of the AE measurements were to characterise damage mechanisms involved at different stages of UEWS tests and to search for correlations between AE activity and the UEWS results. Through the analysis, the AE results do give good accounts on the states of damage mechanisms and progressions involved based on the distinct AE signatures throughout the test. The results hence suggest that AE can be used as the monitoring tool to provide an early-warning system for GRP pipe failure. Nevertheless, the question remains whether the method can actually be used to determine exactly at what state of damage mechanism, the UEWS point is considered to be reached.

The corresponding weepage crack density was determined through microscopic study by examining the post-test microstructure of the pipe wall. Transverse matrix cracks were observed to propagate through the ply thickness, stopping at the adjacent ply. The matrix

cracks were found spaced equidistantly, and the crack density at weepage was calculated to be in the range of 0.7-0.8, which is slightly lower than the predicted value of 0.8-1.0.

Miner's law modelling of the stress-strain response of the UEWS tests shows a good agreement with the experimental results, particularly in the early cycle groups at lower levels of strain. Slight discrepancies were noted at higher strain after the UEWS point had been reached, possibly due to other damage modes such as delamination and fibre breakage occurring that were not accounted for in the model. It has also been shown that cyclic rather than static loading dominates the UEWS test response. Finally, a general lifetime damage model was developed, and reasonably good agreement with the experimental envelopes was achieved.

As this study has demonstrated, the UEWS approach offers an attractive alternative to the existing procedures in ASTM D2292 for re-qualifying GRE pipes. It is envisaged that, with further study, the UEWS procedure may possibly form the basis of a full qualification programme. However, this will only be possible if the procedure can be interpreted in terms of damage progression and related to the hydrostatic design basis (HDB) currently acquired from the ASTM D2992 regression procedure.

6.2. Suggestions for future work

Improvements of the test rig developed for the UEWS test are possible. Currently, the operator has to conduct the test for over six hours, since the operation of loading and unloading of pressures was handled manually. In order to improve the operation, the two-ball valves used in the test rig could be replaced with solenoid valves. A digital input module is required in the control system developed to enable the feeding of the input pressure needed during the UEWS tests, so that the opening and closing of the solenoid valves could be controlled automatically. This would allow the entire procedure of testing and data collection to be conducted automatically.

The results of the UEWS tests indicate that UEWS strength at high temperatures generally degraded except for pure hydrostatic loading where it is increased. However, this appears to contradict with the findings of the regression based procedure described in ASTM D2992, which shows a reduced LCL value at 65°C and 95°C compared to RT. Considering the procedure is a long term rupture test, ageing of laminates could affect the lifetime of the pipe which has not been accounted for in the UEWS test. Hence further investigation of UEWS tests should be performed on aged pipes, which can be achieved by exposing pipe samples in a water bath for a certain time and temperature.

As discussed in detail for the hoop dominating UEWS results, the pipes failed due to high stress concentrations near the end fittings which resulted in the bending of the pipes followed by buckling failure. In order to investigate the true nature of the UEWS and final failure at high hoop loading, the end fittings and the pipe's reinforcement end would probably have to be redesigned to minimise the effects of stress concentrations. Smaller and shorter test samples could minimise these stress concentrations and avoid buckling failure, but it would have to be ensured that this would reflect the true nature of failure in real commercially available pipe products.

Further investigations into the effect of winding angles on the UEWS could provide interesting findings. GRE pipes at higher winding angles such as ±63° and ±75° might be expected to yield lower UEWS points in axial dominated loading but could provide better performance in high hoop loadings. In contrast, pipes with lower winding angles would be expected to have higher UEWS strength in axial dominated loading. Such results would provide engineers with more accurate design limits to improve the performance of specific wound pipes to suit particular loading conditions.

The Miner's law model developed here has proved to provide good prospects for modelling the UEWS stress-strain response with respect to increasing crack density. However, the modelling is dependent on the regression constants used, which means that it is only applicable to the hydrostatic loading condition since no regression data are

available for non-hydrostatic loading. GRE pipe manufacturers must qualify their products based on the procedures elucidated in ASTM D2992, which involve conducting only static and cyclic tests under hydrostatic loading from RT up to 95°C. A second, more general model needs to be developed to overcome this problem.

REFERENCES

1. Fahrer, A., *A Study of the Manufacturing and Characterisation of Filament Wound Reinforced Thermoplastic Pipework,*. PhD Thesis, University of Newcastle, 1997.
2. Gibson, A.G., *Composite materials in the offshore industry.* Metals and materials, 1989. 5(10): p. 590-594.
3. Gibson, A.G. and D.A. Spagni, *Recent developments in the use of composite materials offshore.* The Institute of Marine Engineers (UK), 1991: p. 3-9.
4. Salama, M.M., *Advanced composites for the offshore industry: applications and challenges.* Revue de l'Institute Francais du Petrole, 1995. 50(1): p. 19-26.
5. Frost, S.R., *Applications of polymer composites within the oil industry.* Composites for the Offshore Oil and Gas Industry - Design and Application, 1999: p. 45-54.
6. Daniel, I.M., Ishai, O., *Engineering Mechanics of Composite Materials, 2Ed.Oxford University Press., Inc.* 2006.
7. Muttana Suresh Babu, G.S.S.B., *Composite Fabrication by Filament Winding - An Insight* Available from http://www.tifac.org.in/, 2000.
8. Shen, F.C., *A filament-wound structure technology overview.* Materials Chemistry and Physics, 1995. 42(2): p. 96-100.
9. Lye, S.W. and F.Y.C. Boey, *Development of a low-cost prototype filament-winding system for composite components.* Journal of Materials Processing Technology, 1995. 52(2-4): p. 570-584.
10. Mazumdar, S.K., *Composites Manufacturing: Materials, Product and Process Engineering, CRC Press.* 2002.
11. *Picture courtesy of the Polymer Processing website http://www.polymerprocessing.com/operations/filwind/index.html.*
12. Freeman, W.T. and A.B. Stein, *Filament winding: Waking the sleeping giant.* Aerospace America, 1985. 2(10): p. 44-49.
13. Abdalla, F.H., et al., *Design and fabrication of low cost filament winding machine.* Materials and Design, 2007. 28(1): p. 234-239.
14. Saied, R., *Elevated Temperature Envelopes for Composite Tubing.* PhD Thesis, University of Newcastle, 2004.
15. *Guide to Composites, http://www.netcomposites.com/.* 2008.
16. Agarwal, B.D., Broutman, L.J., *Analysis and Performance of Fiber Composites.* John Wiley & Sons, Inc., 1990.
17. Varma, I.K. and V.B. Gupta, *Thermosetting resin properties.* Chapter 2: Comprehensive composite materials, Elsevier, 2000.

18. May, C.A., *Epoxy Resins Chemistry and technology.* New York: Marcel Dekker, 1.
19. Jones, M.L.C. and D. Hull, *Microscopy of failure mechanisms in filament-wound pipe.* Journal of Materials Science, 1979. 14(1): p. 165-174.
20. Owen, M.J. and D.J. Rice, *Biaxial strength behaviour of glass fabric-reinforced polyester resins.* Composites, 1981. 12(1): p. 13-25.
21. Swanson, S.R., A.P. Christoforou, and G.E. Colvin Jr, *Biaxial testing of fiber composites using tubular specimens.* Experimental Mechanics, 1988. 28(3): p. 238-243.
22. Ellyin, F. and J.D. Wolodko, *Testing facilities for multiaxial loading of tubular specimens.* ASTM Special Technical Publication, 1996. 1280: p. 7-24.
23. Hull, D., Clyne, T.W., *An Introduction to Composite Materials.* Cambridge University Press, 1996.
24. Hull, D., M.J. Legg, and B. Spencer, *Failure of glass/polyester filament wound pipe.* Composites, 1978. 9(1): p. 17-24.
25. Rosenow, M.W.K., *Wind angle effects in glass fibre-reinforced polyester filament wound pipes.* Composites, 1984. 15(2): p. 144-152.
26. Soden, P.D., R. Kitching, and P.C. Tse, *Experimental failure stresses for ±55° filament wound glass fibre reinforced plastic tubes under biaxial loads.* Composites, 1989. 20(2): p. 125-135.
27. Mistry, J., A.G. Gibson, and Y.S. Wu, *Failure of composite cylinders under combined external pressure and axial loading.* Composite Structures, 1992. 22(4): p. 193-200.
28. Hale, J.M., A.G. Gibson, and S.D. Speake, *Biaxial failure envelope and creep testing of fibre reinforced plastic pipes in high temperature aqueous environments.* Journal of Composite Materials, 2002. 36(3): p. 257-270.
29. Hale, J.M., et al., *High temperature failure envelopes for thermosetting composite pipes in water.* Plastics, Rubber and Composites Processing and Applications, 2000. 29(10): p. 539-548.
30. Carvalho, A. and C. Marques, *A new formula to predict the structural life of composite pipes.* JEC Composites Magazine, 2007. 44(33): p. 71-74.
31. Ellyin, F. and M. Martens, *Biaxial fatigue behaviour of a multidirectional filament-wound glass-fiber/epoxy pipe.* Composites Science and Technology, 2001. 61(4): p. 491-502.
32. Frost, S.R., *Design, Failure and Life Predictions of Composite Pipelines and Piping Systems.* SIEP B.V., 1997.
33. Gibson, A.G., et al., *Failure Envelopes for Glass Fiber Pipes in Water up to 160C.* Proceeding 'The 4th MERL International Conference, Oilfield Engineering with Polymer, 3-4 November, pp. 163-177, Institute of Electrical Engineers, London UK., 2003.

34. Kaddour, A.S., P.D. Soden, and M.J. Hinton, *Failure of ±55 degree filament wound glass/epoxy composite tubes under biaxial compression.* Journal of Composite Materials, 1998. 32(18): p. 1618-1645.
35. Meijer, G. and F. Ellyin, *A failure envelope for ±60° filament wound glass fibre reinforced epoxy tubulars.* Composites Part A: Applied Science and Manufacturing, 2008. 39(3): p. 555-564.
36. Mertiny, P. and F. Ellyin. *Performance of high-pressure fiber-reinforced polymer composite pipe structures*. in *American Society of Mechanical Engineers, Pressure Vessels and Piping Division (Publication) PVP*. 2006.
37. Soden, P.D., M.J. Hinton, and A.S. Kaddour, *Biaxial test results for strength and deformation of a range of E-glass and carbon fibre reinforced composite laminates: Failure exercise benchmark data.* Composites Science and Technology, 2002. 62(12-13 SPECIAL ISSUE): p. 1489-1514.
38. Soden, P.D., Leadbetter, D., Griggs, P. R., Eckold, G. C., *The strength of a filament wound composite under biaxial loading.* Composites, 1978. 9(4): p. 247-250.
39. Tarakcioglu, N., L. Gemi, and A. Yapici, *Fatigue failure behavior of glass/epoxy ±55 filament wound pipes under internal pressure.* Composites Science and Technology, 2005. 65(3-4): p. 703-708.
40. Carroll, M., et al., *Rate-dependent behaviour of ±55° filament-wound glass-fibre/epoxy tubes under biaxial loading.* Composites Science and Technology, 1995. 55(4): p. 391-403.
41. Chen, R.X., *Structural analysis for filament-wound cylinder pressure vessel.* Guti Huojian Jishu/Journal of Solid Rocket Technology, 2004. 27(2): p. 105-107.
42. Frost, S.R. and A. Cervenka, *Glass fibre-reinforced epoxy matrix filament-wound pipes for use in the oil industry.* Composites Manufacturing, 1994. 5(2): p. 73-81.
43. Ferry, L., et al., *Interaction between plasticity and damage in the behaviour of [+ ϕ, - ϕ]$_n$ fibre reinforced composite pipes in biaxial loading (internal pressure and tension).* Composites Part B: Engineering, 1998. 29(6): p. 715-723.
44. Joseph, E. and D. Perreux, *Fatigue behaviour of glass-fibre/epoxy-matrix filament-wound pipes: Tension loading tests and results.* Composites Science and Technology, 1994. 52(4): p. 469-480.
45. Perreux, D. and E. Joseph, *The effect of frequency on the fatigue performance of filament-wound pipes under biaxial loading: Experimental results and damage model.* Composites Science and Technology, 1997. 57(3): p. 353-364.
46. Perreux, D. and F. Thiebaud, *Damaged elasto-plastic behaviour of [+ϕ, -ϕ]$_n$ fibre-reinforced composite laminates in biaxial loading.* Composites Science and Technology, 1995. 54(3): p. 275-285.

47. Reifsnider, K.L., et al., *Damage mechanics and NDE of composite laminates, in Mechanics of Composite Materials - Recent Advances.* Pergamon Press, New York, 1983(399-420).
48. Nairn, J.A. and S. Hu, *Matrix microcracking. In: Damage mechanics of composite materials. Talreja, R, editor.* Amsterdam: Elsevier Science, 1994. Chapter 6: p. 187-243.
49. Roberts, S.J., et al., *The effect of matrix microcracks on the stress-strain relationship in fiber composite tubes.* Journal of Composite Materials, 2003. 37(17): p. 1509-1523.
50. Bailey, J.E., Parvizi, A., *On fibre debonding effects and the mechanism of transverse-ply failure in cross-ply laminates of glass fibre/thermoset composites.* Journal of Materials Science, 1981. 16(3): p. 649-659.
51. Varna, J., et al., *Damage in composite laminates with off-axis plies.* Composites Science and Technology, 1999. 59(14): p. 2139-2147.
52. Asp, L.E., L.A. Berglund, and R. Talreja, *Prediction of matrix-initiated transverse failure in polymer composites.* Composites Science and Technology, 1996. 56(9): p. 1089-1097.
53. Broutman, L.J. and S. Sahu, *Progressive Damage of a Glass Reinforced Plastic during Fatigue.* SPI, 24th Annual Technical Conference, Washington D.C., 1969. Section 11-D.
54. Garrett, K.W. and J.E. Bailey, *Multiple transverse fracture in 90° cross-ply laminates of a glass fibre-reinforced polyester.* Journal of Materials Science, 1977. 12(1): p. 157-168.
55. Highsmith, A.L. and K.L. Reifsnider, *Stiffness reduction mechanisms in composite laminates.* . Damage in composite materials, , 1982. ASTM STP 775: p. 103-117.
56. Harrison, R.P. and M.G. Barder, *Damage development in CFRP laminates under monotonic and cyclic stressing.* Fibre Science and Technology, 1983. 18(3): p. pp. 163-180.
57. Nairn, J.A. and S. Hu, *The initiation and growth of delaminations induced by matrix microcracks in laminated composites.* International Journal of Fracture, 1992. 57(1): p. 1-24.
58. Nairn, J.A., S. Hu, and J.S. Bark, *A critical evaluation of theories for predicting microcracking in composite laminates* Journal of Materials Science, 1993. 28(18): p. 5099-5111
59. Hanh, H.T. and S.W. Tsai, *On the behaviour of composite laminates after initial failures.* Journal of Composite Materials, 1974. Vol. 8: p. 280-305.
60. Talreja, R., *Transverse Cracking and Stiffness Reduction in Coposite Laminates.* Journal of Composite Materials, 1985. 19(4): p. 355-375.

61. Allen, D.H. and J.-W. Lee. *Matrix cracking in laminated composites under monotonic and cyclic loadings*. in *American Society of Mechanical Engineers, Applied Mechanics Division, AMD*. 1990.
62. Li, S., S.R. Reid, and P.D. Soden, *A continuum damage model for transverse matrix cracking in laminated fibre-reinforced composites.* Philosophical Transactions of the Royal Society A: Mathematical, Physical and Engineering Sciences, 1998. 356(1746): p. 2379-2412.
63. Norman, L. and G.J. Dvorak, *Progressive transverse cracking in composite laminates.* Journal of Composite Materials, 1988. 22: p. 900-916.
64. Laws, N., G.J. Dvorak, and M. Hejazi, *Stiffness changes in unidirectional composites caused by cracks systems.* Mechanics of Materials, 1983. Vol. 2: p. 123-137.
65. Hashin, Z., *Analysis of cracked laminates: A variational approach.* Mechanics of Materials, 1985. 4: p. 121-136.
66. Praveen, G.N. and J.N. Reddy, *Transverse matrix cracks in cross-ply laminates: Stress transfer, stiffness reduction and crack opening profiles.* Acta Mechanica, 1998. 130(3-4): p. 227-248.
67. Katerelos, D.G., L.N. McCartney, and C. Galiotis, *Effect of off - Axis matrix cracking on stiffness of symmetric angle-ply composite laminates.* International Journal of Fracture, 2006. 139(3-4): p. 529-536.
68. Katerelos, D.T.G., et al., *Analysis of matrix cracking in GFRP laminates using Raman spectroscopy.* Composites Science and Technology, 2007. 67(9): p. 1946-1954.
69. Tao, J.X. and C.T. Sun, *Effect of matrix cracking on stiffness of composite laminates.* Mechanics of Composite Materials and Structures, 1996. 3(3): p. 225-239.
70. Sun, C.T. and J. Tao, *Prediction of failure envelopes and stress/strain behaviour of composite laminates.* Composites Science and Technology, 1998. 58(7): p. 1125-1136.
71. Jones, R.M., *Mechanics of Composite Materials, McGraw-Hill Inc.* 1975.
72. Gemi, L., et al., *Progressive fatigue failure behavior of glass/epoxy (±75)$_2$ filament-wound pipes under pure internal pressure.* Materials and Design, 2009. 30(10): p. 4293-4298.
73. Frost, S.R., *Predicting the long term fatigue behaviour of filament wound glass/epoxy matrix pipes.* Proceeding of the 10th international Conference of Composite Materials (ICCM 10), 1995. 1: p. 649-656.
74. Hull, D., *Research on composite materials at Liverpool University. I. Failure of filament wound tubes.* Physics in Technology, 1982. 13(5): p. 183-189.

75. Ellyin, F., et al., *The behavior of multidirectional filament wound fibreglass/epoxy tubulars under biaxial loading.* Composites Part A: Applied Science and Manufacturing, 1997. 28(9-10): p. 781-790.
76. Berthelot, J.M. and J.F. Le Corre, *A model for transverse cracking and delamination in cross-ply laminates.* Composites Science and Technology, 2000. 60(7): p. 1055-1066.
77. Kashtalyan, M. and C. Soutis, *Analysis of local delaminations in composite laminates with angle-ply matrix cracks.* International Journal of Solids and Structures, 2002. 39(6): p. 1515-1537.
78. Kashtalyan, M. and C. Soutis, *Analysis of composite laminates with intra- and interlaminar damage.* Progress in Aerospace Sciences, 2005. 41(2): p. 152-173.
79. Rebière, J.L. and D. Gamby, *A criterion for modelling initiation and propagation of matrix cracking and delamination in cross-ply laminates.* Composites Science and Technology, 2004. 64(13-14): p. 2239-2250.
80. Takeda, N. and S. Ogihara, *Initiation and growth of delamination from the tips of transverse cracks in CFRP cross-ply laminates.* Composites Science and Technology, 1994. 52(3): p. 309-318.
81. O'Brien, T.K. *Analysis of local delaminations and their influence on composite laminate behavior* in *ASTM Special Technical Publication*. 1985.
82. Talreja, R., *Stiffness properties of composite laminates with matrix cracking and interior delamination.* Engineering Fracture Mechanics, 1986. Vol. 25(5/6): p. 751-762.
83. Wang, A.S.D., N.N. Kishore, and C.A. Li, *Crack development in graphite-epoxy cross-ply laminates under uniaxial tension.* Composites Science and Technology, 1985. 24(1): p. 1-31.
84. Nagendra, V.A. and R. Talreja, *A mechanistic model for fatigue damage evolution in composite laminates.* Mechanics of Materials, 1998. 29: p. 123-140.
85. Kashtalyan, M. and C. Soutis, *Effect of delaminations induced by transverse cracks and splits on stiffness properties of composite laminates.* Composites Part A: Applied Science and Manufacturing, 2000. 31(2): p. 107-119.
86. Noh, J. and J. Whitcomb, *Effect of delaminations on opening of transverse matrix cracks.* Journal of Composite Materials, 2005. 39(15): p. 1353-1370.
87. Mertiny, P. and A. Gold, *Quantification of leakage damage in high-pressure fibre-reinforced polymer composite tubular vessels.* Polymer Testing, 2007. 26(2): p. 172-179.
88. Pabiot, J., P. Krawczak, and C. Monnier, *Behaviour of Glass-Fibre Composite Pipes under Internal Pressure as a Function of Composite Cohesion Parameters.* 49th Annual Conf. Composite Institute, The Society of the Plastic Industry, Inc., 1994: p. 7-9.

89. Mieras, H.J.M.A., *Irreversible Creep of Filament-Wound Glass-Reinforced Resin Pipes.* Plastics & Polymers, 1973. 41: p. 84-88.
90. Legg, M.J. and D. Hull, *Effect of resin flexibility on the properties of filament wound tubes.* Composites, 1982. 13(4): p. 369-376.
91. Tanigushi, K., M. Ohira, and M. Ishii, *The Effect of Matrix Resins on the Mechanical Properties of Fibreglass Reinforced Pipes for Oil and Gas Production.* 46th Annual Conf. Composite Institute, The Society of the Plastics Industry, Inc., 1991: p. 18-21.
92. Orifici, A.C., I. Herszberg, and R.S. Thomson, *Review of methodologies for composite material modelling incorporating failure.* Composite Structures, 2008. 86(1-3): p. 194-210.
93. Spencer, B. and D. Hull, *Effect of winding angle on the failure of filament wound pipe.* Composites, 1978. 9(4): p. 263-271.
94. Soden, P.D., Kitching, R., Tse, P. C., Tsavalas, Y., Hinton, M. J., *Influence of winding angle on the strength and deformation of filament-wound composite tubes subjected to uniaxial and biaxial loads.* Composites Science and Technology, 1993. 46(4): p. 363-378.
95. Highton, J., A.B. Adeoye, and P.D. Soden, *Fracture Stresses for +- 75 Degree Filament Wound GRP Tubes under Biaxial Loads.* Journal of Strain Analysis for Engineering Design, 1985. 20(3): p. 139-150.
96. Nahas, M.N., *Analysis of non-linear stress-strain response of laminated fibre-reinforced composites.* Fibre Science and Technology, 1984. 20(4): p. 297-313.
97. Evans, J.T. and A.G. Gibson, *Composite angle ply laminates and netting analysis.* Proceeding 'The Royal Society London', 2002. A(458): p. 3079-3088.
98. Hinton, M.J. and P.D. Soden, *Predicting failure in composite laminates: the background to the exercise.* Composites Science and Technology, 1998. 58(7): p. 1001-1010.
99. Soden, P.D., M.J. Hinton, and A.S. Kaddour, *A comparison of the predictive capabilities of current failure theories for composite laminates.* Composites Science and Technology, 1998. 58(7): p. 1225-1254.
100. Soden, P.D., A.S. Kaddour, and M.J. Hinton, *Recommendations for designers and researchers resulting from the world-wide failure exercise.* Composites Science and Technology, 2004. 64(3-4): p. 589-604.
101. Azzi, V.D. and S.W. Tsai, *Anisotropic strength of composites - Investigation aimed at developing a theory applicable to laminated as well as unidirectional composites, employing simple material properties derived from unidirectional specimens alone.* Experimental Mechanics, 1965. 5(9): p. 283-288.
102. Tsai, S.W. and E.M. Wu, *A General Theory of Strength for Anisotropic Materials.* Journal of Composite Materials, 1971. 5: p. 58-80.

103. Hinton, M.J., P.D. Soden, and A.S. Kaddour, *Strength of composite laminates under biaxial loads.* Applied Composite Materials, 1996. 3(3): p. 151-162.
104. Puck , A. and W. Schneider, *On Failure Mechanisms and Failure Criteria of Filament Wound Glass Fibre/Resin Composites.* Plastics & Polymers, 1969. 37: p. 270-273.
105. Sim, D.F. and V.H. Brogdon, *Fatigue behaviour of composites under different loading modes.* Fatigue of Filamentary materials. ASTM STP 636, 1977: p. 185-205.
106. Philippidis, T.P. and A.P. Vassilopoudos, *Fatigue strength prediction under multiaxial stress.* Journal of Composite Materials, 1999. 33(17): p. 1578-1599.
107. Hashin, Z., *Failure Criteria for Unidirectional Fibre Composites.* Journal of Applied Mechanics, 1980. 47: p. 329-334.
108. Rotem, A., *Prediction of laminate failure with the Rotem failure criterion.* Composites Science and Technology, 1998. 58(7): p. 1083-1094.
109. Puck , A. and H. Schurmann, *Failure analysis of FRP laminates by means ofphysically based phenomenological models.* Composite Science Technology, 1998. 58(7): p. 1045.
110. Sun, C.T., J. Tao, and A.S. Kaddour, *The prediction of failure envelopes and stress/strain behavior of composite laminates: Comparison with experimental results.* Composites Science and Technology, 2002. 62(12-13 SPECIAL ISSUE): p. 1673-1682.
111. Mistry, J., *Theoretical investigation into the effect of the winding angle of the fibres on the strength of filament wound GRP pipes subjected to combined external pressure and axial compression.* Composite Structures, 1992. 20(2): p. 83-90.
112. Hernandez-Moreno, H., et al., *Influence of winding pattern on the mechanical behavior of filament wound composite cylinders under external pressure.* Composites Science and Technology, 2008. 68(3-4): p. 1015-1024.
113. Mertiny, P., F. Ellyin, and A. Hothan, *An experimental investigation on the effect of multi-angle filament winding on the strength of tubular composite structures.* Composites Science and Technology, 2004. 64(1): p. 1-9.
114. Lea R.H. and C. Yang, *Improving the mechanical properties of composite pipe using multi-axial filament winding.* Proc. of NACE Annual Conference COROSSION, 1998: p. 458.
115. Schutte, C.L., *Environmental durability of glass-fiber composites.* Materials Science and Engineering R: Reports, 1994. 13(7): p. 265-324.
116. Lundgren, J.E. and P. Gudmundson, *Moisture absorption in glass-fibre/epoxy laminates with transverse matrix cracks.* Composite Science Technology, 1994. 59: p. 1983-1991.

117. Kotsikos, G., et al., *Evaluation of effects of pre-exposure in marine environments of structural glass reinforced composites by acoustic emission testing.* Material Evaluation, 2000. 58: p. 1320-1325.
118. Komai, K.e.a., *The Influence of Water on the Mechanical Properties and Fatigue Strength of Angle-Ply Carbon/Epoxy Composites,.* JSME Int. J., series 1, 1989. 32: p. 588-595.
119. Perreux, D. and C. Suri, *A study of a coupling between the phenomena of water absorption and damage in glass/epoxy composite pipe.* Composite Science Technology, 1997. 57: p. 1403-1413.
120. Mandell, J.F., Huang, D.D. and McGarry, F.J., *Tensile Fatigue Performance of Glass Fibre Dominated Composites.* Composite Technology Review, 1981. 3: p. 96-102.
121. Mandell, J.F., McGarry, F.J., Hsieh, A.J.-Y. and Li, C.G., *Tensile Fatigue of Glass Fibers and Composites with Conventional and Surface Compressed Fibers.* Polymer Composites, 1985. 6: p. 168-174.
122. E. Vauthier, et al., *Interaction between hygrothermal ageing and fatigue damage in unidirectional glass/epoxy composites.* Composites Science and Technology, 1998. 58: p. 687-692.
123. Ellyin, F. and C. Rohrbacher, *Effect of aqueous environment and temperature on glass-fibre epoxy resin composites.* Journal of Reinforced Plastics and Composites, 2000. 19(17): p. 1405-1427.
124. Ellyin, F., *Durability of glass-fibre reinforced polymer composites in aqueous and high temperature environments.* Polymers and Polymer Composites, 2004. 12(4): p. 277-288.
125. Ellyin, F. and R. Maser, *Environmental effects on the mechanical properties of glass-fiber epoxy composite tubular specimens.* Composites Science and Technology, 2004. 64(12): p. 1863-1874.
126. Chiou, P.L. and W.L. Bradley, *Moisture-induced degradation of glass/epoxyfilament wound composite tubes.* Journal of Thermoplastic Composite Materials 1996. 9(2): p. 118-128.
127. Hale, J.M., A.G. Gibson, and S.D. Speake, *Tensile strength testing of GRP pipes at elevated temperatures in aggressive offshore environments.* Journal of Composite Materials, 1998. 32(10): p. 969-986.
128. Mertiny, P. and F. Ellyin. *Selection of optimal processing parameters in filament winding*. in *International SAMPE Technical Conference*. 2001.
129. Lee, S.Y. and G.S. Springer, *Filament winding cylinders. III. Selection of the process variables.* Journal of Composite Materials, 1990. 24(12): p. 1344-1366.
130. Lee, S.Y. and G.S. Springer, *Filament winding cylinders. I. Process model* Journal of Composite Materials, 1990. 24 (12): p. 1270-1298.

131. Lee, S.Y. and G.S. Springer, *Filament winding cylinders. II. Validation of the process model* Journal of Composite Materials 1990. 24(12): p. 1299-1243.
132. Cohen, D., *Influence of filament winding parameters on composite vessel quality and strength.* Composites Part A: Applied Science and Manufacturing, 1997. 28(12): p. 1035-1047.
133. Mertiny, P. and F. Ellyin, *Influence of the filament winding tension on physical and mechanical properties of reinforced composites.* Composites Part A: Applied Science and Manufacturing, 2002. 33(12): p. 1615-1622.
134. Dvorak, G.J. and A.P. Suvorov, *The effect of fibre pre-stress on residual stress and the onset of damage in symmetric laminates.* Composite Science Technology, 2000. 60: p. 1129-1139.
135. Talreja, R., *Fatigue of Composite Materials.* Technomatic Publishing Inc. Lancaster, Pennsylvania, US, 1987.
136. Reifsneider, K.L., *Fatigue of Composite Materials.* Elsvier Science Publisher B.V., 1990.
137. Dharan, C.K.H., *Fatigue Behaviour of Fibre -reinforced polymers and advanced composites.* American Society of Mechanical Engineers (Paper), 1977(77 -DE-41).
138. Talreja, R., *Fatigue of composite materials: damage mechanisms and fatigue-life diagrams.* Proceedings of The Royal Society of London, Series A: Mathematical and Physical Sciences, 1981. 378(1775): p. 461-475.
139. Owen, M.J. and J.R. Griffiths, *Evaluation of biaxial stress failure surfaces for a glass reinforced polyester resin under static and fatigue loading.* Journal of Materials Science, 1978. 13: p. 1521-1537.
140. Krempl, E., et al., *Uniaxial and biaxial fatigue properties of thin walled composite tubes.* Journal of the American Helicopter Society, 1988. 33(3): p. 3-10.
141. Krempl, E. and N. Tyan Min. *Graphite/epoxy [±45°] tubes-their static axial and shear and fatigue behaviour under completely reversed load controlled loading*. in *Journal of Composite Materials*. 1982.
142. Bredemo, R., *Damage development during uniaxial fatigue of filament wound tubes.* SICOM report 92-001. Pitea (Sweden): Swedish Institute of composites., 1992.
143. Kujawski, D., A.S. Chiu, and F. Ellyin, *An effective stress parameter for long-term fatigue strength of fiber-reinforced plastic pipes.* Journal of Composites Technology and Research, 1996. 18(3): p. 215-220.
144. Kujawski, D., F. Ellyin, and M.S. Culen, *The fatigue behaviour of filament-wound fiberglass/epoxy tubes under cyclic pressure.* Journal of Reinforced Plastics and Composites, 1998. 17(3): p. 268-281.

145. Rousseau, J., D. Perreux, and N. Verdie?re, *The influence of winding patterns on the damage behaviour of filament-wound pipes.* Composites Science and Technology, 1999. 59(9): p. 1439-1449.
146. Kaynak, C. and O. Mat, *Uniaxial fatigue behavior of filament-wound glass-fiber/epoxy composite tubes.* Composites Science and Technology, 2001. 61(13): p. 1833-1840.
147. Guedes, R.M., *Creep and fatigue lifetime prediction of polymer matrix composites based on simple cumulative damage laws.* Composites Part A: Applied Science and Manufacturing, 2008. 39(11): p. 1716-1725.
148. S.Subramanian, K.L.R., W.W.Stinchcomb, *A cumulative damage model to predict the fatigue life of composite laminates including the effect of a fibre-matrix interface.* Int. J. Fatigue, 1994. 17(5): p. 343-351.
149. Wu, F. and W. Yao, *A fatigue damage model of composite materials.* International Journal of Fatigue. 32(1): p. 134-138.
150. Yao, W.X. and N. Himmel, *A new cumulative fatigue damage model for fibre-reinforced plastics.* Composites Science and Technology, 2000. 60(1): p. 59-64.
151. Ye, L., *On fatigue damage Accumulation and material degradation in composite materials.* Composite Science and Technology, 1989. 36: p. 339-350.
152. Miner, M.A., *Cumulative damage in fatigue.* J Appl Mech, 1945. 12: p. 59-64.
153. Owen, M.J. and R.J. Howe, *The accumulation of damage in glass-reinforced plastic under tensile and fatigue loading.* Journal Physics D: Applied Physics, 1972. 5: p. 1637-1649.
154. Paris, P.C., *The growth of cracks due to variations of loads.* Ph.D thesis, Lehigh University, 1960.
155. Suresh, S., *Fatigue of materials.* 2nd ed. Cambridge University Press., 1998.
156. Christensen, R.M., *A physically based cumulative damage formalism.* International Journal of Fatigue, 2008. 30(4): p. 595-602.
157. Broutman, L.J. and S. Sahu, *A new theory to predict cumulative damage in fibre-glass reinforced composites.* Composite Materials Testing and Design, 1972. ASTM STP(497): p. 170-188.
158. Z. Fawaz and F. Ellyin, *Fatigue failure model for fibre reinforced materials under general loading conditions.* Journal of Composite Materials, 1994. 28(15): p. 1432-1451.
159. Inoue, A., T. Fujii, and H. Kawakami, *Effect of loading path on mechanical response of a glass fabric composite at low cyclic fatigue under tension/torsion biaxial loading.* Journal of Reinforced Plastics and Composites, 2000. 19(2): p. 111-123.
160. Adden, S. and P. Horst, *Stiffness degradation under fatigue in multiaxially loaded non-crimped-fabrics.* International Journal of Fatigue, 2010. 32(1): p. 108-122.

161. Marino Quaresimin, Luca Susmel, and R. Talreja, *Fatigue behaviour and life assessment of composite laminates under multiaxial loadings.* International Journal of Fatigue, 2010. 32(1): p. 2-16.
162. Hashin, Z., *Cumulative damage theory for composite materials: Residual life and residual strength methods.* Composites Science and Technology, 1985. 23(1): p. 1-19.
163. Reifsnider, K.L. and W.W. Stinchcomb. *Stiffness change as a fatigue damage parameter for composite laminates*. in *American Society of Mechanical Engineers, Aerospace Division (Publication) AD*. 1983.
164. Reynolds, W.N., *Nondestructive testing (NDT) of fibre reinforced composite materials.* Material and Design, 1985. 5(6): p. 256-270.
165. Scott, I.G. and C.M. Scala, *A review of non-destructive testing of composite materials.* NDT International, 1982. 15(2): p. 75-86.
166. Barre, S. and M.L. Benzeggagh, *On the use of acoustic emission to investigate damage mechanisms in glass fibe reinforced polypropylene.* Composite Science Technology, 1994. 52: p. 369-376.
167. Barnes, C.A. and G. Ramirez, *Acoustic emission testing of carbon fibre composite offshore drilling risers.* 6th International Symposium on acoustic emission from composite materials (AECM-6) 1998: p. 13-22.
168. Kaiser, J., *"Untersuchen uiber das Auftreten Gerauschen Beim Zugversuch" (Investigation of Acoustic Emission in Tensile Testing).* Ph.D. thesis, Technische Hochscule, Munich, Germany, 1950.
169. Fowler, T.J., *Acoustic emissions of fibre reinforced plastics.* Journal Technical Councils of ASCE, 1979: p. 281-289.
170. Pollock, A., *Acoustic Emission Inspection.* Metals Handbook, 1989. 9th Edition, ASM International: p. 278-294.
171. Prevorovsky, Z., et al., *Ultrasonic scanning and acoustic emission of composite tubes subjected to multiaxial loading.* Ultrasonics, 1998. 36(1-5): p. 531-537.
172. Ramirez, G., M.D. Engelhardt, and T.J. Fowler, *On the endurance limit of fiberglass pipes using acoustic emission.* Journal of Pressure Vessel Technology, Transactions of the ASME, 2006. 128(3): p. 454-461.
173. Ameron, I.C., *Quick guide into ISO 14692.* Internal Publication of Ameron - Fiberglass-Composite Pipe Division, 2006.
174. 14692-2:2002, E.I., *The European Standard, Petroleum and natural gas industries: Glass-reinforced plastics (GRP) piping.* 2002.
175. *ASTM D2992, Standard Practice for Obtaining Hydrostatic or Pressure Design Basis for Fiberglass (Glass-Fiber-Reinforced Thermosetting Resin) Pipe and Fittings.* American Society for Testing and Materials, 1996.
176. *Picture curtesy of http://www.ameron-fpg.com/files/pdf/EB_1.pdf.*

177. Gibson, A.G., et al., *Novel approach to qualification of non-metallic pipe systems - As applied to reinforced thermoplastic pipe.* Plastics, Rubber and Composites, 2005. 34(7): p. 301-304.
178. www.iso14692.co.uk.
179. Schwencke, H.F., De Ruyter van Stevenick, A.W. , *The Ultimate Elastic Wall Stress (UEWS) of Wavistrong Pipes (A criterion for the determination of the working pressure of a GRP pipe).* 1968. 68-11(Shell Publication).
180. FuturePipes, I., *Engineering Guide for Wavistrong filament wound epoxy pipe systems.* Wavistrong Engineering Guide, 2001.
181. Gibson, R.F., *Principles of Composite Material Mechanics, McGraw-Hill, Inc.* 1994.
182. *Standard Practice for Determining Dimensions of "Fiberglass" (Glass-Fiber-Reinforced Thermosetting Resin) Pipe and Fittings.* American Society for Testing and Materials, 1997 (reapproved 2006).
183. Stephens, R.C., *Strength of Materials: Theory and examples.* Edward Arnold (Publisher) Ltd, 1975: p. 168.
184. J.T.Evans, A.G.G., *Composite angle ply laminates and netting analysis.* Proceeding 'The Royal Society London', 2002. A(458): p. 3079-3088.
185. A. Thionnet, J.R., *Laminated composites under fatigue loading: A damage development for tranverse cracking.* Composite Science and Technology, 1994. 52: p. 173-181.
186. Guedes, R.M., *Lifetime predictions of polymer matrix composites under constant or monotonic load.* Composites Part A: Applied Science and Manufacturing, 2006. 37(5): p. 703-715.
187. D.T.G. Katerelos, M.K., C. Soutis, C. Galiotis, *Matrix cracking in polymeric composites laminates: Modelling and experiments.* Composites Science and Technology, 2008. 68: p. 2310-2317.
188. Talreja, R., *Transverse cracking and stiffness reduction in composite laminates.* Journal of Composite Materials, 1985. 19(4): p. 355-375.
189. Gudmundson, P. and Z. Weilin, *An analytic model for thermoelastic properties of composite laminates containing transverse matrix cracks.* International Journal of Solids and Structures, 1993. 30(23): p. 3211-3231.
190. Gudmundson, P. and S. Ostlund, *Prediction of thermoelastic properties of composite laminates with matrix cracks.* Composites Science and Technology, 1992. 44: p. 95-105.
191. Azzi, V.D. and S.W. Tsai, *Elastic moduli of laminated anisotropic composites - Experimental program, using glass-filament-reinforced resin cross-ply and angle-ply plates and cylindrical pressure vessels as test specimens, confirms the validity of the theory.* Experimental Mechanics, 1965. 5(6): p. 177-185.

192. Hale, J.M. and A.G. Gibson, *Coupon tests of fibre reinforced plastics at elevated temperatures in offshore processing environments.* Journal of Composite Materials, 1998. 32(4): p. 387-404.
193. *Plastics-Determination of compressive properties.* British Standard, BE EN ISO 604:2003, 2003.

APPENDICES

Appendix A: Engineering drawing for adhesive bonded end fitting

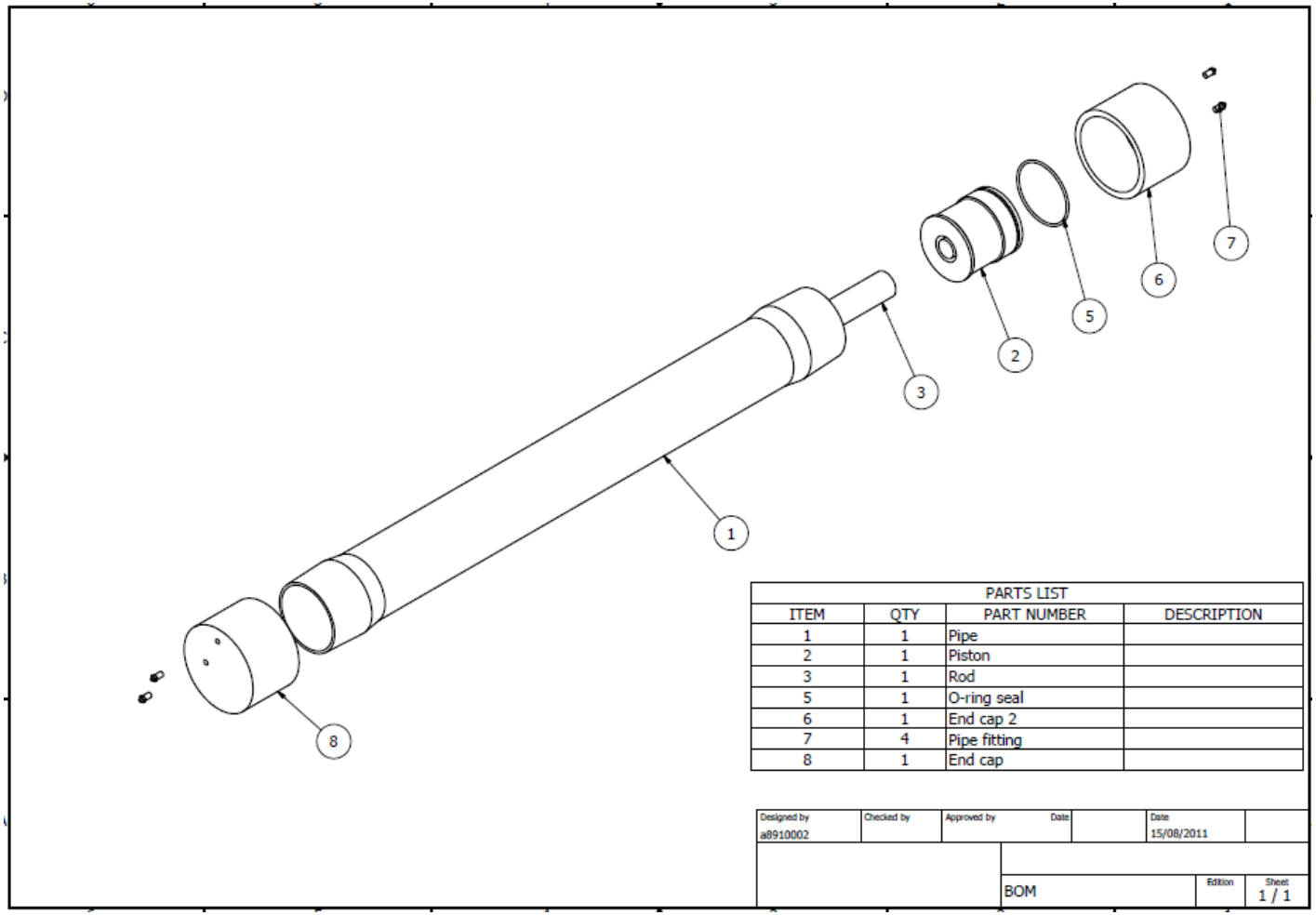

PARTS LIST			
ITEM	QTY	PART NUMBER	DESCRIPTION
1	1	Pipe	
2	1	Piston	
3	1	Rod	
5	1	O-ring seal	
6	1	End cap 2	
7	4	Pipe fitting	
8	1	End cap	

Designed by	Checked by	Approved by	Date	Date
a8910002				15/08/2011

BOM | Edition | Sheet 1 / 1

A-A (0.15 : 1)

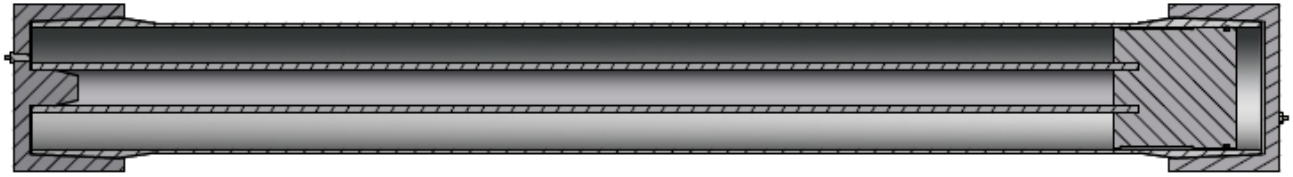

Designed by	Checked by	Approved by	Date		Date	
Shukry					15/08/2011	

Newcastle University			
	xsection	Edition	Sheet 1 / 1

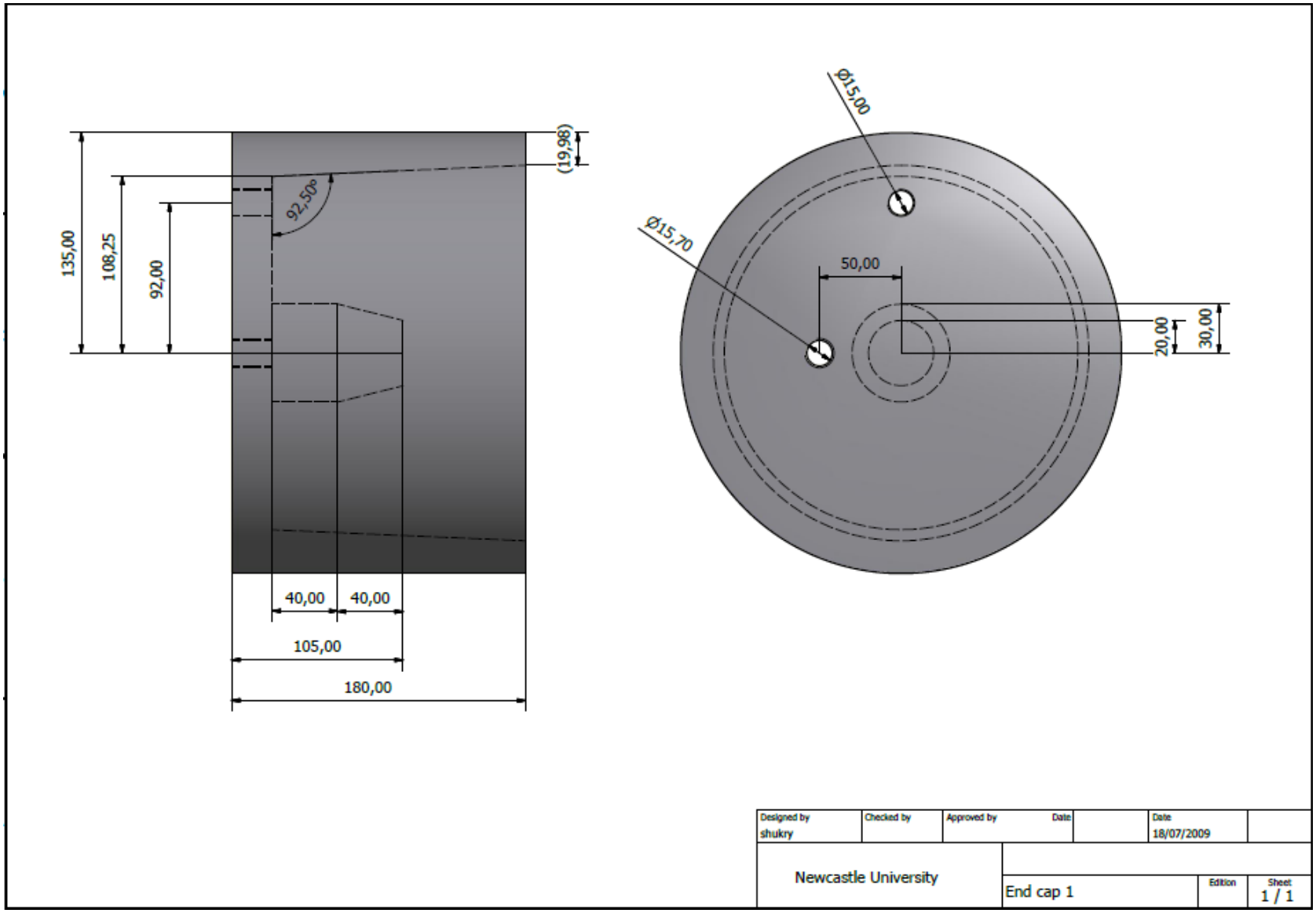
135,00
108,25
92,00
92,50°
(19,98)
40,00
40,00
105,00
180,00
Ø15,00
Ø15,70
50,00
20,00
30,00
Designed by
shukry
Checked by
Approved by
Date
Date
18/07/2009
Newcastle University
End cap 1
Edition
Sheet
1 / 1

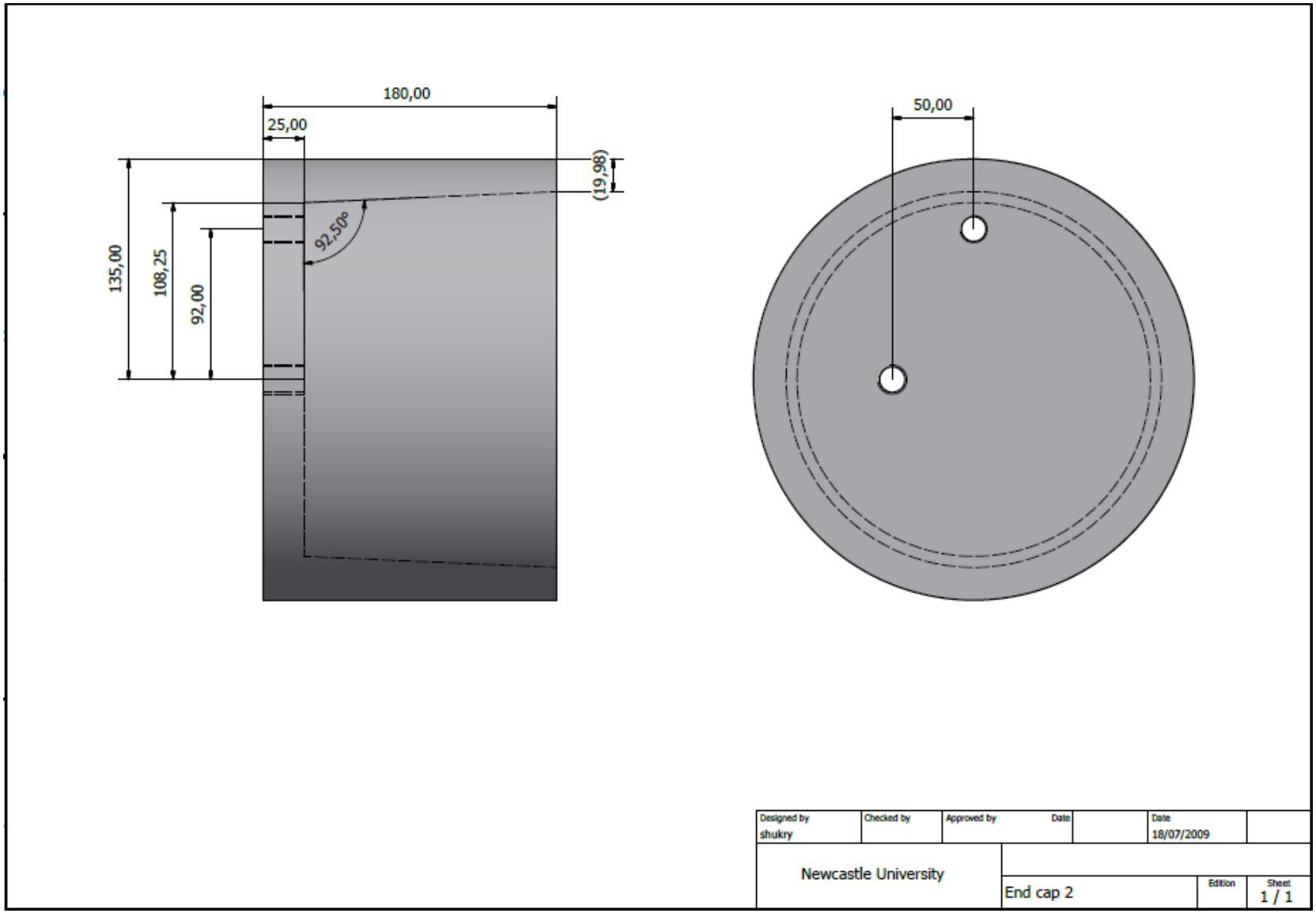
180,00
25,00
(19,98)
92,50°
135,00
108,25
92,00
50,00
Designed by
shukry
Checked by
Approved by
Date
Date
18/07/2009
Newcastle University
End cap 2
Edition
Sheet
1 / 1

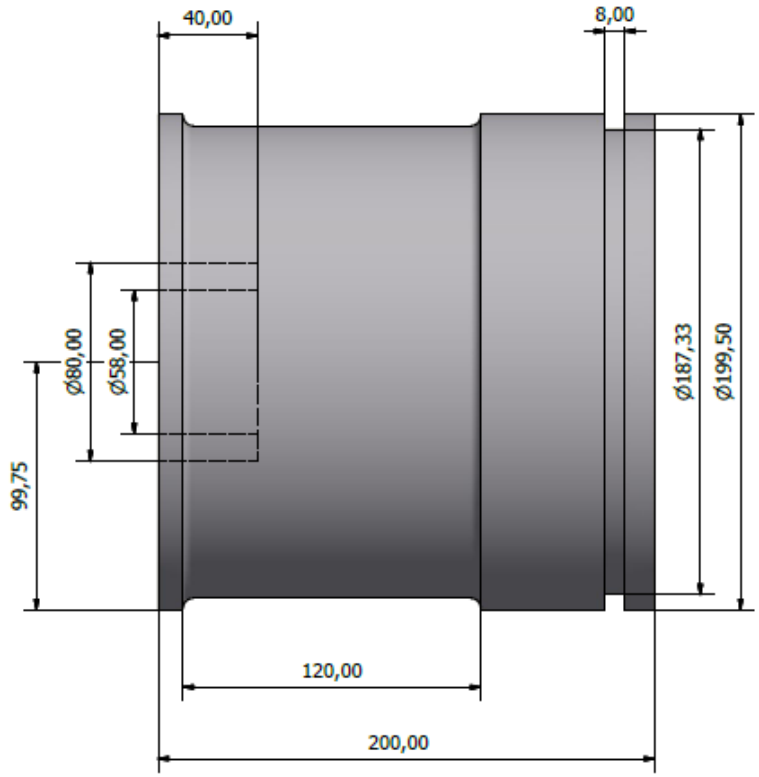

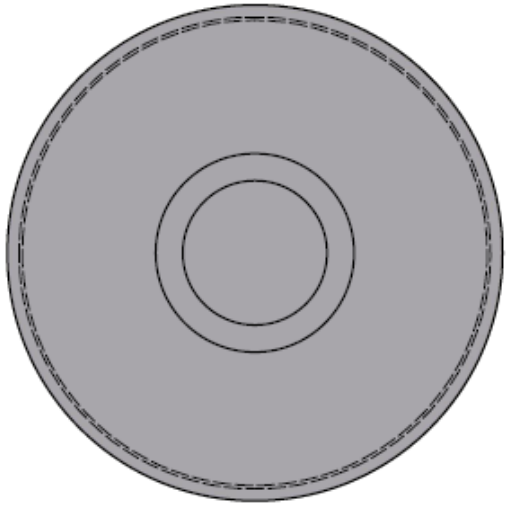

Designed by	Checked by	Approved by	Date		Date	
shukry					18/07/2009	

Newcastle University	Head Piston	Edition	Sheet
			1 / 1

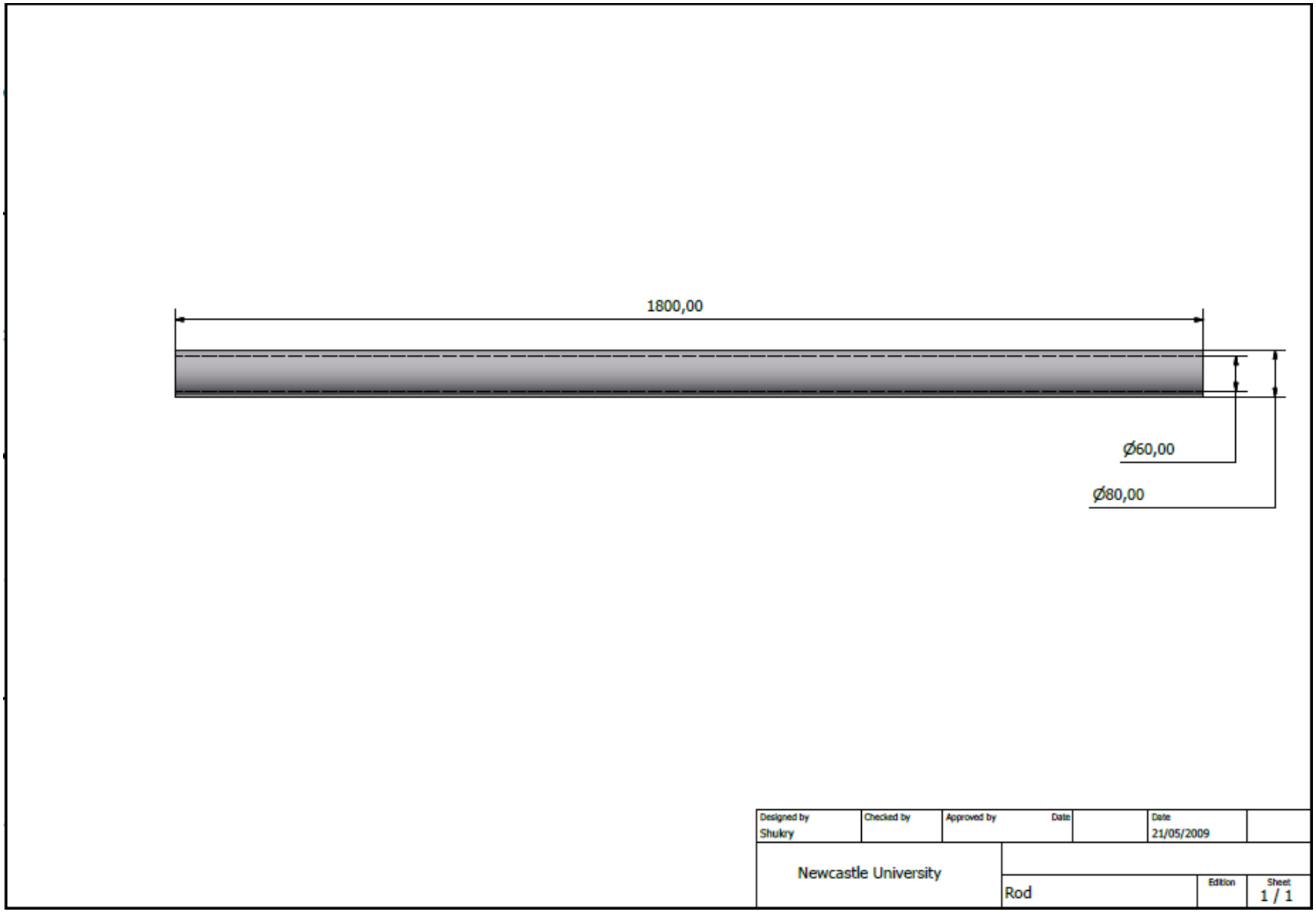
1800,00
Ø60,00
Ø80,00
Designed by
Shukry
Checked by
Approved by
Date
Date
21/05/2009
Newcastle University
Rod
Edition
Sheet
1 / 1

Appendix B: Engineering drawing for mechanical end fitting

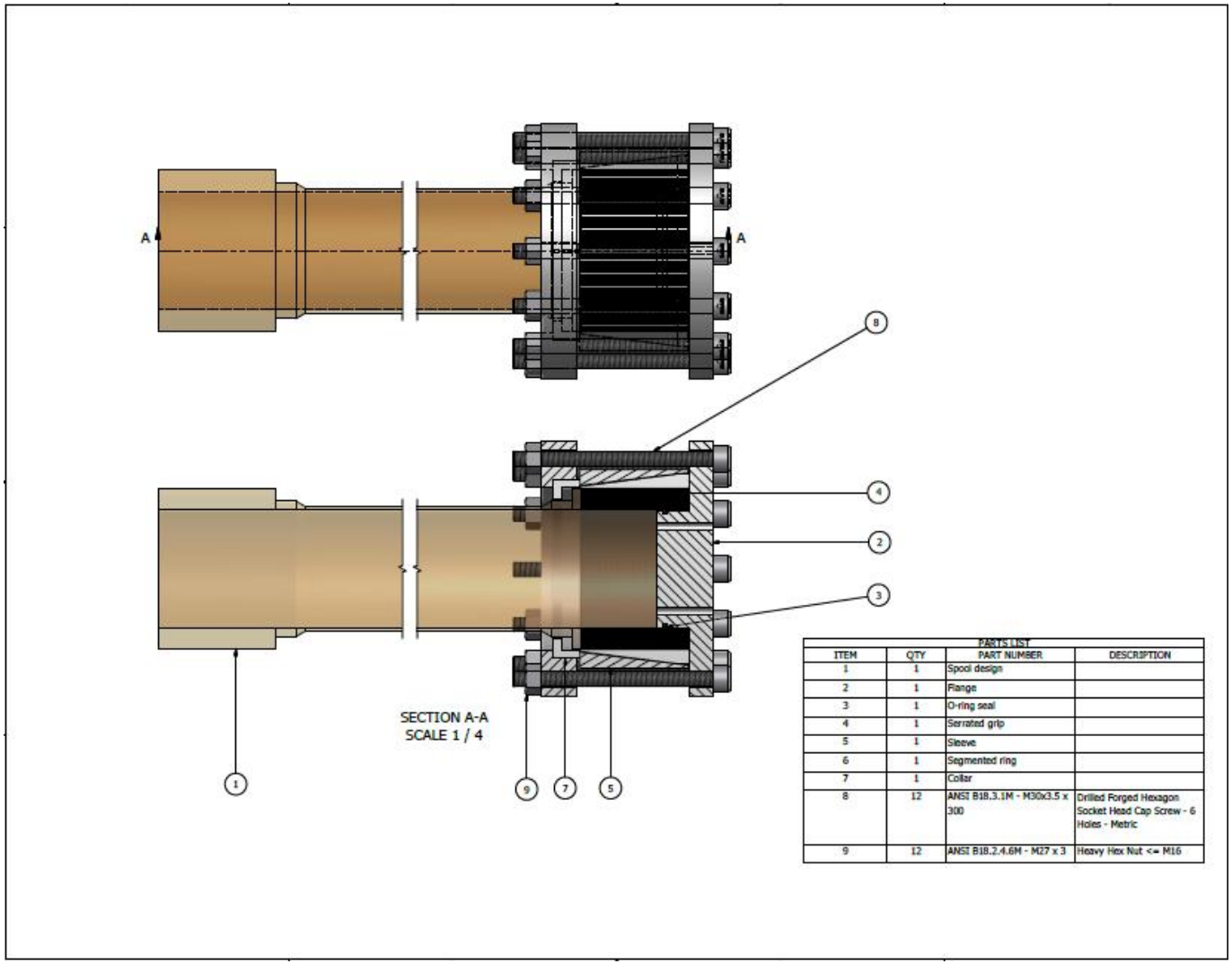

PARTS LIST

ITEM	QTY	PART NUMBER	DESCRIPTION
1	1	Spool design	
2	1	Flange	
3	1	O-ring seal	
4	1	Serrated grip	
5	1	Sleeve	
6	1	Segmented ring	
7	1	Collar	
8	12	ANSI B18.3.1M - M30x3.5 x 300	Drilled Forged Hexagon Socket Head Cap Screw - 6 Holes - Metric
9	12	ANSI B18.2.4.6M - M27 x 3	Heavy Hex Nut <= M16

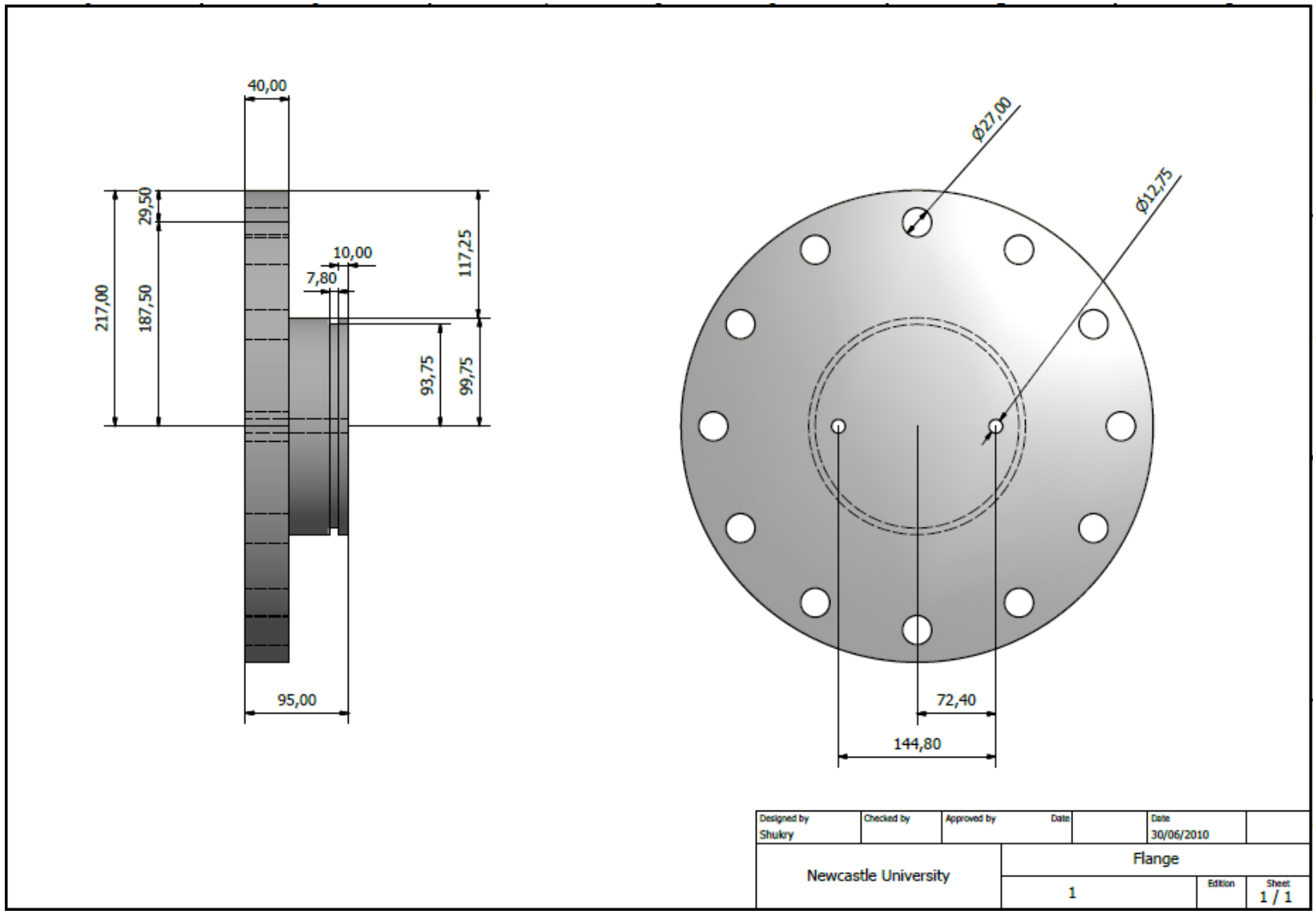
40,00
29,50
187,50
217,00
10,00
7,80
117,25
93,75
99,75
95,00
Ø27,00
Ø12,75
72,40
144,80
Designed by
Shukry
Checked by
Approved by
Date
Date
30/06/2010
Newcastle University
Flange
1
Edition
Sheet
1 / 1

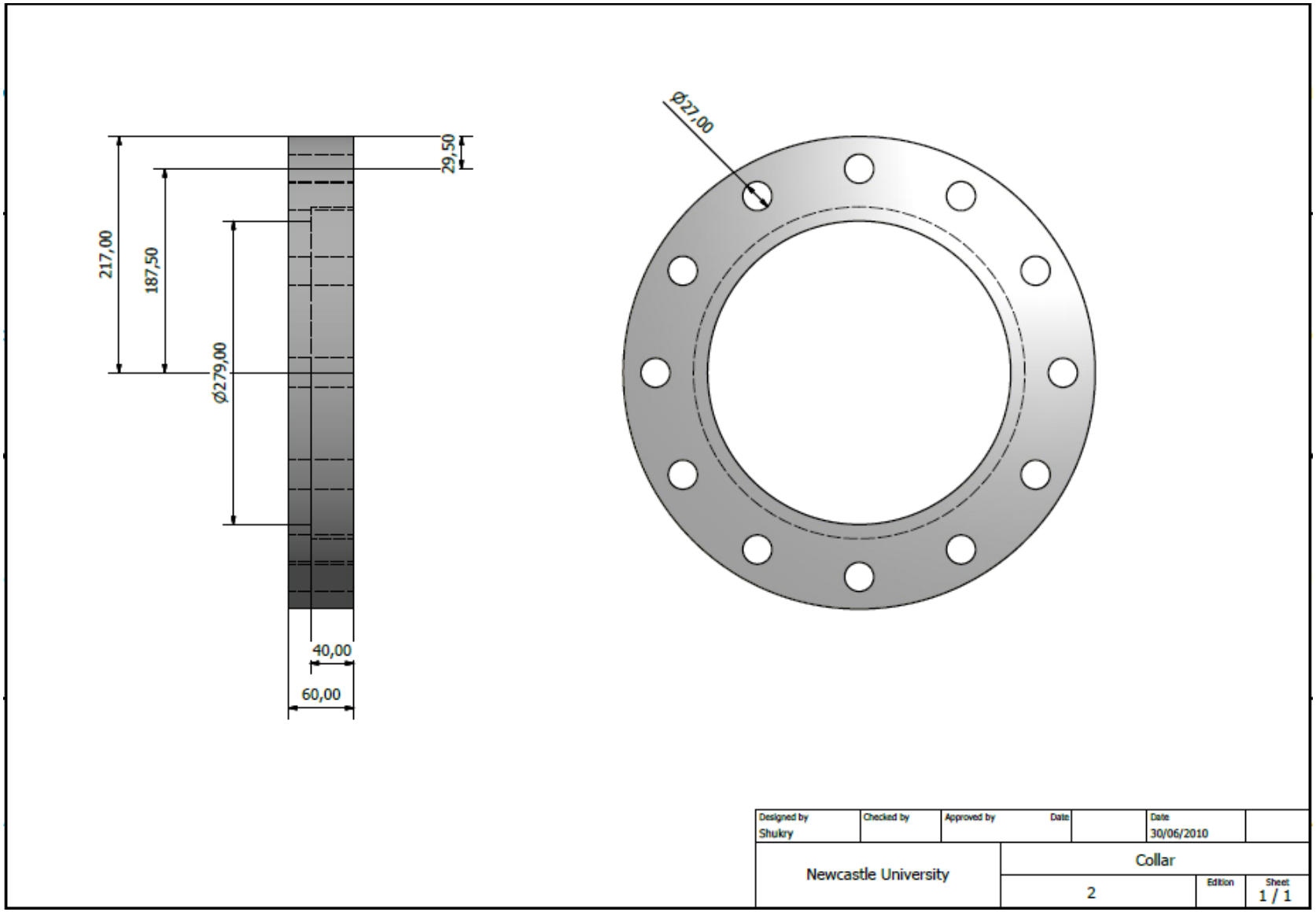
29,50
217,00
187,50
Ø279,00
40,00
60,00
Ø27,00
Designed by
Shukry
Checked by
Approved by
Date
Date
30/06/2010
Newcastle University
Collar
2
Edition
Sheet
1 / 1

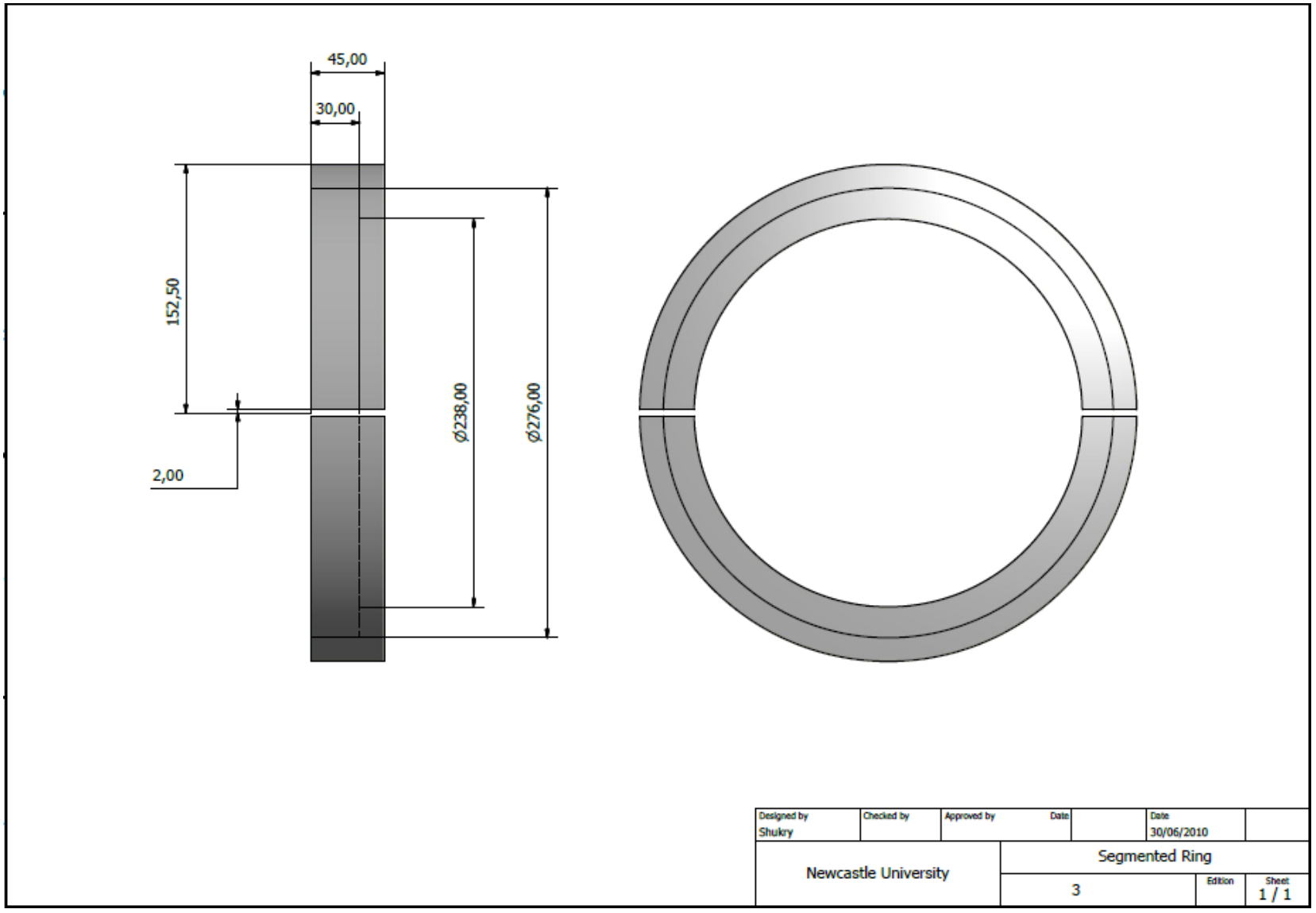
45,00
30,00
152,50
2,00
Ø238,00
Ø276,00
Designed by
Shukry
Checked by
Approved by
Date
Date
30/06/2010
Newcastle University
Segmented Ring
3
Edition
Sheet
1 / 1

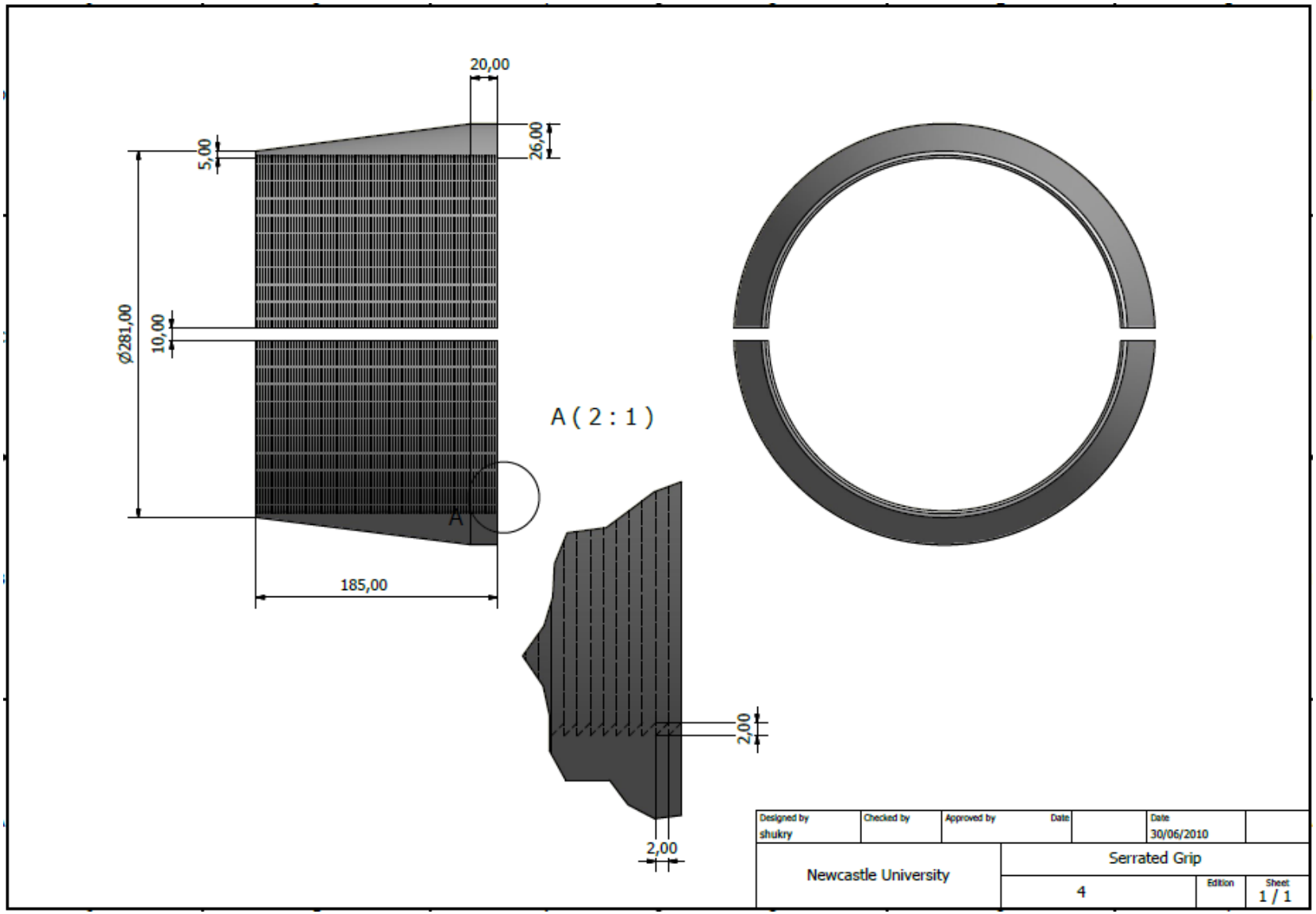
20,00
26,00
5,00
Ø281,00
10,00
A (2 : 1)
A
185,00
2,00
2,00
Designed by
shukry
Checked by
Approved by
Date
Date
30/06/2010
Newcastle University
Serrated Grip
4
Edition
Sheet
1 / 1

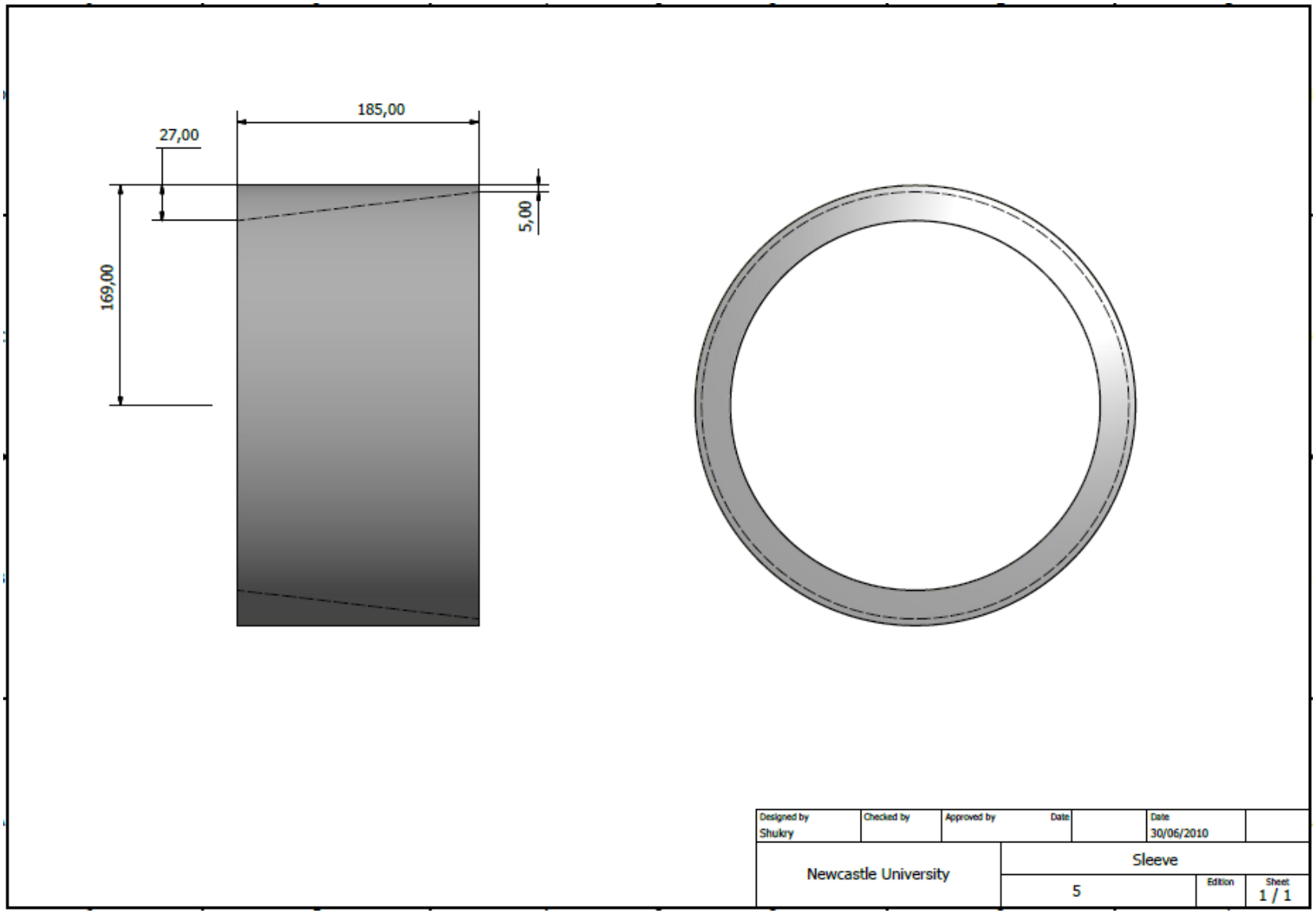
185,00
27,00
5,00
169,00
Designed by
Shukry
Checked by
Approved by
Date
Date
30/06/2010
Newcastle University
Sleeve
5
Edition
Sheet
1 / 1

Appendix C: Engineering drawing for pressure intensifier/reducer

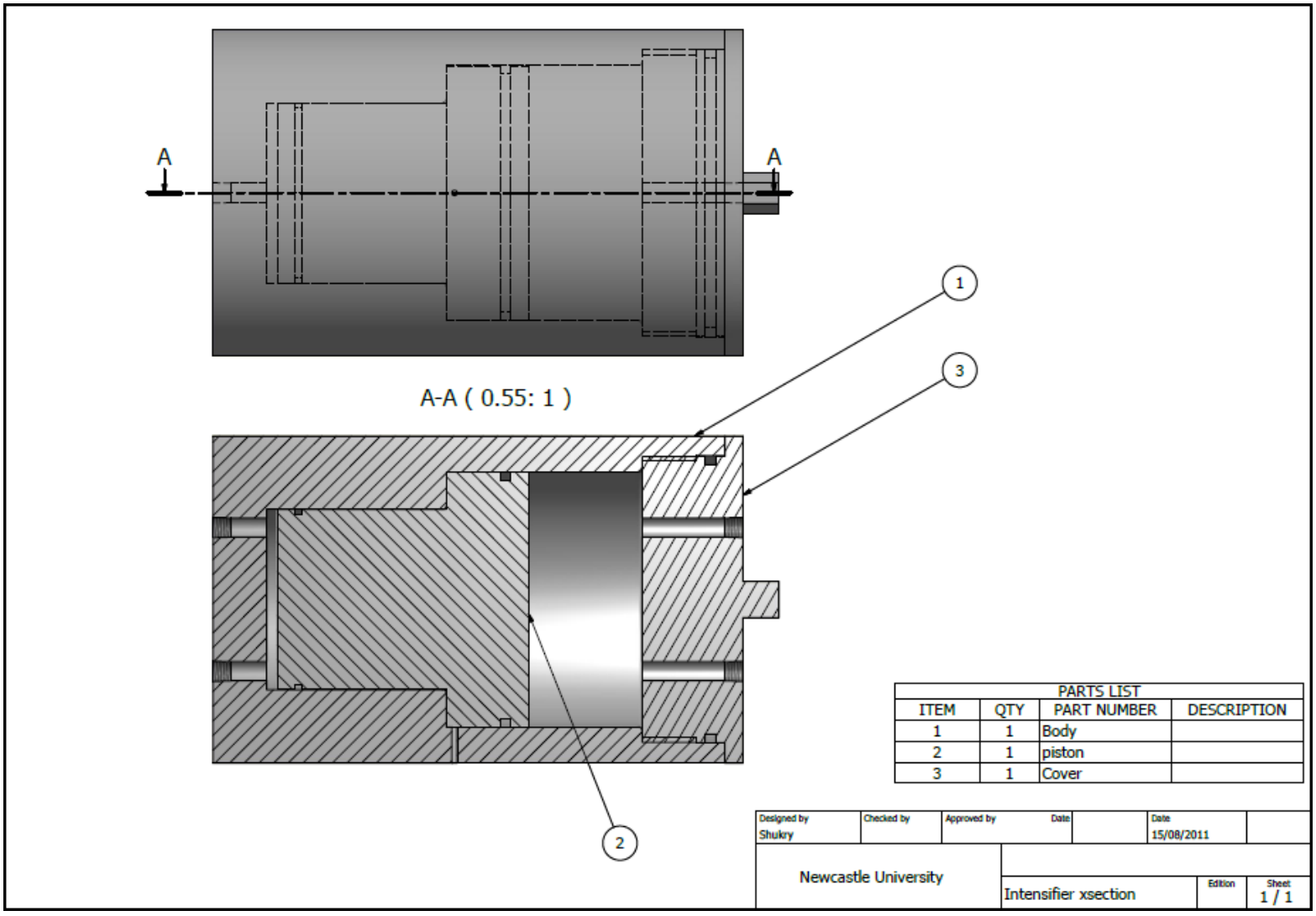

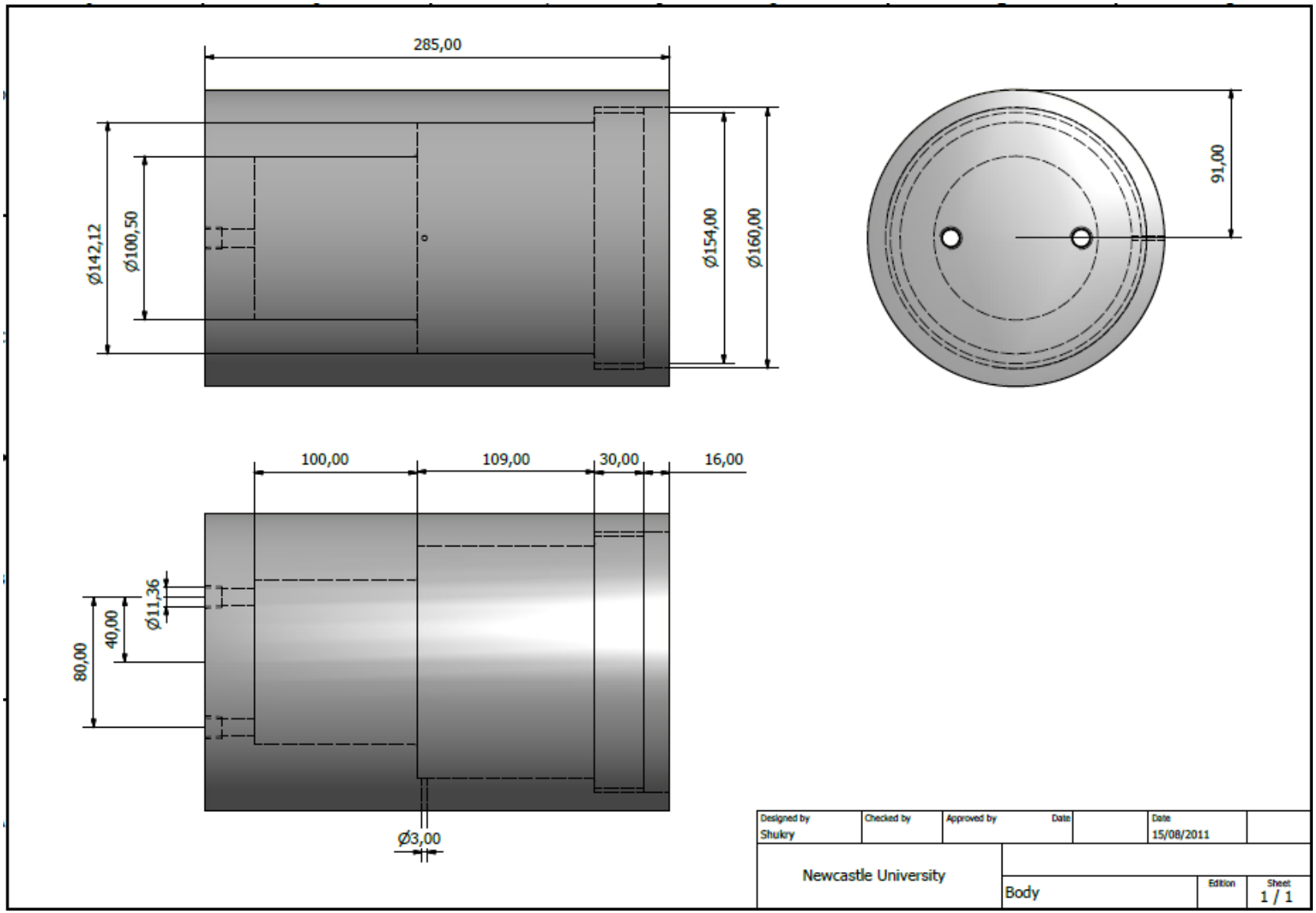
285,00
Ø142,12
Ø100,50
Ø154,00
Ø160,00
91,00
100,00
109,00
30,00
16,00
Ø11,36
40,00
80,00
Ø3,00
Designed by
Shukry
Checked by
Approved by
Date
Date
15/08/2011
Newcastle University
Body
Edition
Sheet
1 / 1

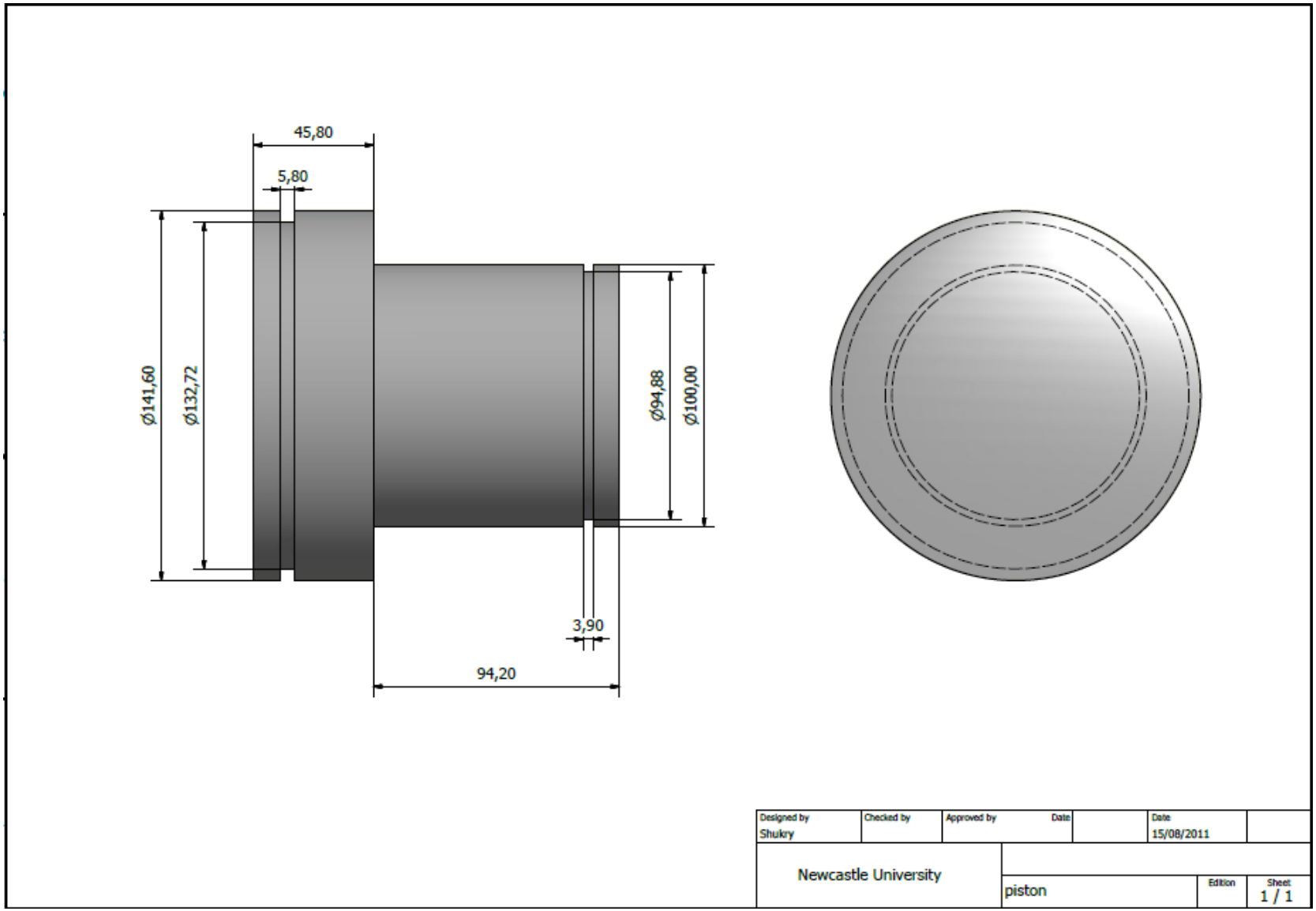
45,80
5,80
Ø141,60
Ø132,72
Ø94,88
Ø100,00
3,90
94,20
Designed by
Shukry
Checked by
Approved by
Date
Date
15/08/2011
Newcastle University
piston
Edition
Sheet
1 / 1

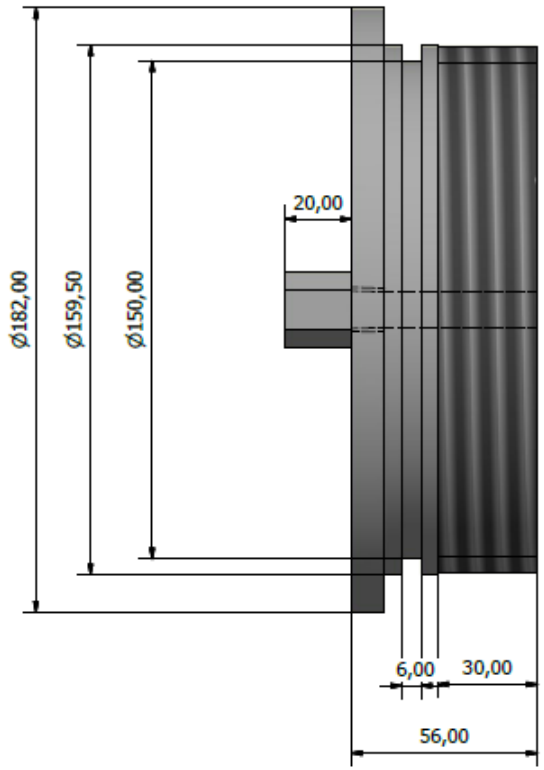

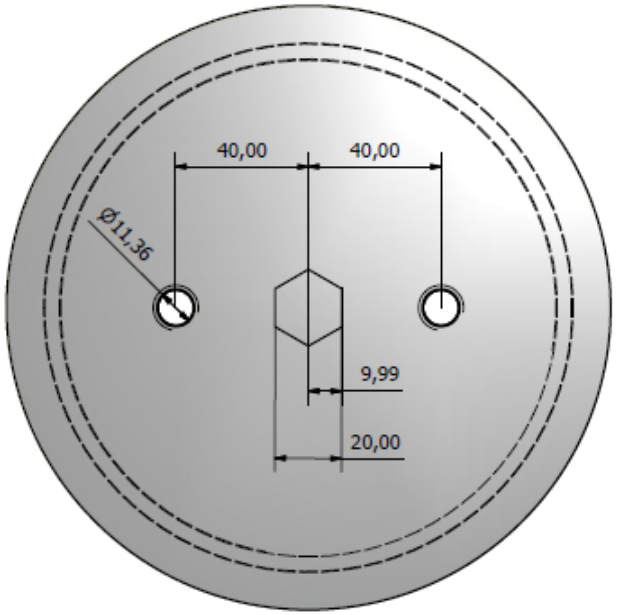

Designed by	Checked by	Approved by	Date		Date	
Shukry					15/08/2011	

Newcastle University			
	Cover	Edition	Sheet 1 / 1